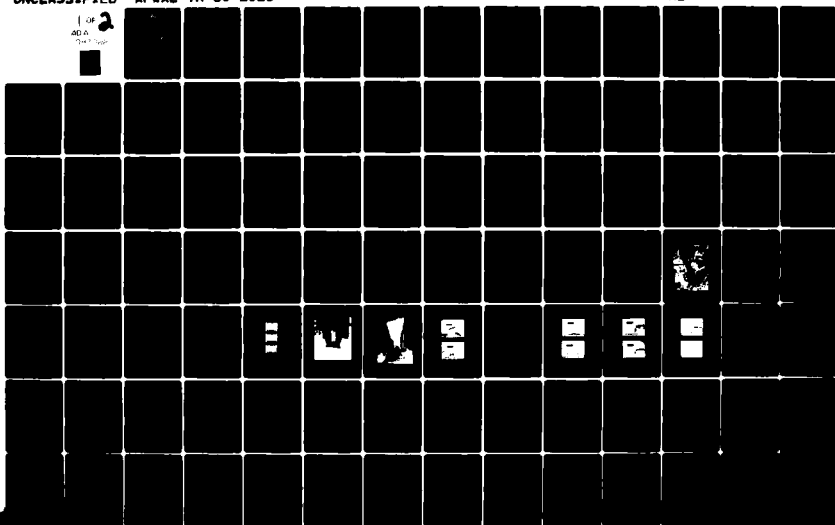


AD-A087 022

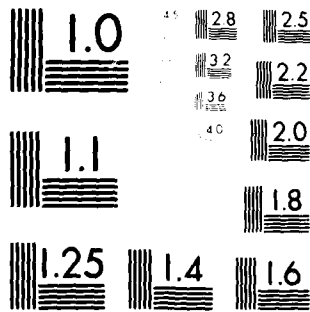
AIR FORCE WRIGHT AERONAUTICAL LABS WRIGHT-PATTERSON AFB OH F/G 10/2  
TESTS OF A LIGHTWEIGHT 200 KW MHD CHANNEL AND DIFFUSER.(U)  
MAR 80 J F HOLT, J PEARSON  
AFWAL-TR-80-2021

UNCLASSIFIED

NL



8702



MICROCOPY RESOLUTION TEST CHART  
NBS 1963-A

AFWAL-TR-80-2021

**LEVEL**

2

ADA087022

TESTS OF A LIGHTWEIGHT 200 KW MHD CHANNEL AND DIFFUSER

Energy Conversion Branch  
Aerospace Power Division

DTIC  
ELECTE  
JUL 23 1980  
S D C

March 1980

TECHNICAL REPORT AFWAL-TR-80-2021

Final Report for Period March 1977 through December 1978

Approved for public release; distribution unlimited.

DDC FILE COPY

AERO PROPULSION LABORATORY  
AIR FORCE WRIGHT AERONAUTICAL LABORATORIES  
AIR FORCE SYSTEMS COMMAND  
WRIGHT-PATTERSON AIR FORCE BASE, OHIO 45433


80 7 22 019


NOTICE

When Government drawings, specifications, or other data are used for any purpose other than in connection with a definitely related Government procurement operation, the United States Government thereby incurs no responsibility nor any obligation whatsoever; and the fact that the government may have formulated, furnished, or in any way supplied the said drawings, specifications, or other data, is not to be regarded by implication or otherwise as in any manner licensing the holder or any other person or corporation, or conveying any rights or permission to manufacture use, or sell any patented invention that may in any way be related thereto.

This report has been reviewed by the Office of Public Affairs (ASD/PA) and is releasable to the National Technical Information Service (NTIS). At NTIS, it will be available to the general public, including foreign nations.

This technical report has been reviewed and is approved for publication.

  
JAMES F. HOLT  
Physicist  
High Power Branch  
Aerospace Power Division

  
JOSEPH F. WISE  
Technical Area Manager  
Energy Conversion Branch  
Aerospace Power Division

FOR THE COMMANDER

  
ROBERT R. BARTHELEMY  
Acting Chief  
Aerospace Power Division

"If your address has changed, if you wish to be removed from our mailing list, or if the addressee is no longer employed by your organization please notify AFWAL/POOC, W-PAFB, OH 45433 to help us maintain a current mailing list".

Copies of this report should not be returned unless return is required by security considerations, contractual obligations, or notice on a specific document.

SECURITY CLASSIFICATION OF THIS PAGE (When Data Entered)

REPORT DOCUMENTATION PAGE		READ INSTRUCTIONS BEFORE COMPLETING FORM
1. REPORT NUMBER AFWAL-TR-80-2021	2. GOVT ACCESSION NO. AD-A087 022	3. RECIPIENT'S CATALOG NUMBER
4. TITLE (and Subtitle) TESTS OF A LIGHTWEIGHT 200 KW MHD CHANNEL AND DIFFUSER.	5. TYPE OF REPORT & PERIOD COVERED Final Report March 1977 - December 1978	
7. AUTHOR(s) James F. Holt and Jerome Pearson	6. PERFORMING ORG. REPORT NUMBER	
9. PERFORMING ORGANIZATION NAME AND ADDRESS Aero Propulsion Laboratory and Flight Dynamics Laboratory Wright-Patterson AFB, OH 45433	8. CONTRACT OR GRANT NUMBER(s)	
11. CONTROLLING OFFICE NAME AND ADDRESS Aero Propulsion Laboratories (AFWAL/POOC) AF Wright Aeronautical Laboratories Wright-Patterson AFB, OH 45433	10. PROGRAM ELEMENT, PROJECT, TASK AREA & WORK UNIT NUMBERS	
14. MONITORING AGENCY NAME & ADDRESS (if different from Controlling Office)  1276	12. REPORT DATE March 1980	
	13. NUMBER OF PAGES 175	
	15. SECURITY CLASS. (of this report)	
	15a. DECLASSIFICATION DOWNGRADING SCHEDULE	
16. DISTRIBUTION STATEMENT (of this Report) Approved for public release; distribution unlimited.  163145		
17. DISTRIBUTION STATEMENT (of the abstract entered in Block 20, if different from Report)  17,26		
18. SUPPLEMENTARY NOTES		
19. KEY WORDS (Continue on reverse side if necessary and identify by block number) MHD Power MHD Generator MHD Energy Converter Structural Vibration		
20. ABSTRACT (Continue on reverse side if necessary and identify by block number) A 200 kW lightweight MHD generator channel and diffuser were tested over a regime of 235 individual firings of the open cycle combustor system. The diagonal conducting wall channel delivered full rated power with no inter-electrode breakdown. Vibration measurements indicated no fatigue of the channel structure.		

DD FORM 1 JAN 73 1473

EDITION OF 1 NOV 65 IS OBSOLETE

SECURITY CLASSIFICATION OF THIS PAGE (When Data Entered)

892.662

B

AFWAL-TR-80-2021

## FOREWORD

This report documents the results of testing a lightweight MHD channel and diffuser which were developed for the Air Force by Maxwell Laboratories, Inc. The period of testing was from March 1977 through December 1978; the report was submitted in January 1980. This test program was done under Project 3145, Task 314526, at the Aero Propulsion Laboratory (APL). The authors, Messrs. James F. Holt and Jerome Pearson, wish to express their appreciation for the valuable assistance in running tests and setting up instrumentation, to Messrs. D. C. Rabe, J. L. Knight, and W. C. Bourne of APL, Flight Dynamics Lab personnel Messrs. Roger E. Thaller and David L. Banaszak; to the employees of Universal Energy Systems Messrs. R. Darrah, R. Clericus, G. Wolfe, and others for assistance in running tests and operating the facility. Acknowledgment also is due to Messrs. R. F. Cooper and R. L. Verga, and Dr. P. E. Stover of APL for their contributions toward making possible the MHD program. We also acknowledge the help of Dr. D. W. Swallow, formerly of Maxwell Laboratories, Inc., who helped set up the channel and diffuser installation and contributed advice on the test program.

Accession For	
NTIS GRA&I	<input checked="checked" type="checkbox"/>
DDC TAB	<input type="checkbox"/>
Unannounced	<input type="checkbox"/>
Justification	
By _____	
Distribution/	
Availability Codes	
Dist	Avail and/or special
A	

AFWAL-TR-80-2021

# TABLE OF CONTENTS

SECTION	PAGE
I INTRODUCTION	1
II TEST SETUP	3
1. MHD Test Setup	3
2. Vibration Test Setup and Procedure	6
III MHD CHANNEL RESISTANCE AND POWER TESTS	11
1. First Test Series, LWC 001/LWC 013	11
a. Channel Resistance Tests	11
b. Power Generation Tests	16
2. Second Test Series, LWC 014/LWC 051	19
3. Third Test Series, LWC 052/LWC 235, Power Tests	19
4. Voltage Spectral Analysis	24
IV VIBRATION TEST RESULTS	25
V DISSECTION OF MHD CHANNEL	31
VI CONCLUSIONS	33
APPENDIX, CHARACTERISTICS OF EXPERIMENTAL EQUIPMENT	37
REFERENCES	164

## LIST OF ILLUSTRATIONS

FIGURE	PAGE
1 Lightweight Channel/Diffuser System Installed at the APL MHD Facility	41
2 MHD Channel Load Circuit	42
3 Magnetic Field Distribution for 2.3 Tesla Center Field for the APL Magnet	43
4 Accelerometer Locations on MHD Channel	44
5 Block Diagram of Data Recording Package	45
6 Block Diagram of Data Analysis System	46
7 Circuit for Measuring Channel Resistance	47
8 MHD Channel Resistance Signals, LWC 001, 002, and 003	48
9 Lightweight Channel (LWC) after Several Power and Vibration Tests	49
10 LWC After 225 Test Runs	50
11 Voltage vs. Time, LWC 004 and 005	51
12 LWC 004 Voltage Profile, at 2.9 Sec	52
13 Voltage vs. Time, LWC 006 and 007	53
14 Voltage vs. Time, LWC 062 and 064	54
15 Voltage vs Time, LWC 069 and 076	55
16 LWC 211 Load Voltage	56
17 LWC 211 Load Current	57
18 LWC 211 Voltage Profile at 8.0 Sec	58
19 LWC 211 Combustor Wall Exit Water Temperature	59
20 LWC 211 Right Half Nozzle Exit Water Temperature	60
21 LWC 211 Electrode No. 1 Exit Water Temperature	61
22 LWC 211 Electrode 3 Exit Water Temperature	62
23 LWC 211 Electrode 9 Exit Water Temperature	63



## LIST OF ILLUSTRATIONS (Cont'd)

FIGURE	PAGE
24 LWC 211, Electrode 21 Exit Water Temperature	64
25 LWC 211, Electrode 27 Exit Water Temperature	65
26 LWC 211, Electrode 35 Exit Water Temperature	66
27 LWC 211, Electrode 50 Exit Water Temperature	67
28 LWC 211, Electrode 59 Exit Water Temperature	68
29 LWC 211, Electrode 70 Exit Water Temperature	69
30 Relative Differential Temperature Drop, $\Delta T/T_s$ vs. Electrode Number	70
31 LWC 205, Load Voltage	71
32 LWC 205, Load Current	72
33 LWC 205, Voltage Profile at 15.0 Sec	73
34 MHD Generator Output Voltage Linear Spectrum, 0-20 kHz	74
35 LWC 013, Vibration Amplitude at Beginning of Firing of Main Combustor, Channel One	75
36 LWC 013, Vibration Amplitude at End of Main Combustor Run, Channel One	76
37 LWC 013, Vibration Amplitude at Beginning Run, Channel Two	77
38 LWC 013, Vibration Amplitude at End of Run, Channel Two	78
39 LWC 013, Vibration Amplitude at Beginning of Run, Channel Three	79
40 LWC 013, Vibration Amplitude at End of Run, Channel Three	80
41 LWC 013, Vibration Amplitude at Beginning of Run, Channel Five	81
42 LWC 013, Vibration Amplitude at End of Run, Channel Five	82
43 LWC 013, Vibration Amplitude at Beginning of Run, Channel Six	83

## LIST OF ILLUSTRATIONS (Cont'd)

FIGURE	PAGE
44 LWC 013, Vibration Amplitude at End of Run, Channel Six	84
45 LWC 013, Vibration Amplitude at Beginning Run, Channel Seven	85
46 LWC 013 Vibration Amplitude at End of Run, Channel Seven	86
47 LWC 013, Vibration Amplitude at Beginning of Run, Channel Eight	87
48 LWC 013, Vibration Amplitude at End of Run, Channel Eight	88
49 LWC 013, Vibration Amplitude at Beginning of Run, Channel Nine	89
50 LWC 013, Vibration Amplitude at End of Run, Channel Nine	90
51 LWC 013, Vibration Amplitude at Beginning of Run, Channel Ten	91
52 LWC 013, Vibration Amplitude at End of Run, Channel Ten	92
53 LWC 013, Vibration Amplitude at Beginning of Run, Channel 11	93
54 LWC 013, Vibration Amplitude at End of Run, Channel 11	94
55 LWC 013, Vibration Amplitude at Beginning of Run, Channel 12	95
56 LWC 013, Vibration Amplitude at End of Run, Channel 12	96
57 LWC 013, Vibration Power Spectrun for Channel One	97
58 LWC 013, Vibration Power Spectrum for Channel Two	98
59 LWC 013, Vibration Power Spectrum for Channel Three	99
60 LWC 013, Vibration Power Spectrum for Channel Five	100
61. LWC 013, Vibration Power Spectrum for Channel Six	101

## LIST OF ILLUSTRATIONS (Cont'd)

FIGURE	PAGE
62 LWC 013, Vibration Power Spectrum for Channel Seven	102
63 LWC 013, Vibration Power Spectrum for Channel Eight	103
64 LWC 013, Vibration Power Spectrum for Channel Nine	104
65 LWC 013, Vibration Power Spectrum for Channel Ten	105
66 LWC 013, Vibration Power Spectrum for Channel Eleven	106
67 LWC 013, Vibration Power Spectrum for Channel Twelve	107
68 Accelerometer 3 PSD, 0-500 Hz, Run LWC 003	108
69 Channel Five PSD, 0-500 Hz, Run LWC 003	109
70 Channel Six PSD, 0-500 Hz, Run LWC 003	110
71 Channel Seven PSD, 0-500 Hz, Run LWC 003	111
72 Channel Eight PSD, 0-500 Hz, Run LWC 003	112
73 Channel Nine PSD, 0-500 Hz, Run LWC 003	113
74 A Channel Ten PSD, 0-500 Hz, Run LWC 003	114
75 Channel Eleven PSD, 0-500 Hz, Run LWC 003	115
76 Channel Twelve PSD, 0-500 Hz, Run LWC 003	116
77 Channel One PSD, 0-500 Hz, Run LWC 013	117
78 Channel Three PSD, 0-500 Hz, Run LWC 013	118
79 Channel Five PSD, 0-500 Hz, Run LWC 013	119
80 Channel Six PSD, 0-500 Hz, Run LWC 013	120
81 Channel Seven PSD, 0-500 Hz, Run LWC 013	121
82 Channel Eight PSD, 0-500 Hz, Run LWC 013	122
83 Channel Nine PSD, 0-500 Hz, Run LWC 013	123
84 Channel Ten PSD, 0-500 Hz, Run LWC 013	124
85 Channel 11 PSD, 0-500 Hz, Run LWC 013	125
86 Channel 12 PSD, 0-500 Hz, Run LWC 013	126

## LIST OF ILLUSTRATIONS (Cont'd)

FIGURE	PAGE
87 Channel One PSD, 0-500 Hz, Run LWC 023	127
88 Channel Three PSD, 0-500 Hz, Run LWC 023	128
89 Channel Four PSD, 0-500 Hz, Run LWC 023	129
90 Channel Five PSD, 0-500 Hz, Run LWC 023	130
91 Channel Six PSD, 0-500 Hz, Run LWC 023	131
92 Channel Seven, PSD, 0-500 Hz, Run LWC 023	132
93 Channel Nine PSD, 0-500 Hz, Run LWC 023	133
94 Channel Ten PSD, 0-500 Hz, Run LWC 023	134
95 Channel Twelve PSD, 0-500 Hz, Run LWC 023	135
96 Channel x PSD, 0-500 Hz, Run LWC 023	136
97 Channel y PSD, 0-500 Hz, Run LWC 023	137
98 Channel z PSD, 0-500 Hz, Run LWC 023	138
99 PSD for Channels $(1+3)/2$ , 0-500 Hz, Run LWC 013	139
100 PSD for Channels 1-3, 0-500 Hz, Run LWC 013	140
101 PSD for Channels $(5+7)/2$ , 0-500 Hz, Run LWC 013	141
102 PSD for Channels 5-7, 0-500 Hz, Run LWC 013	142
103 PSD for Channels $(6+8)/2$ , 0-500 Hz, Run LWC 013	143
104 PSD for Channels 6-8, 0-500 Hz, Run LWC 013	144
105 PSD for Channels $(9+11)/2$ , 0-500 Hz, Run LWC 013	145
106 PSD for Channels 9-11, 0-500 Hz, Run LWC 013	146
107 PSD for Channels $(10+12)/2$ , 0-500 Hz, Run LWC 013	147
108 PSD for Channels 10-12, 0-500 Hz, Run LWC 013	148
109 Beam Approximation to MHD Channel Modes	149
110 How the Lightweight Channel Was Cut Apart After Tests	150
111 Typical Cross Section of Electrode Wall	151

## LIST OF ILLUSTRATIONS (Concluded)

FIGURE	PAGE
112 Some Anode Wall Electrodes Near the Upstream End of the Channel	152
113 Cathode Wall Electrodes Near Middle of Channel	153
114 Channel Sidewall	153
115 Main Load Resistor Schematic	154
116 Main Load Resistor Circuit and Leakage Through Water Paths When Main Load = 10.86 Ohms; Equivalent Circuit	155
117 V/I for Current Leakage in Water Around Main Load Resistor to Ground	156
118 Ballast Resistors for LW MHD Channel	157
119 Top View, Schematic of MHD Channel and Diffuser Water Supply and Return	158
120 Cooling Water Connections for the Diffuser	159
121 MHD Channel Electrode Water Circuit Schematic	160-161
122 Fuel Flow Rate vs. Fuel Line Pressure Drop	162
123 Seed Flow vs. Seeder Dial Setting	163

LIST OF TABLES

TABLE	PAGE
I Summation of Tests	2
II Nominal Operating Characteristics	5
III Data Recorded During MHD Channel Tests	9
IV Test Sequence and Results	12-14
V Calculated MHD Channel RMS Displacement	29
VI Channel and Diffuser Water Data	38
VII Dimensional Comparisons of AFAPL Channel and Diffusers	40

SECTION I  
INTRODUCTION

A diagonal conducting wall MHD channel with fiberglass external wall was developed with the goal of light weight, to deliver 200 kW for a series of tests including three 20 sec runs spaced in time by 20 seconds each (Reference 1). The channel and lightweight diffusers were built and delivered by Maxwell Laboratories, Inc., under contract F33615-76-C-2001. This report describes the main results of tests conducted by AFAPL in evaluating the channel and its design. The purpose of the tests was to establish a minimum operational life rather than to test constancy of operation.

Table I summarizes test results which are explained in some detail in the following sections.

A description of vibration test results is placed in a separate section of the report.

The channel and diffuser performance design goals were met, and the channel and diffuser after 235 tests of 32 minutes total were still in good operating condition. Vibration measurements over the first few dozen runs indicate that the channel did not suffer any mechanical fatigue.

Vibration measurements were conducted by Flight Dynamics Lab (FDL) for the purpose of determining the level of vibrational power density at failure were the structure to fail, or for determining a tolerable operating level of vibration intensity in the more fortunate case, which was encountered, wherein the channel stayed intact. We did not attempt to increase the vibration artificially for the purpose of life testing. The system was not specially shock mounted or treated in any special way to reduce vibration.

Dissecting the channel after the complete test series showed no evidence of interelectrode arcing.

TABLE I  
SUMMATION OF TESTS

Total number of tests 235.  
Duration of tests, approximately 5 to 60 sec.  
Total channel run time, 32 minutes.  
Maximum DC power generated, 240 kW.  
Maximum vibrational channel wall acceleration, 70 g.  
Typical channel spectral vibration energy density,  $10^{-2} \text{ g}^2/\text{Hz}$ .  
Initial end-to-end channel cold resistance, over 150k ohms.  
Final end-to-end channel cold resistance, 100k ohms.  
Initial end-to-end channel hot resistance, 1700 ohms.  
Final end-to-end channel hot resistance, 80 ohms.



## SECTION II

### TEST SETUP

#### 1. MHD TEST SETUP

The channel design goals were 200 kW electrical power, and at least three successive tests of 20 sec separated by periods of 20 sec resting time, at that power level.

Figure 1 shows the installation. Water cooling circuits for individual electrodes of the diagonal conducting wall MHD channel are shown in the appendix. The rate of water flow to the channel was 20% less than the amount specified by Maxwell for the tests. For that reason the first tests were limited to 5 seconds' duration or less; the risk of overheating the electrodes was thought to be too great to run tests of longer duration.

The MHD channel was cooled with deionized water. The diffuser was cooled with tap water. The combustor and nozzle were cooled with treated water. Leakage resistance to ground, from the treated water-cooled load bank, was in the neighborhood of 200 to 300 ohms. See the appendix. Since the MHD channel load resistance was in the neighborhood of 6 to 10 ohms for maximum power, possibly 5% of the load power was hidden in water leakage paths of load bank and diffusers. Numbers for total delivered power, quoted for the tests, do not add this hidden power. The load bank leakage circuit resistance appeared to be linear up to 40 volts; beyond that voltage there is no linearity data. The voltage on the load bank for maximum power tests was typically 1300 volts.

In the first few power tests, a previous seeder calibration curve was followed; by pre-weighing the quantity of cesium carbonate seed powder placed in the seeder hopper, and timing the run-out of seed from observed voltage data during power tests, the seed for these first tests was found to be going through the seeder unusually fast. Seed rates were ultimately based on the observed seed run-out rate data.

In the first power test series, runs LWC 004 through 013, the seed was sieved through 20 and 40 mesh screens. This produced an exceptionally uniform seed that flowed unusually fast through the seeder. In the later tests, very fine seed was mixed into the double screened material so that the mixture resembled the seed used in the original calibration curve. Run-out measurements showed that the seed of the later tests did follow the original calibration curve fairly well. The very fine seed was approx. 0.001 inch in diameter.

Fuel jets for the combustor were 8 stainless steel tubes of approximately 0.040 inch i.d. A filter in the fuel supply line dropped the fuel pressure considerably. The fuel flow rate measured with a rotary flow meter for toluene vs. pressure drop between fuel tank and combustor is shown in the appendix. This data taken before the start of power testing, by using a flame tube substituted for the MHD channel, was found to be different after approximately 100 power tests with the channel. The preset pressure on the fuel tank had to be increased to give the proper flow rate for the later tests. The cause of the change was not ascertained. A description of the MHD test facility and general operating conditions are given in AFAPL-TR-74-99 (Reference 2).

Nominal operating conditions for the MHD channel tests are given in Table II. The MHD channel load circuit and magnetic field profile are shown schematically in Figures 2 and 3. The load resistor consisted of a bank of stainless steel tubes with bypass switches arranged so that the load value could be changed over a range of approximately 4 to 32 ohms. See the appendix for the resistor schematic. The ballast resistors were chosen according to proportional scaling of axial position of electrodes, from the ballast resistor distribution used in diagonal conducting wall channel tests from previous research (Reference 2).

The channel inlet transition piece was grounded to the frame of the facility at the combustor end; the downstream or diffuser end was the high voltage positive end, and the diffuser, also at that voltage, was insulated from ground and was spaced so that its outlet was approximately

TABLE II  
NOMINAL OPERATING CONDITIONS

Channel

Inlet, 2.5 X 10.0 cm (1 X 4 in)

Outlet, 7.3 X 14.0 cm (3 X 5.5 in)

Length, 106 cm (41 5/8 in)

Number of electrodes, 70

Electrode thickness, 0.635 cm (0.25 in)

Coolant, deionized water, 113 gpm at 102 psig

Diffuser

Length, 96.5 cm (38 in)

Coolant, untreated water, 111 gpm at 35 psig

Combustor

Fuel, toluene, flow rate 0.15 kg/sec

Oxidizer, gaseous oxygen, flow rate 0.6 kg/sec

Seed, cesium carbonate, flow rate 30 to 50 grams/sec

Burn time, 5 to 60 sec

Pressure, 130 psig

Flow

M 2 inlet to channel

Static pressure inlet to channel, 1 atm

Load Resistance 6 to 10 ohms

18 inches from the exhaust stack. The exhaust of the diffuser traveled through open space for this distance and was water quenched in the exhaust stack.

Usually the thermocouple and accelerometer leads were disconnected from their amplifier channels during power generation tests, although some later temperatures were taken with the magnet on.

The timing of pilot flame, fuel, oxygen, and seeder was set so that the pilot flame came on about 2 sec before the main combustor flame came on; oxygen was turned on just before the fuel; after somewhat less than 1 sec of main combustor flame the seeder was turned on. The seeder was turned off about 1 sec before the main combustor flame came on. The MHD magnet was operated continuously; typically it was started about 30 to 60 sec before firing the combustor.

## 2. VIBRATION TEST SETUP AND PROCEDURE

The channel is constructed of a series of hollow copper coolant tubes which serve as electrodes, separated by ceramic insulation and covered by a layer of 2 cm (3/4 in) thick fiberglass. The coolant tubes are connected externally by plastic tubing to complete the water flow system. The inside dimensions of the channel vary from 2.5 x 10 cm (1 x 4 in) at the rocket exhaust inlet to 7.3 x 3.6 cm (2 7/8 x 5 3/8 in) at the diffuser; the channel length is 106 cm (41 5/8 in). The channel has end flanges bolted to the nozzle and to the exit diffuser. After the electrically conductive rocket exhaust has travelled the length of the MHD channel, it is slowed in the diffuser and exhausted to the atmosphere. The Channel is clamped at the flanges to vertical beams mounted on the false floor of the test stand. The 96.5-cm long diffuser is likewise supported by a beam 180 cm from the exit flange of the MHD channel. During power generation the large magnet faces are rolled into position close around the channel.

Accelerometers were chosen to measure the channel dynamic responses because of their simplicity and accuracy. The severity of vibration can

be inferred from channel acceleration, and the vibratory displacements can be derived from twice integrating the accelerometer outputs. Strain gages could be used to provide a direct readout of vibratory strain, but would prove very difficult to mount and calibrate on the irregular fiberglass channel.

The MHD channel wall accelerations were sensed by the 12 Columbia Research Laboratories Model 902H accelerometers numbered as shown in Figure 4. Odd numbered accelerometers were used to determine the channel transverse vibration in the horizontal plane and, by using the differences in response between 1 and 3, 5 and 7, and 9 and 11, to determine the horizontal breathing modes of the walls. Similarly, the even numbered accelerometers were used to determine the MHD channel transverse and breathing vibrations in the vertical plane.

After MHD run number LWC 13, three of the 902H accelerometers were moved to a mounting block on the combustor flange. These accelerometers, labelled x, y, and z in Figure 4, were used to measure the longitudinal, transverse, and vertical accelerations, respectively, of the combustor flange.

The accelerometer outputs were conditioned by Intech Model A2318 automatic-gain-controlled amplifiers and recorded in a portable instrument package by a Leach Model 3200A FM tape recorder. A datametrics Type SP105 time-code generator provided a 1000-Hz, amplitude-modulated, IRIG G time code which was recorded on the tape. A voice signal was also recorded during each of the MHD runs. The instrument package was configured for 115 VAC power, which was available in the control room. A block diagram of the on-site vibration data acquisition system is shown in Figure 5.

MHD run number LWC 24 was the last record on which vibration data were collected. Between LWC 24 and LWC 68, a signal proportional to the voltage generated by the MHD channel was recorded on track 7 of the recorder. This signal was obtained from a voltage divider with

bandpass 0 to 2 kHz. At run number LWC 68, this network was electrically trimmed for a bandpass flat within 3% from zero to 10 kHz.

Accelerations were recorded on 16 MHD test runs during May-July of 1977, as listed in Table III. Each record was approximately 30 seconds long, so that the actual MHD firing time of 3-6 seconds could be recorded with certainty. The signal proportional to the MHD-generated voltage was recorded during 14 runs, as listed in Table III.

To properly record starting transients during the first 0.1 second, the amplifiers were locked into pre-calculated gain settings during the last 15 test runs. Between tests, the accelerometers remained on the channel and the instrument package remained in the MHD facility control room. During MHD electrical power testing, however, all the accelerometers were disconnected from the Intech amplifiers.

Magnetic tapes recorded during the tests were returned to the Flight Dynamics Laboratory for analysis and retention. A block diagram of the FDL analysis system is shown in Figure 6. The data were played back on a laboratory recorder meeting IRIG Standard No. 106-72 and converted to digital form. These digitized data were used for time histories with 24 microsecond resolution. Using the Fast Fourier Transform, power spectral densities of all accelerometer signals were computed from zero to 500 Hz with a resolution of 1.22 Hz and from zero to 10 kHz with a resolution of 6.79 Hz.

TABLE III  
DATA RECORDED DURING MHD CHANNEL TESTS

<u>Date 1977</u>	<u>MHD Run No.</u>	<u>MHD Firing Time (Sec)</u>	<u>Data Recorded</u>	<u>Comments</u>
May				
4	001	3.5 (est)	Accel No. 1-12	No. 4 bad
6	002	1.7 (est)	No. 1-12	No. 4 bad
6	003	3.5 (est)	No. 1-12	No. 4 bad
June				
10	012	4 (est)	No. 1-12	No. 4 bad
10	013	4.5 (est)	No. 1-12	No. 4 bad
July				
26	014	6.9	Accel's No. 1, 3-7, 9, 10, 12, x, y, z	
26	015	5.6	"	
27	016	3.2	"	
27	017	3.3	"	
27	018	5.6	"	
27	019	5.7	"	
27	020	5.8	"	
28	021	5.6	"	
28	022	5.6	"	
28	023	5.6	"	
28	024	5.6	"	
Sep	(SEP 19, 1977 ACCELEROMETERS REMOVED & WIRES DISCONNECTED)			
20	052	5.3	MHD Output Voltage	Recorder @ 30 ips
20	053	5.7	MHD Output Voltage	Recorder @ 30 ips

TABLE III (Concluded)

<u>Date 1977</u>	<u>MHD Run No.</u>	<u>MHD Firing Time (Sec)</u>	<u>Data Recorded</u>	<u>Comments</u>
20	054	5.3	MHD Output Voltage	Recorder @ 30 ips
20	055	4.8	MHD Output Voltage	Recorder @ 30 ips
20	056	5.6	MHD Output Voltage	Recorder @ 30 ips
20	057	5.7	MHD Output Voltage	Recorder @ 30 ips
20	058	6.4	MHD Output Voltage	Recorder @ 30 ips
29	068	4.5	MHD Output Voltage	Recorder @ 60 ips
29	069	5.7	MHD Output Voltage	Recorder @ 60 ips
29	070	5.0	MHD Output Voltage	Recorder @ 60 ips
29	074	4.5	MHD Output Voltage	Recorder @ 60 ips
29	075	5.3	MHD Output Voltage	Recorder @ 60 ips
29	076	5.8	MHD Output Voltage	Recorder @ 60 ips
29	077	5.8	MHD Output Voltage	Recorder @ 60 ips



### SECTION III

#### MHD CHANNEL RESISTANCE AND POWER TESTS

##### 1. FIRST TEST SERIES, LWC 001/LWC 013

###### a. Channel Resistance Tests

Tests were consecutively numbered LWC xxx with x representing the numerical digits. Table IV gives a synopsis of the entire test run program. A current source applied through a sensing resistor in series with the longitudinal leakage resistance path of the MHD channel served in the first series of tests to determine the channel leakage resistance during flame. This approach was the same as that used in previous work (Reference 3). Cold end-to-end resistance of the channel by ohmmeter was approximately 100,000 ohms or greater.

Photographs of the voltage across the MHD channel and across the sensing resistance allow determination of the longitudinal leakage resistance. Figure 7 shows the schematic of the leakage resistance measuring circuit, while Figure 8 shows signals recorded during application of the flame without seed or magnet. The magnet during these resistance tests must be rolled away from the vicinity of the channel so that the residual magnetic field does not impart induced emf in channel that will hide the low value of voltage drop when the approximately 40 volts source of current is used. If much less applied voltage is used, as in an ohmmeter, the MHD induced voltage accompanied by the earth's magnetic field will cause interference with the resistance measurements.

Since the diffuser was cooled with tap water, leakage of current through the water circuit of the diffuser to ground had to be accounted for. Measurement showed the resistance to ground through the water path of the diffuser was 1070 ohms with the water temperature around 60°F. The value would be expected to vary depending on the conductivity of the water, deposit of impurities on the water hoses, and water temperature.

TABLE IV  
TEST SEQUENCE AND RESULTS

Run No. LWC-	Test Objective(s)	Run Time Sec	DC Power kW	Channel Res. Ohms	Remarks
001	Vibration; Resistance	2.5		>1170	propellant rate = 0.48 kg/sec; no digital data
002	Vibration; Resistance	2.0		>1600	full propellant rate 0.6 kg/sec
003	Vibration; Resistance	5.0		>1660	
004	Power	5.1	70		Reduced B-field, 400 amps, 1.66T
005	Power	5.0	118		Load res. shorted at 3.0 sec; full B field, 2.3T
006	Power	4.3	118		Load res. shorted at 1.0 sec; full B-field, 2.3T
007	Power	4.3	92		1.66T B-field strength
008	Power	3.6	94		No data - instrumentation trouble
009	Power	4.3	70		1.66T
010	Power	0.9			1.66T run incomplete
011	Power	3.7	65		1.66T
012-024	Vibration; Resistance	5.6		~180	resistance value corrected for wiring error
025-038	Power	5.6	200		corrected data; full B-value 2.3T from here on
Special cold channel resistance test. With 500V applied, end-end resistance = 90K ohms.					
039-043	Resistance	5.6		87	data corrected for wiring error

TABLE IV (CONTINUED)

Run No. LWC	Test Objective(s)	Run Time Sec	DC Power kW	Channel Res. Ohms	Remarks
044-051	Power; vary O/F ratio	5.6	-200		10.86 $\Omega$ load. Max. power at about O/F = 2.5. Corrected power data
052-062	Power	5.6	192		10.86 $\Omega$ load
063-077	Power, vary $R_L$	5.6			4.26 to 15.74 $\Omega$ load
078-085	Resistance	5.6			
086-099	Power, vary $R_L$	5.6			4.26 to 12.63 $\Omega$ load
100-105	Power	5.6	218 to 236		8.46 $\Omega$ load
106-110	Power, varied seed	5.6			8.46 $\Omega$ load
111-116	Power; vary B-field	5.6			8.46 $\Omega$ load
117-121	Resistance	5.6			
122	Power	5.6			8.46 $\Omega$ load
123-127	Resistance	5.6			
128-139	Power	5.6	202		8.46 $\Omega$ load
140-150	Resistance	5.6		70	
151-157	Power	5.6			8.46 $\Omega$ load
158-169	Resistance	5.6			
170-171	Power	5.6			8.46 $\Omega$ load
172-193	Extended duration, power	12.2 to 42	196-220		
194	Extended duration, resistance	40			instrumentation trouble
195	Extended duration, power	10.3			8.46 $\Omega$ load
196-200	Extended duration, power, variable load	5.8 to 45	222		15.74 to 4.26 $\Omega$ loads
201-202	Power, vary magnet current	40.6			

TABLE IV (CONCLUDED)

Run No. LWC	Test Objective(s)	Run Time Sec	DC Power kW	Channel Res. Ohms	Remarks
203	Extended Duration, resistance	60.9			instrumentation trouble
204-217	Power	5.6-5.8	217-247		2.5 to 12.63 $\Omega$ load
218-223	Power, variable load	5.6-5.8	216		2.5 to 12.63 $\Omega$ load
224-227	Extended duration, resistance	10 to 19.8 sec		65-89	

In the third run with the lightweight channel the longitudinal resistance from the oscilloscope, is  $1660 \pm 200$  ohms. However, this value, measured with flame in the channel, shows that the original insulation resistance of the channel is sufficient to make the leakage insignificant compared to the normal 10 ohm MHD power load resistance circuit.

It was decided on the first flame run with the channel (no magnet), that since the cooling water flow rate specification for the channel was only 80% of the designed rate, the propellant rate would be reduced, in an effort to cut down the heat transfer rate to the walls of the channel. If the channel stood this initial heat flux the following runs would be done at an increased propellant rate. After the first run, which lasted for about three seconds, observation of the channel interior showed a discolored strip and eroded spot on the electrode wall about two thirds downstream of the channel inlet. The strip was perpendicular to the axis of flow on all four walls; one electrode wall had erosion and more discoloration than the other parts, and was also dished out about 1/16 inch deep and about 1 inch diameter. The electrode wall had apparently been covered about that depth in some areas with alumina in the final smoothing out of the channel and this spot was the first instance of major flaking of the alumina. Although the presence of the alumina covering the electrodes may have not been intended in the design, it was apparently applied by the technician finishing the interior of the channel. In later tests more of this alumina coating came off the electrode walls; on the side walls there appeared to be no alumina coating; there the individual electrode screens could be seen. We filled the particularly rough spot with castable alumina, cured it overnight with a heat lamp, and, upon successive firings of the channel, observed that the patch appeared to adhere rather well.

The excess alumina coating inside the channel seemed to flake off considerably after the first run, for there were apparently abundant flakes of alumina inside the channel after the run. It seemed that the initial thermal shock of heating and quick cooling loosened the coating.

Successive firings of the channel quickly caused the electrode walls to be unusually rough, mostly resulting from removal of the surplus alumina coating plus unevenness in electrode placement. This roughness, developing quickly in the early tests, did not seem to worsen much in the remaining tests. Early photographs of the channel interior after a few tests (Figure 9) and of the interior after over about 100 tests (Figure 10) show little difference in its appearance, although in the earlier picture some cast magnesia flakes remain stuck to the electrode walls.

After the first test we thought there may have been a transverse shock at the location of discoloration in the channel, about two thirds of the way downstream. Calculation of the location of the hypothetical shock was not accurate enough to be convincing. Pressure data on the first run were not valid, unfortunately. However, since it appeared that the channel was being overheated at that location, and investigation showed that the water-cooling circuit was not at fault, it was decided to run succeeding tests with full 0.6 kg/sec propellant rate. Since in the following tests the channel functioned well with full propellant flow rate, we concluded that there was probably a "standing" shock in the first run.

#### b. Power Generation Tests

The first power run LWC 004 (Figure 11) was conducted with 1.66 Tesla magnetic field strength instead of the full 2.3 Tesla, in order to guard against inadvertent short circuiting in the channel or overloading of the circuit that might happen when a new test series is started. Seed was started at the beginning of the flame and was stopped after three seconds. During the firing there are noise pulses visible on the signal spaced at slightly less than 1/2 second apart; these should be disregarded. In following oscilloscope traces similar noise pulses may be seen; if they are regular in time, they have been introduced from the data system and should be disregarded.

The most apparent characteristic of the voltage signal of LWC 004 is the gradual buildup of voltage. From previous observations of the seeder gear acceleration, it was apparent that the voltage buildup is very similar in rise time to that of the seeder rpm during the first second or two of voltage. The seed rate was shown to be about 10% by weight of propellant, so that the seed should have been plentiful to produce maximum electrical conductivity in the flame. However, since the seed had been sifted between 20 and 40 mesh screens, so that there was not any very fine material, it was surmised that the coarse character of the seed, which had not been tried in previous power tests with other channels, prevented sufficient evaporation of seed in the combustor. The flame may have been under-seeded, as a result of insufficient seed evaporation. Considering the one half to one second rise time of the seeder motor speed we conclude that the gradual rise of voltage seems reasonable, and had there been adequate seeding from using finer seed material, it seems the voltage would have risen to a higher level. In previous power tests with other MHD channels this gradual rise of voltage was not observed. Perhaps when finer seed is used, enough of the extra fine material feeds around the seeder gear so that the rise time of voltage is much faster than the rise time of the seeder speed. Even when fine seed is used, after the initial sharp rise of voltage to near maximum there is a more gradual buildup to maximum.

In run LWC 004 (Figure 11a) the DC power into the load resistor was 60 kW; an assumption of an additional 15% dissipated in the ballast resistors gives total delivered power of 80 kW DC. Scaling power proportional to the square of applied magnet field strength gives 150 kW at 2.3 Tesla. If one extrapolates the DC power to a steady-state plateau as indicated by the shape of the voltage output, scaling yields considerably more than 200 kW DC power as the ultimate potential total output for 2.3 Tesla.

In the same run LWC 004, the profile of the electrode voltage is an approximately linear rise with distance along the MHD channel (Figure 12).

The successful test at 80% of full magnetic field strength indicated that the test at full magnetic strength should go well; apparently there were no glaring oversights or faults in the load circuit or instrumentation. Figure 11b shows the oscilloscope trace for the second power test with 2.3 Tesla magnetic field strength, to be LWC 005. At about one second into power delivery the load resistor arced to ground from the high potential end of the resistor. There was then a sudden drop in voltage which lasted for about 2 seconds until seeding stopped. The arc then extinguished, and some noisy voltage signal is seen during the last two seconds of the run. Inspection of the load resistor, which consisted of a bank of vertical water-cooled stainless steel tubes showed that the tubes had swayed during the run, probably from vibration or noise, and touched the grounded frame of the load bank, thus setting up the arc. This fault was repaired and the third power test was undertaken.

In the third power test, LWC 006 (Figure 13a) the load bank arced to ground from a different place as result of moisture released on the previous power test; although the moisture had been wiped off the insulators, there was sufficient moisture left to cause an arc to start along the surface of the insulator, and the oscilloscope trace of the voltage across the load resistor looked very much like that of the previous test. By extrapolating the voltage curve beyond the time of the start of the arc, as before, the expectable total delivered DC power level should have been well in excess of 200 kW, probably in the neighborhood of 230 kW. The arc on LWCH 006 started earlier and lasted for over 3 seconds.

Voltage profiles for LWC 005 and LWC 006 up until the time of the load arcing were similar to that of the first power test LWC 004 except that the maximum voltage was higher; a fairly linear voltage distribution was observed.

After repairing the load resistor bank no more difficulty with load resistor arcing was met, and succeeding tests proceeded well from that standpoint.



Power tests immediately following those of the load arcs were made with reduced magnetic field strength, as in LWC 004.

In LWC 007 (Figure 13b) the load resistor power reached a DC level of 80 kW, with an estimated total delivered power of 115 kW. Several tests were conducted with the same operating conditions, in which these results were repeated, as shown by LWC 011.

Observation of channel pressure profiles indicated supersonic flow throughout the channel. The cold end-to-end resistance of the channel continued to be on the order of a hundred thousand ohms or greater.

## 2. SECOND TEST SERIES, LWC 014/LWC 051

In this series of tests, measurement of the hot channel wall resistance, vibration measurements, and measurement of power output were performed. The data indicated an unusually low resistance between the inlet end of the channel and a point about one third of the distance from inlet to outlet, although initial inspection showed nothing wrong in the test setup. Eventually a misconnection was discovered in the patch board used to connect the channel electrodes to the load and instrumentation. After correcting this error the channel behaved well and voltage profile and other data appeared normal. During this series of tests valid and valuable vibration data was obtained, and some debugging of the system operation and equipment was carried out. The vibration data are discussed in a separate section.

## 3. THIRD TEST SERIES, LWC 052/LWC 235, POWER TESTS

The objectives were to maximize MHD power output, and to measure the end-to-end resistance of the hot MHD channel without seed application.

In this test series the power was maximized with respect to O/F (oxygen-to-fuel) ratio and with respect to load resistance, with fixed 0.6 kg/sec propellant rate. The maximum power vs O/F was obtained at  $O/F = 2.5$ . Keeping this O/F ratio, varying the load resistance, and

with a seed rate of 40 to 50 grams/sec cesium carbonate, maximum power was produced at 6 to 10 ohms.

In run LWC 062 (Figure 14a) calculation of DC load power from  $V^2/R$ , where V is the maximum DC load voltage on the high speed data system and R is load resistance, yielded 190 kW; calculation of DC load power from VI, where I is the measured maximum DC load current on the strip chart, yielded 168 kW.

In LWC 064 (Figure 14b)  $V^2/R$  was 179.5 kW while VI totaled 169 kW. Adding an additional 15% to the lower values for dissipation of power in the ballast resistors gives approximately 200 kW (196 kW) total power delivered. (Itemized calculation of power dissipated in the ballast resistors has shown that their total dissipation is 15% of the load power.)

Arcing between certain electrode pairs was suspected, since the apparent voltage difference was seen to be low, or opposite the desired polarity for power production. These electrode pairs were mostly in the downstream group of electrodes that attach to the ballast resistors. One electrode pair in the upstream ballast electrode group exhibited opposite polarity part of the time. However, examination of the voltage differences between these questioned electrode pairs, and also voltage differences between unquestionably properly working electrode pairs, showed no positive evidence of arcing anywhere. This result correlates with the observation of "no visible evidence of arcing" after the channel was dissected. Although the average or DC level of voltage seemed abnormal for the suspected electrode pairs, a normal amount of fluctuation seemed to be present in the difference voltage. Unfortunately differential pickups were not used for measuring differential electrode voltages. The difference electrode voltage was determined by subtracting voltages that were picked up in single-ended circuits with the ground reference at the channel inlet potential. Since there was a  $10^{-4}$  sec time delay between consecutive data channels, the noise appearing on each channel introduces noise in the subtracted values. An estimate of the noise

expected when consecutive voltage channels are subtracted shows that the expected noise is significant. It was not possible to determine positively from the numerical data whether any arcing existed. From observing voltage profiles taken later, on a peg wall channel, it appears that the particular nonlinearities seen in the LWC voltage profiles were caused by non-optimum ballast resistance values, and by a few small mis-calibrations of the voltage pickup divider resistors.

The overall conclusion is that there was no arcing, and that the local undesired or opposite current flow was caused essentially by unsuitable values in magnetic field strength and/or ballast resistances at the channel ends or possibly by other faulty local phenomena. Since the magnetic field strength as well as plasma velocity is decreasing at the downstream end of the channel, the power production capability of the channel there is low or perhaps even negative per unit length of channel under certain conditions, and to properly match the ballast resistors to the generator at the downstream end may require some experimentation.

An advantage of using the finer seed, which was used in all tests after LWC 013, is that the hash or noise fluctuations on the load voltage are diminished by the finer seed. As in previous experience, the level of noise is dependent also on O/F ratio, although no effort was made to investigate this effect.

Figure 15a and b represents load voltage in typical runs during which the noise or hash level is about as low as ever obtained with the powdered seed, and in which the feeding of seed is fairly constant. In run LWC 076 although the average value of seeding appears to be constant there are voltage fluctuations of 1/10 to 1/8 second duration which appear to be caused from seeder fluctuations. The constancy of DC voltage in run LWC 069 shows that the seeder functioned perfectly. As in previous test programs, the technique of introducing powdered cesium carbonate was adequate but not dependable. There is typically a gradual rise of DC level after the first half second of load power. This rise

may be connected with the gradual seeder speed increase, and possibly with heating the MHD electrodes. Reference 5 discusses calculations of rise time for heating typical electrodes.

Run LWC 211 (Figures 16 through 29) was typical of the later, long duration runs; the seed stopped near the middle of the run at about 40 sec of main combustor running. Calculation of VI for the load power gives 200 kW in the main load resistance. Adding 15% for power dissipated in the ballast resistors gives a total of 230 kW delivered to the external load circuit during seeding.

Figure 18, also run LWC211, is a typical voltage profile plotted for 8.0 sec of computer run time, which is about 4 sec after start of combustion. The only jog in the central portion of the channel voltage is at around electrode 45, about two-thirds the channel length from the inlet. This jog occupies 2 electrode spaces, which is the distance between data contacts there. It could be caused by various deficiencies other than arcing; for example, serious offsetting of the electrode wall may contribute to it; bad electrical contact or miscalibration of signal channels may cause it. The unevenness in the curve at the end portions is systemic and is apparently caused by wrong adjustment of the values for the trimmer resistors to match the channel operating characteristics.

Some channel electrode water temperatures are shown in Figures 21 through 29. The 70 electrodes here are numbered consecutively starting at the entrance end of the channel. The length of the water path should affect the water temperature. Although electrode 1 has theoretically the greatest heat flux rate, its water temperature is less than 70 F at the end of the run. Electrode 50 shows a water temperature increase of 150 F with an actual water temperature of 200 F, close to boiling. As seen in the appendix, the water circuit for electrode 50 shows only two electrodes in the water circuit. Electrode 35 also shows a temperature rise of 130 F, giving a total water temperature of around 180 F. This electrode is in a circuit with three other electrodes. The last electrode, 70, has a water temperature near 200 F, and it is individually cooled.

There does not appear to be a correlation between water temperature and length of the water path through the associated electrodes, for a limited sampling consisting of about 5 water exits. In carrying out the long duration runs, the water was either chilled artificially, or the advantage of the outside air temperature was used to lower the water temperature below normal room temperature. Without this precaution, the water would have boiled after about 7 seconds of running the combustor. A plot of the relative differential water temperature drop  $\Delta T/T_s$ , where  $\Delta T$  is the temperature drop upon cutting out seed, and  $T_s$  is the temperature rise above water inlet temperature with seed applied, Figure 30, shows that the ratio increases with axial distance from the channel inlet. This means that the additional percent of total heat flux to the channel wall while seeding is less near the channel inlet. Since the ratio of wall roughness (electrode stepping) to channel height is greater near the channel inlet, the variation of  $\Delta T/T_s$  with distance seems plausible. The stepping offsets between electrodes would also be expected to introduce scatter in this data. An estimate of electrode surface wall temperature based on observed water temperature indicated that the original electrode ceramic was possibly being somewhat overheated, with a temperature around 2200 to 2300K, leading to some loss of ceramic material as was found when the channel was finally taken apart at the end of testing. (As the ceramic ablates or wears away, the ceramic surface temperature will decrease; eventually there will be an equilibrium surface temperature at which the ceramic will not readily ablate.) Since the electrode copper protects the insulator, one would not expect appreciable insulator spalling; in the dissected channel we found the insulators to be in good condition.

The combustor wall exit water temperature (Figure 19) and the nozzle water exit temperature (Figure 20) have a considerable amount of noise fluctuation; it is not related to MHD load current, since there is appreciable noise before the start of load current.

Figures 31 through 33 show data plots for run number LWC 205, an extended duration run which lasted for a minute. The seed was not

continuously flowing for the run duration. The two interruptions of load power in the latter half of the run are caused by seed temporarily sticking in the powder seeder hopper at the inlet to the seeding gear. Multiplying load voltage by load current (times 1.15, to account for ballast resistor power) gives 238 kW maximum at end of the run, and 218 kW DC power in the first half. The axial distance voltage profile closely matches the profile for run LWC 211 and others. The sharp drop in voltage at electrode 58 is seen also in a voltage profile for a peg-wall MHD channel operated with similar resistance values in a separate test program. Considering the observed test data and the resistance distribution, the sharp drop appears to be caused by using a ballast resistance series of overall too great a resistance scale in the downstream end region. To remove the drop and smooth the profile, experimentation is necessary. The voltage profile remained essentially consistent through all tests starting from the first power runs.

#### 4. VOLTAGE SPECTRAL ANALYSIS

A point of interest is the fluctuation of the electrical output from the MHD generator. During several runs the voltage output of the generator was sampled and analyzed by a spectral analyzer. A typical result is shown in Figure 34 on a linear scale from zero to 20 kHz in frequency and on a logarithmic scale in voltage output. The voltage output is broadband, with no significant energy at discrete frequencies. These data were recorded with a data channel frequency response that was flat from zero to 10 kHz.

## SECTION IV

### VIBRATION TEST RESULTS

Analog time histories of the accelerometer responses were first played back through an oscillograph to determine the character of the signals. Examples of these time histories are shown for run number LWC 13 in Figures 35-56. Accelerometer Number 4 responses were not obtained on this run because of electronic problems.

The typical MHD run is characterized by an abrupt, high-amplitude transient lasting about 0.02 second as the mainburner is turned on, followed by a steady-state firing period of several seconds, and climaxed by acutoff transient of about 0.05 second. In these time histories, most of the steady-state firing response is deleted in order to show the details of the starting and ending transients. The pilot burner was turned on before these records begin. For all the plots, the overall rms acceleration of the plotted portion is shown in the upper right-hand corner in g rms, summed over the frequency range of zero to 10 kHz. The time resolution of these computer-generated plots is 24 microseconds. During the starting and ending transients, instantaneous accelerations as high as 75 g were recorded. The acceleration peaks during steady-state firing were normally in the 15 g range. The rms values range from 2.5 to 10 g rms for the various accelerometers.

These time histories are random signals which are non-stationary, especially at the beginning and at the end. The steady-state portion of the firing, however, is nearly stationary and can be analyzed spectrally. All the spectra presented in this report represent the steady-state portion of the MHD firings. Examples of frequency spectra for the individual accelerometers are shown for run number LWC 13 in Figures 57-67 for the full frequency range of the instrumentation. The frequency resolution of these acceleration spectral densities is 6.787 Hz. Because the accelerometers have a flat frequency response to 6 kHz and the tape recorder is 3 dB down at 10 kHz, the decrease in response above 5 kHz is apparently a characteristic of the rocket exhaust excitation.

These acceleration responses were normally in the range of  $0.01 \text{ g}^2/\text{Hz}$  except for narrow peaks at 2-3 kHz which reach  $0.05 - 0.1 \text{ g}^2/\text{Hz}$ . The highest spectrum measured was accelerometer Number 11 for run LWC 13 (Figure 66). This accelerometer, on the side of the channel nearest the rocket nozzle, showed a peak of  $1 \text{ g}^2/\text{Hz}$  at a frequency of 4500 Hz. A measure of the overall energy in the response is the rms acceleration in g's, which is shown for each accelerometer in the upper right corner. The highest overall acceleration recorded was by accelerometer Number 11 during run Number LWC 13, 7.11 g rms summed over the frequency range of zero to 10 kHz.

To determine the effects of continued firings on the vibration responses, data were analyzed at selected runs over a long series of firings. The firing numbers and durations are shown in Table III. An expected change due to deterioration of the channel walls would be a change in the damping of the vibration modes. These modes may be identified with individual response peaks in the lower frequency range of the acceleration responses. By measuring any change in the widths of these response peaks over a series of runs, a change in damping of the mode would be observable. An increase in damping could be caused, for example, by the development of cracks in the material.

To show the lower frequency modes more clearly, accelerometer responses were analyzed from zero to 500 Hz. The results for run Number LWC 3 are shown in Figures 68-76, those for run number LWC 13 in Figures 77-86, and those for run Number LWC 23 in Figures 87-98. Accelerometers 1, 2, and 4 are missing from run LWC 3, and accelerometers 2 and 4 are missing from run LWC 13. For run LWC 23, accelerometers 2, 8, and 11 were replaced by accelerometers x, y, and z on the combustor flange.

These responses showed little indication of any change in damping with wear on the channel. Although the random character of the rocket exhaust excitation results in fluctuations in the relative amplitudes at different frequencies from run to run, distinct modes can be identified.



Accelerometer Number 3, for example, on the side of the channel near the diffuser end, showed a prominent mode at 53 Hz. The width of this mode during run LWC 3 (Figure 68) showed a Q of 18, from the relation  $Q = f/\Delta f$ , where  $\Delta f$  is the frequency bandwidth at the half-power points. This same response peak at 53 Hz during run LWC 13 (Figure 78) and during run LWC 23 (Figure 88) had the same bandwidth, to within the accuracy of the 1.22 Hz frequency resolution, indicating little or no change in damping for this mode over 20 firings. Similar results were obtained for the mode at 43 Hz. This method, however, is limited to detecting gross damping changes because of the 1.22 Hz frequency resolution. The resolution is limited by the amount of data available during one firing.

The responses from a single firing were also analyzed with respect to accelerometer position along the channel, to determine any change in character of the excitation along the channel length. No clear pattern of distinct differences was found, either in the overall rms accelerations or in the frequency content, between the diffuser end and the rocket end of the channel.

The responses from different firings show different overall amplitudes, which may be due to differences in the propellant flow rates and combustion temperatures. The rms responses of firing Numbers LWC 3 and LWC 23 can be compared directly. The rms responses for firing Number LWC 13 were not obtained.

The individual accelerometer frequency responses show several peaks which might be interpreted as overall vibration modes of the channel. To distinguish between bending and breathing modes, the accelerometer signals on opposite sides were combined by both adding and subtracting the signals. These responses are shown for run LWC 13 in Figures 99-108. The results showed no correlation between the motion of opposite sides of the channel. Apparently the modes of the structure were so highly damped by the visco-elastic fiberglass coating that the four sides moved independently.

The fatigue life of the MHD channel can be estimated as follows. The MHD channel is approximated as a beam with pinned ends of height  $h$  and length  $L$ , as shown in Figure 109. The transverse deflection of the wall vibrating in the  $n$ th mode is

$$y_n(x,t) = y_0 \sin\left(\frac{n\pi x}{L}\right) \sin \omega_n t \quad (1)$$

where  $y_0$  is the peak deflection. The moment  $M$  at any point is given by the relation  $M = EI \frac{d^2 y}{dx^2}$ , where  $E$  is Young's modulus of the material,  $I$  is the moment of inertia of the beam cross-section ( $I = bh^3/12$ ), and  $b$  and  $h$  are the width and height of the beam, respectively. The maximum stress occurs at the surface of the beam and is given by  $\sigma = Mh/2I$ .

From these relations we derive

$$\sigma_{rms} = y_{rms} \left(\frac{Eh}{2}\right) \left(\frac{n\pi}{L}\right)^2 \quad (2)$$

To find the actual displacements of the MHD channel walls from the accelerometer frequency responses, the latter were transformed by  $1/\omega^2$  and converted to rms displacement. These results of wall deflections for runs LWC 12 and LWC 13 are shown in Table V. These deflections can be used to estimate the stress levels and thus the expected fatigue life of the structure. The maximum deflections observed during these runs is seen to be 0.00431 meters rms for accelerometer 12.

To evaluate the rms stress produced by this response peak, refer to Figure 99, which is typical. This particular plot is an average of accelerometers 1 and 3, near one end of the beam. From this and the other figures the peak at 17.3 Hz appears to be the first mode, so the 53 Hz peak may be identified as the third mode,  $n = 3$ .

From the channel wall geometry,  $L$  is 1 meter,  $h$  is 0.6 cm, and we may assume  $E = 3$  to 5 million PSI ( $2.1-3.5 \times 10^{10}$  N/m<sup>2</sup>), from

TABLE V  
CALCULATED MHD CHANNEL RMS DISPLACEMENT

Run No.	Pickup No.	Displacement rms (m)
LWC 12	1	0.00459
	3	0.00263
	5	0.00352
	7	0.00334
	6	0.00123
	8	0.00392
	9	0.00407
	10	0.00123
	11	0.00404
	12	0.00431
LWC 13	1	0.00395
	3	0.00280
	5	0.00286
	7	0.00283
	6	0.00124
	8	0.00366
	9	0.00354
	10	0.00104
	11	0.00399
	12	0.00365

measurements on similar fiberglass. From AFFDL-TR-74-112, page 514, data are given for the  $\sigma$ -N curves (N cycles to failure at stress level  $\sigma$ ) for 181-S Type III glass fabric. Applying these values gives the following results:

<u><math>E, 10^{10} \text{ N/m}^2 (10^6 \text{ PSI})</math></u>	<u><math>\sigma, 10^7 \text{ N/m}^2 (10^3 \text{ PSI})</math></u>	<u>Lifetime</u>
2.07 (3.0)	2.4 (3.48)	105 hrs
2.76 (4.0)	3.2 (4.64)	7.9 hrs
3.45 (5.0)	4.0 (5.80)	31 min

These results show that the fatigue life is so strongly dependent on the value of E that no reliable prediction can be made. A more refined estimate could be obtained by directly measuring the modulus of the material in a laboratory force-deflection test, and then measuring the stress levels during firing with strain gages.

## SECTION V

### DISSECTION OF MHD CHANNEL

After the tests had been completed, the lightweight channel was taken apart to examine closely the amount of wear or damage to the electrodes and insulators. The channel was sawed lengthwise as indicated in Figure 110. Observation of the interior of the channel showed that there was substantial loss of insulator material between the electrodes, and greater loss of zirconia ceramic material from the cast portion of the electrode around the nichrome screen. See also Figure 111. Approximately half of the zirconia was gone from the electrode fillings. The insulators between electrodes were cupped below the electrode surfaces as much as 1/16 inch in several places. In one place, at the very entrance to the channel, the insulator was undercut to approximately 1/8 inch. The channel sidewalls were hardly worn away at all; it was not possible to detect any substantial difference between new and worn conditions of the sidewalls.

Figure 112 shows some anode wall electrodes (top of test rig), near the upstream end of the channel. Here the insulator and zirconia filling can be seen to be considerably worn away. Note that the electrode metal does not show any appreciable wear. There were no water leaks in the channel.

Figure 113 shows some cathode wall electrodes near the middle of the channel which also evidence some deterioration of the electrode insulators and zirconia fillings. In the middle of the figure there is one electrode that showed atypical deterioration. One side of the copper electrode material was badly consumed; the electrode screen can be seen apparently still in good condition, and apparently the other side of the electrode metal is in good condition. This electrode appears to be possibly not positioned right originally, with some alumina used to smooth out the difference in level between it and the adjoining electrodes. This particular electrode was the only one in the channel that was severely consumed, although it still did not leak water. Because of the type

of construction of the electrodes, the water passages were inherently well protected unless mechanical forces should cause rupture.

Figure 114 is a photograph of one of the sidewalls, both of which looked in like-new condition, after the tests. Here the screens can be seen as ridges with fine detail stripes across them. The black dark rows next to the screens are the slightly recessed zirconia fillings around the screens. Outside the dark rows, the copper edges of the side electrode frame structure can be discerned. Since the sides of the electrode frames were on a slant with respect to the channel axis, the side structure of the frames were narrower than the electrodes, causing the sidewall assembly to look crowded. In spite of this obvious handicap, of having narrow structures and spacings to work with, the sidewall assemblies had surprisingly good integrity after the tests. The nature of the electrode structure and the construction procedure of the electrodes apparently led naturally to considerably more difficulty in positioning the electrodes than sides. To achieve acceptably smooth walls there should be a machining process during or after channel assembly, which would machine out the offsets built into the hand assembly process.

The channel was in surprisingly good overall condition after the tests; the channel was obviously very well and carefully built. From the appearance of the channel interior, as well as from the test data, one would surmise that the channel could have run for many more minutes or perhaps hours without failure.

## SECTION VI

### CONCLUSIONS

A composite lightweight MHD channel and lightweight diffuser were tested for some 235 separate firings with a total time of 32 minutes, after which the channel and diffuser were still delivering full rated power of 200 kW<sub>e</sub>. Water temperature checks of the channel electrodes indicate that some of the electrodes were experiencing original local surface temperatures of about 2300 K. After the tests, the interior of the channel was intact and considerable erosion of the electrode ceramic fillings was observable, and moderate erosion of the alumina between the electrodes was visible. The sidewalls suffered no apparent impairment, and there were no water leaks.

Vibration measurements showed that the maximum accelerations on the channel were in the neighborhood of 70 g, during start up and stop. No breathing modes of vibration were detectable, and no structure fatigue could be detected.

After the test program the channel was dissected, and close inspection of the electrodes, including separating some individual electrodes, showed no evidence of interelectrode arcing or damage by seed. This result is due possibly to a careful regime of purging moist air from the channel and continued bleeding of dry nitrogen into the channel during off times.

The implications of this test program for future development and design of MHD equipment is that the composite approach for channel structure is viable, and that lightweight diffusers can also be developed using comparatively lightweight composite outer walls tied to the metal duct interior. Generally, larger high power channels for portable generators should be designed for about 250 to 500 MW/m<sup>3</sup>. Although the overall power density for this channel was in the neighborhood of 40 MW/m<sup>3</sup>, this program still provided the confidence that a significant lifetime could be reasonably expected when lightweight composite channels

and diffusers are built for portable power systems of the 10 to 50 MW magnitude of electrical power. In scaling the estimated weight of such high power channels, one should realize that the channel tested in this effort was built primarily for performance, and secondarily for light weight. As a result the weight is considerably greater than necessary; the size is large enough to contain a boundary layer of some 0.5 cm thick near the exit. A design study (Reference 8) has claimed that a 25 MW<sub>e</sub> channel-diffuser could be produced with a weight of 115 kg, not including coolant, with a channel maximum local power density of 250 MW/m<sup>3</sup>.

The interpretation of the "wall resistance" tests directly in terms of resistance of the channel walls may not be entirely correct according to the following discussion. As the signals show, the "wall resistance" increases in each test with time. This effect persists no matter how many prior runs have been made without seeding the plasma. It seems that after a few runs all the seed must have been removed from the seeder and associated plumbing, and the plasma is then unseeded; the resistance of the unseeded plasma should be of the order of 10<sup>4</sup> times the resistance of the cesium seeded plasma. Resistance of the seeded plasma from end to end of the channel is of the order of 10 ohms as evidenced by the apparent internal resistance of the generator when loaded. When the channel is run without seed and without magnetic field applied, the beginning resistance is typically a few tens of ohms, then the resistance gradually climbs to around 80 ohms after a few seconds. This behavior is that of a channel having previously a few dozen seeded runs; the new channel exhibited one or two thousand ohms without seed. The phenomenon of increasing resistance with time could be explained as follows.

Seed penetrates to considerable depth into the insulators when the channel is run a few dozen times with seed applied. Applying the unseeded flame bakes seed out of the insulator over a shallow depth; after flame shutdown seed from deeper in the insulator migrates to the surface region previously baked out. Re-application of unseeded flame repeats the phenomenon. The "wall leakage" conductance being measured may be partly comprised of conductance through the plasma boundary layer as a result



of seed bakeout. This still does not account for the fact that there is the same power delivered to the external load at the beginning and end of a run when seed is applied; seed baking out into the boundary layer should lead to a boundary layer leakage current because the velocity there does not support a significant induced emf. However, if the seed bakeout plasma conductance component is near the edge or slightly beyond the boundary layer momentum thickness, then perhaps this component could add to the generated voltage during seeding, at least enough to make up for any additional conductance leakage.

To understand the wall leakage conductance problems a special program of investigation is needed.

AFWAL-TR-80-2021

## APPENDIX

### CHARACTERISTICS OF EXPERIMENTAL EQUIPMENT

Some details of the system test setup are recorded here that will help to explain the procedure and interpretation of data.

Figure 115 is a schematic of the main load resistor bank. This resistor consists of 22 stainless steel water-cooled tubes connected at each end by hoses of approximately 1 foot length; each hose attaches to a grounded water manifold. By lumping the resistance to ground into two equivalent resistors, the MHD channel load circuit can be simplified to the equivalent circuit of Figure 116. A volt-ampere curve for conduction through the load resistor water is given in Figure 117. The equivalent circuit was developed from a consideration of synthesizing a parallel path equivalent to 138 ohms. Since the diffuser and downstream end of the channel is connected to ground only through water connections which are of comparatively high resistance, while the upstream of the channel is separated from ground only by one channel insulator and the intervening plasma, the leakage resistance of the water paths is approximated by the 320 ohm resistance. The 243 ohm water resistance is shunted by the much lower upstream channel resistance. Load circuit ballast resistors are given in Figure 118.

Table VI gives the channel and diffuser water supply flows. Figure 119 shows a top view of the layout of channel and the water manifolds, while Figure 120 is a schematic of the cooling water connections to the diffuser.

Cooling water connections for the various MHD channel electrodes are shown in Figure 121. The upstream (near the channel inlet) electrodes are afforded the shortest coolant paths, and the length of coolant path gradually is increased with distance downstream. This is the Maxwell arrangement of connections.

TABLE VI  
CHANNEL AND DIFFUSER WATER DATA

MHD Channel:

Deionized water for MHD channel. Supply pressure at channel manifolds, 102 psig. Exits of channel manifolds empty into tank about 5 feet above level of MHD channel; the tank at atmospheric pressure.

Exit end of channel, manifold flow = 46.5 gpm

Entrance end of channel, manifold flow = 66.5 gpm

Lightweight Diffuser:

Pressure at hard water supply, inlet to facility, 35 psig while running; 50 psig when not running.

Inboard return manifold flow = 37 gpm

Outboard return manifold flow = 60.3 gpm

---

The fuel flow rate was calibrated by collecting fuel over measured time, and also by observing a calibrated flow rate turbine meter. Figure 122 gives a curve for flow rate vs. pressure drop, as experienced in the beginning of the tests. This curve was ascertained from tests with a flame tube in place of the MHD channel. Later MHD tests showed that this curve was not being followed closely. The fuel flow rate was a few percent lower than predicted by this curve, and fuel pressure setting had to be thus adjusted. No reason for this change was found.

The oxygen flow rate was determined from observations of static pressure upstream of a choked venturi of 0.772 cm diameter. (Static pressure in this case was essentially the same as total pressure; thus, reliance on a total pressure pickup was not necessary, although there was measurement of the total pressure also.) Flow through the venturi is calculated by the equation,  $m = 0.185 P/T^{1/2}$ , where  $m$  is flow in kg/sec,

P is the upstream total pressure, and T is the absolute temperature. Discussion of the equation is given in Reference 7. The coefficient 0.185 was independently derived by APL, and by Systems Research Laboratories in earlier work.

In Figure 123 an early seed flow calibration is shown, along with two typical points obtained for seed flow during actual tests. It is seen that the calibration follows the early curve fairly well. However, the dotted curve was not relied upon for knowing the seed level; the seed rate was determined by weighing the seed amount before a series of tests, and averaging the flow rate over the time taken to run out of seed. The time was determined from observing the oscilloscope voltage vs. time. In the first series of tests, the seed flow rates were about 50% greater than those shown in the Figure 123 data, because the seed was specially sifted through 20 and 40 mesh screens, which permitted smoother flow than ordinary. In the later tests, seed containing 50% very fine material was used, for which the flow is well represented by the figure.

Table VII gives channel dimensions as compared to APL diagonal conducting wall and heat sink peg wall channels.

TABLE VII  
 DIMENSIONAL COMPARISONS OF APL CHANNELS AND DIFFUSERS  
 (All Dimensions Are in Millimeters)

	<u>Channel Entrance</u>		<u>Channel/Diffuser Interface</u>		<u>Diffuser Exit</u>		<u>Overall Length</u>	
	<u>Width</u>	<u>Height</u>	<u>Width</u>	<u>Height</u>	<u>Width</u>	<u>Height</u>	<u>Channel</u>	<u>Diffuser</u>
Heat Sink	24.9	99.8	72.6	140	72.6	200	857	965
Diagonal Conducting Wall	24.9	99.8	72.6	140	72.6	200	989	965
Lightweight	24.9	99.8	72.6	140	72.6	200	1054	965



Figure 1. Lightweight Channel/Diffuser System Installed at the  
APL MIP Facility

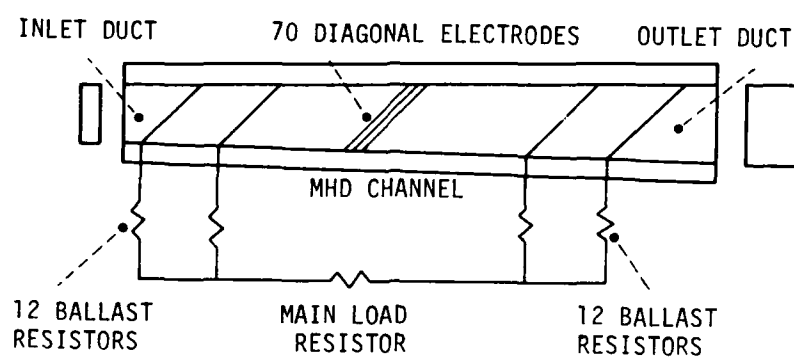


Figure 2. MHD Channel Load Circuit

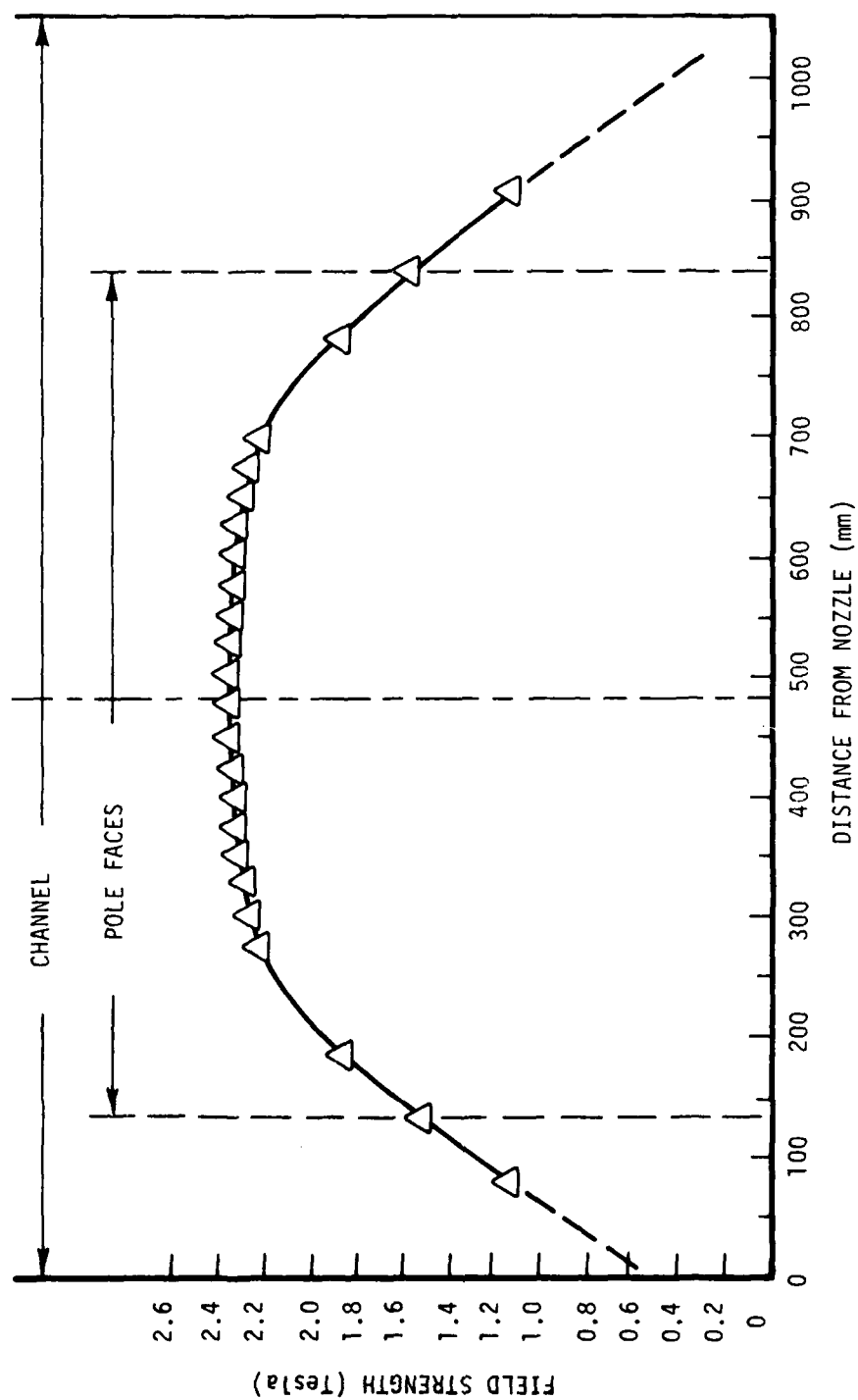


Figure 3. Magnetic Field Distribution for 2.3 Tesla Center Field for the APL Magnet



ACCEL NO.	X(in)	RECTRK	ACCEL NO.	X	RECTRK	ACCEL NO.	X	TRK
1	28 3/4	1	6	19 1/2	6	11	10 3/8	11
2	28 5/8	2	7	19 3/4	7	12	10 3/4	12
3	28 1/2	3	8	19 1/2	8	x	---	8
4	28 1/4	4	9	10 1/2	9	y	---	11
5	19 3/4	5	10	10 3/8	10	z	---	2

x - Distance from combustor end to center of accelerometer  
Columbia Model 902H Accelerometers

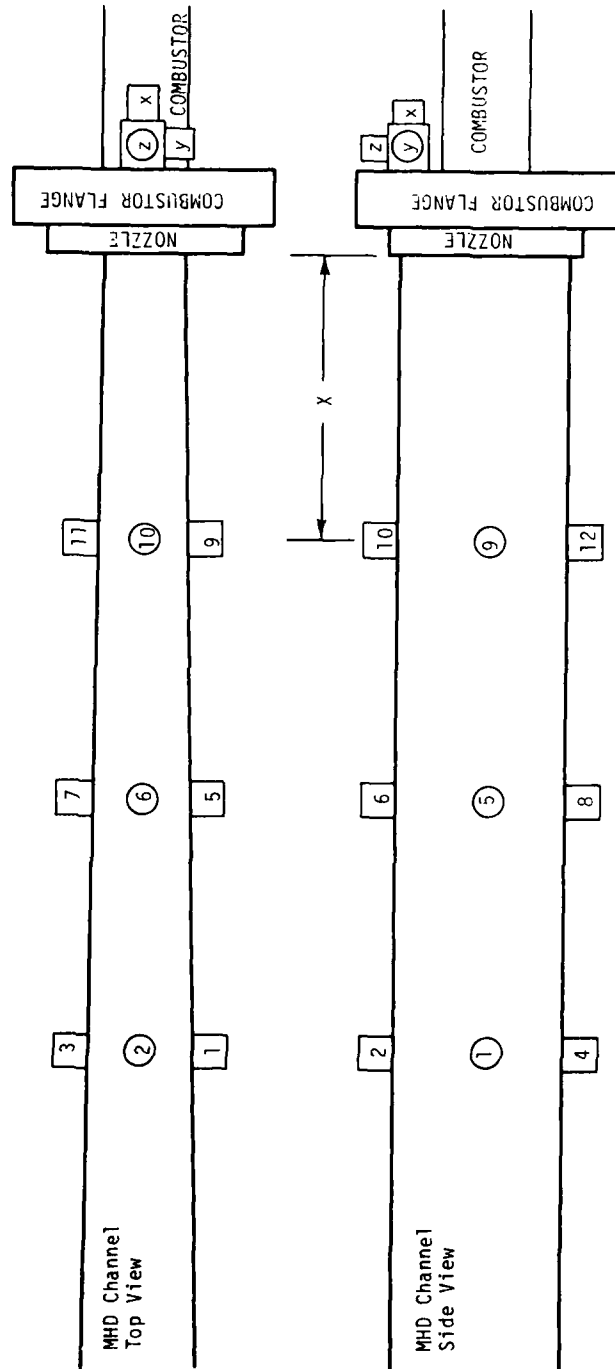


Figure 4. Accelerometer Locations on MHD Channel

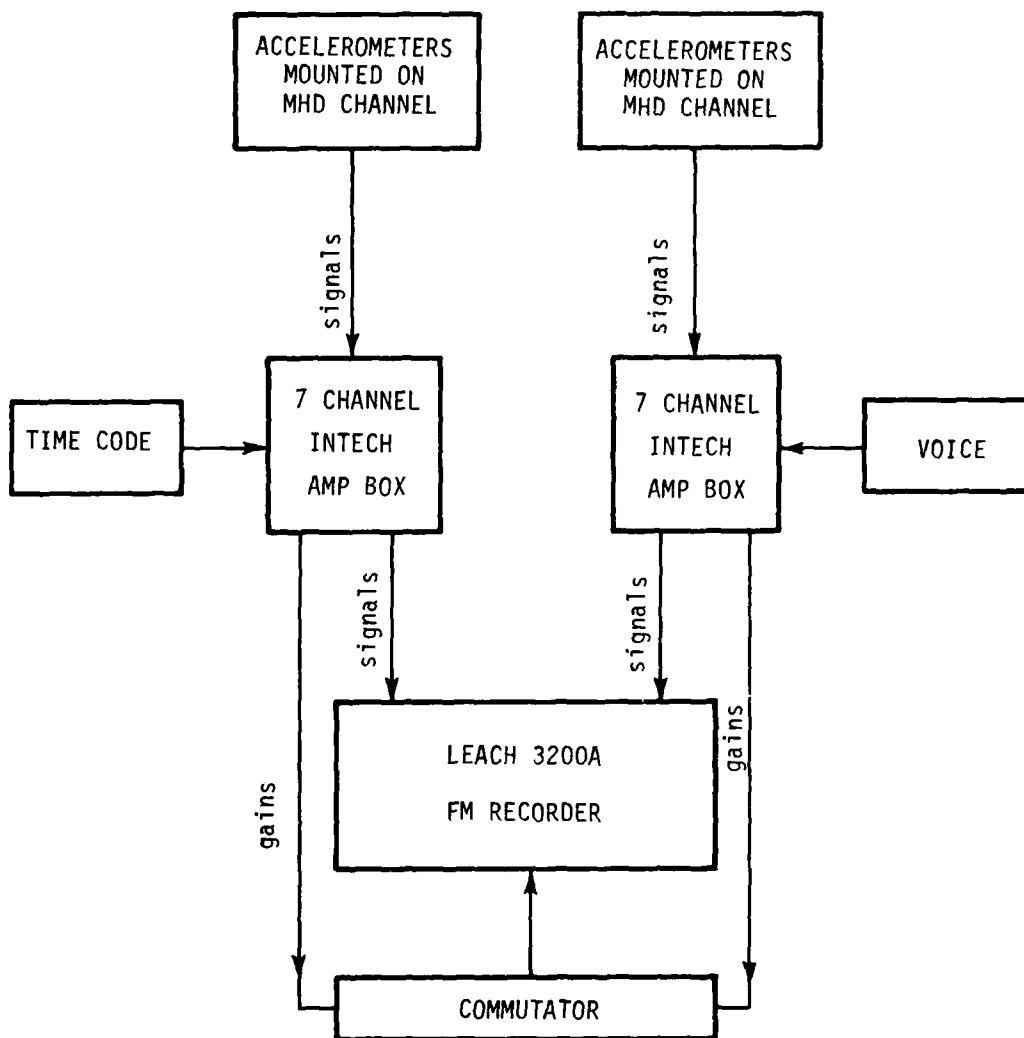


Figure 5. Block Diagram of Data Recording Package

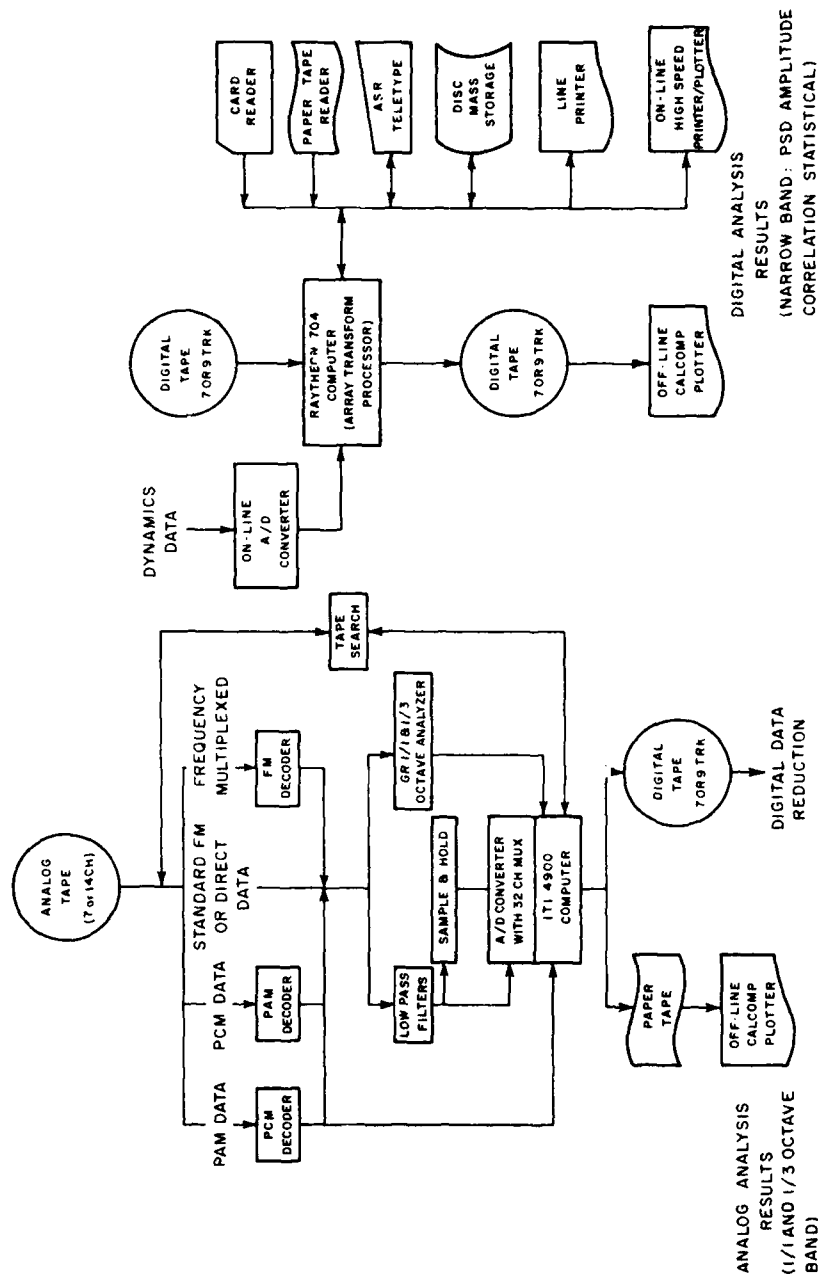
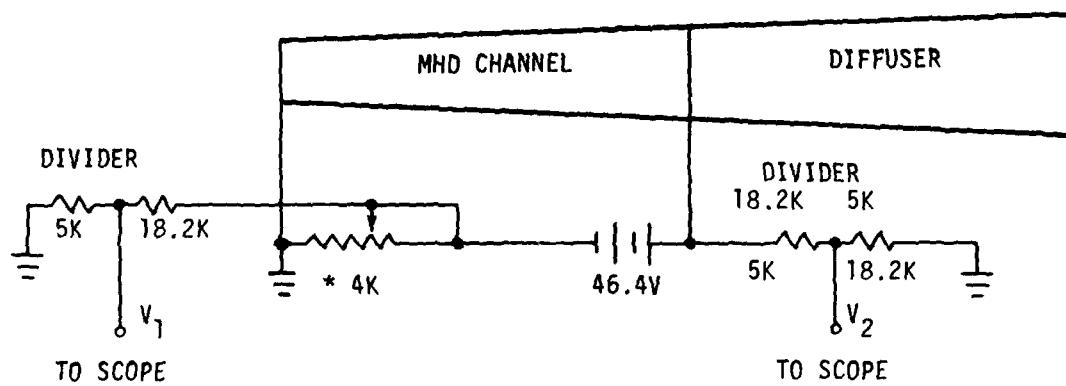


Figure 6. Block Diagram of Data Analysis System



\* Adjusted to give 4000 ohms to gnd, total incl divider.

Figure 7. Circuit for Measuring Channel Resistance

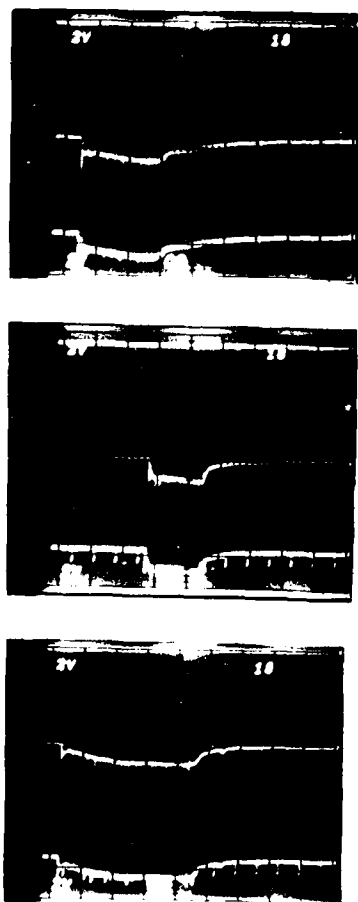


Figure 8. MHD Channel Resistance Signals, LWC 001, 002, and 003  
(Scale 2 V/div, 1 sec/div)



Figure 9. Lightweight Channel (LWC) After Several Power and Vibration Tests



Figure 10. LWC After 225 Test Runs

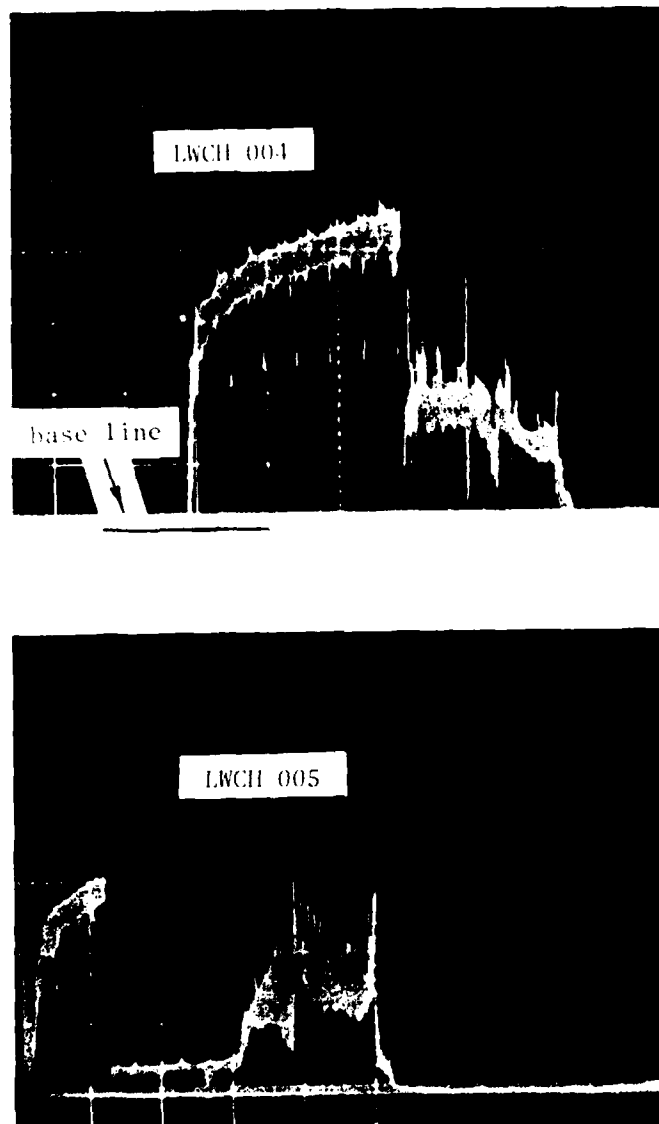


Figure 11. Voltage vs. Time, LWC 004 and 005  
(Vertical 400V/cm, horizontal 1 sec/cm)



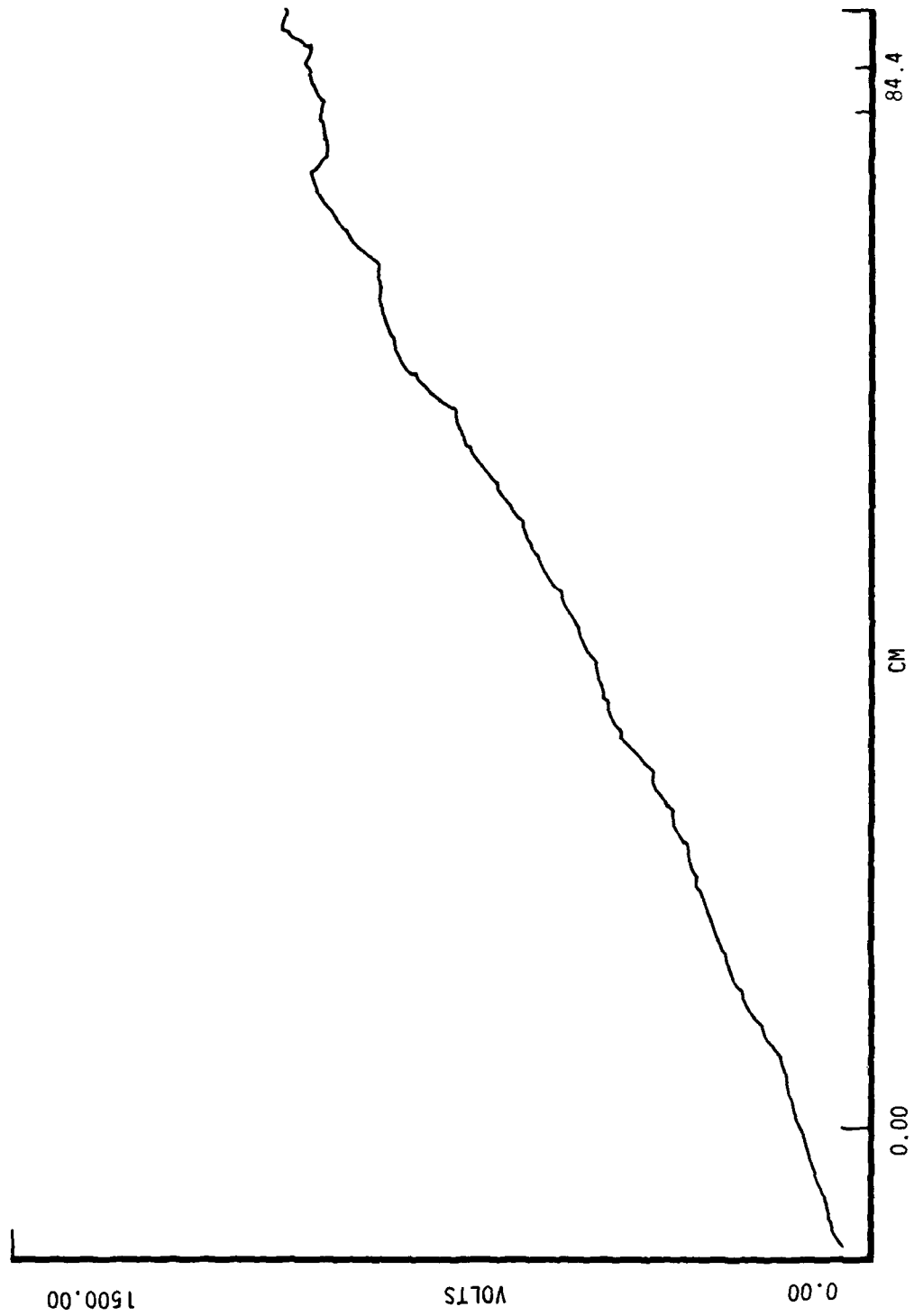


Figure 12. LWC 004 Voltage Profile, at 2.9 Sec

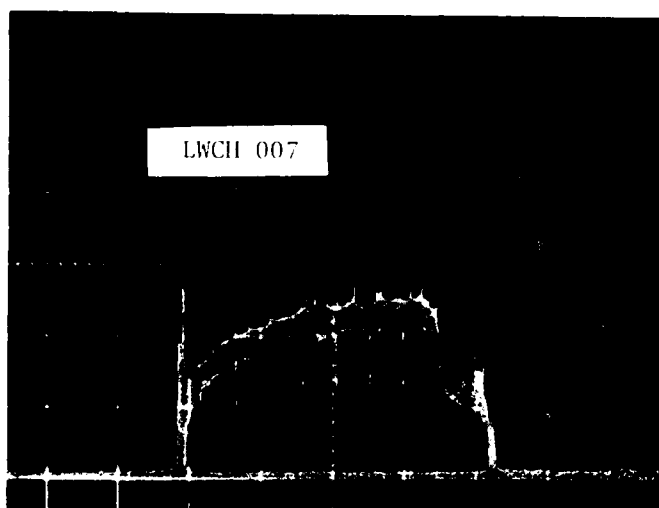
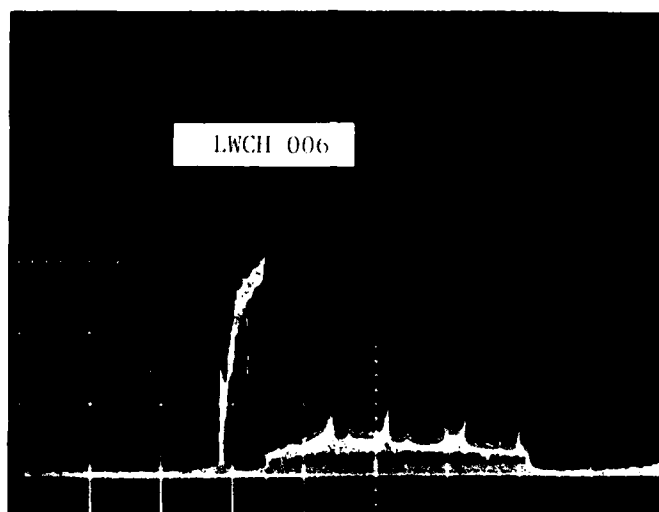


Figure 13. Voltage vs. Time, LWC 006 and 007  
(Vertical 400V/cm, horizontal, sec/cm)

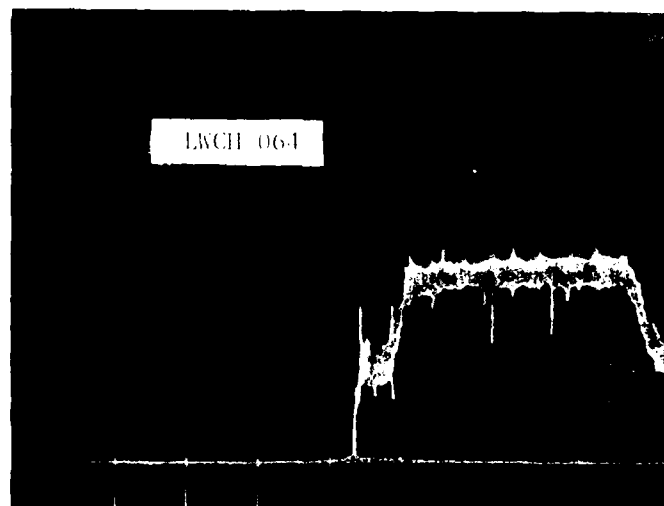
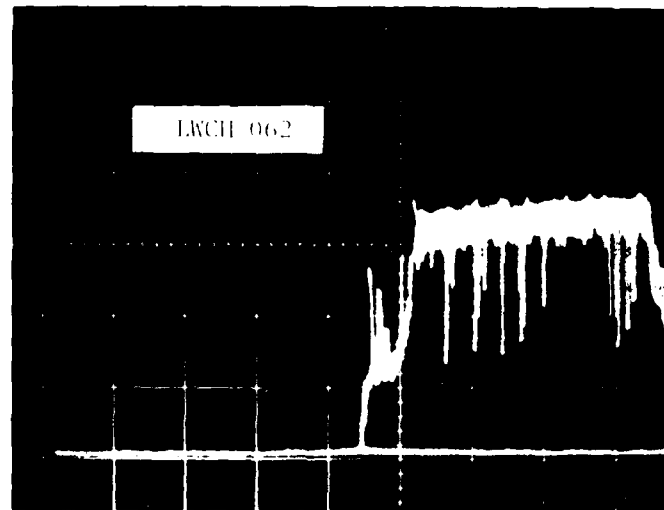


Figure 14. Voltage vs. Time, LWC 062 and 064  
(Vertical 400V/cm, horizontal 1 sec/cm)

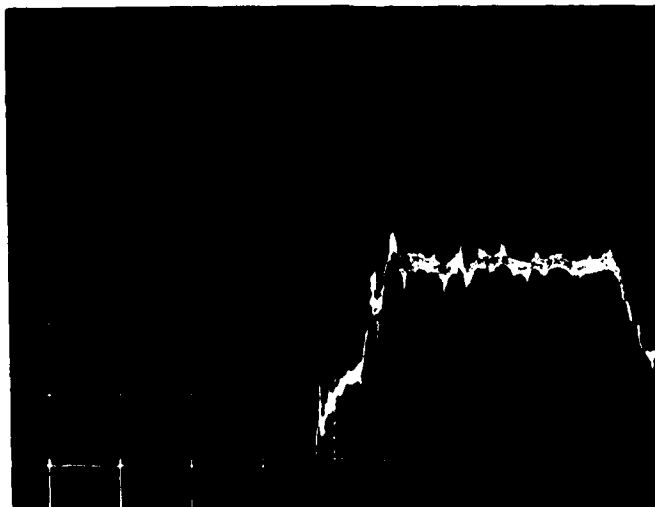


Figure 15. Voltage vs. Time, LWC 069 and 076  
(Vertical 400V/cm, horizontal 1 sec/cm)

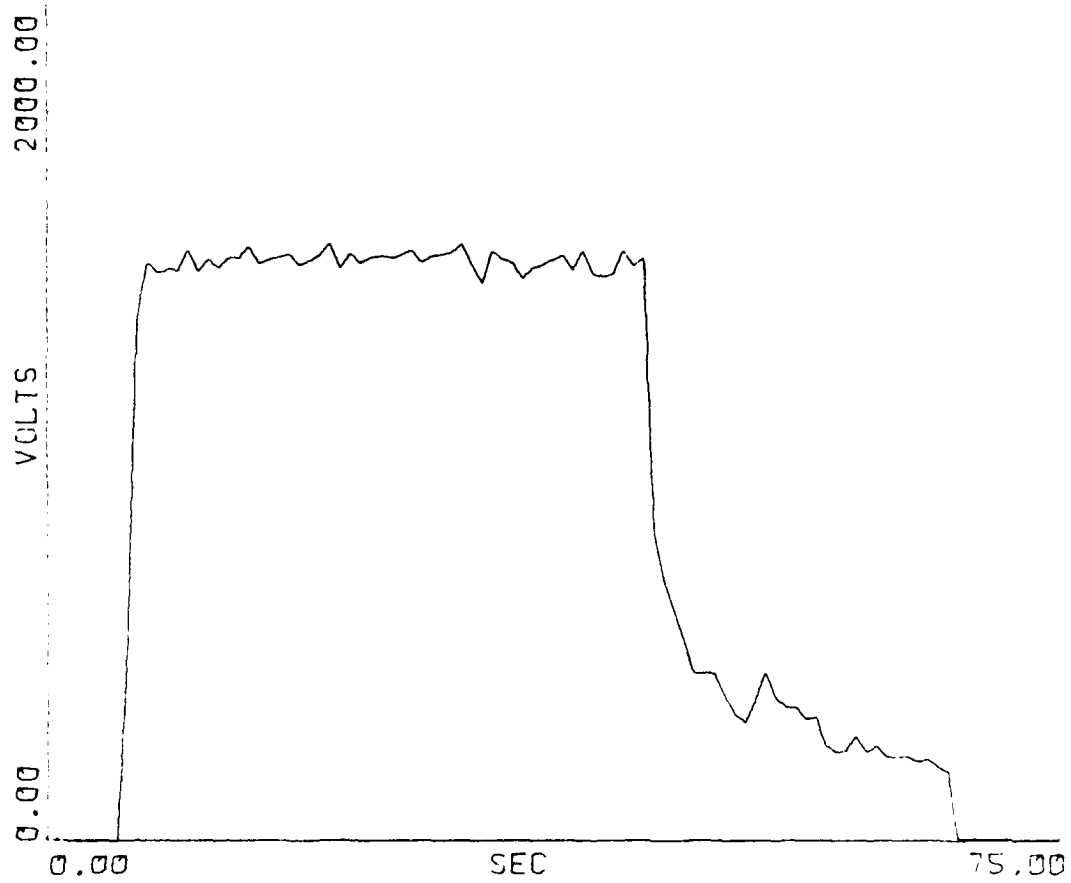


Figure 16. LWC 211 Load Voltage

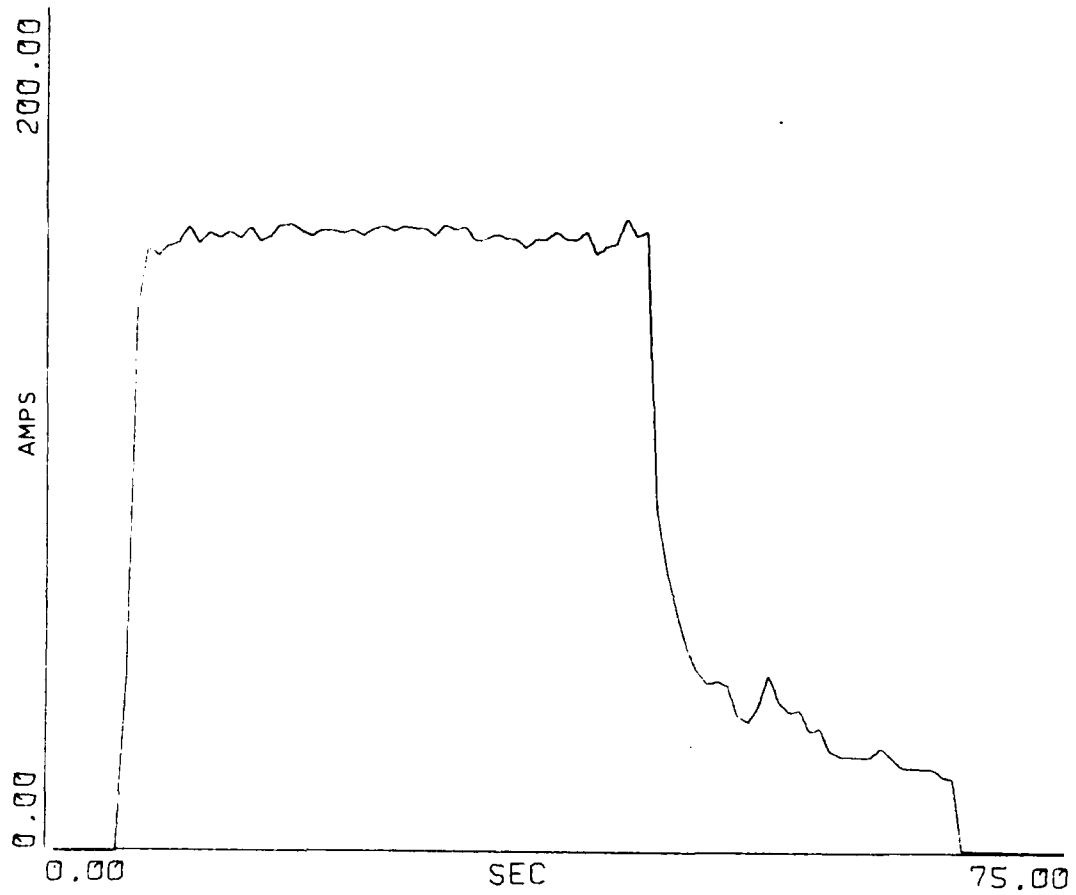


Figure 17. LWC 211 Load Current

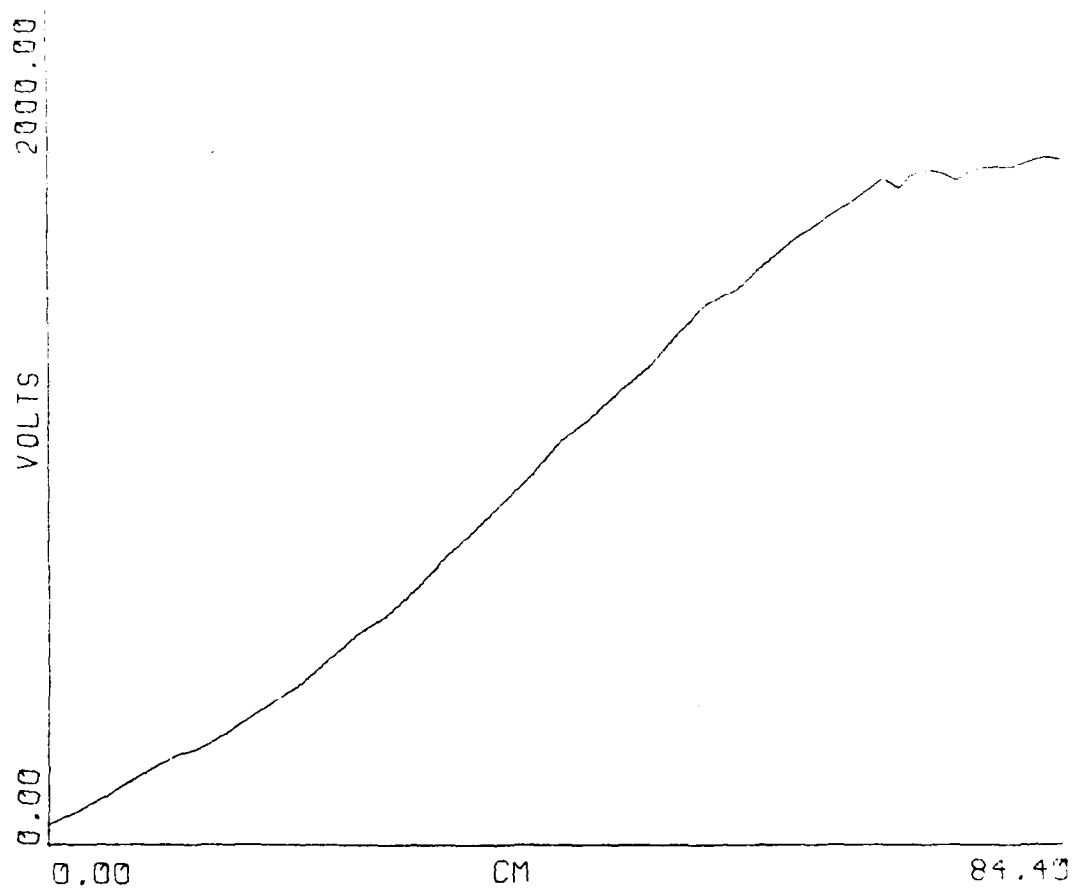


Figure 18. LWC 211 Voltage Profile at 8.0 Sec

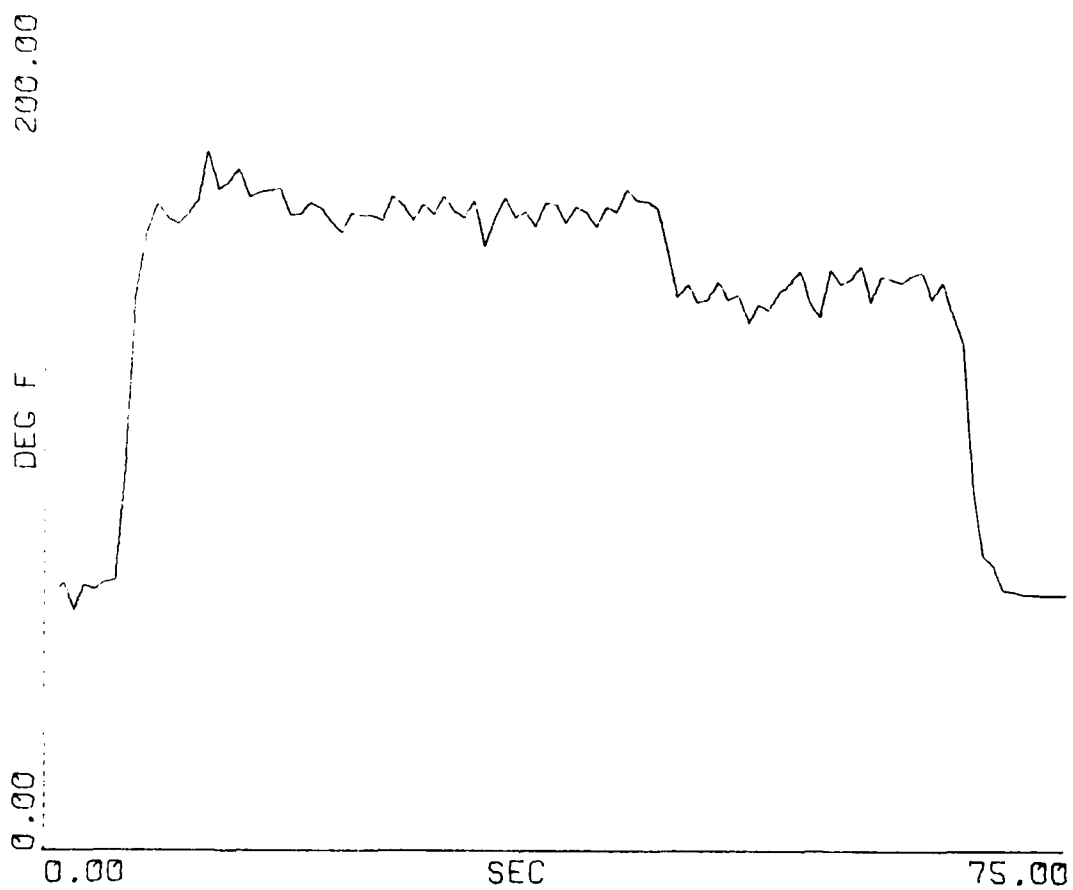


Figure 19. LWC 211 Combustor Wall Exit Water Temperature



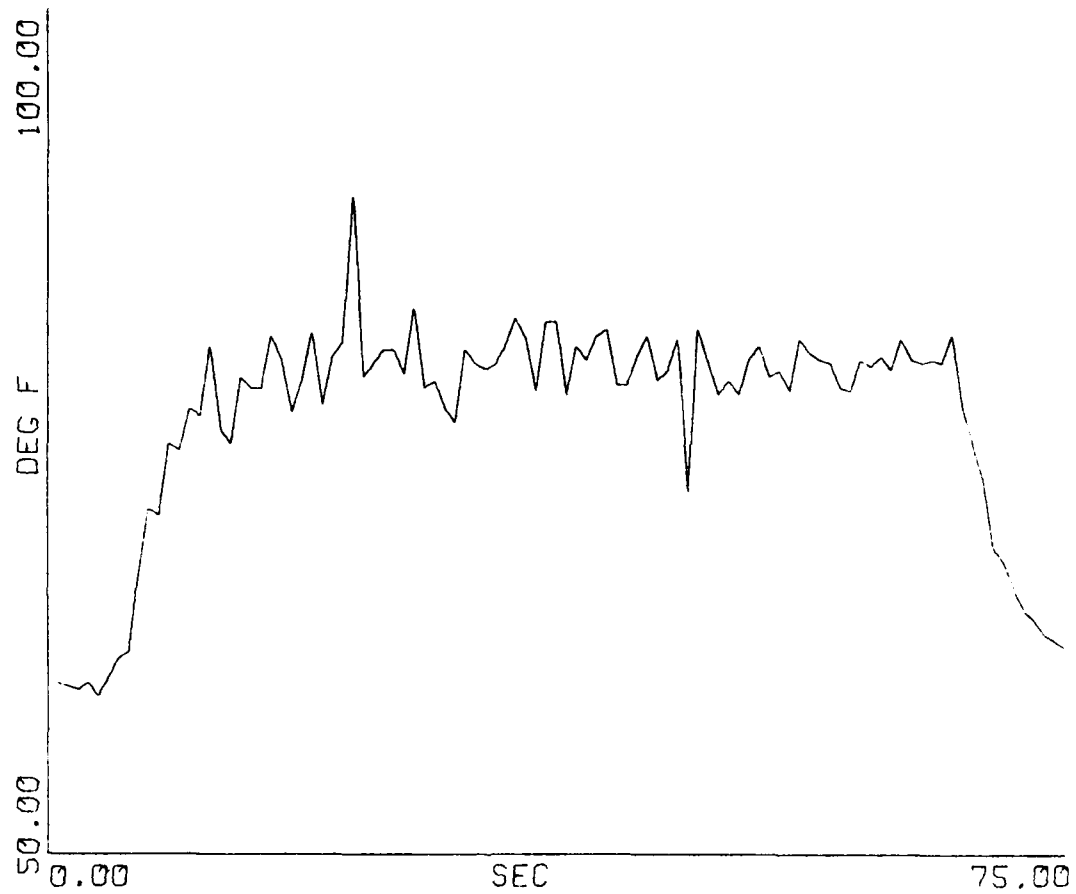


Figure 20. LWC 211 Right Half Nozzle Exit Water Temperature

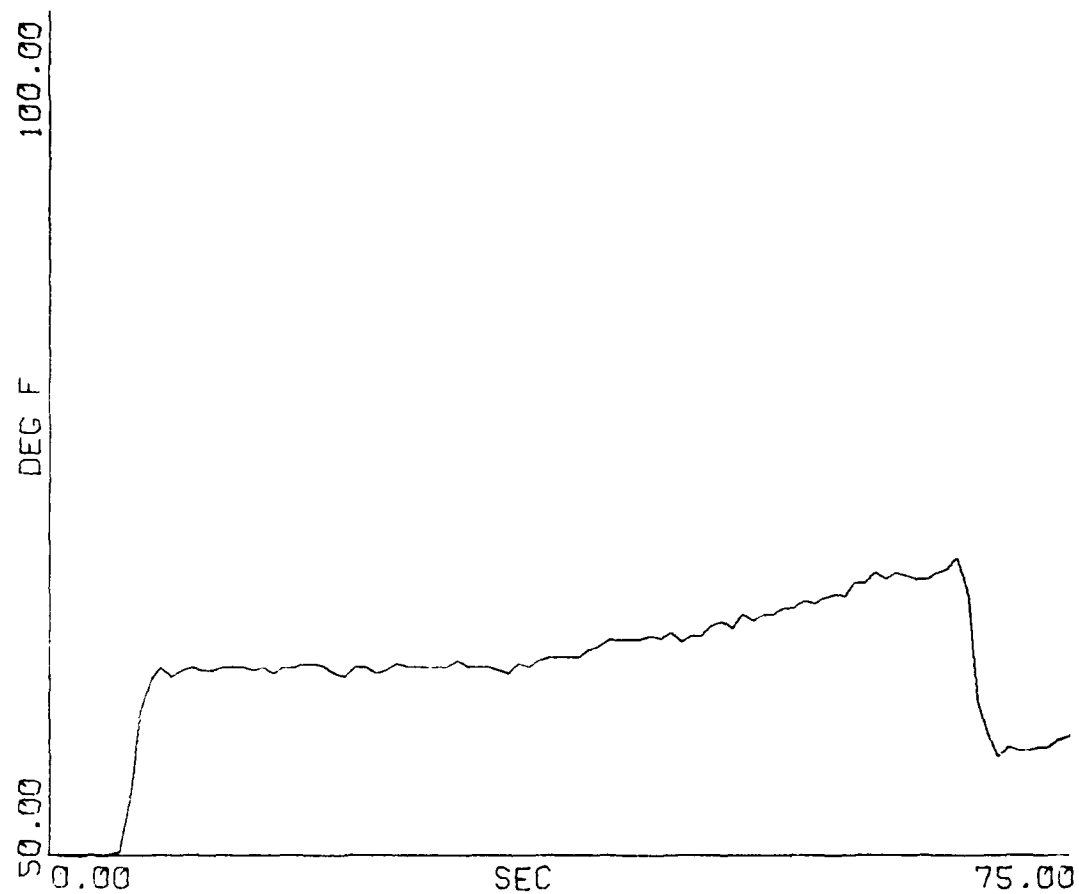


Figure 21. LWC 211 Electrode No. 1 Exit Water Temperature

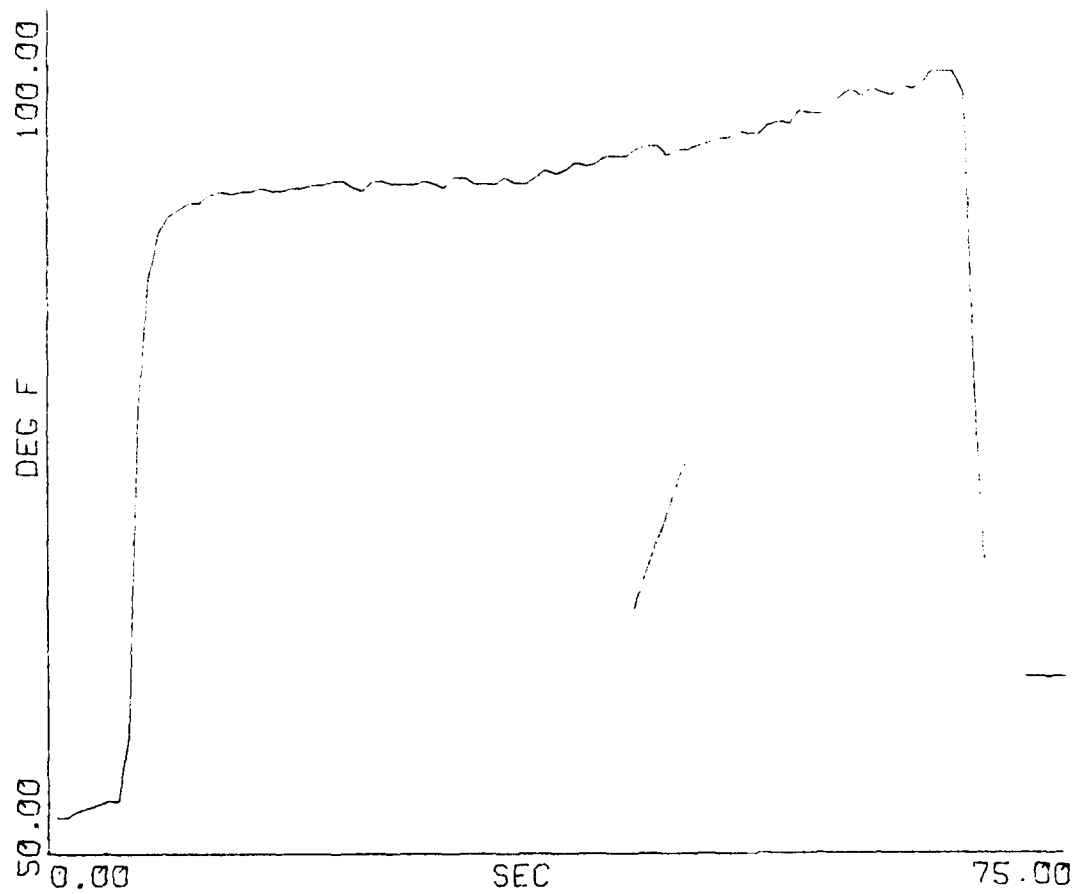


Figure 22. LWC 211 Electrode 3 Exit Water Temperature

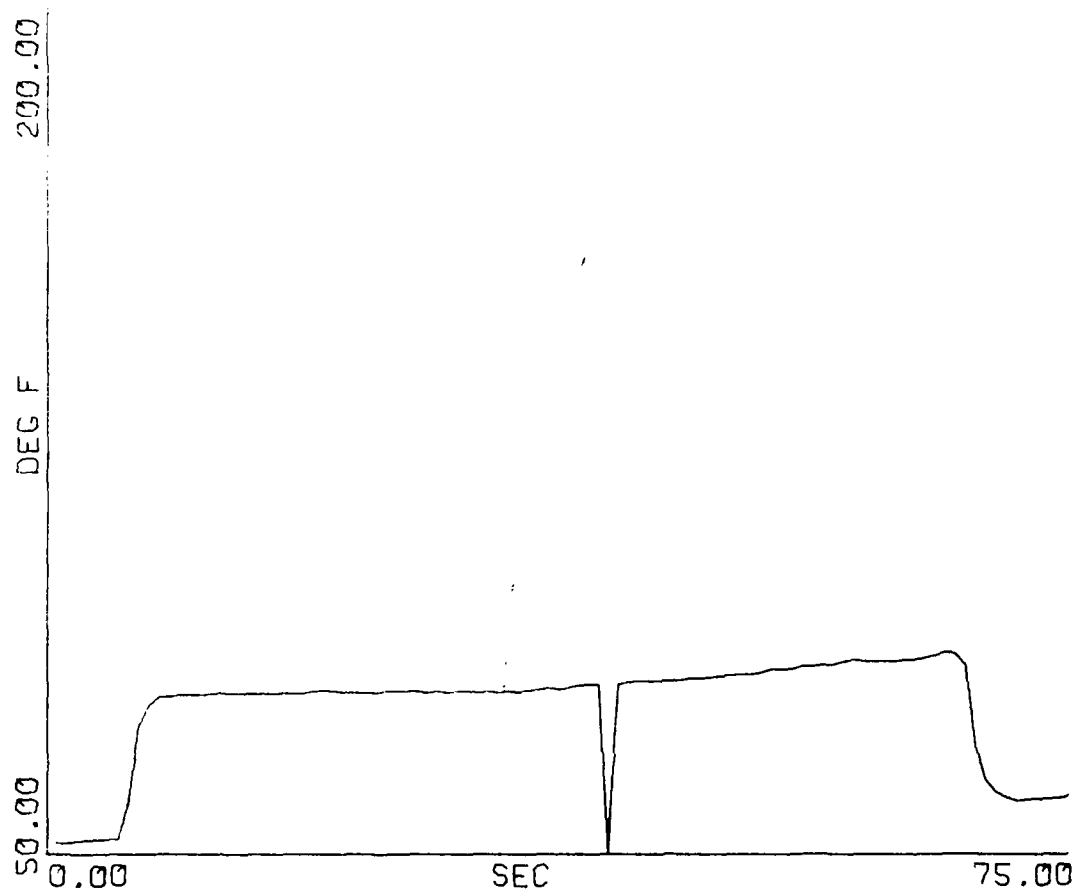


Figure 23. LWC 211 Electrode 9 Exit Water Temperature

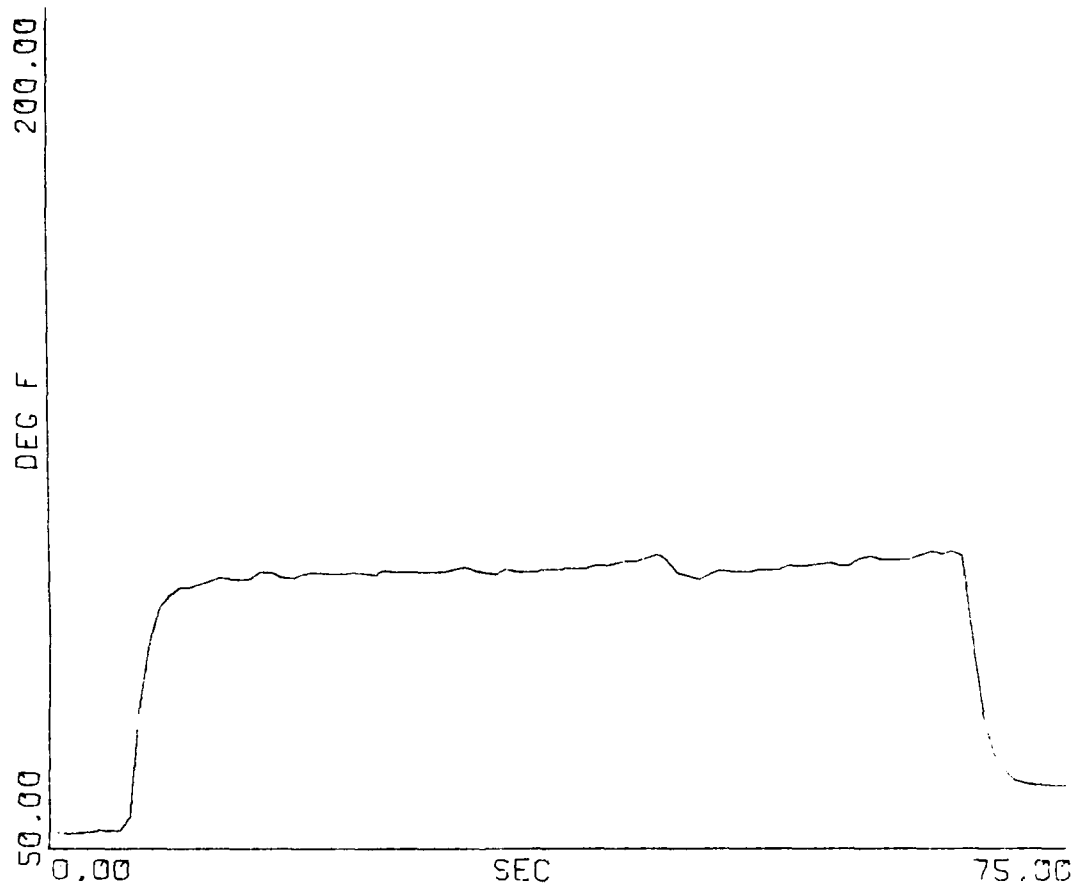


Figure 24. LWC 211 Electrode 21 Exit Water Temperature

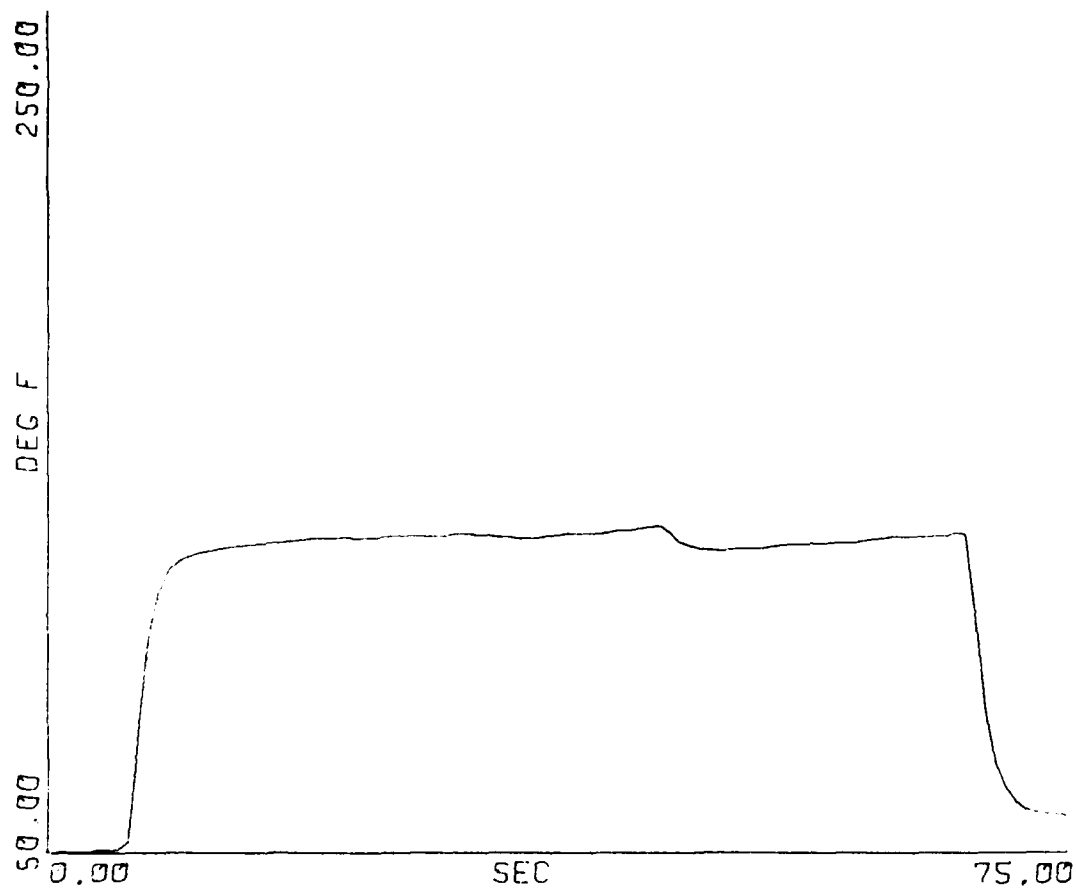


Figure 25. LWC 211, Electrode 27 Exit Water Temperature

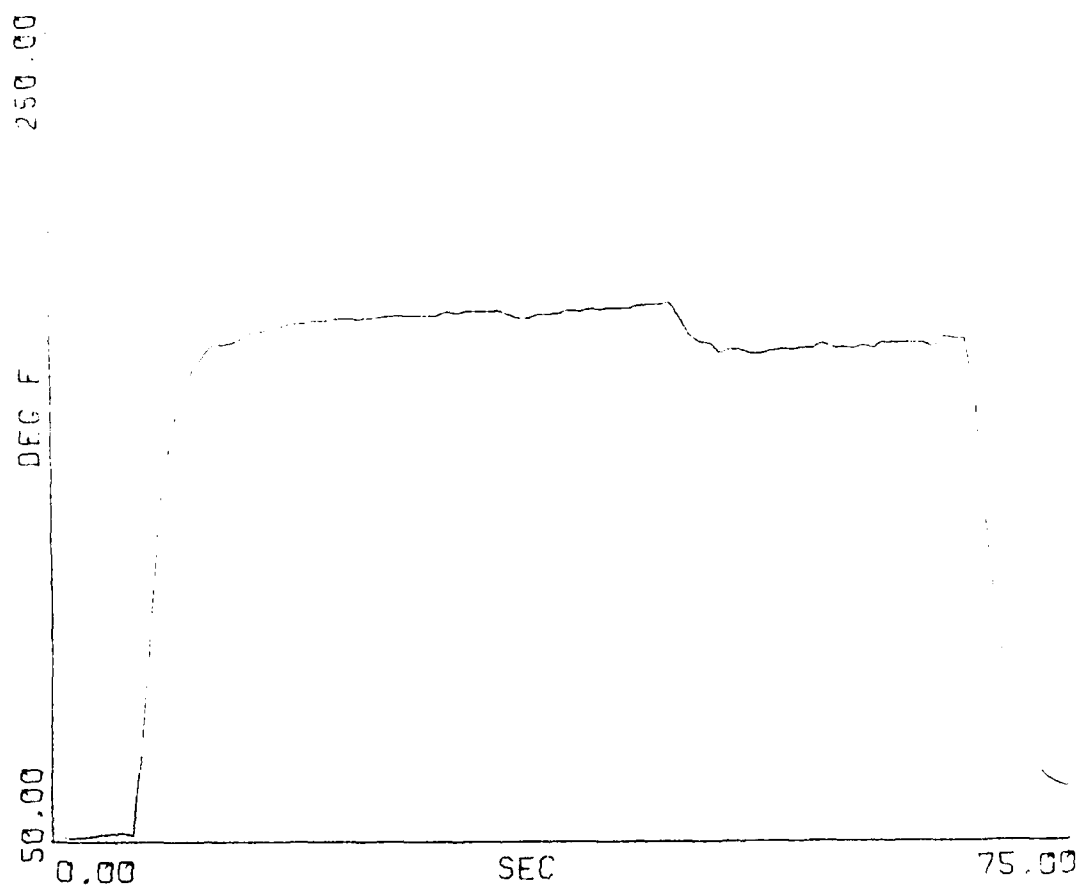


Figure 26. LWC 211, Electrode 35 Exit Water Temperature

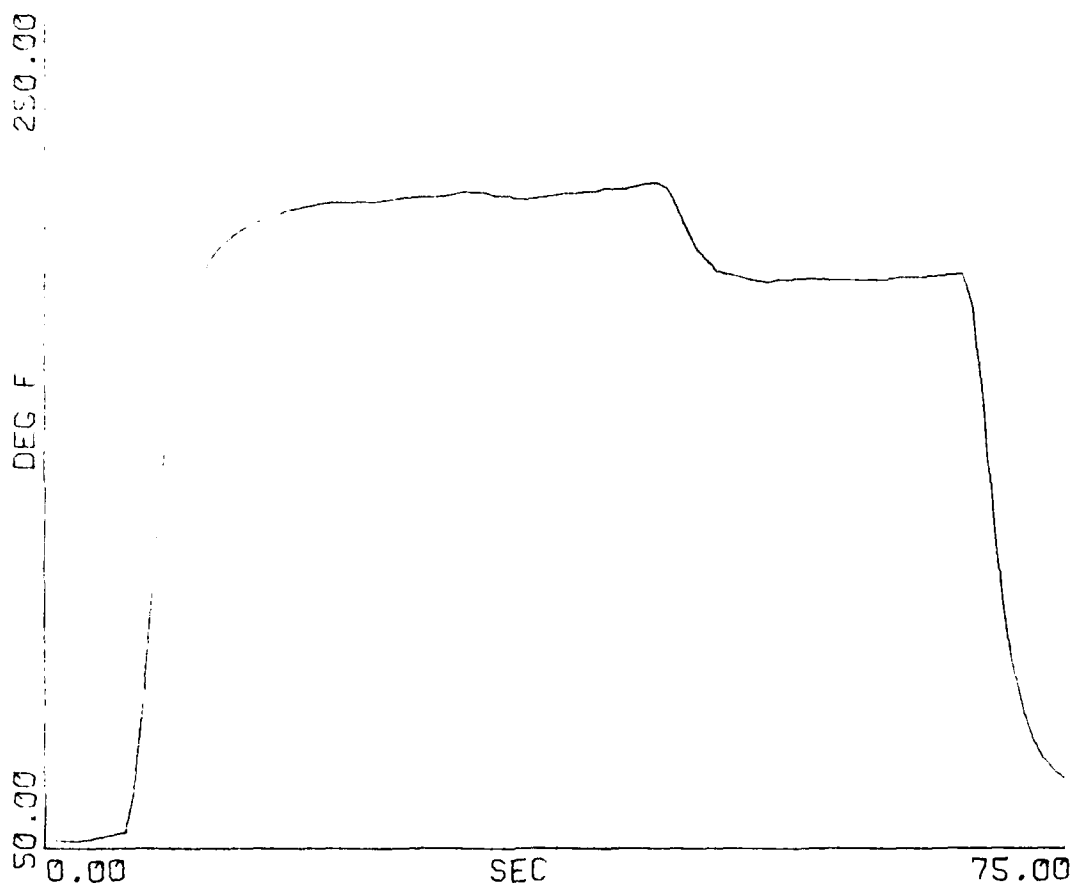


Figure 27. LWC 211, Electrode 50 Exit Water Temperature



AFWAL-TR-80-2021

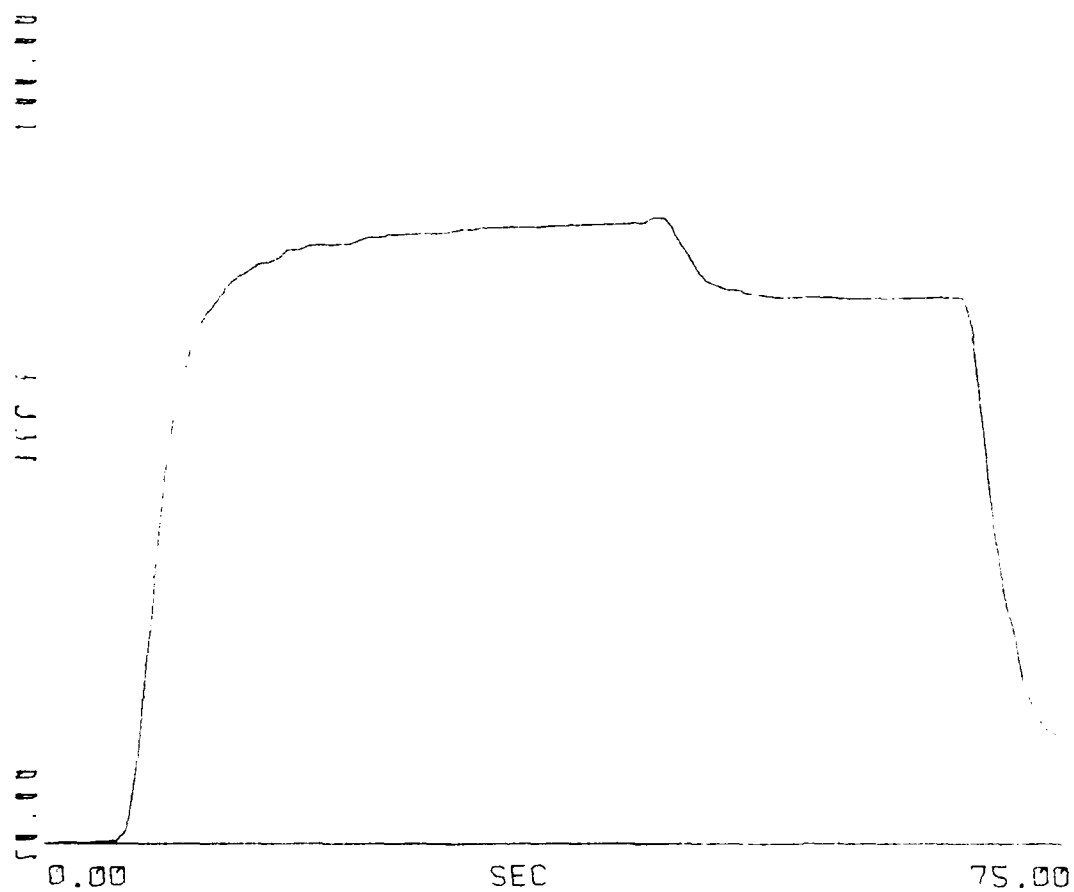


Figure 28. LWC 211, Electrode 59 Exit Water Temperature

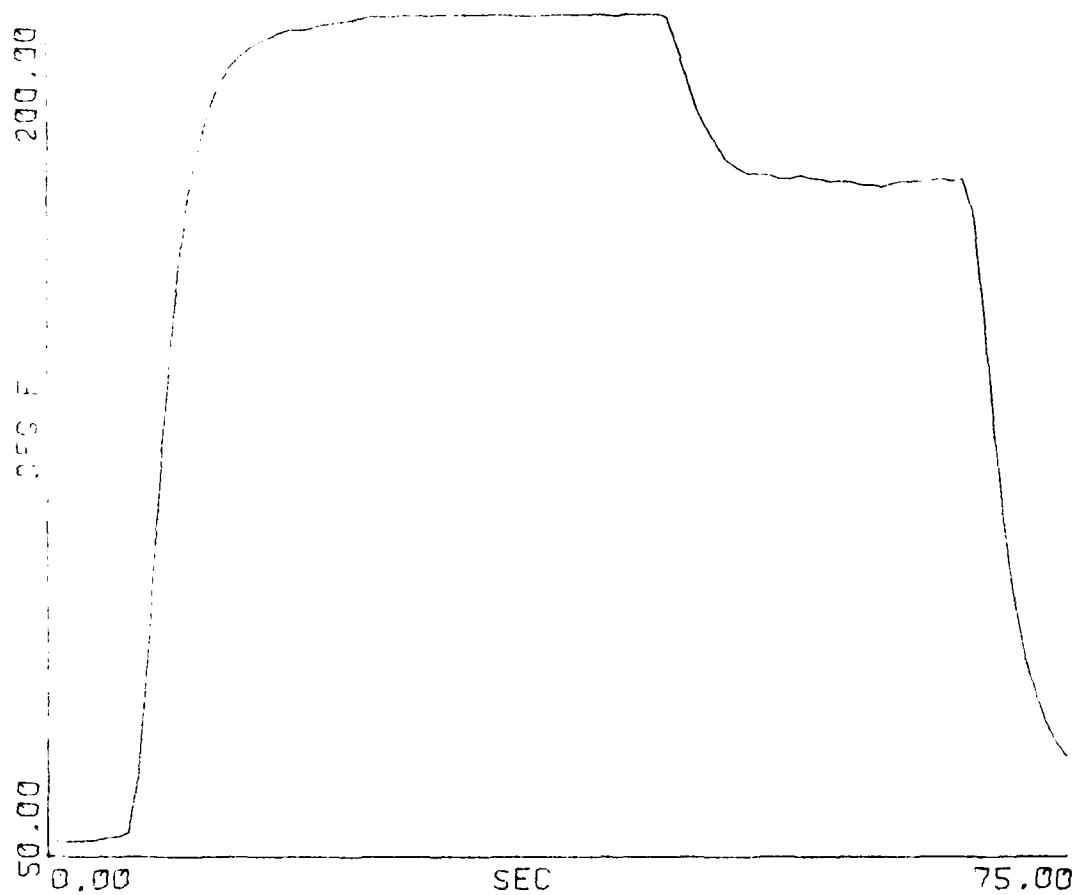


Figure 29. LWC 211, Electrode 70 Exit Water Temperature

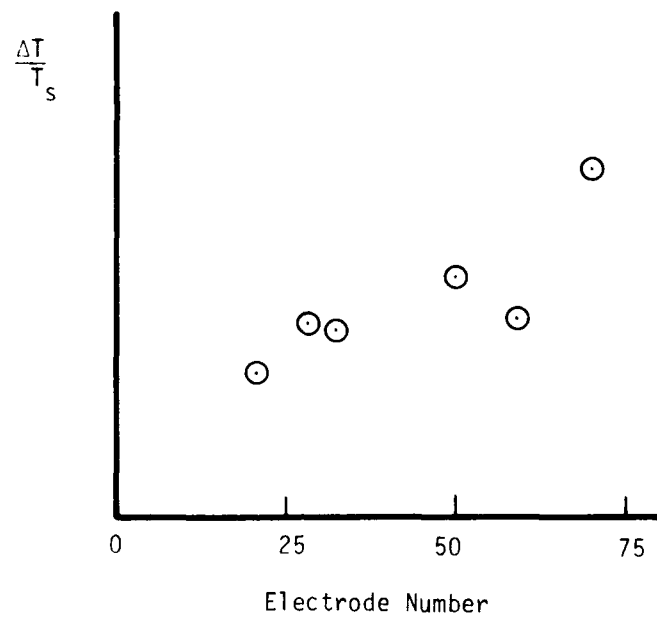


Figure 30. Relative Differential Temperature Drop,  $\Delta T/T_s$  vs. Electrode Number

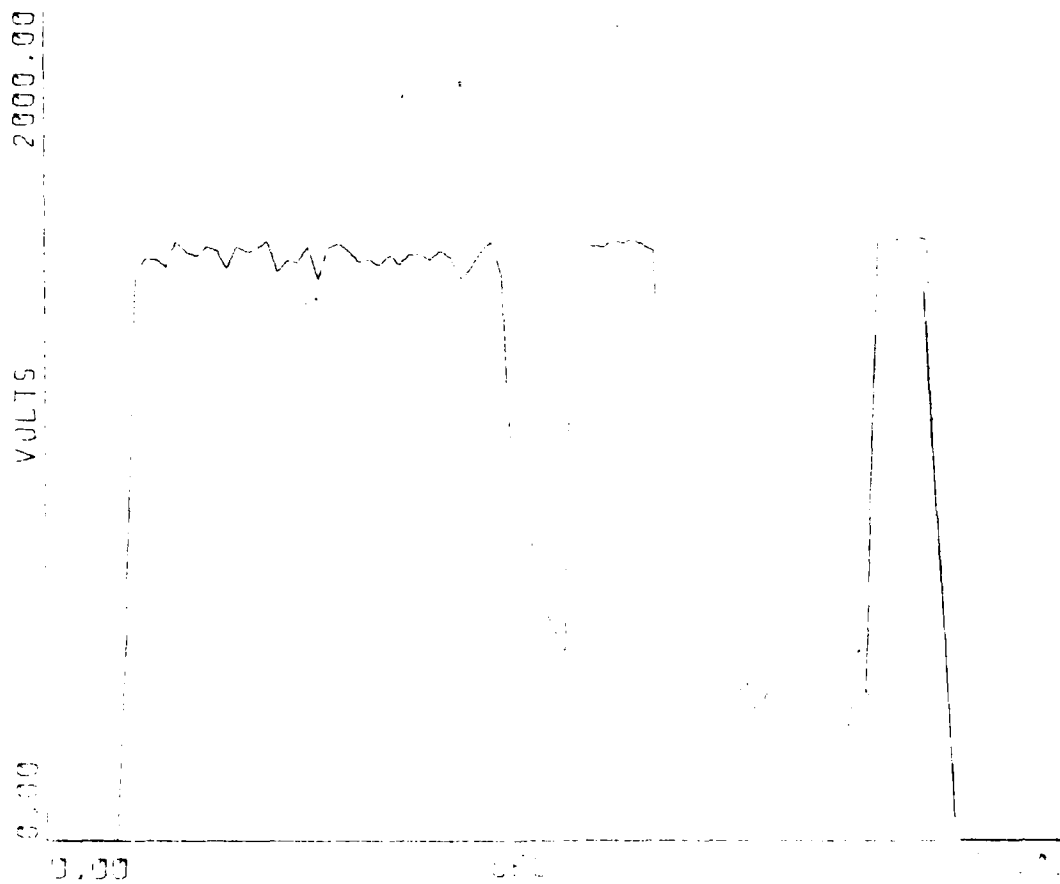


Figure 31. LWC 205, Load Voltage

AFWAI -TR-80-2021

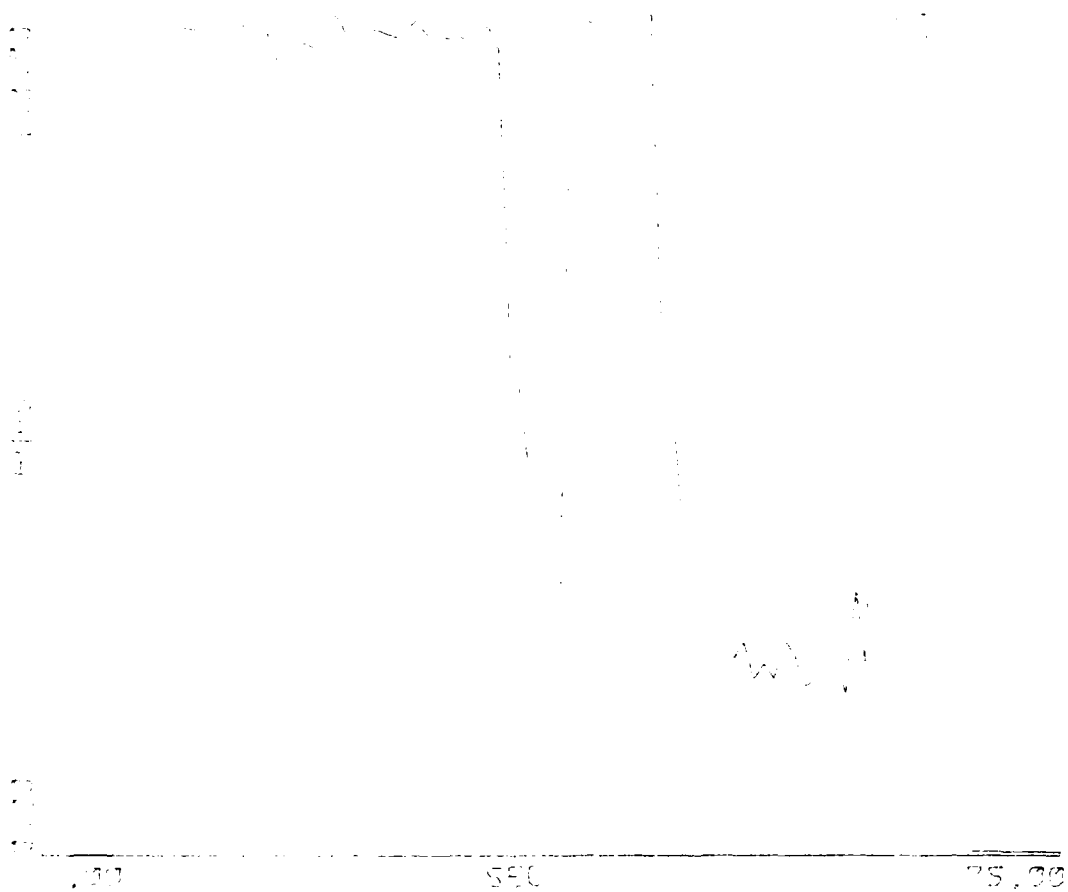


Figure 32. LWC 205, Load Current

Electrode 58

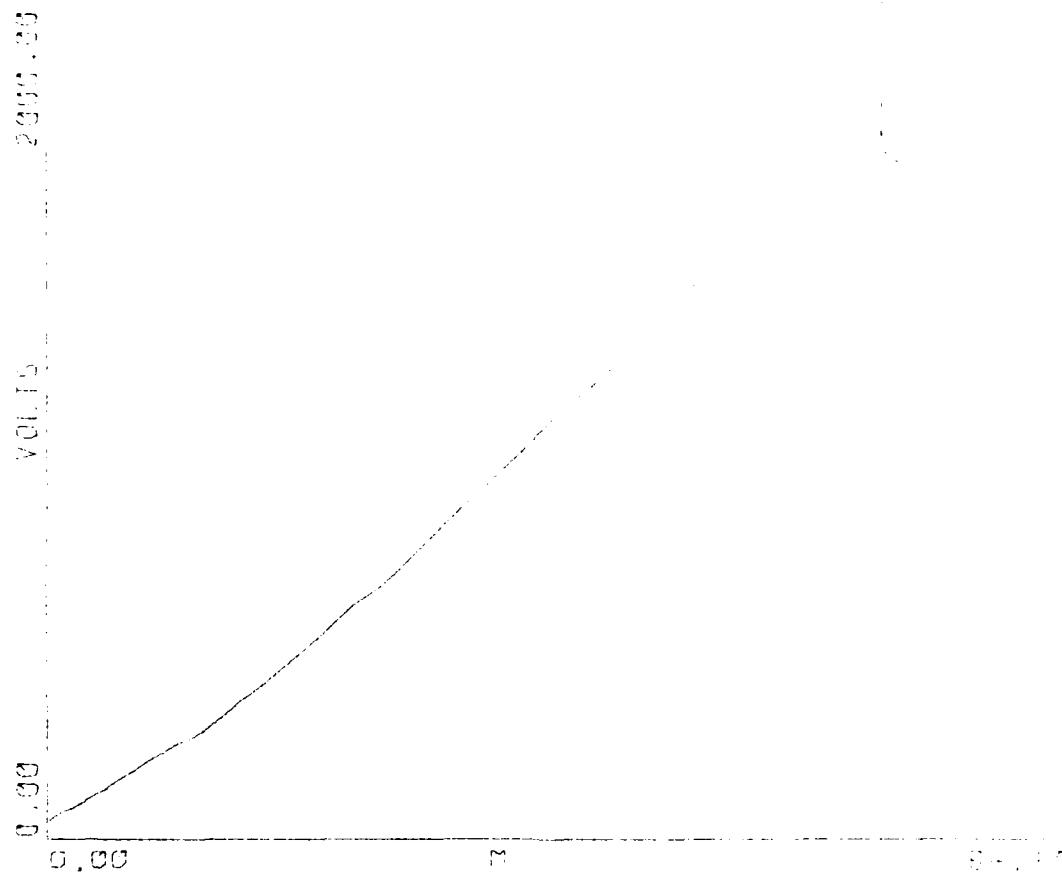


Figure 33. LWC 205, Voltage Profile at 15.0 Sec

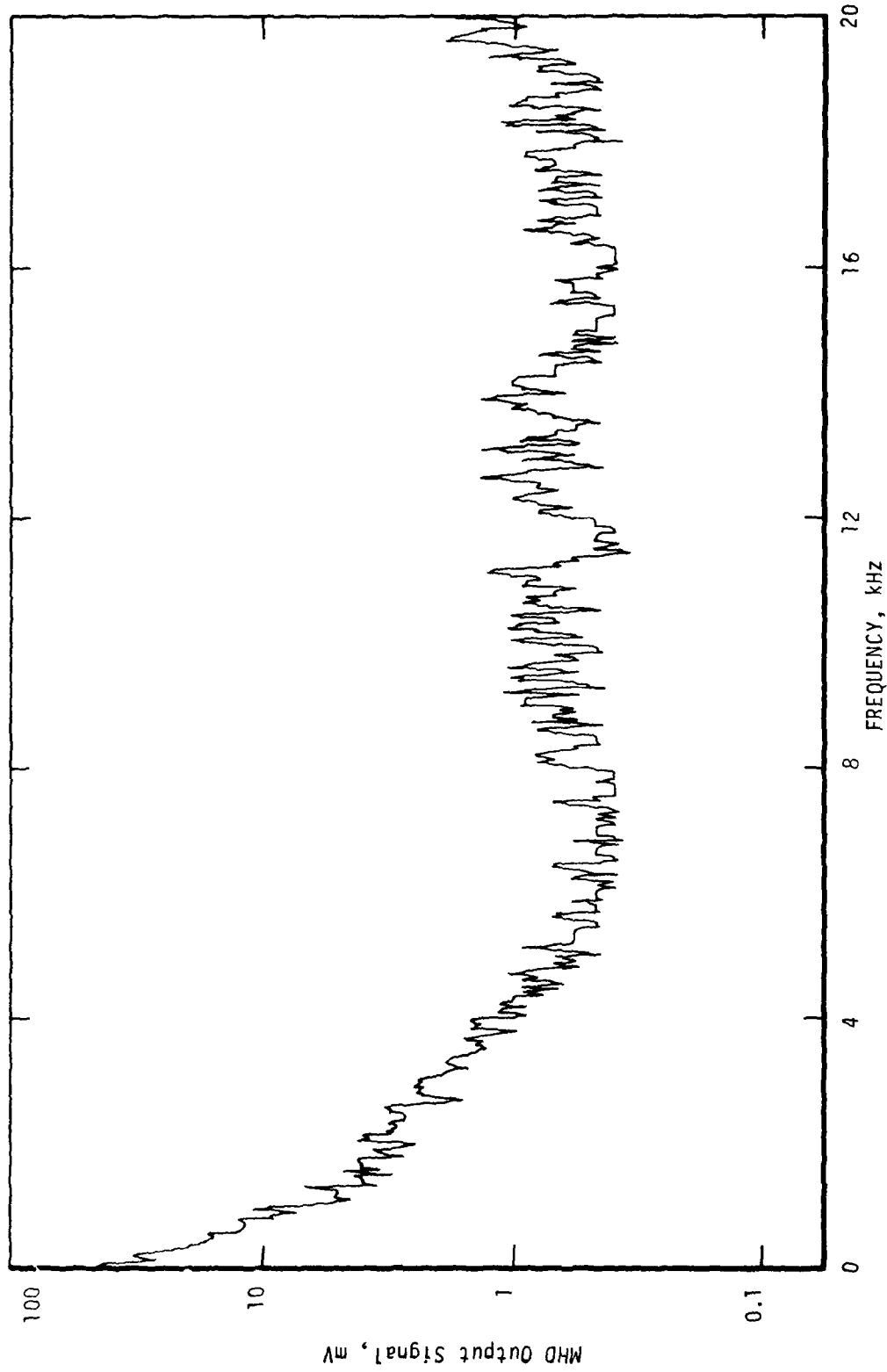


Figure 34. MHD Generator Output Voltage Linear Spectrum, 0-20 kHz

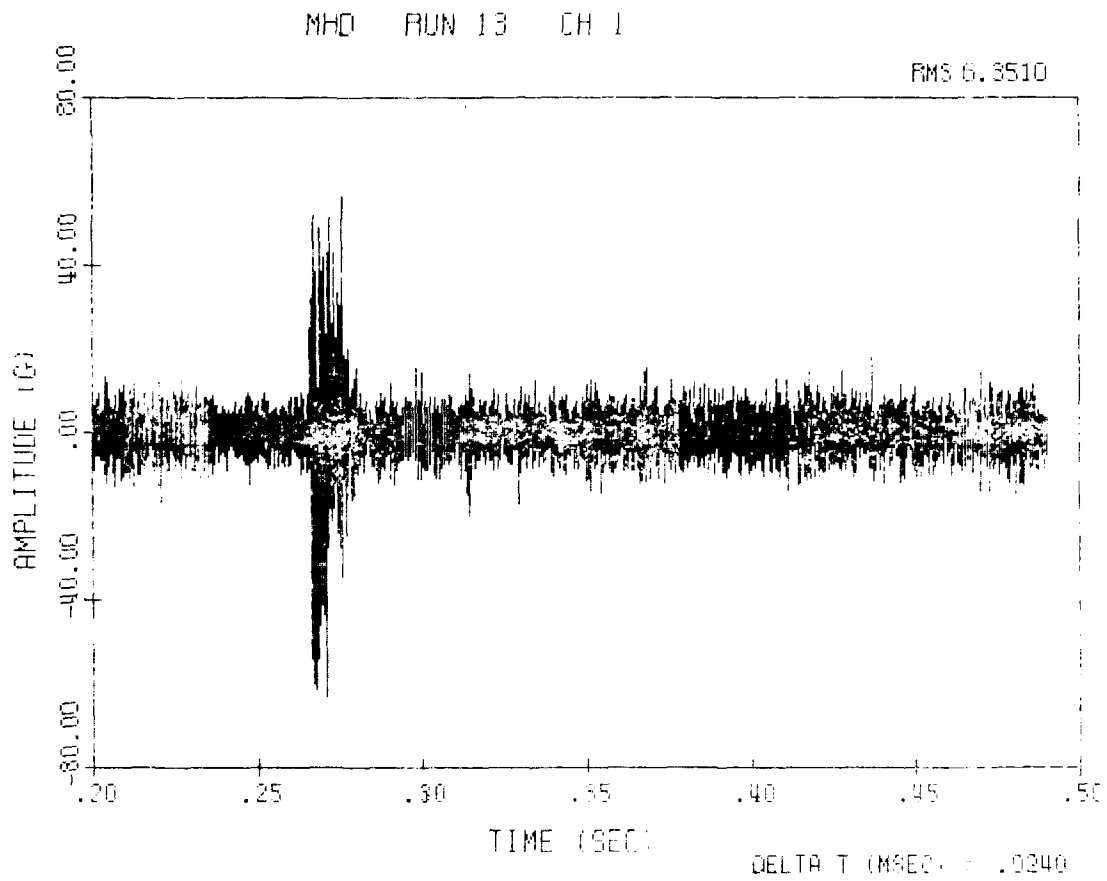


Figure 35. LWC 013, Vibration Amplitude at Beginning of Firing of Main Combustor, Channel One



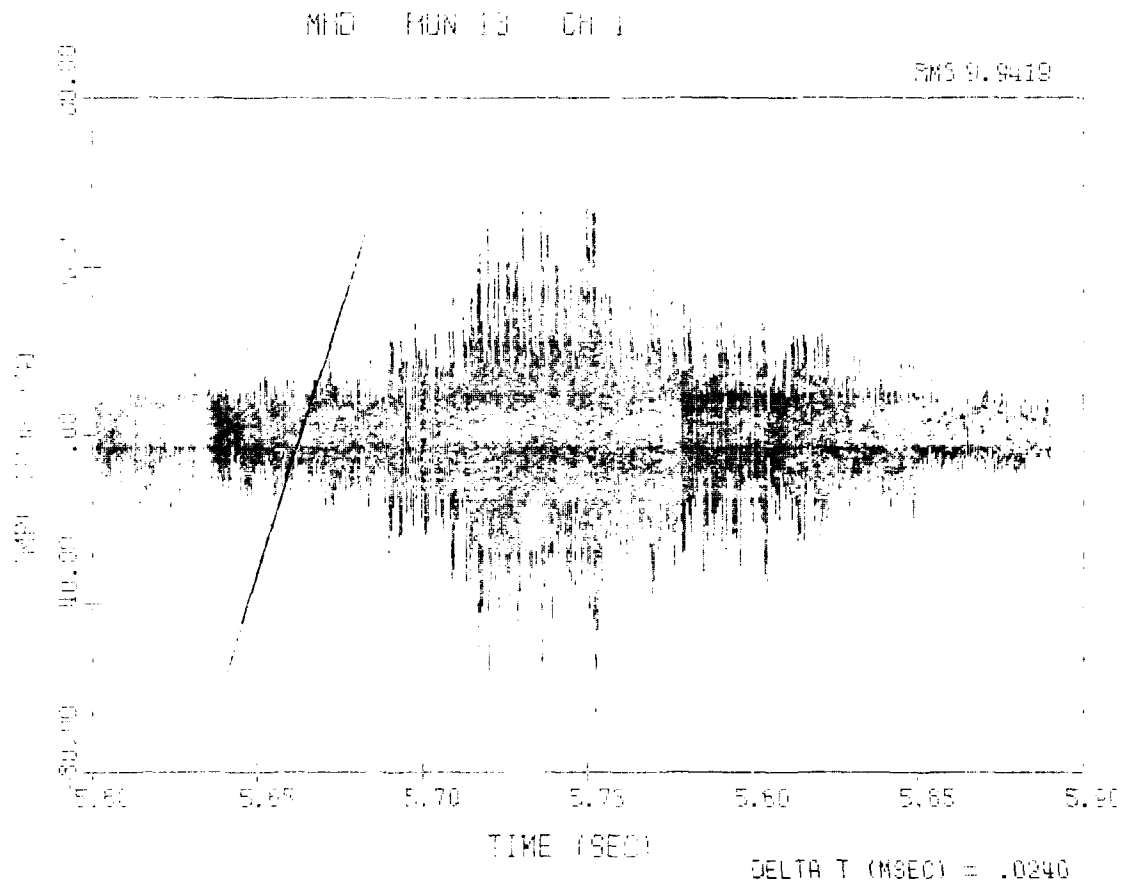


Figure 36. LWC 013, Vibration Amplitude at End of Main Combustor Run, Channel One

AFWAL-TR-80-2021

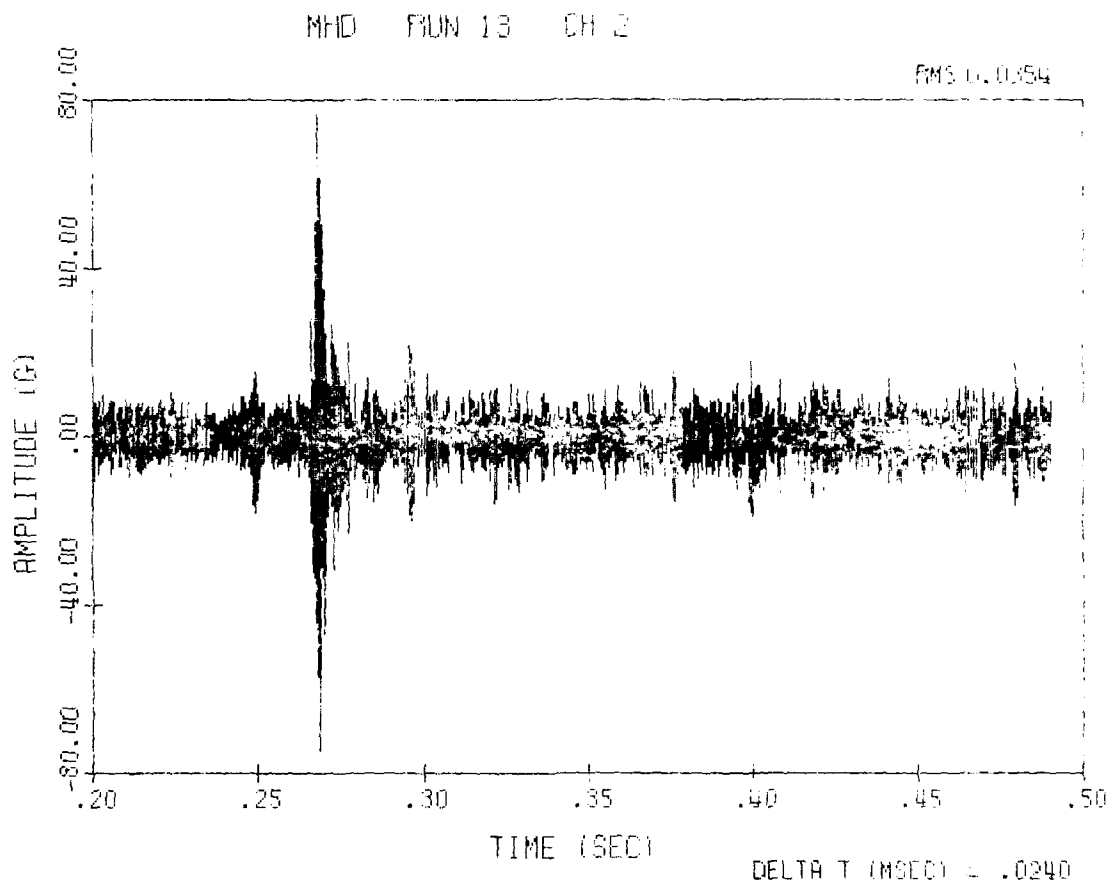


Figure 37. LWC 013, Vibration Amplitude at Beginning Run, Channel Two

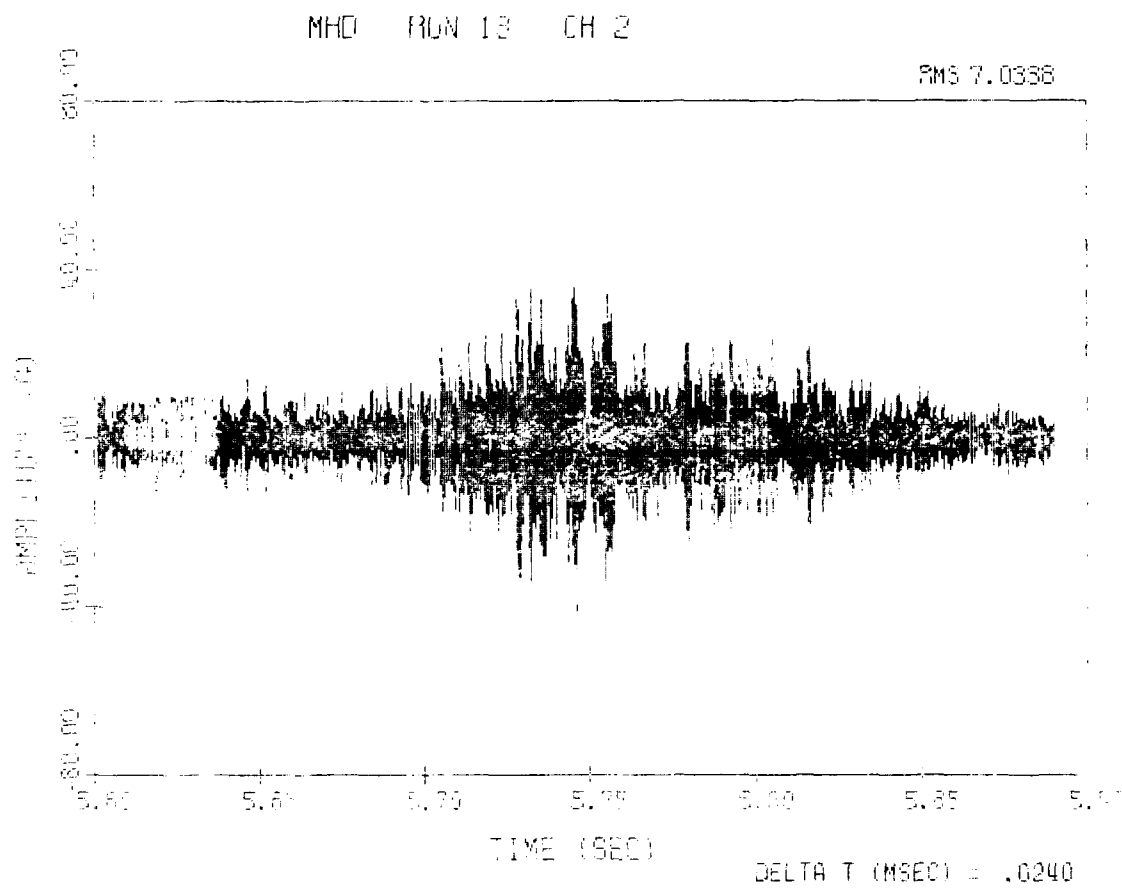


Figure 38. LWC 013, Vibration Amplitude at End of Run, Channel Two

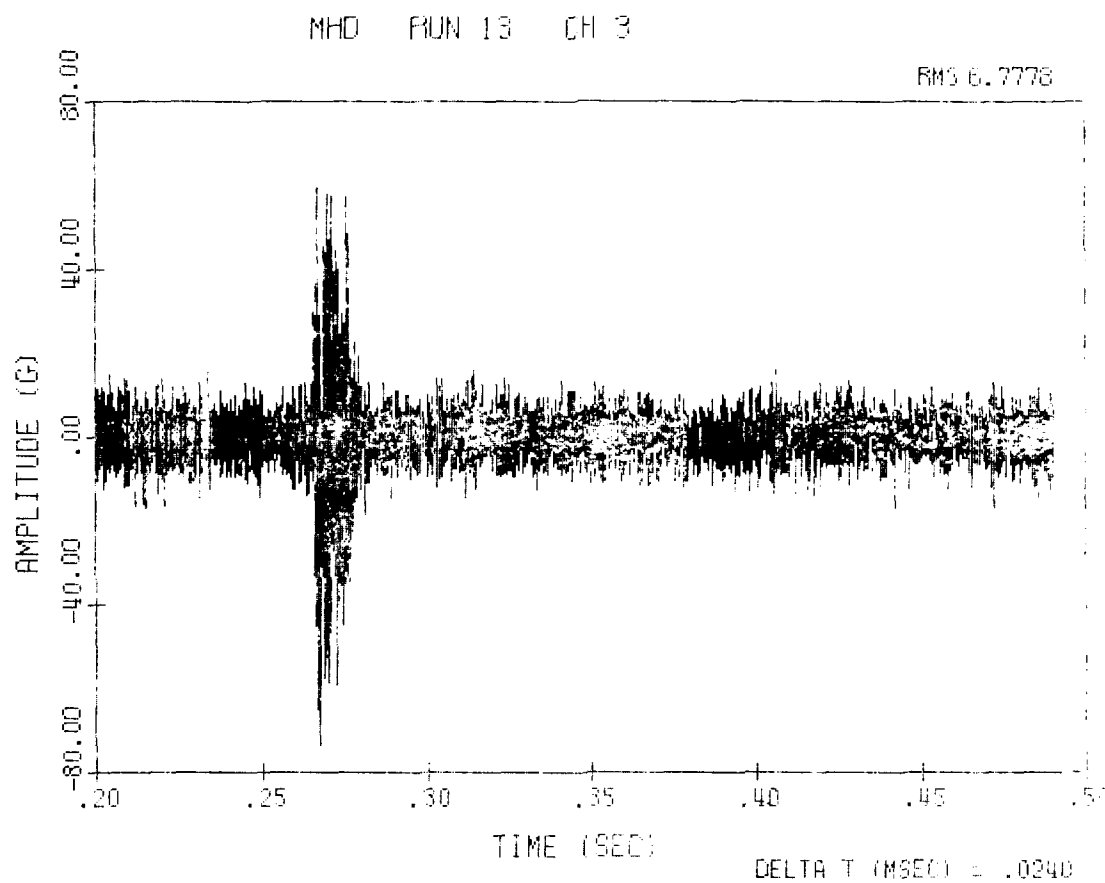


Figure 39. LWC 013, Vibration Amplitude at Beginning of Run, Channel Three

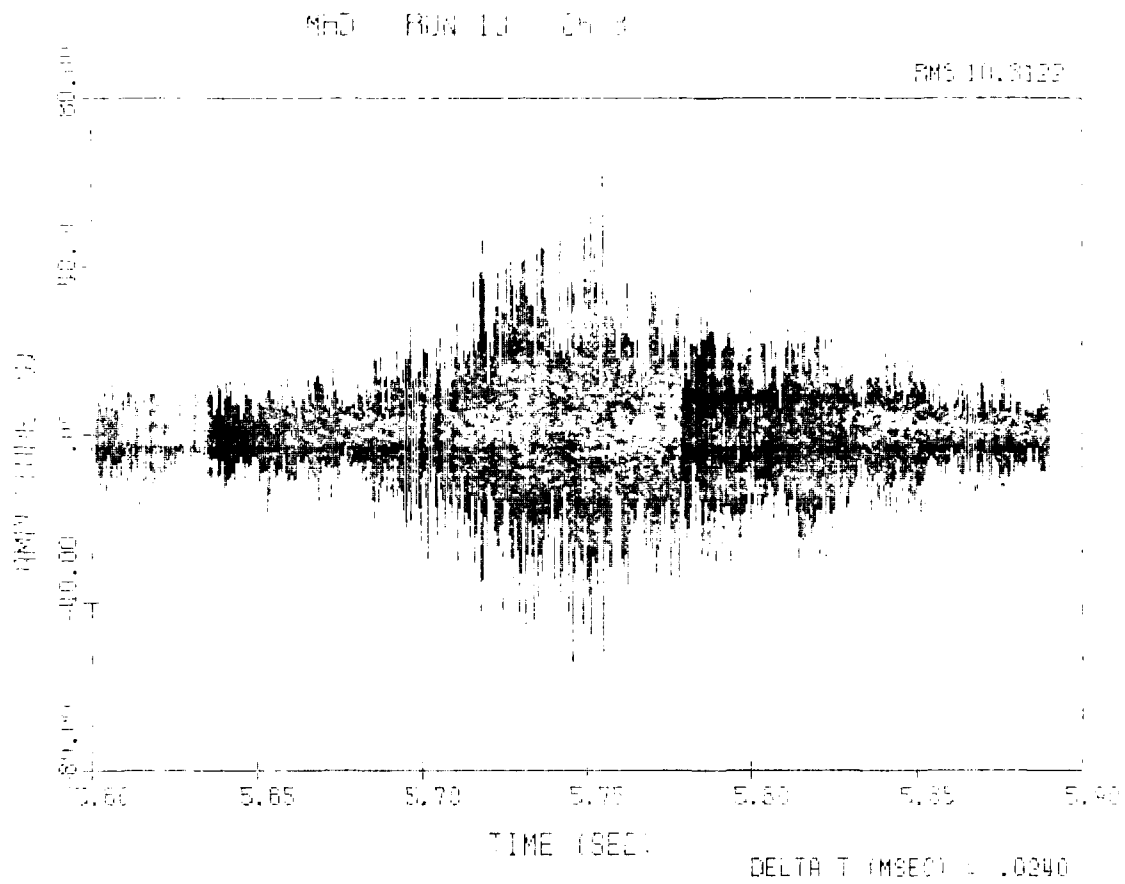


Figure 40. LWC 013, Vibration Amplitude at End of Run, Channel Three

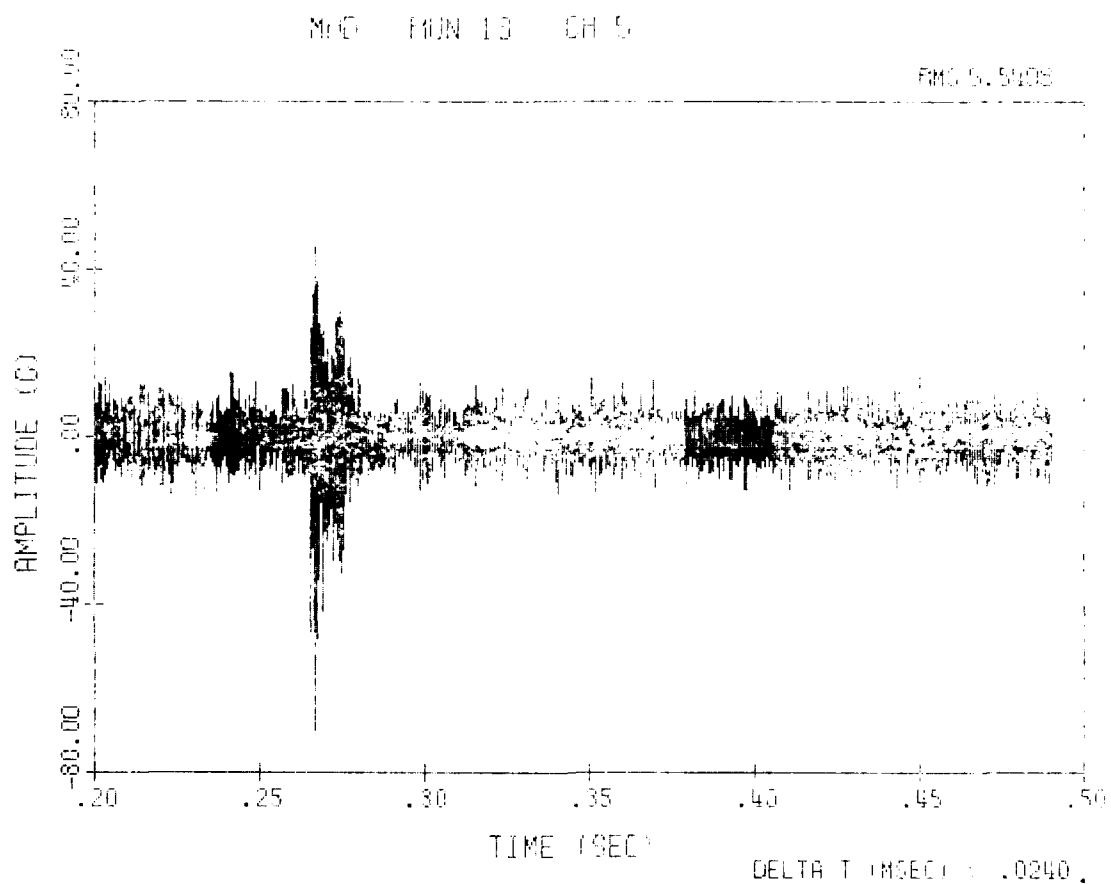


Figure 41. LWC 013, Vibration Amplitude at Beginning of Run Channel Five

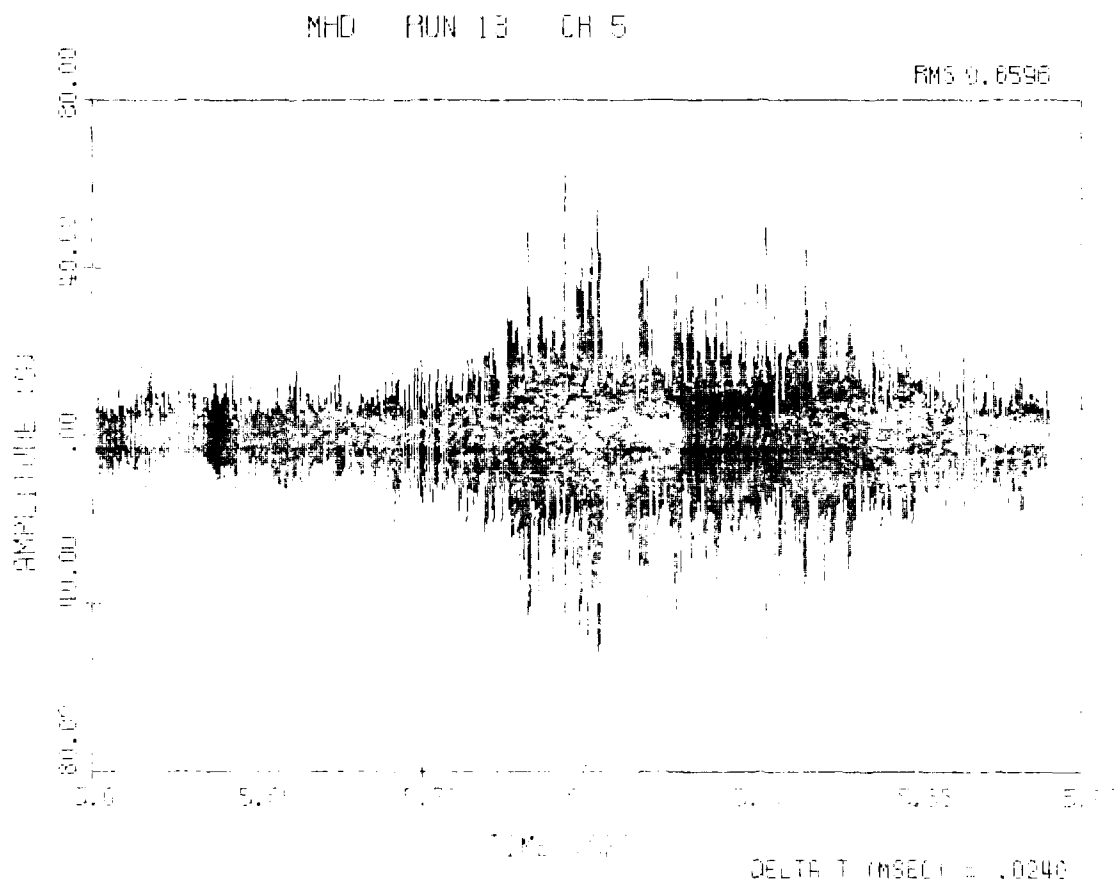


Figure 42. LWC 013, Vibration Amplitude at End of Run, Channel Five

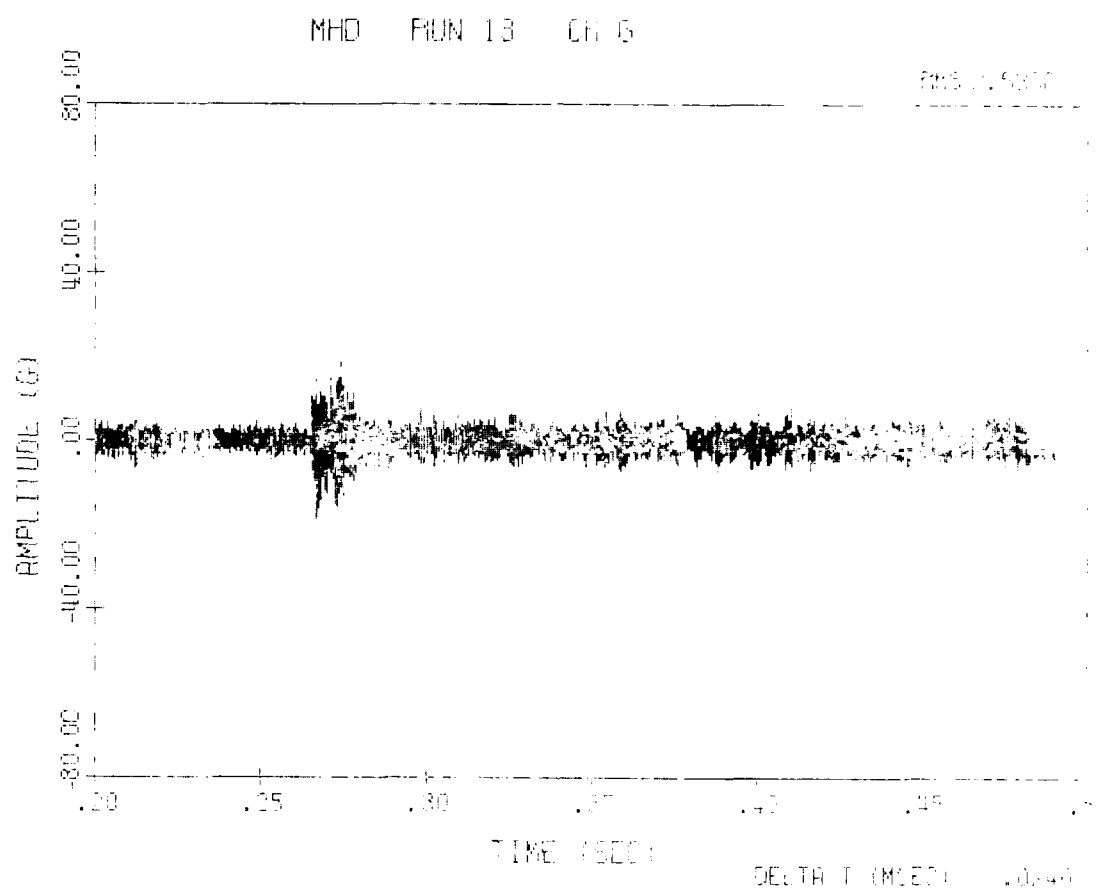


Figure 43. LWC 013, Vibration Amplitude at Beginning of Run, Channel Six



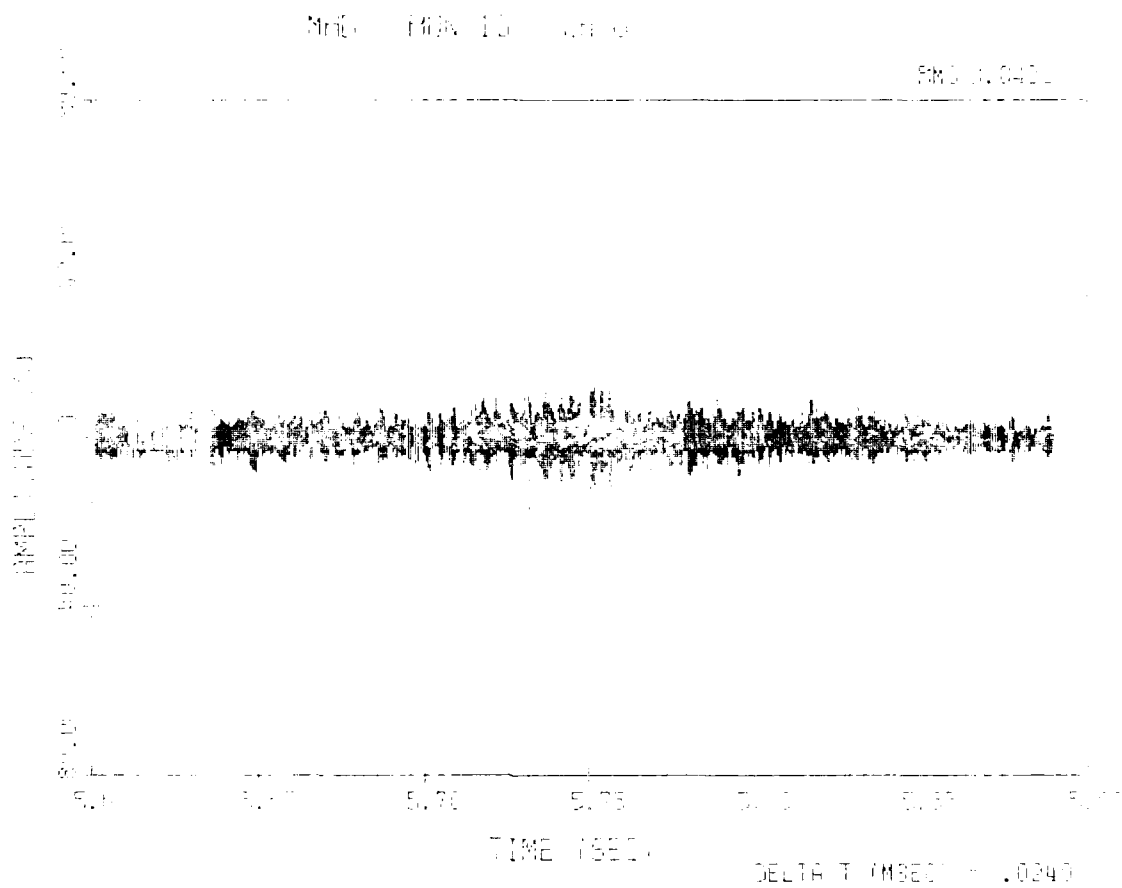


Figure 44. LWC 013, Vibration Amplitude at End of Run, Channel Six

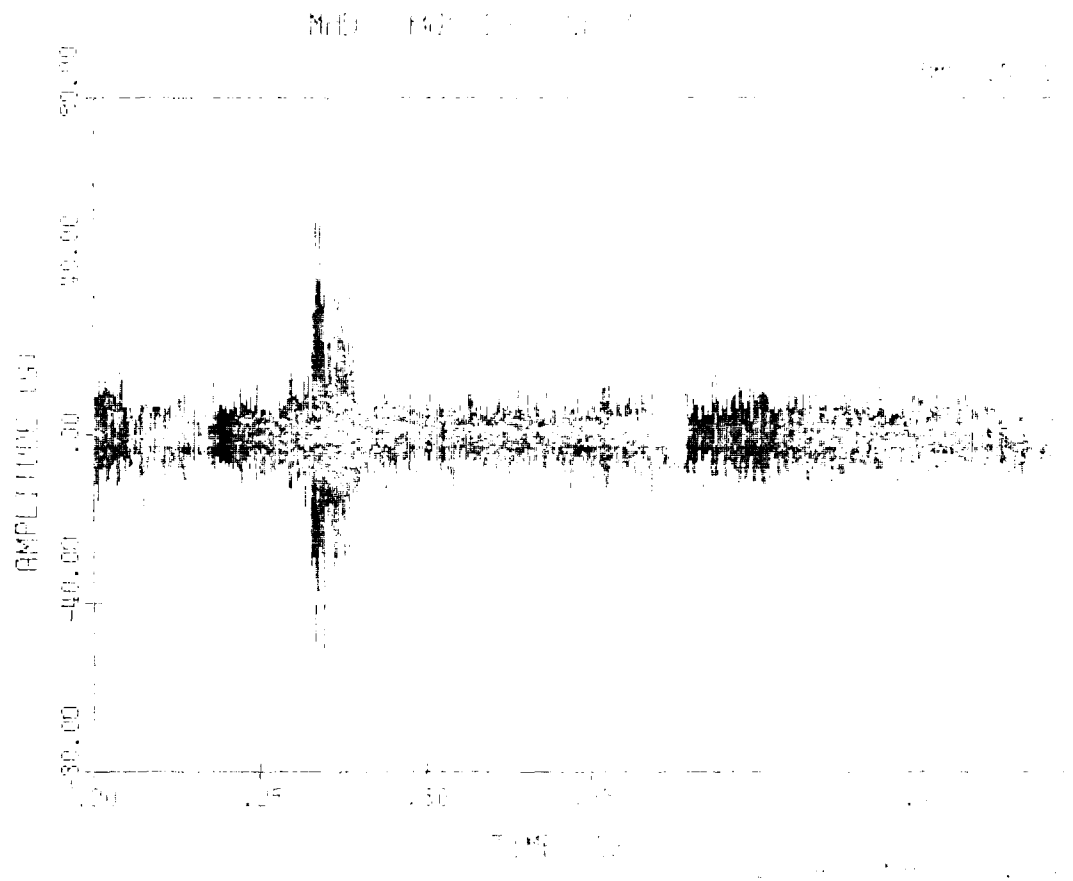


Figure 45. LWC 013, Vibration Amplitude at Beginning Run, Channel Seven

AD-A087 022

AIR FORCE WRIGHT AERONAUTICAL LABS WRIGHT-PATTEPSON AFB OH F/G 10/2

TESTS OF A LIGHTWEIGHT 200 KW MHD CHANNEL AND DIFFUSER.(U)

MAR 80 J F HOLT, J PEARSON

AFWAL-TR-80-2021

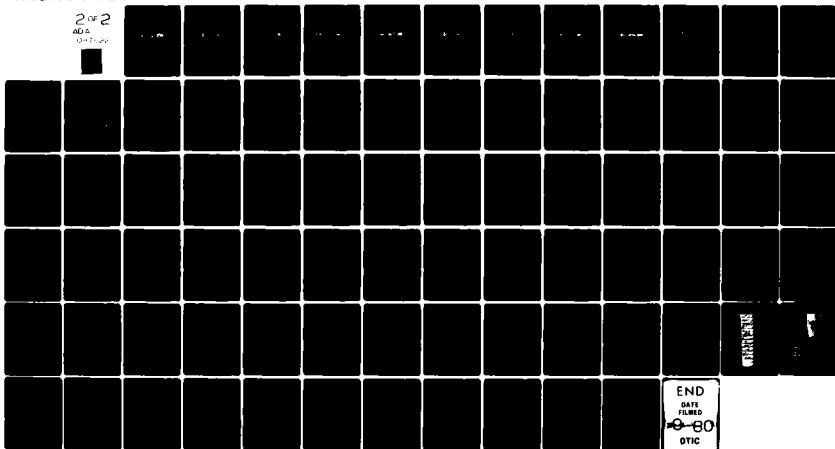
NL

UNCLASSIFIED

2 OF 2

AD-A

011-100



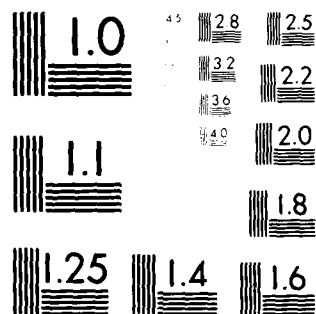
END

DATE

FILMED

9-80

DTIC



MICROCOPY RESOLUTION TEST CHART  
NATIONAL BUREAU OF STANDARDS - 1963-A

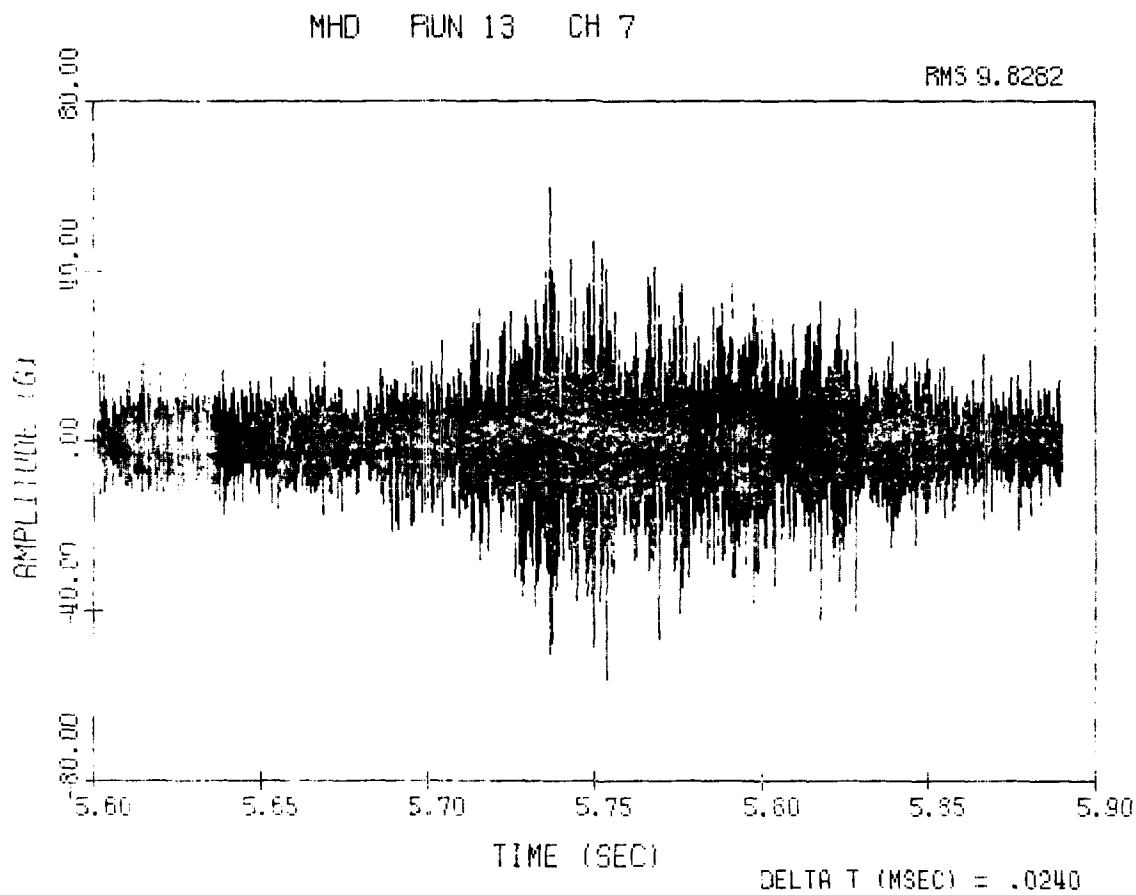


Figure 46. LWC 013, Vibration Amplitude at End of Run, Channel Seven

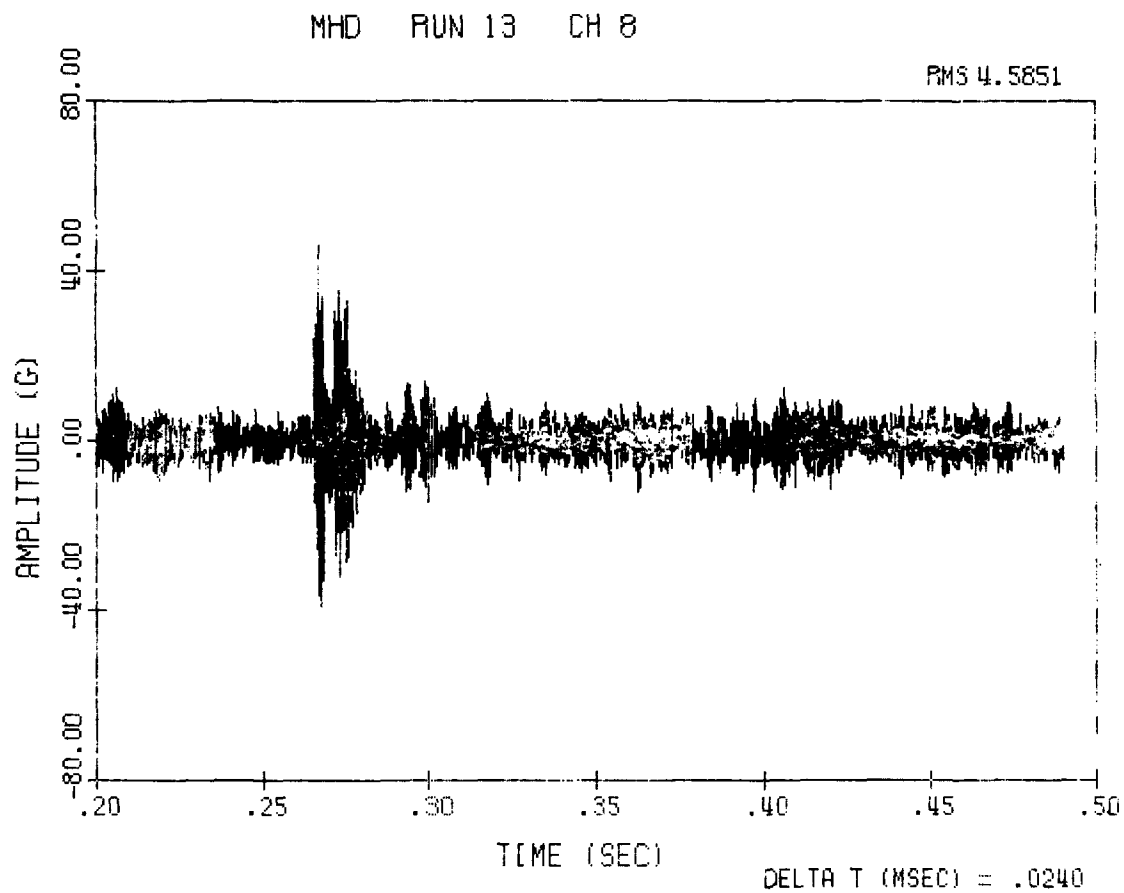


Figure 47. LWC 013, Vibration Amplitude at Beginning of Run, Channel Eight

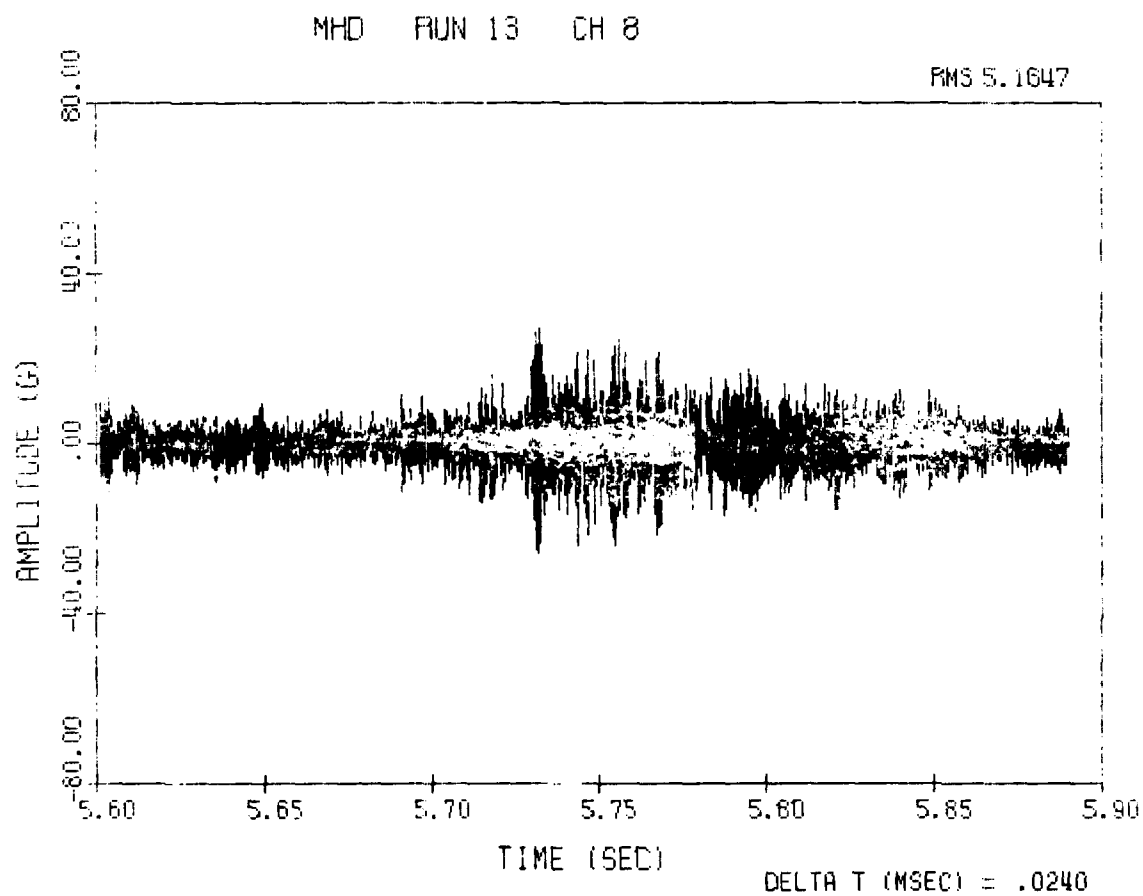


Figure 48. LWC 013, Vibration Amplitude at End of Run, Channel Eight

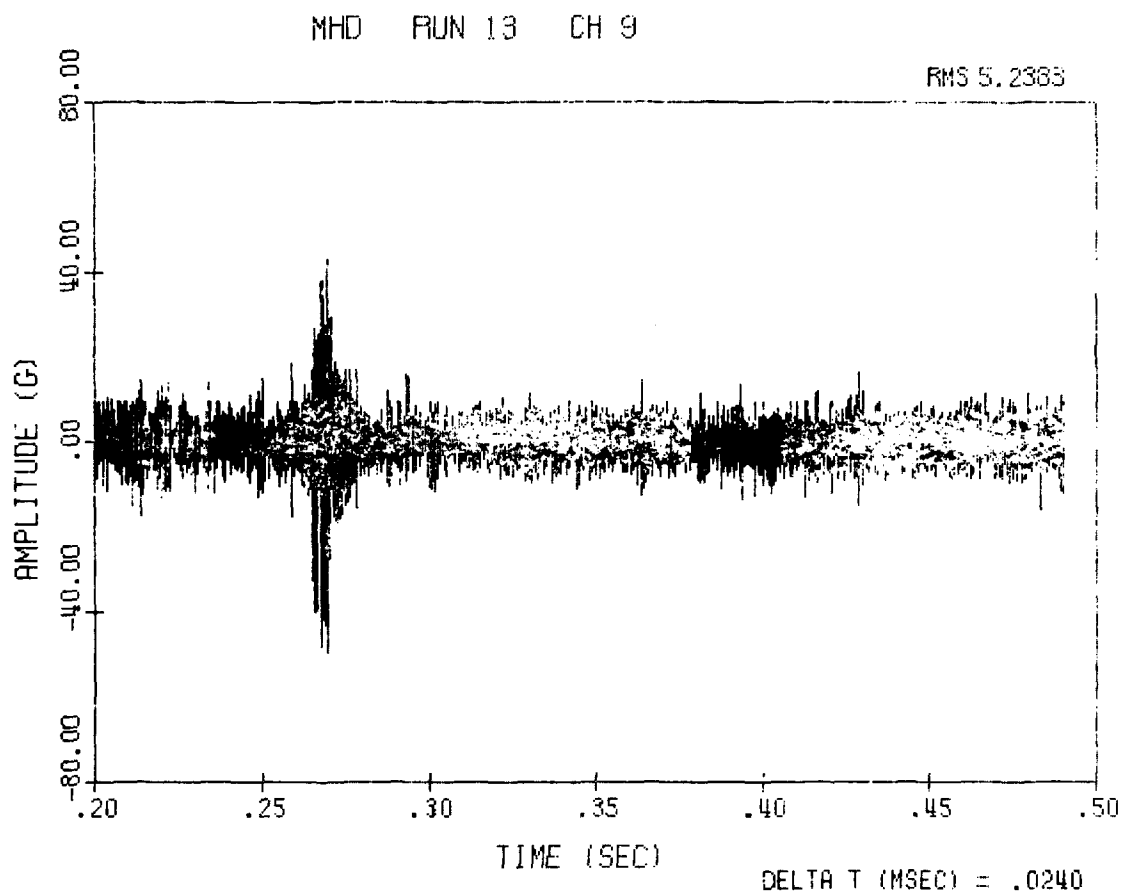


Figure 49. LWC 013, Vibration Amplitude at Beginning of Run, Channel Nine



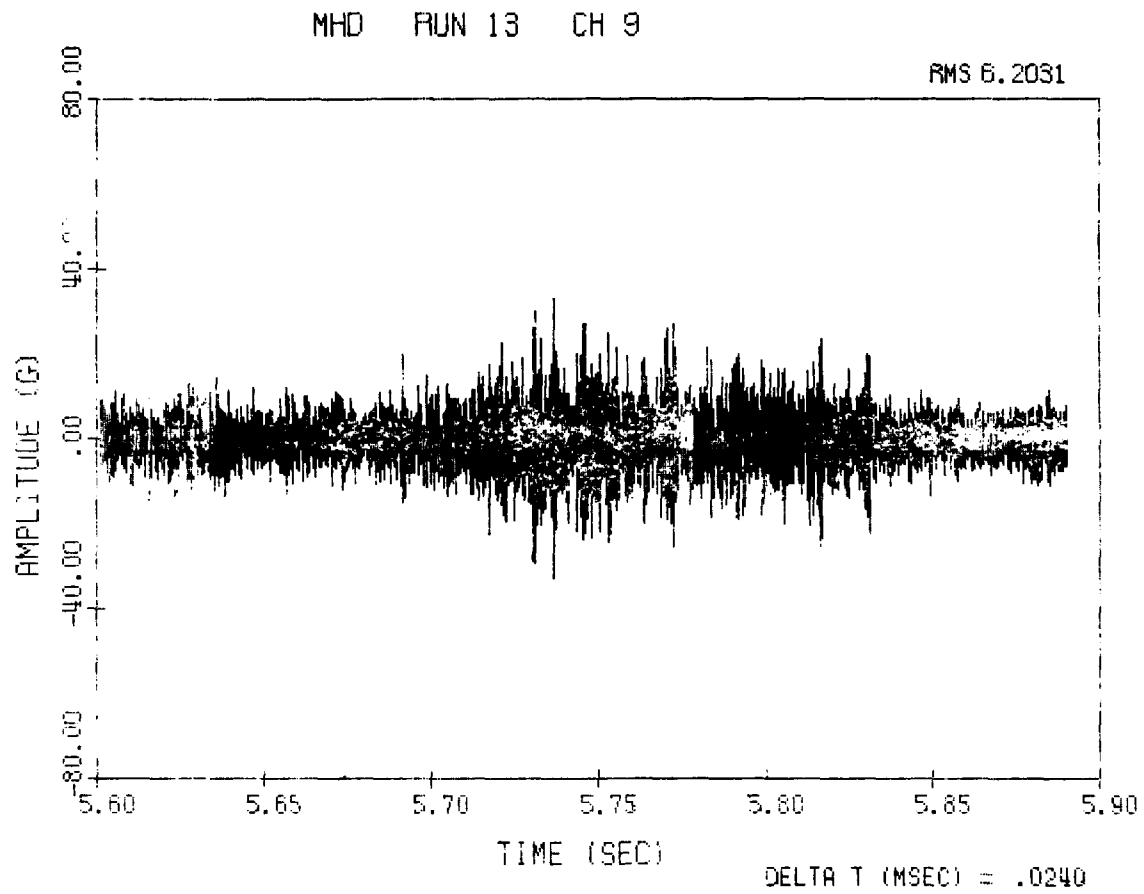


Figure 50. LWC 013, Vibration Amplitude at End of Run, Channel Nine

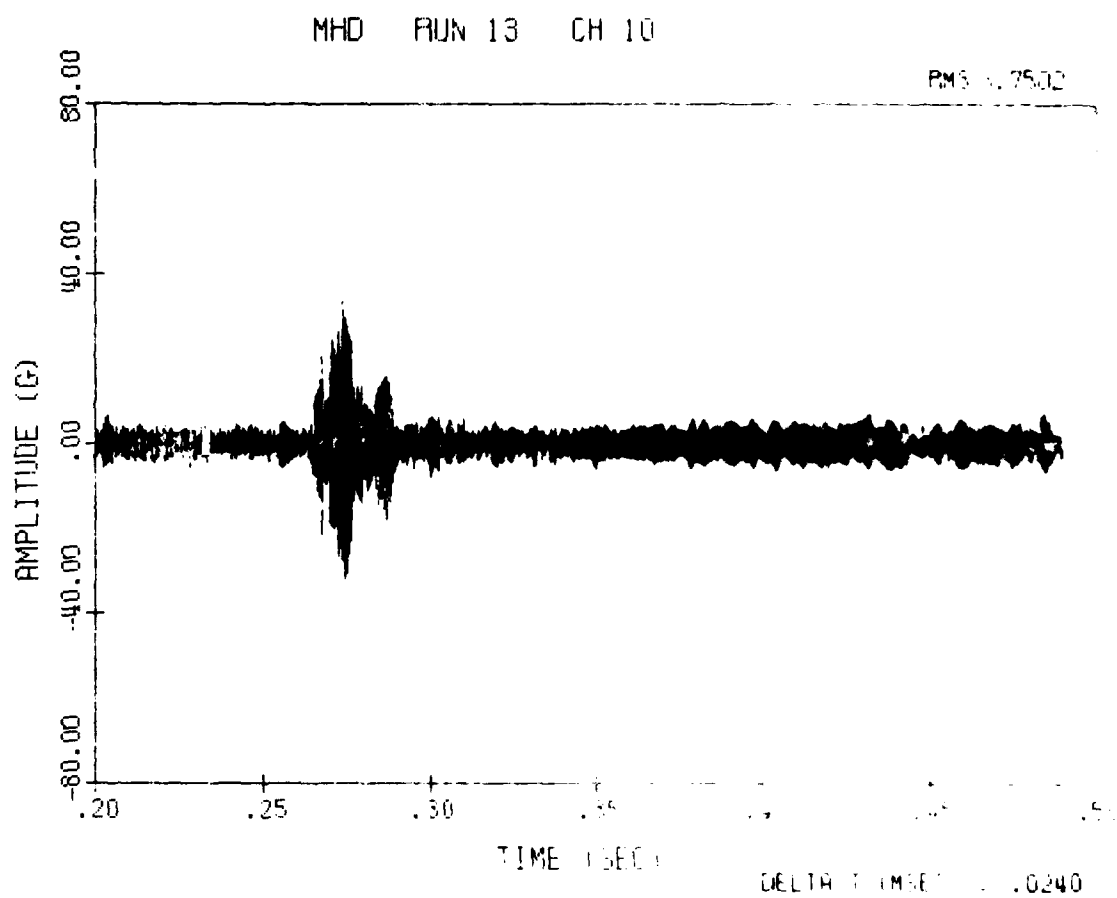


Figure 51. LWC 013, Vibration Amplitude at Beginning of Run, Channel Ten

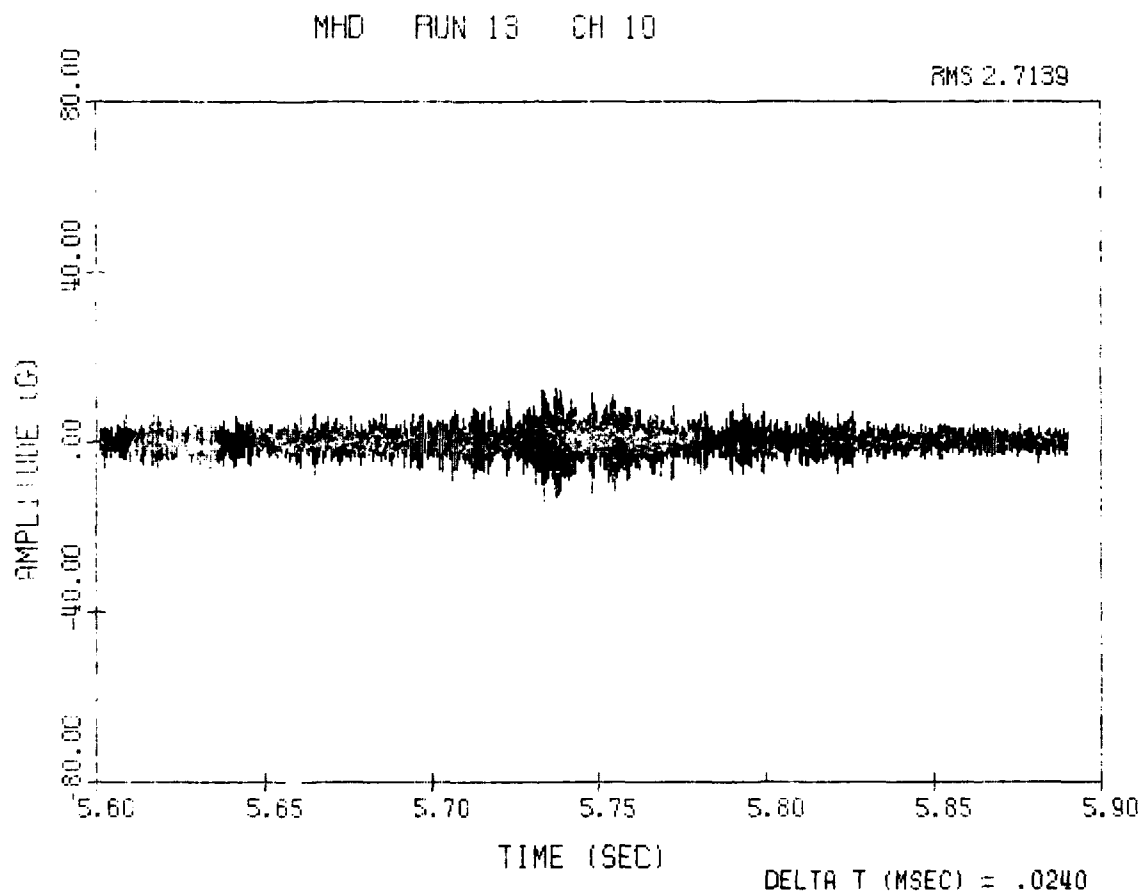


Figure 52. LWC 013, Vibration Amplitude at End of Run, Channel Ten

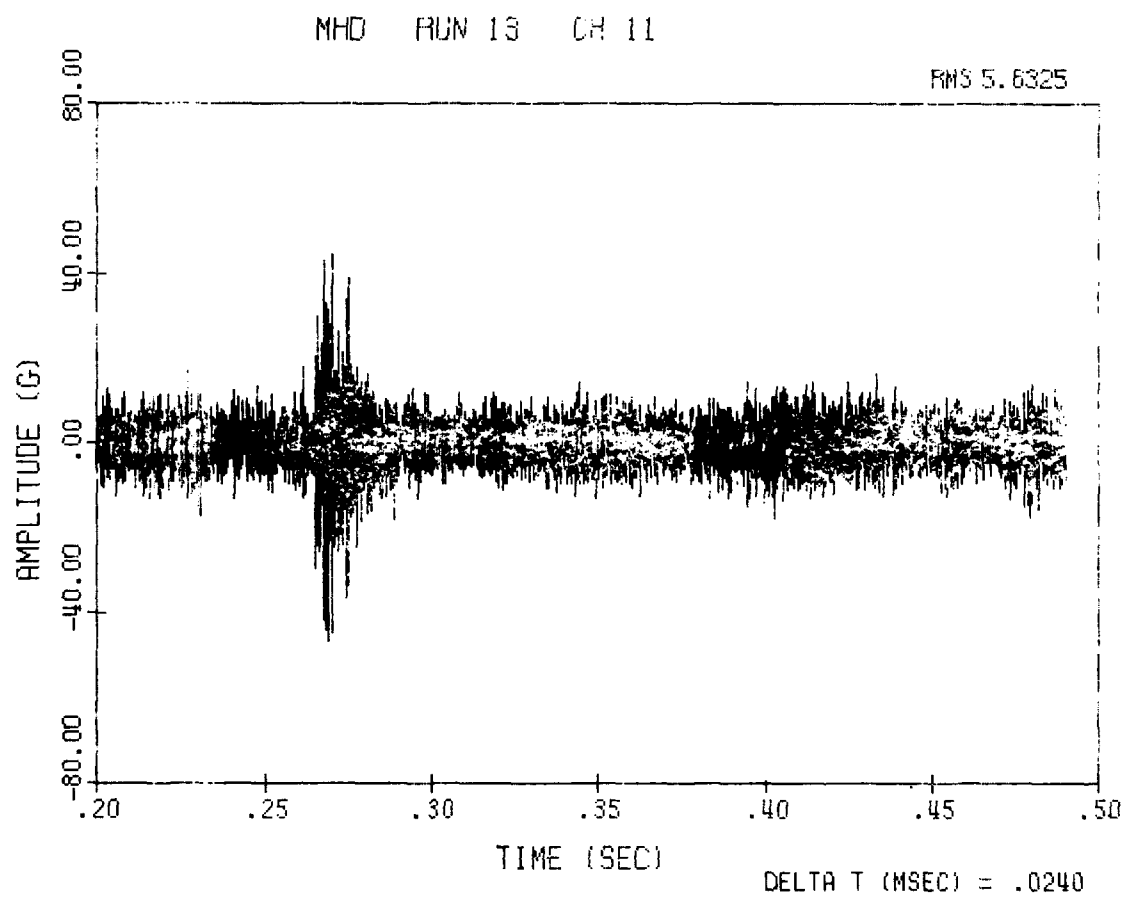


Figure 53. LWC 013, Vibration Amplitude at Beginning of Run, Channel 11

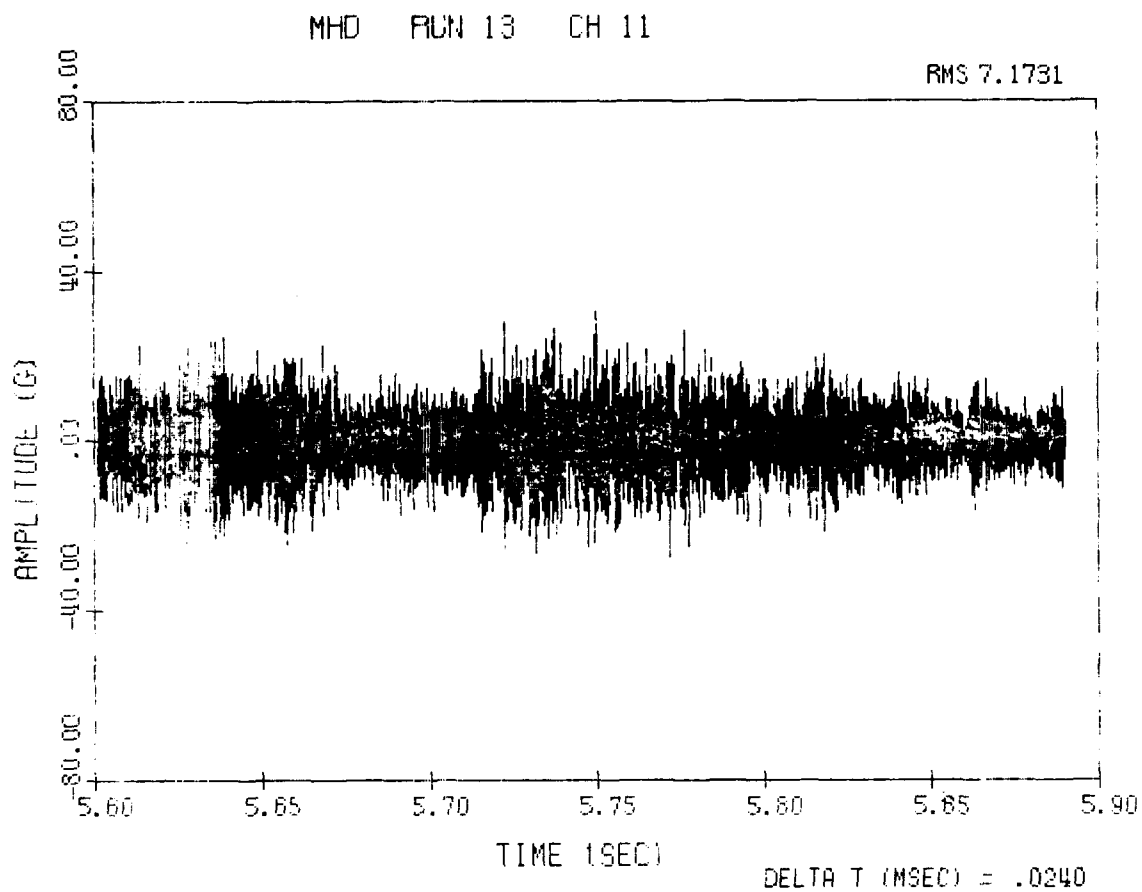


Figure 54. LWC 013, Vibration Amplitude at End of Run, Channel 11

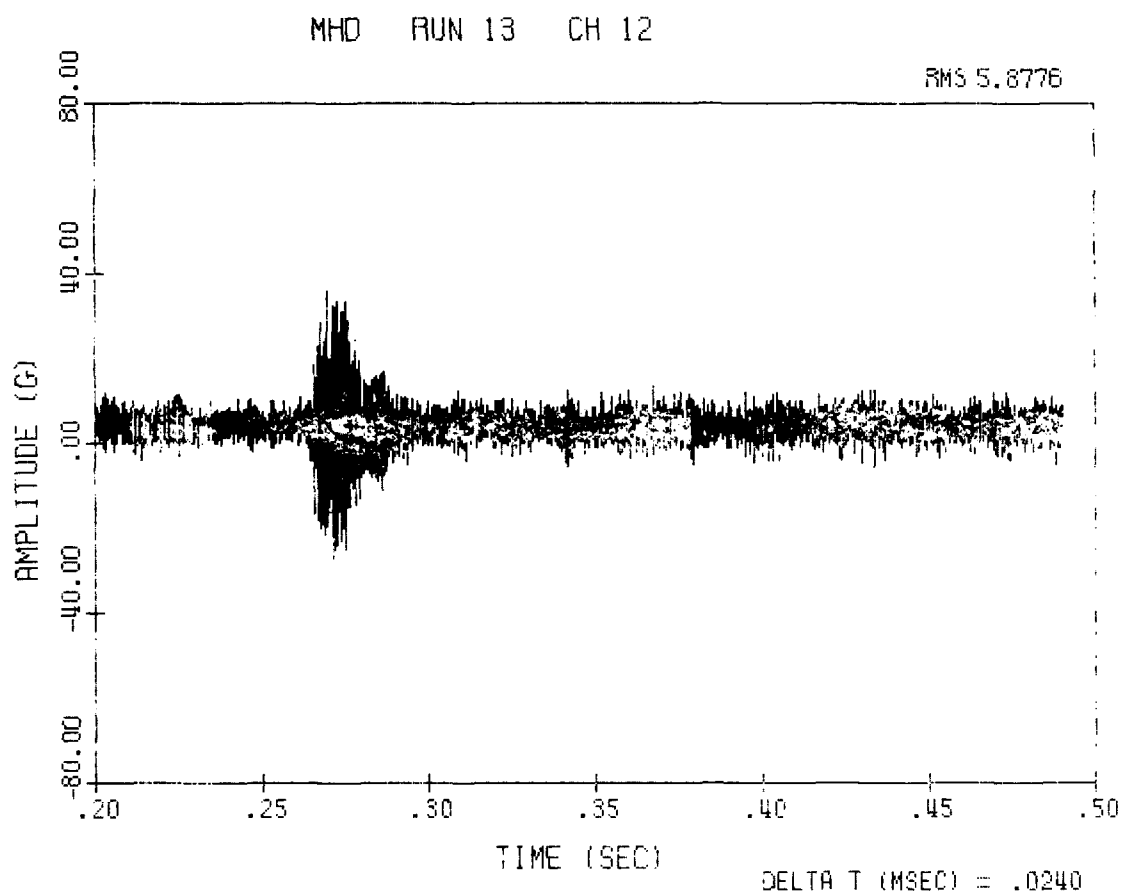


Figure 55. LWC 013, Vibration Amplitude at Beginning of Run, Channel 12

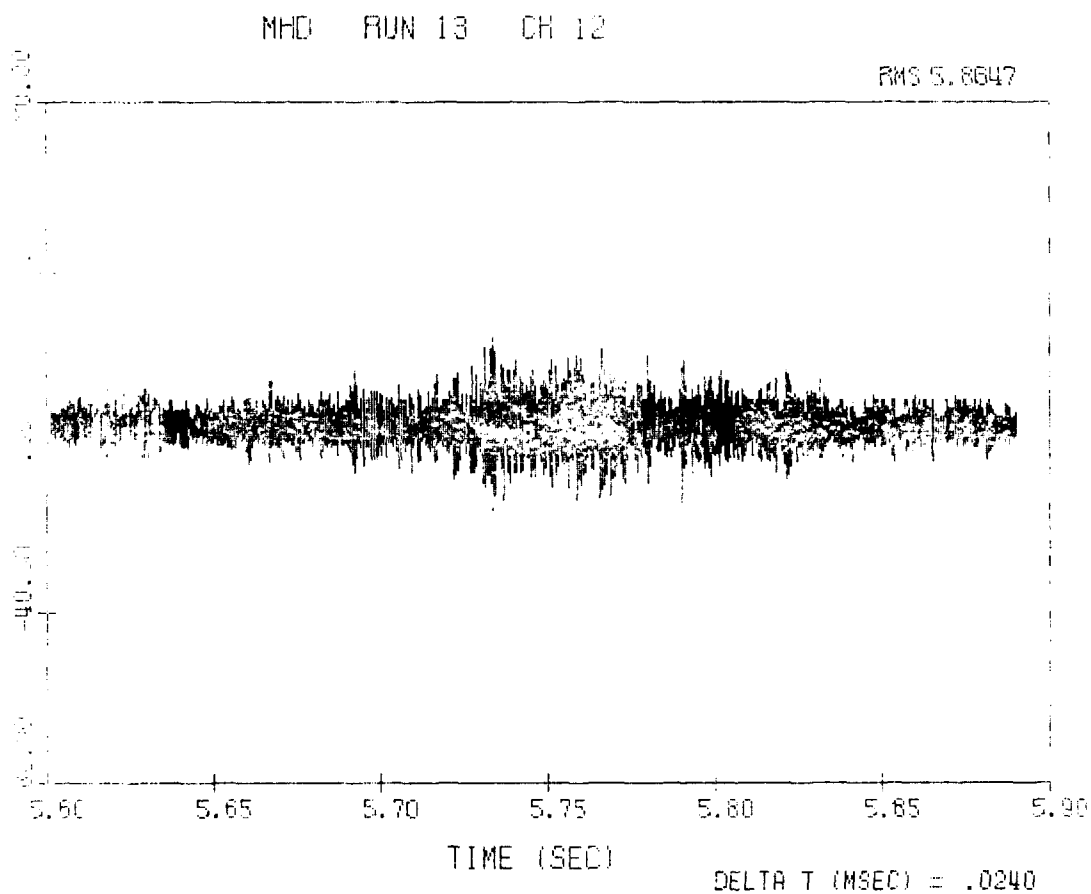


Figure 56. LWC 013, Vibration Amplitude at End of Run, Channel 12

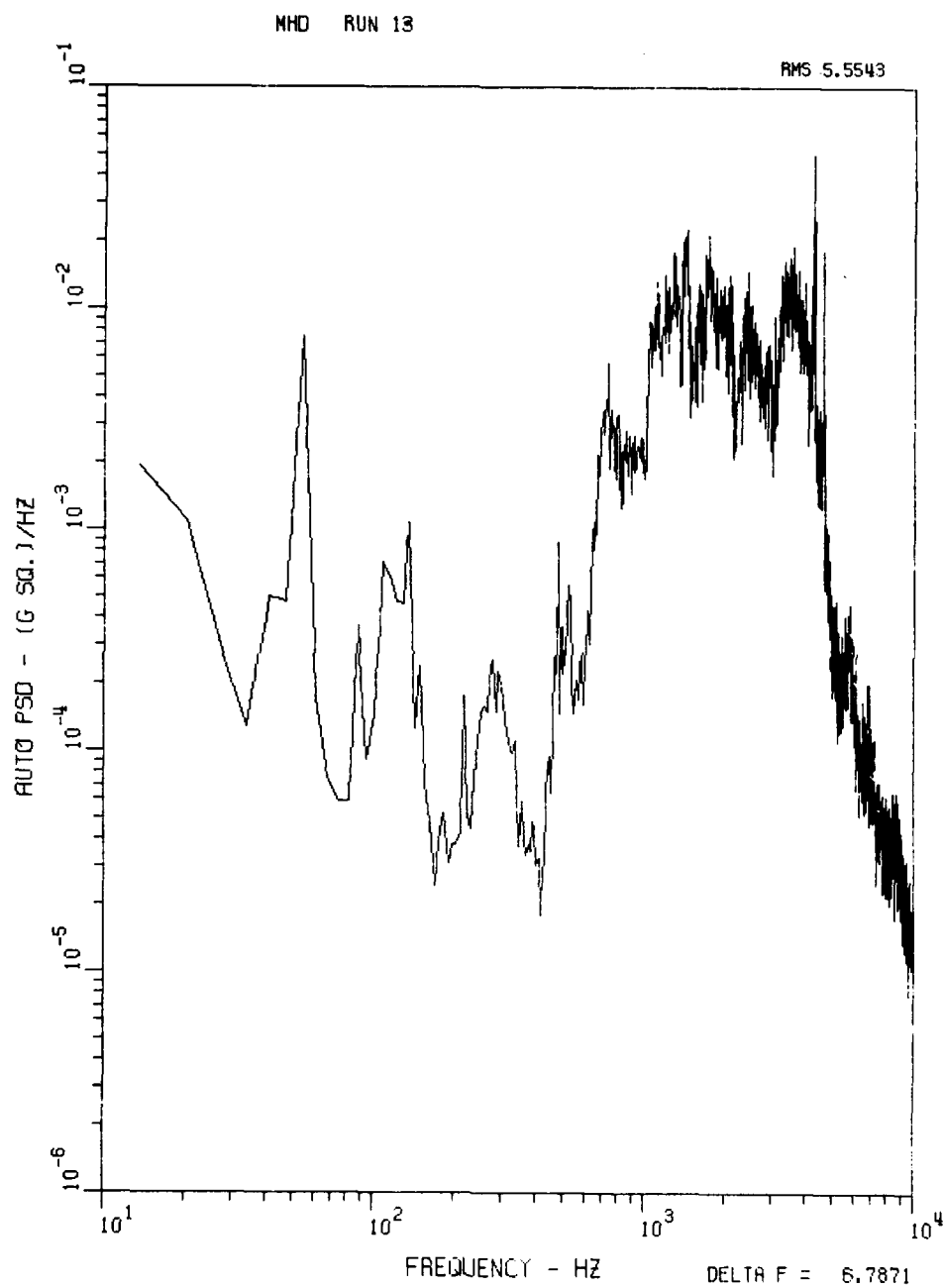


Figure 57. LWC 013, Vibration Power Spectrum for Channel One



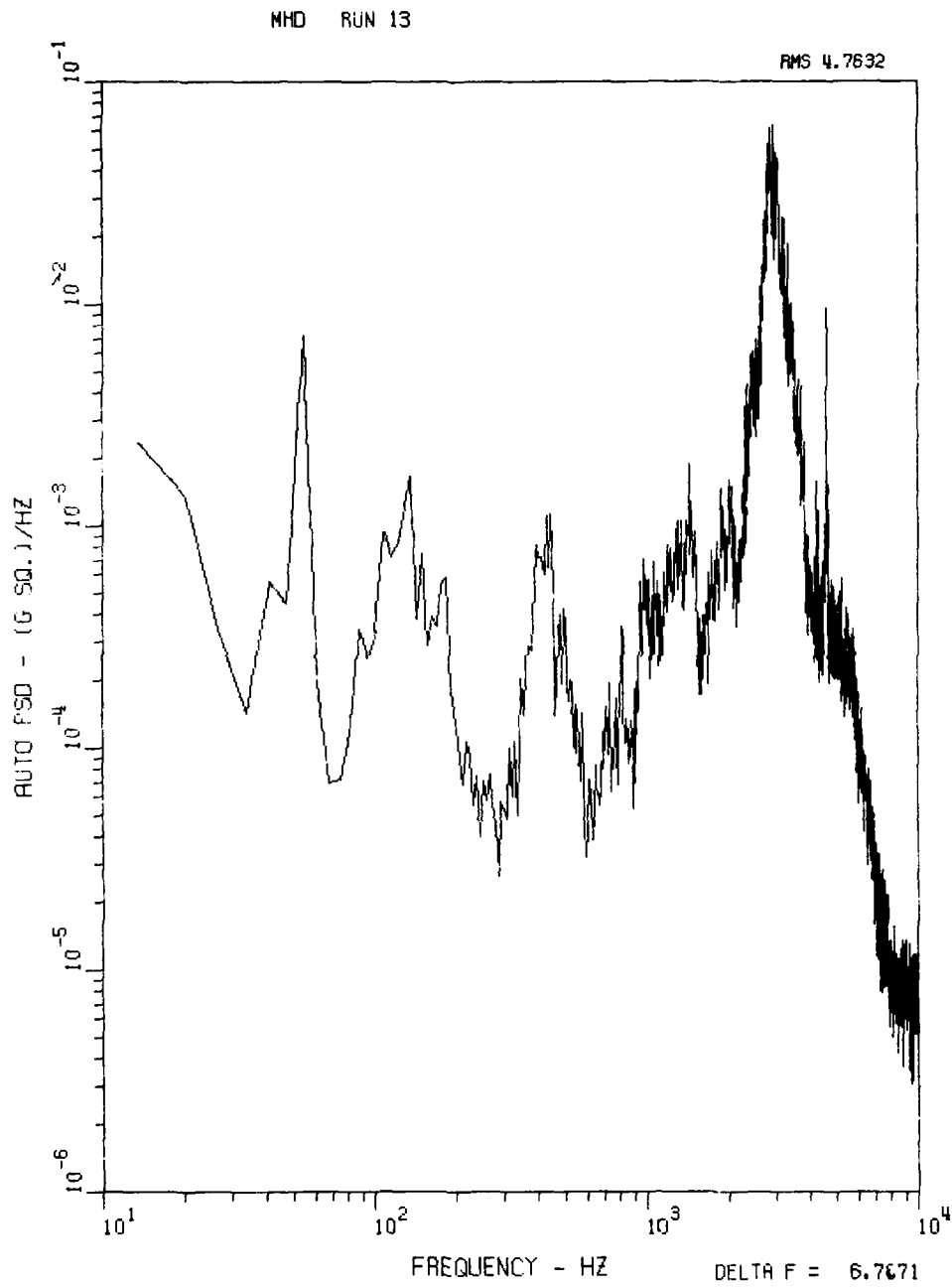


Figure 58. LWC 013, Vibration Power Spectrum for Channel Two

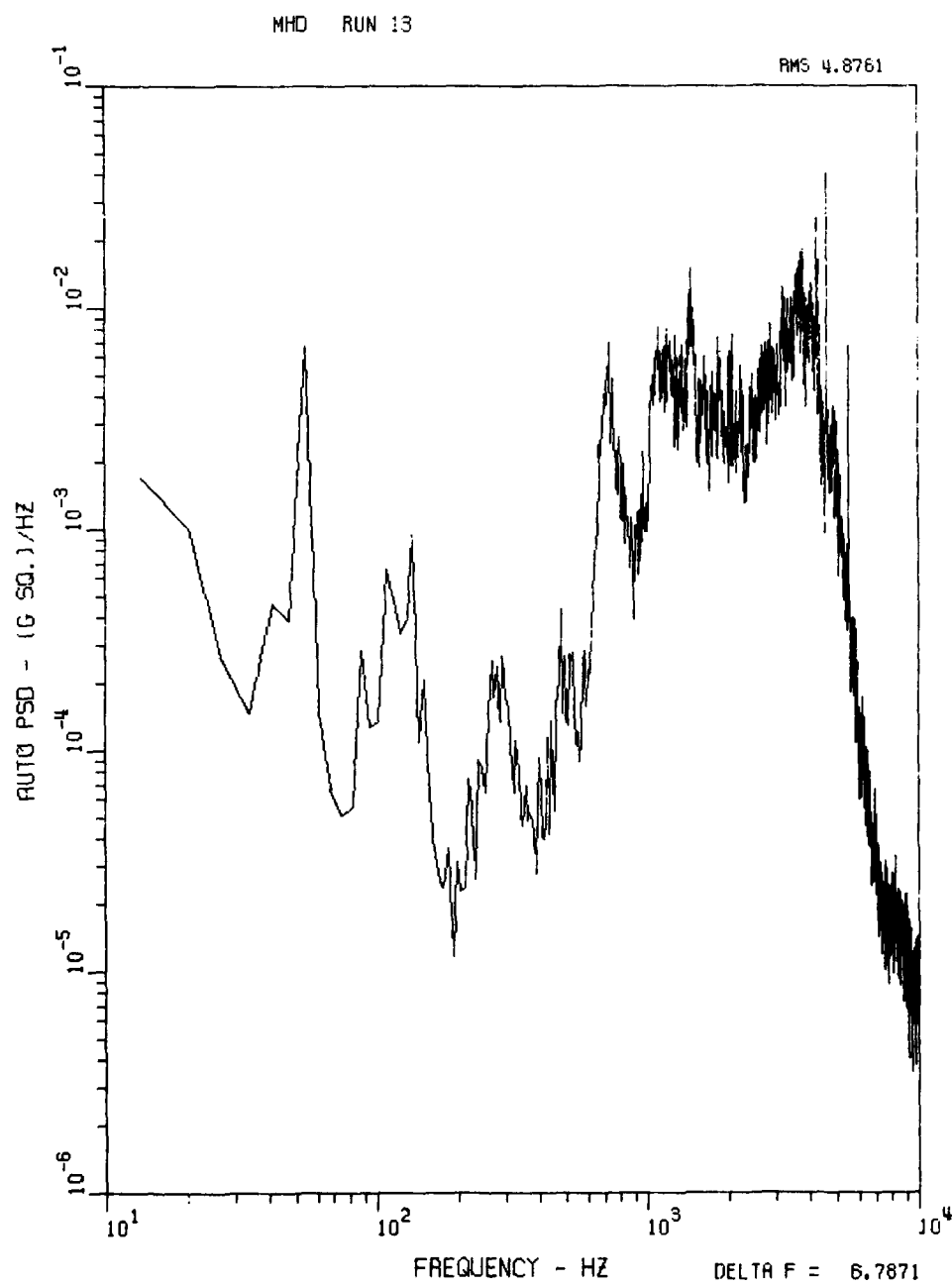


Figure 59. LWC 013, Vibration Power Spectrum for Channel Three

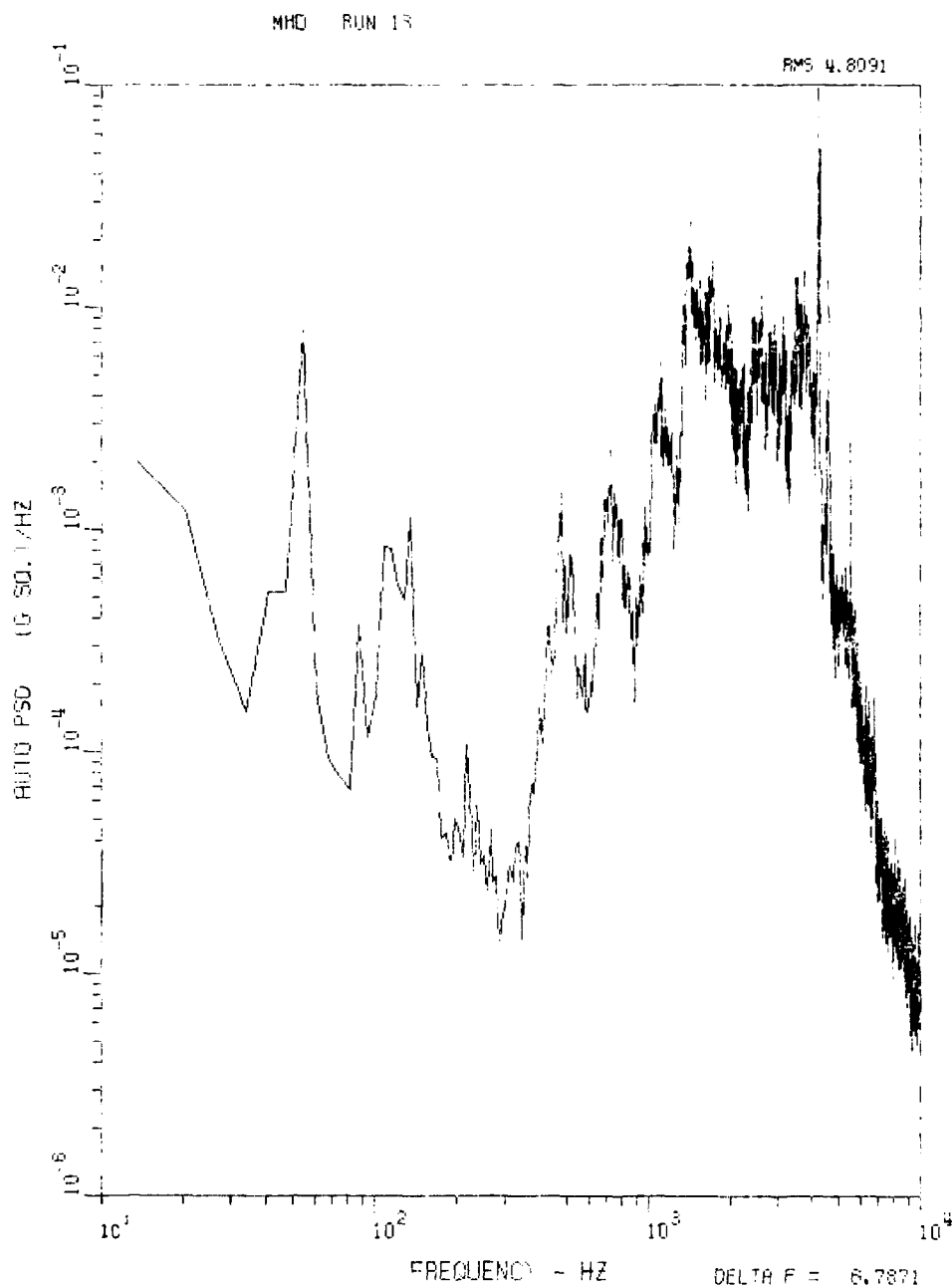


Figure 60. LWC 013, Vibration Power Spectrum for Channel Five

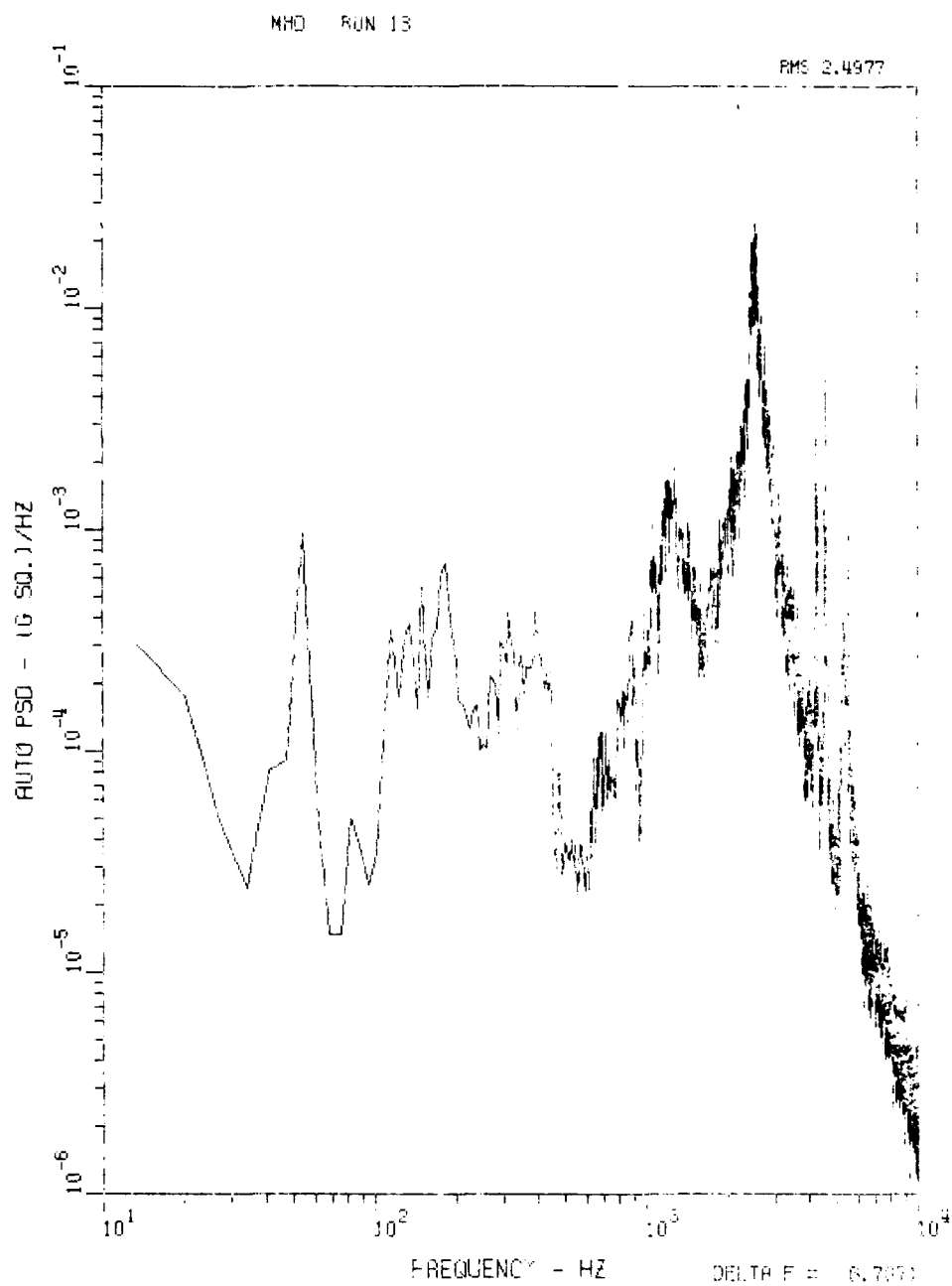


Figure 61. LWC 013, Vibration Power Spectrum for Channel Six

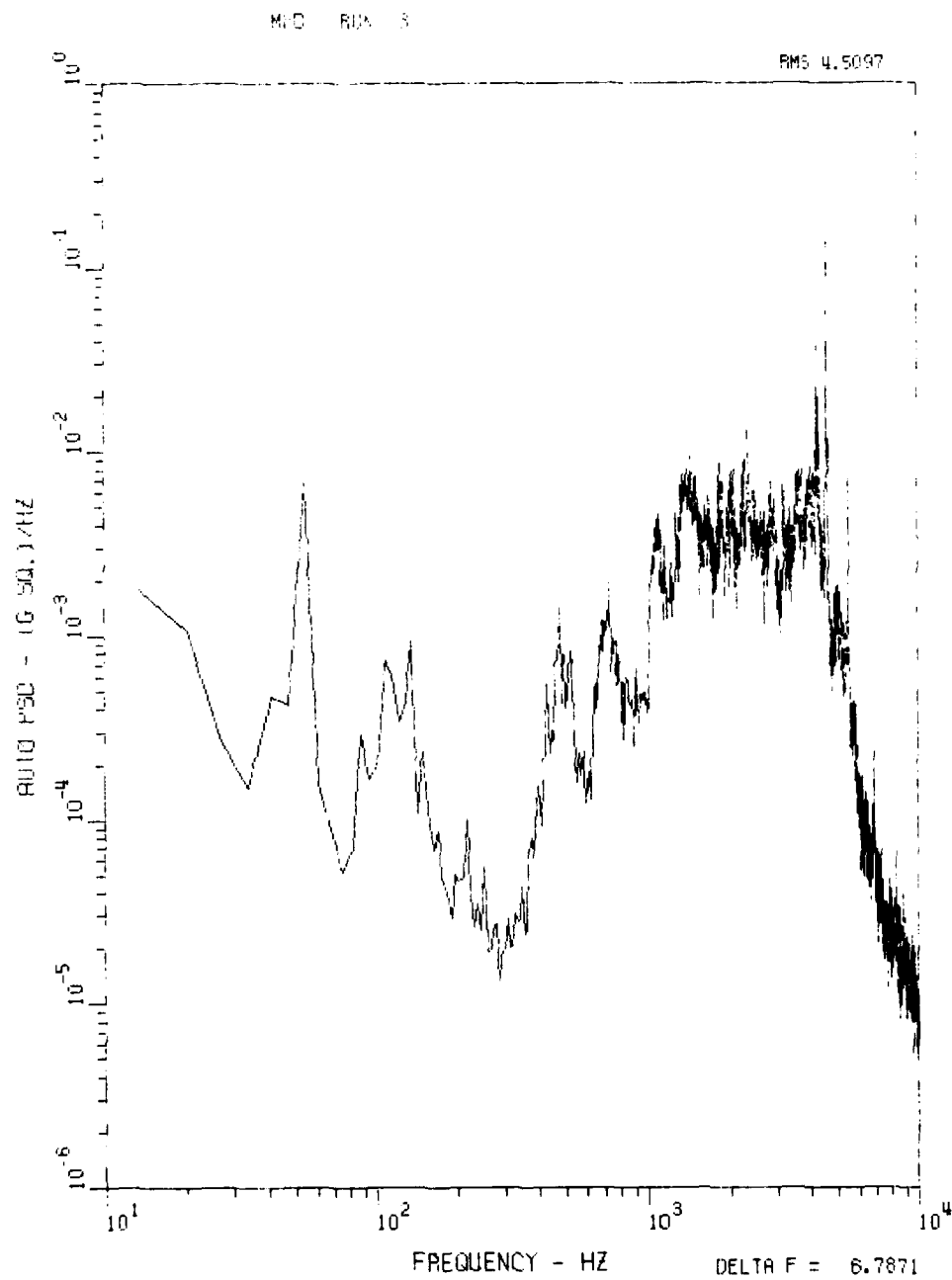


Figure 62. LWC 013, Vibration Power Spectrum for Channel Seven

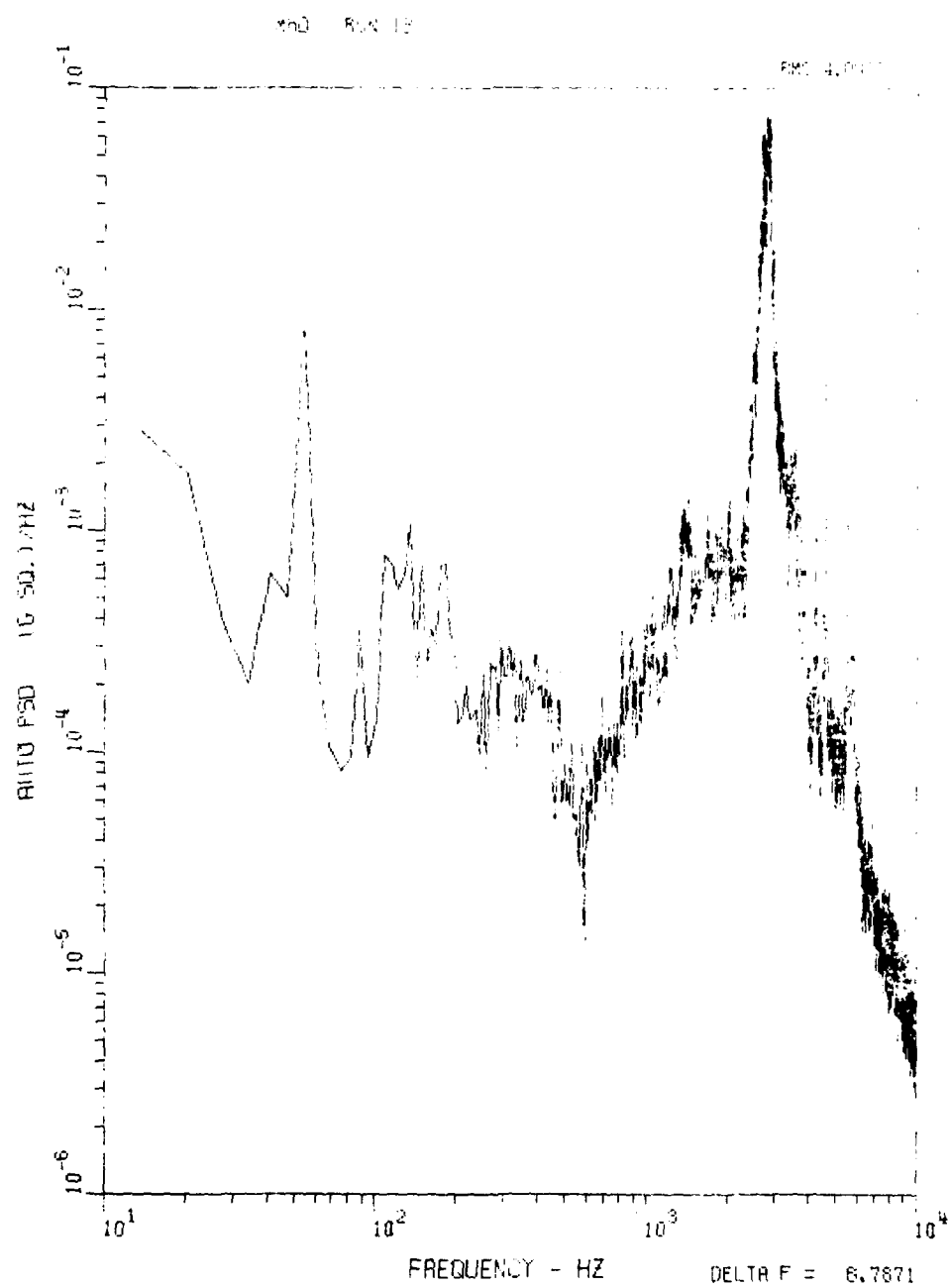


Figure 63. LWC 013, Vibration Power Spectrum for Channel Eight

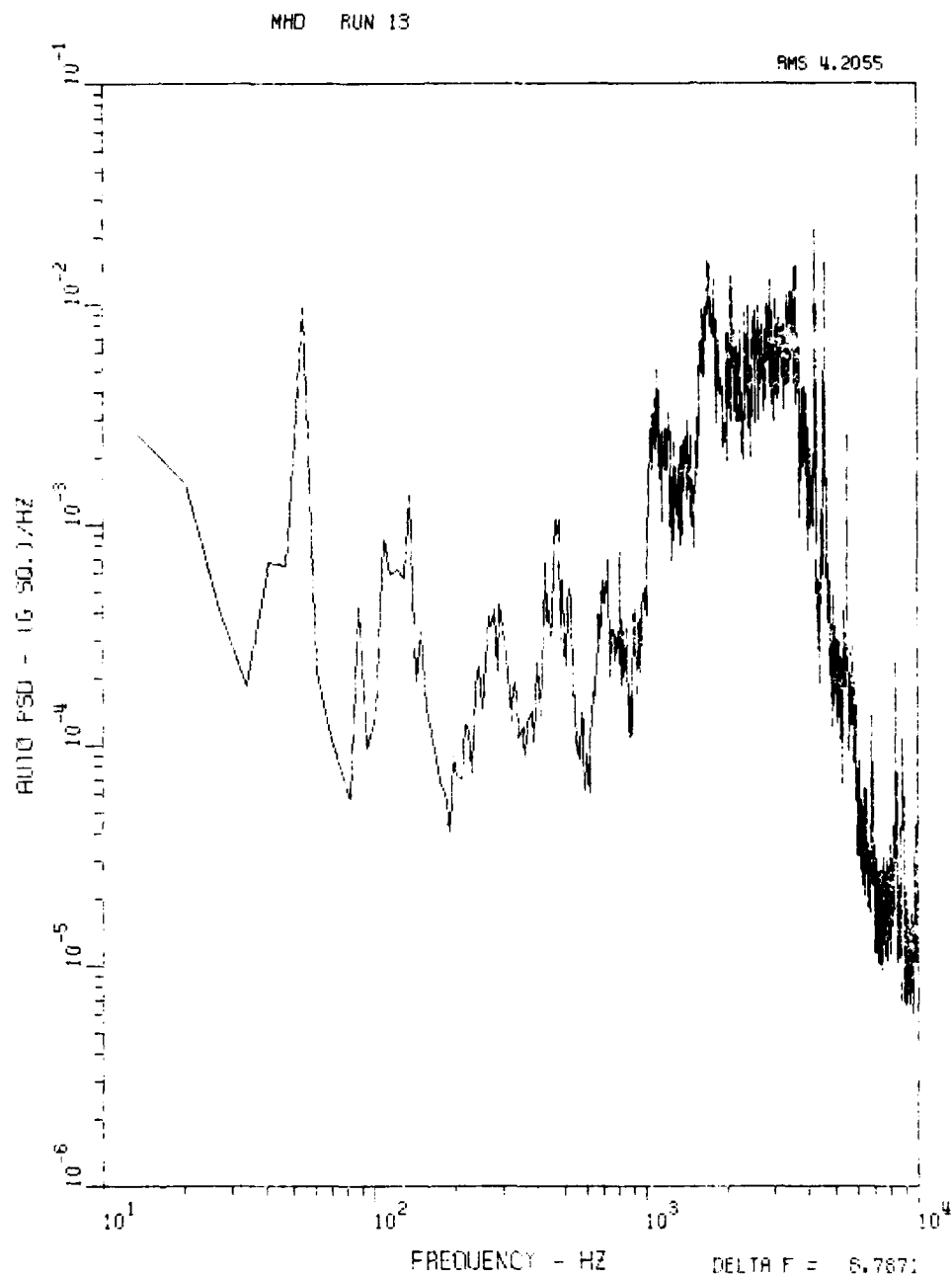


Figure 64. LWC 013, Vibration Power Spectrum for Channel Nine

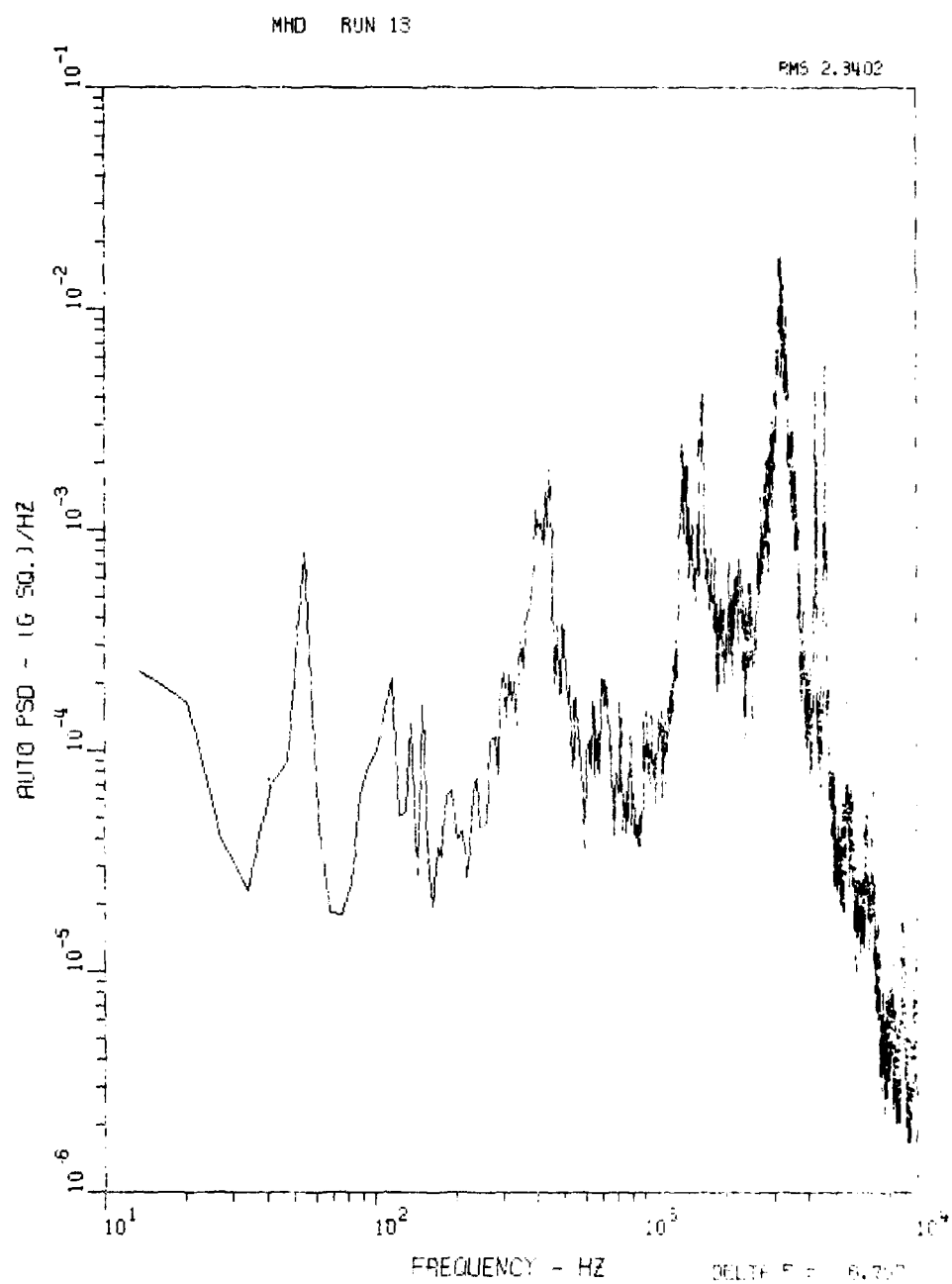


Figure 65. LWC 013, Vibration Power Spectrum for Channel Ten



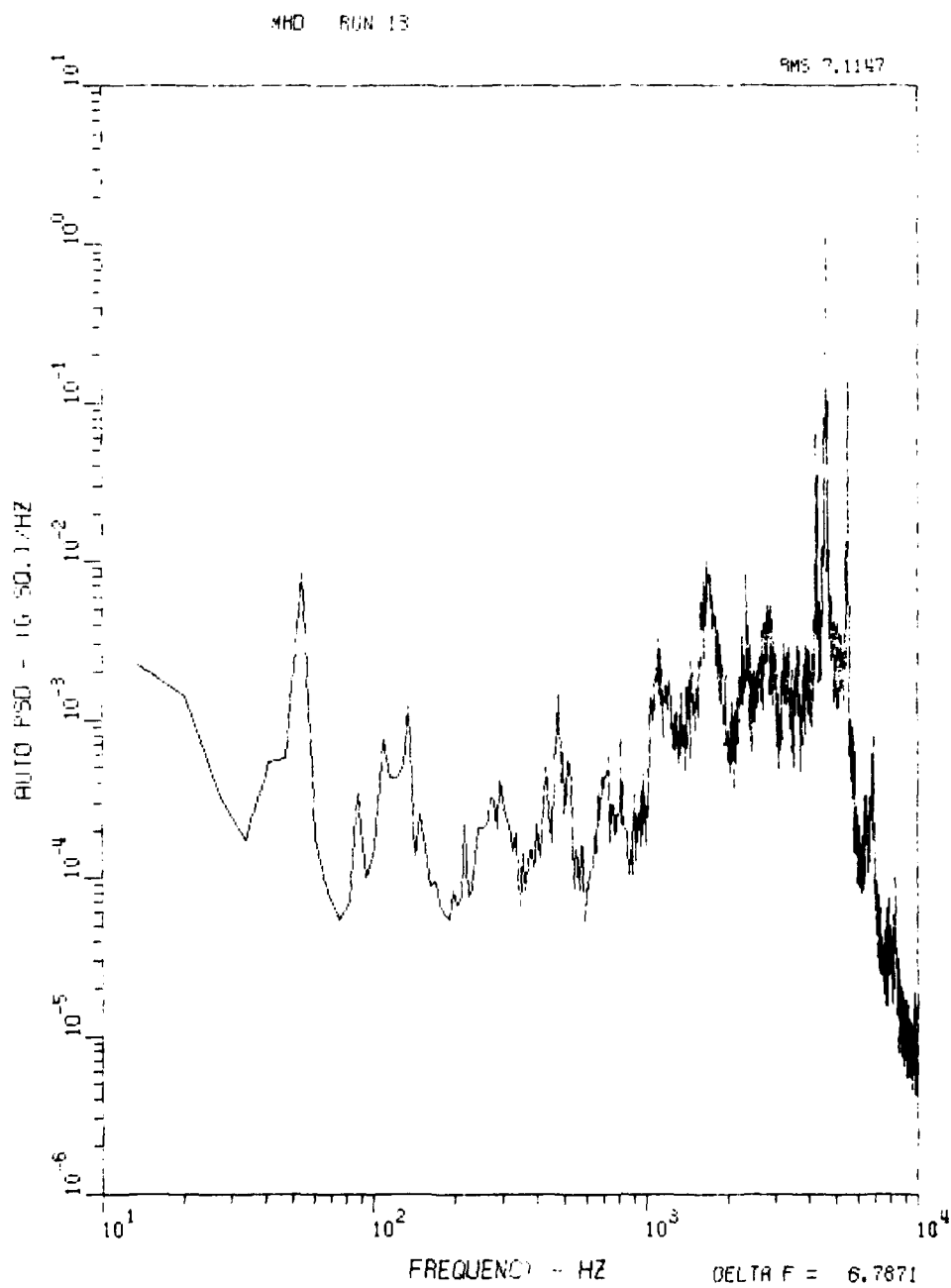


Figure 66. LWC 013, Vibration Power Spectrum for Channel Eleven

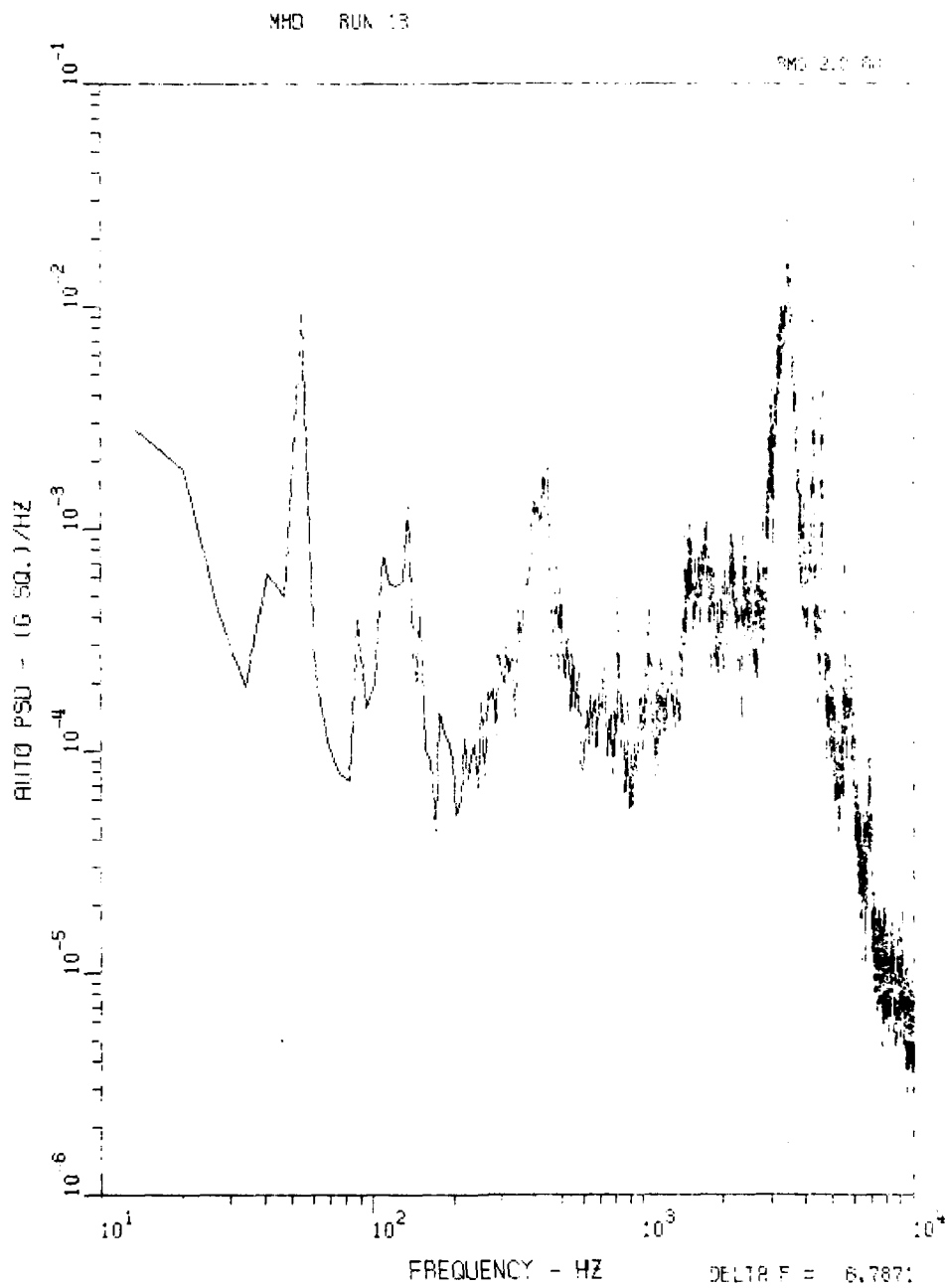


Figure 67. LWC 013, Vibration Power Spectrum for Channel Twelve

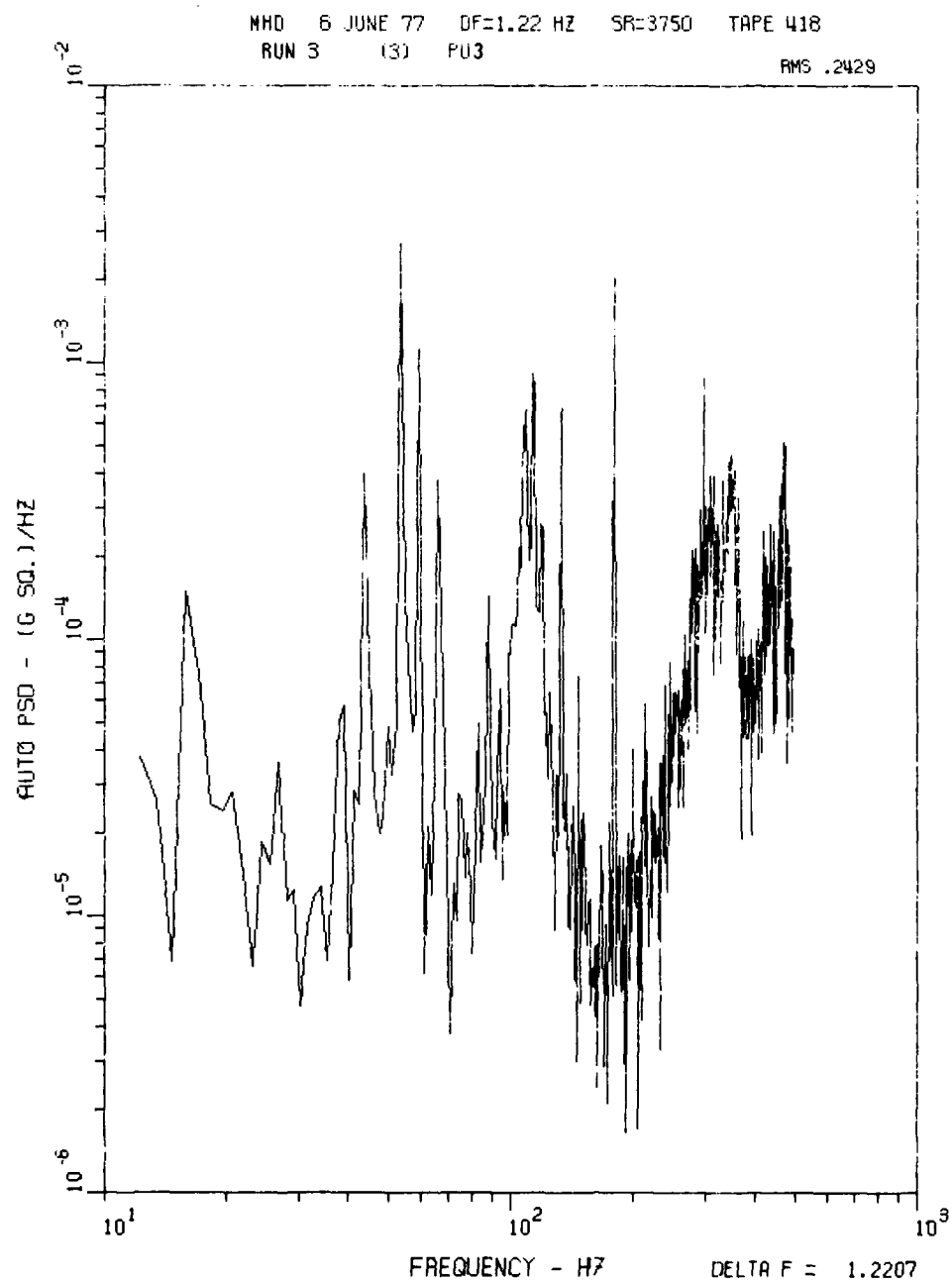


Figure 68. Accelerometer 3 PSD, 0-500 Hz, Run LWC 003

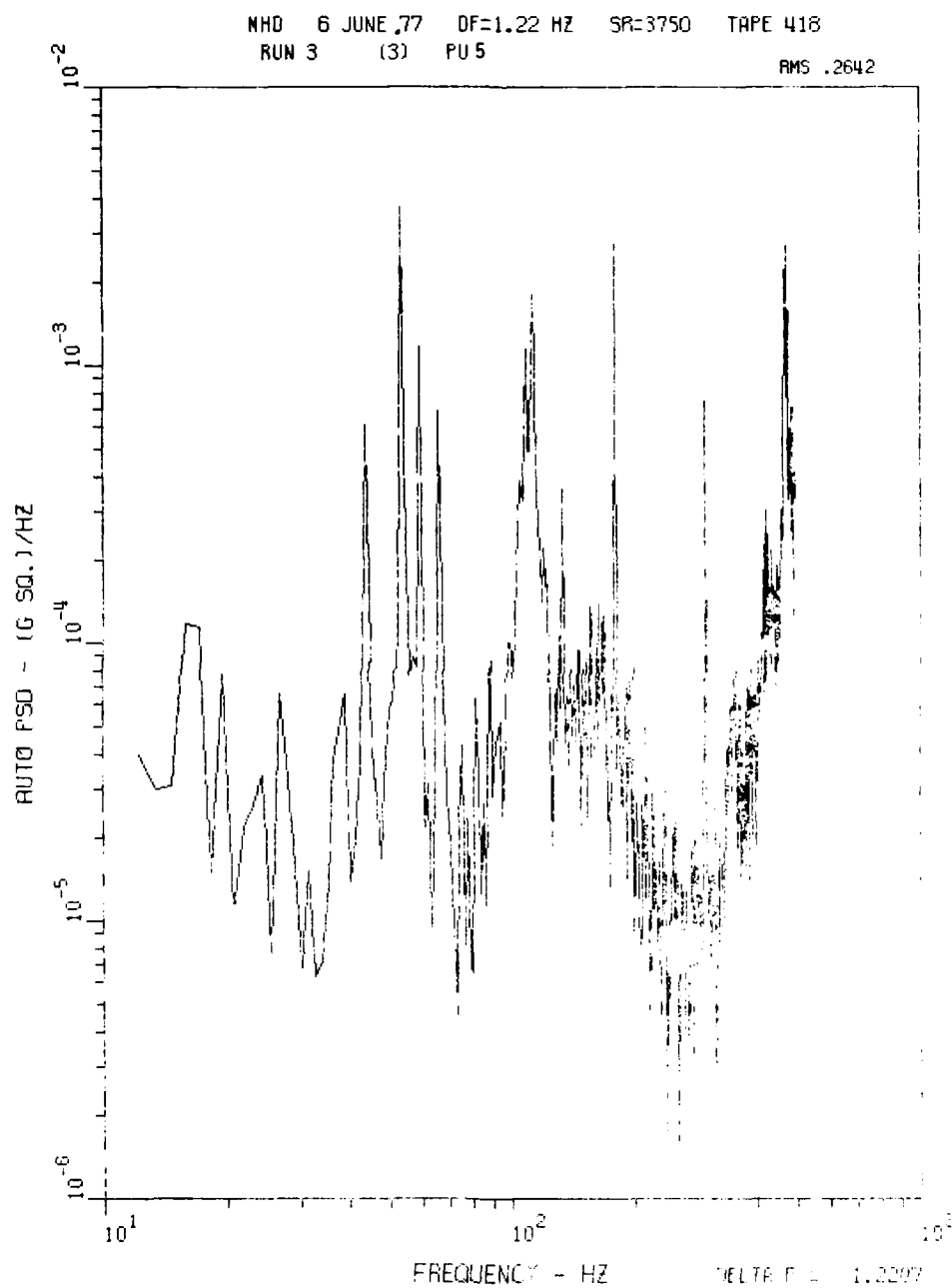


Figure 69. Channel Five PSD, 0-500 Hz, Run LWC 003

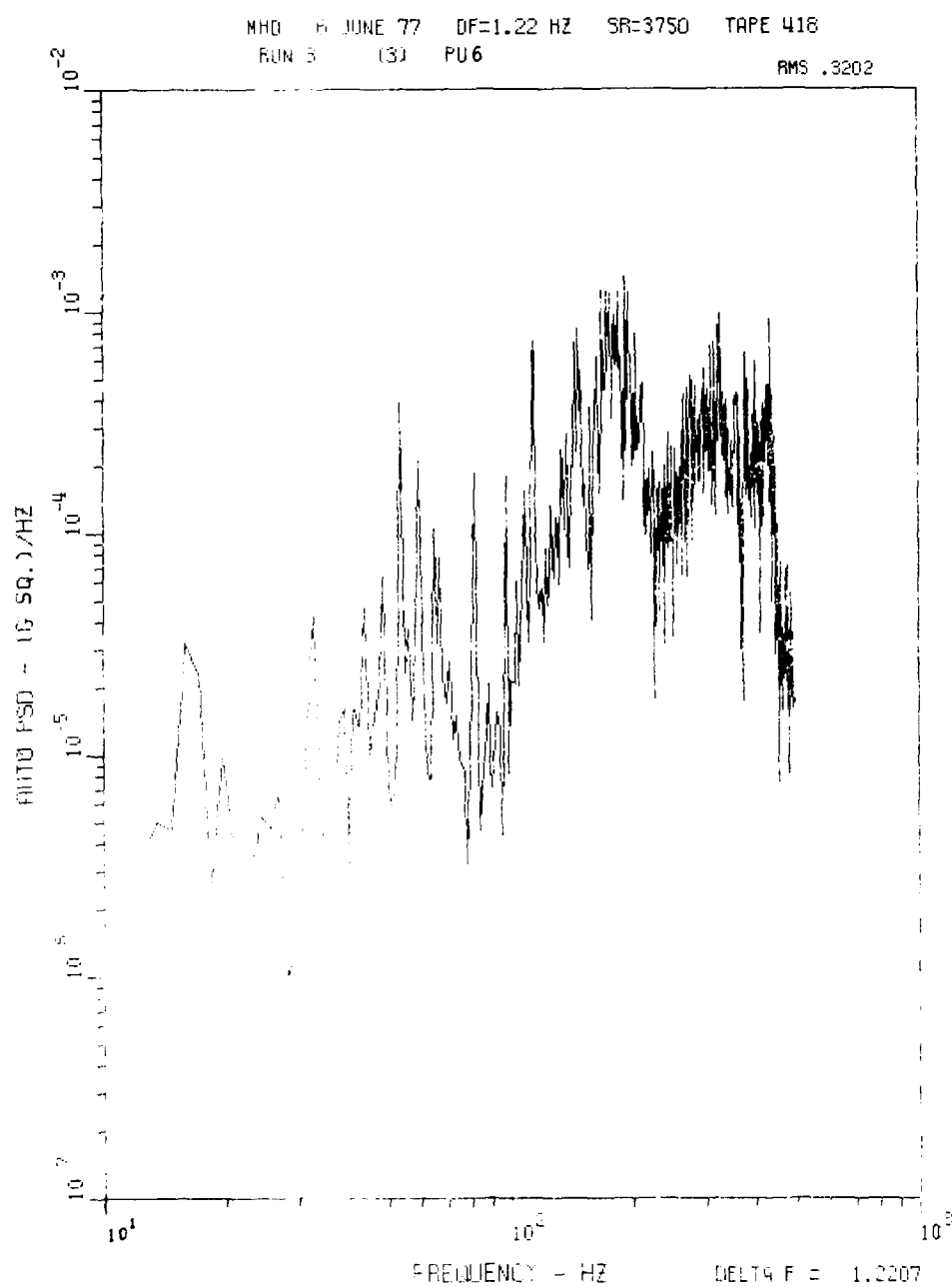


Figure 70. Channel Six PSD, 0-500 Hz, Run LWC 003

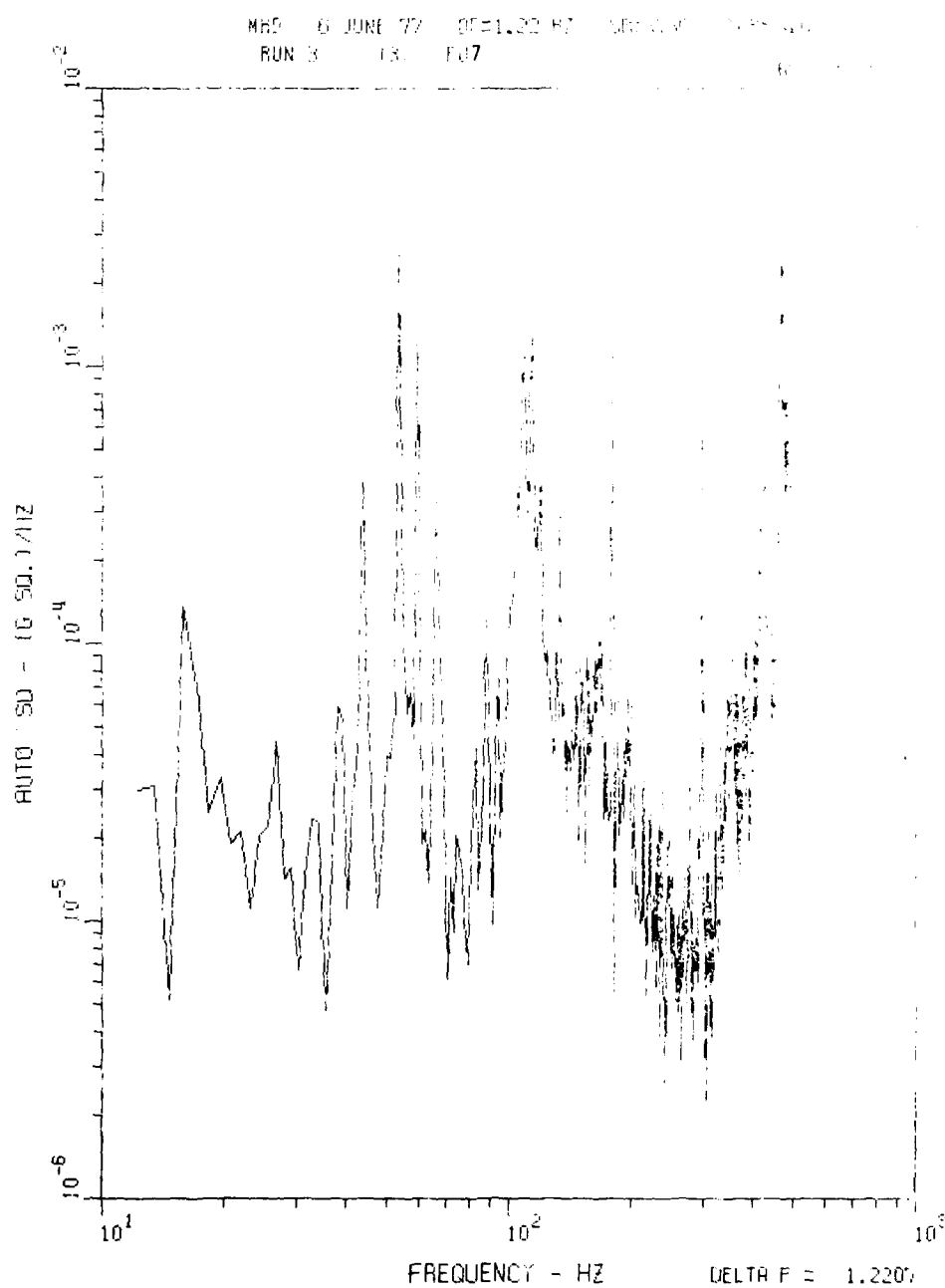


Figure 71. Channel Seven PSD, 0-500 Hz, run LWC 003

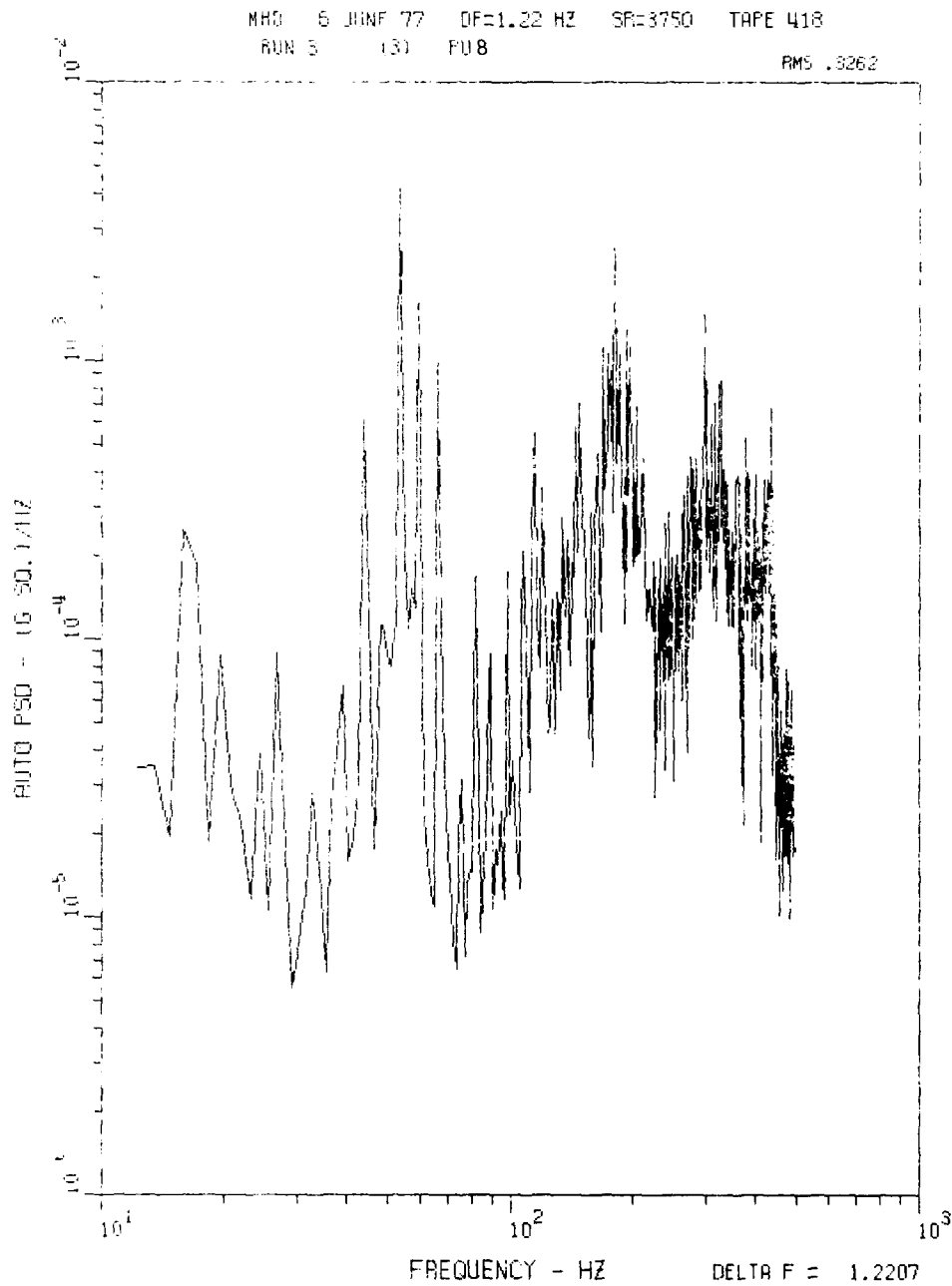


Figure 72. Channel Eight PSD, 0-500 Hz, Run LWC 003

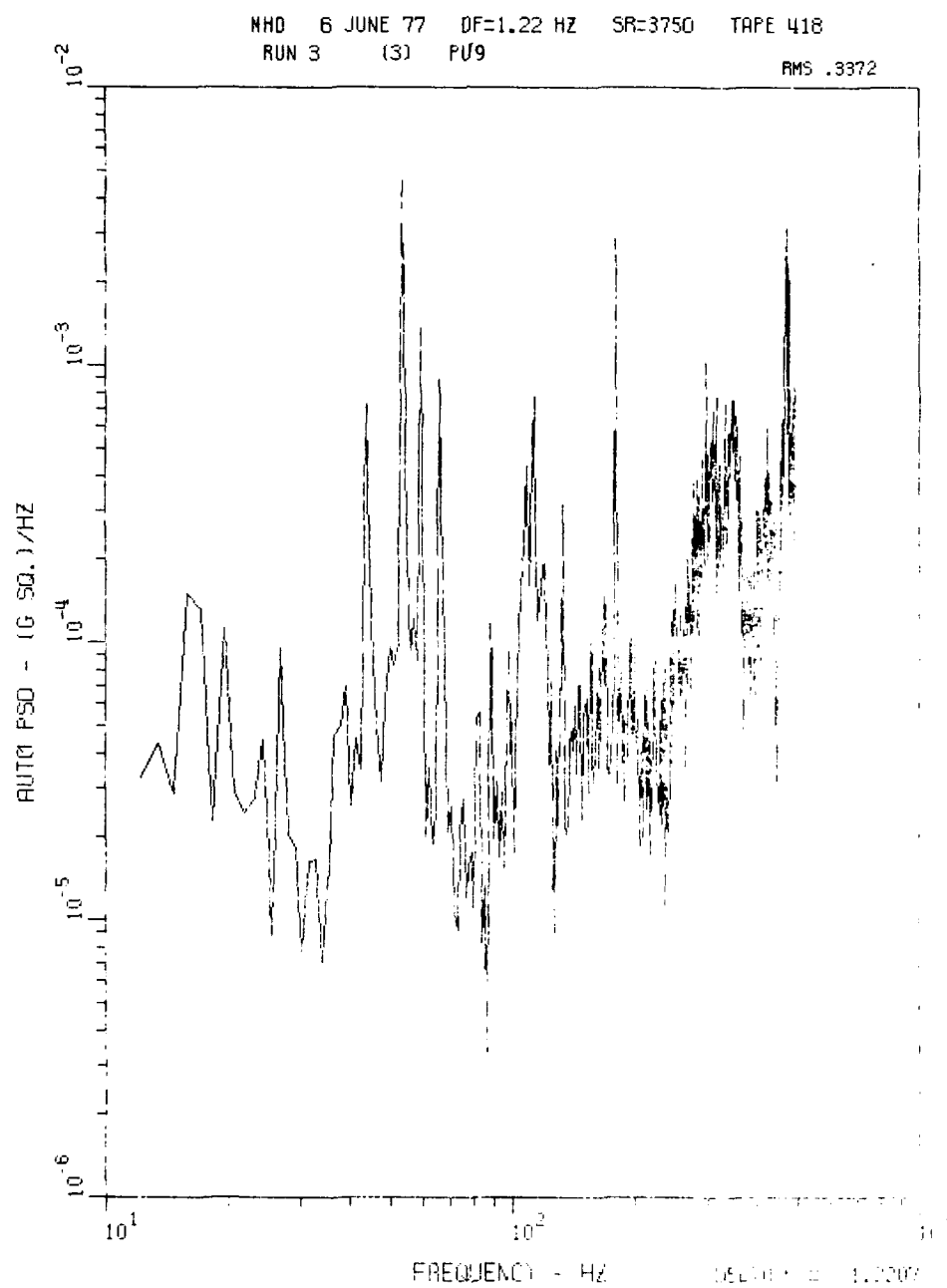


Figure 73. Channel Nine PSD, 0-500 Hz, Run LWC 003



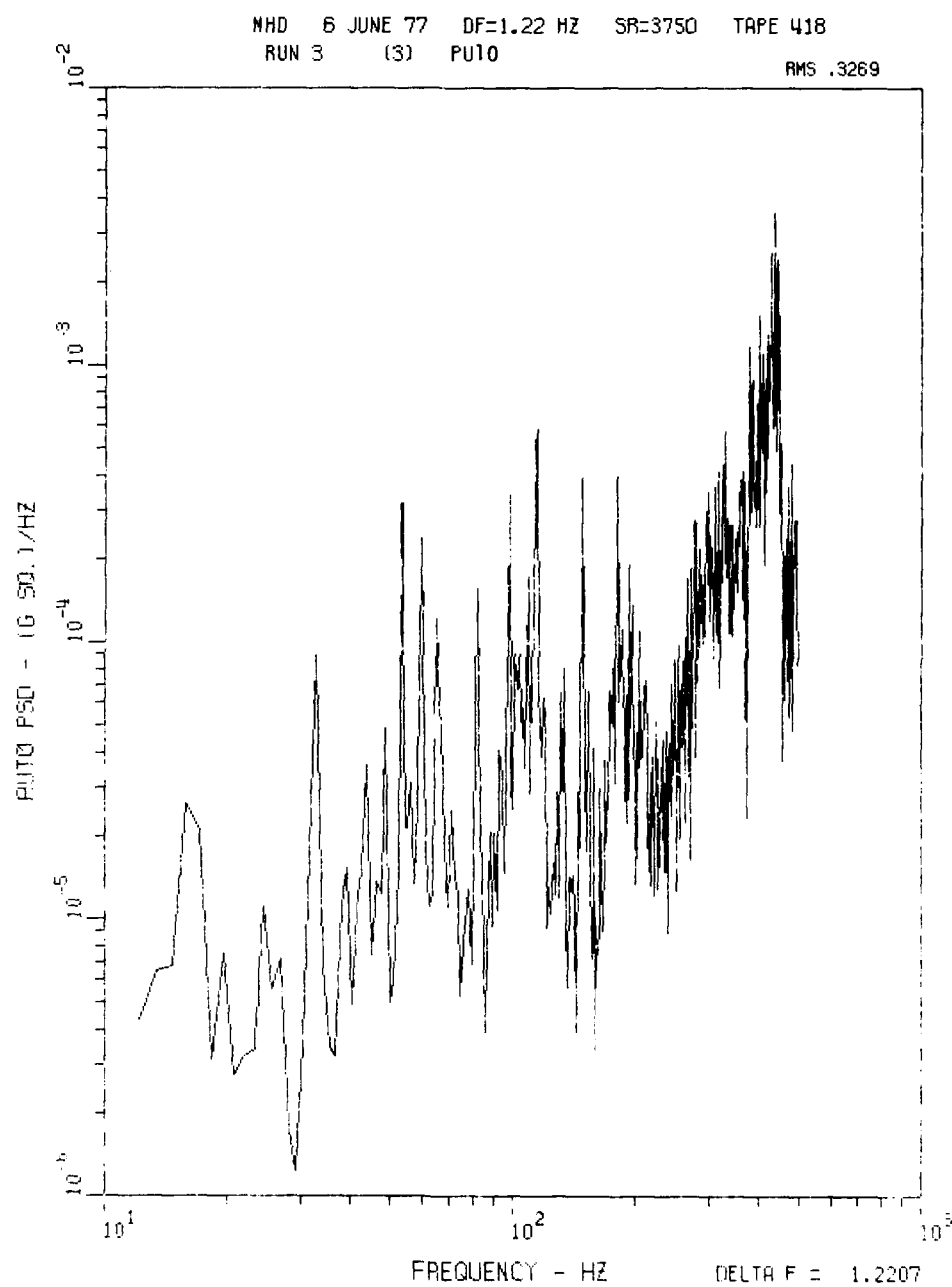


Figure 74. A Channel Ten PSD, 0-500 Hz, Run LWC 003

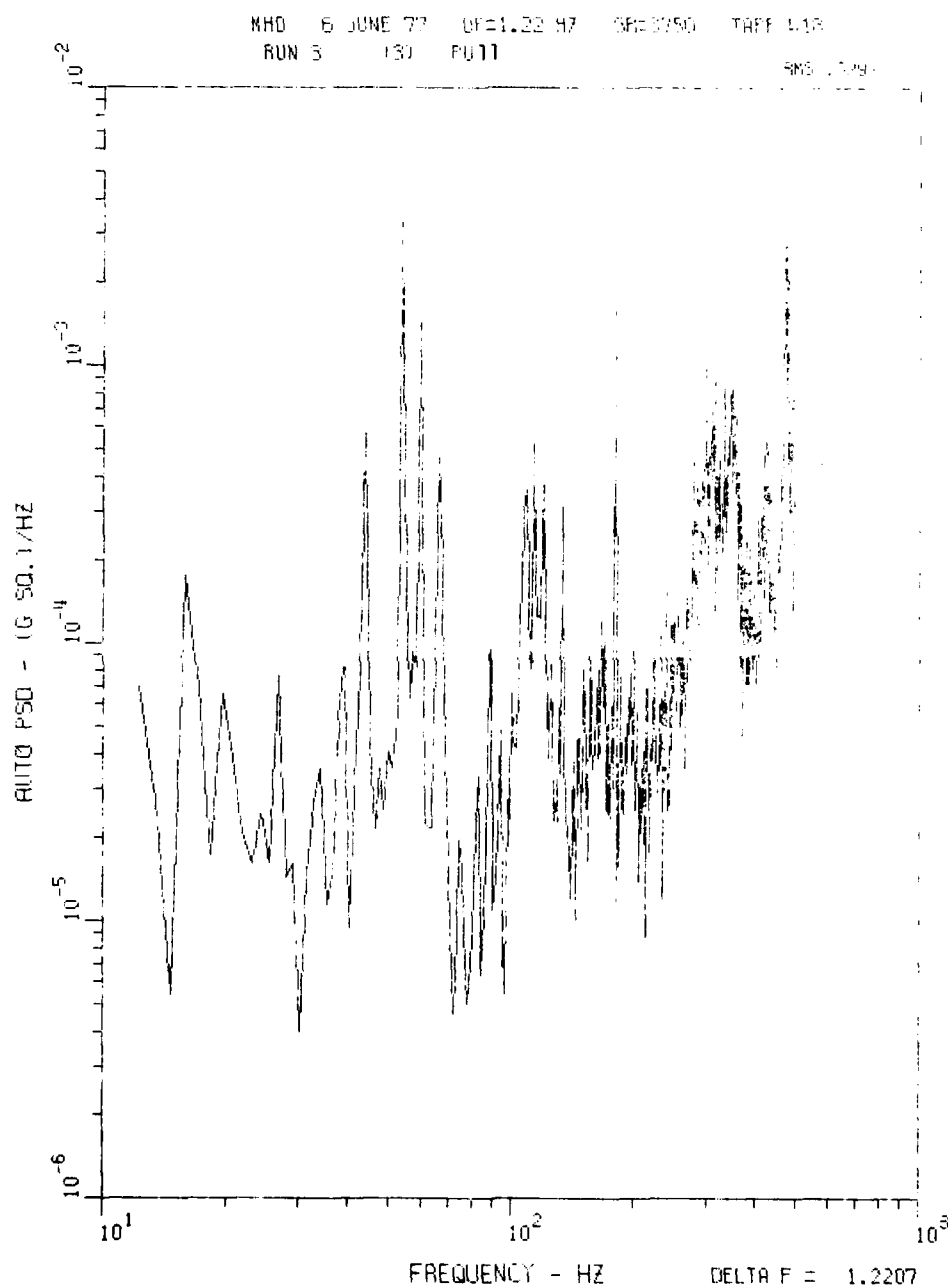


Figure 75. Channel Eleven PSD, 0-500 Hz, Run LWC 003

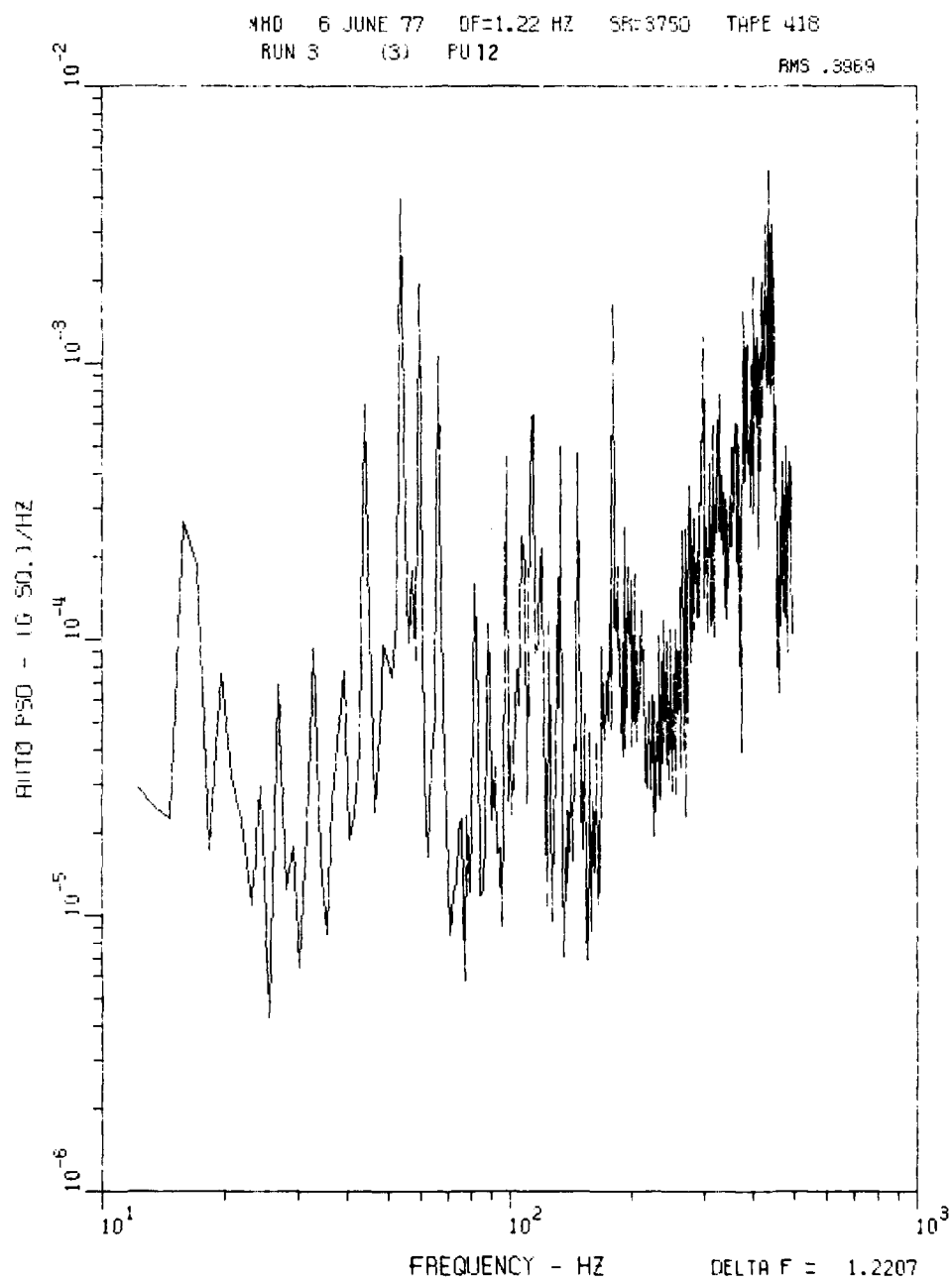


Figure 76. Channel Twelve PSD, 0-500 Hz, Run LWC 003

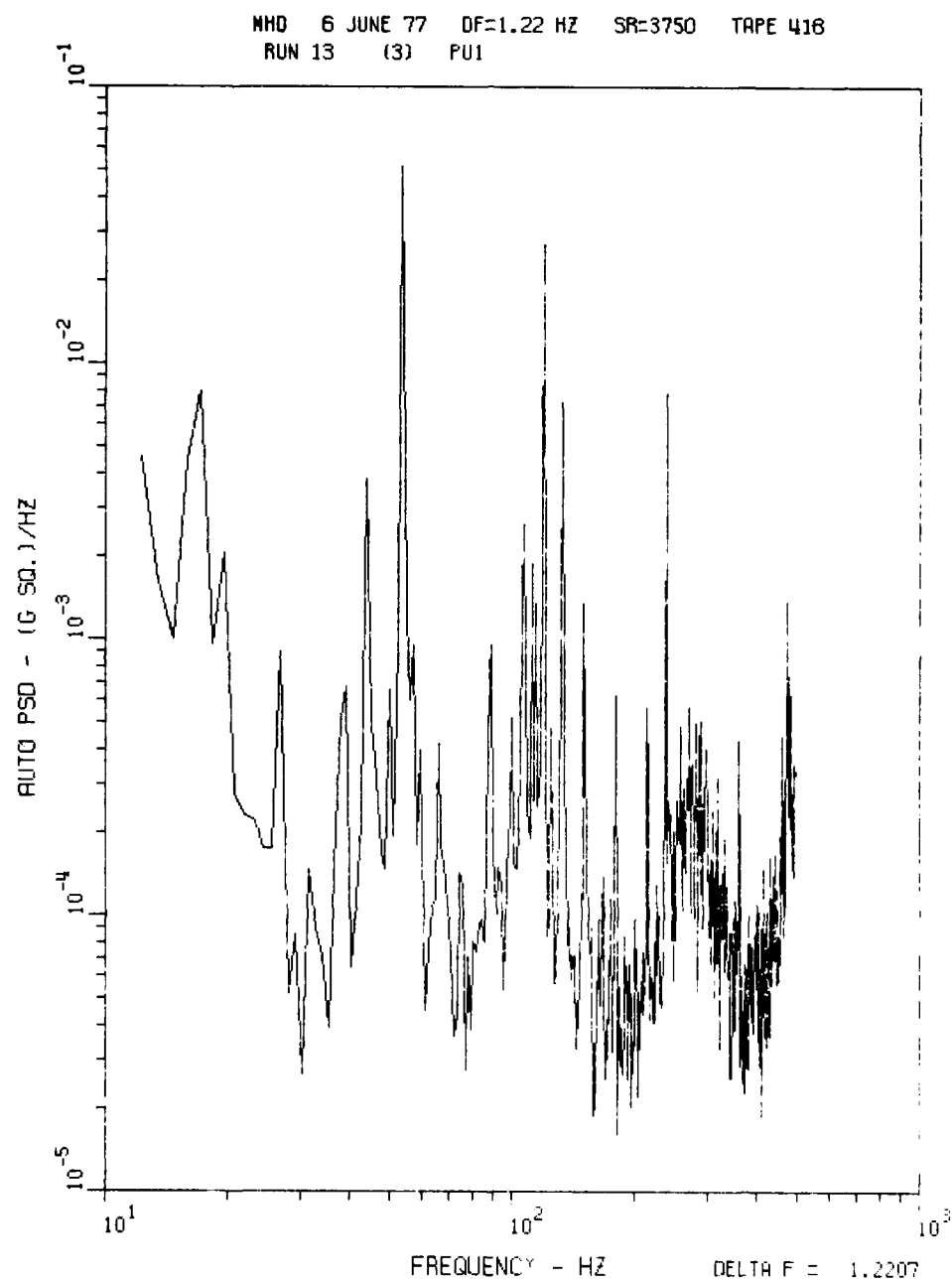


Figure 77. Channel One PSD, 0-500 Hz, Run LMC 013

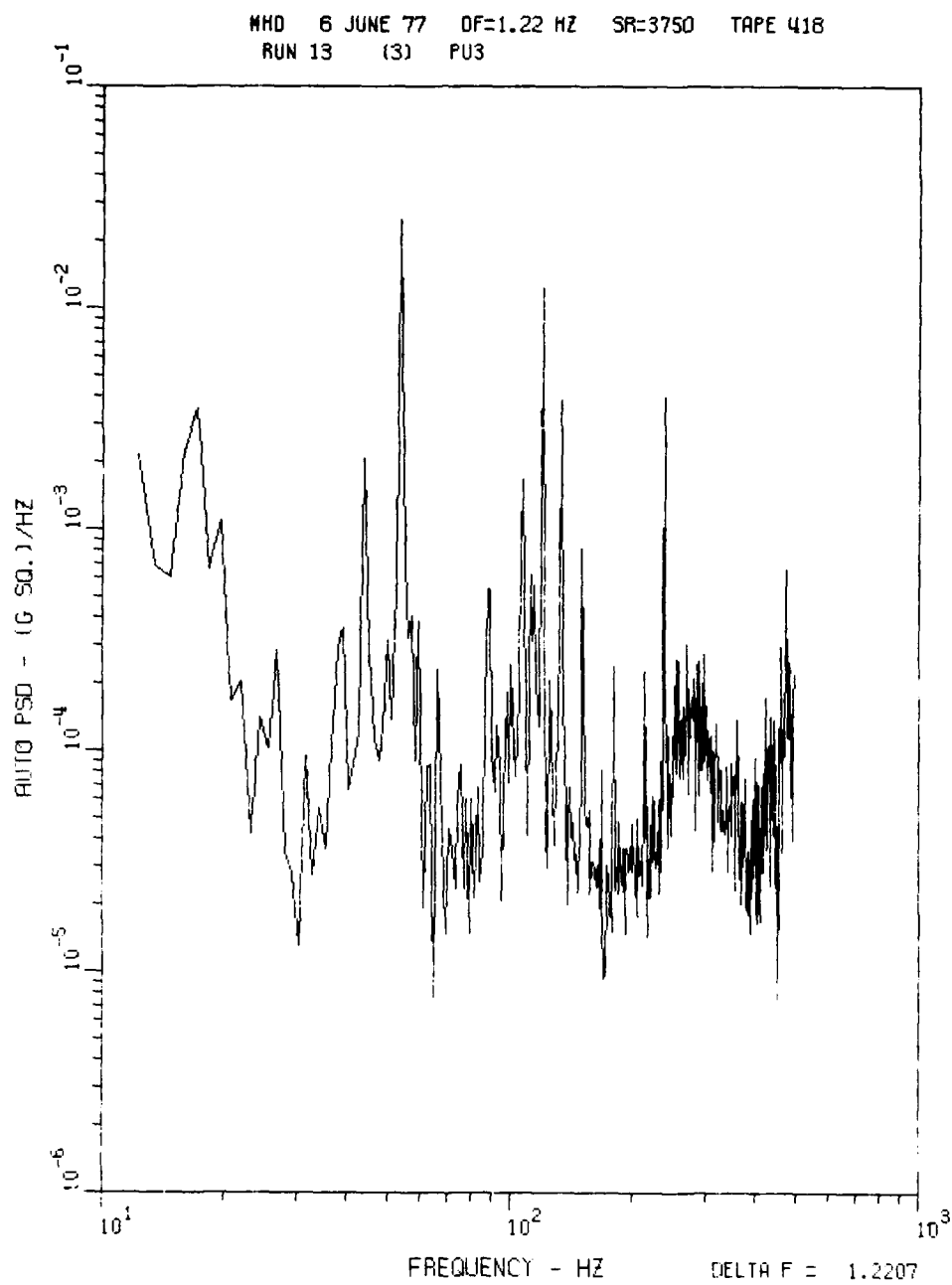


Figure 78. Channel Three PSD, 0-500 Hz, Run LWC 013

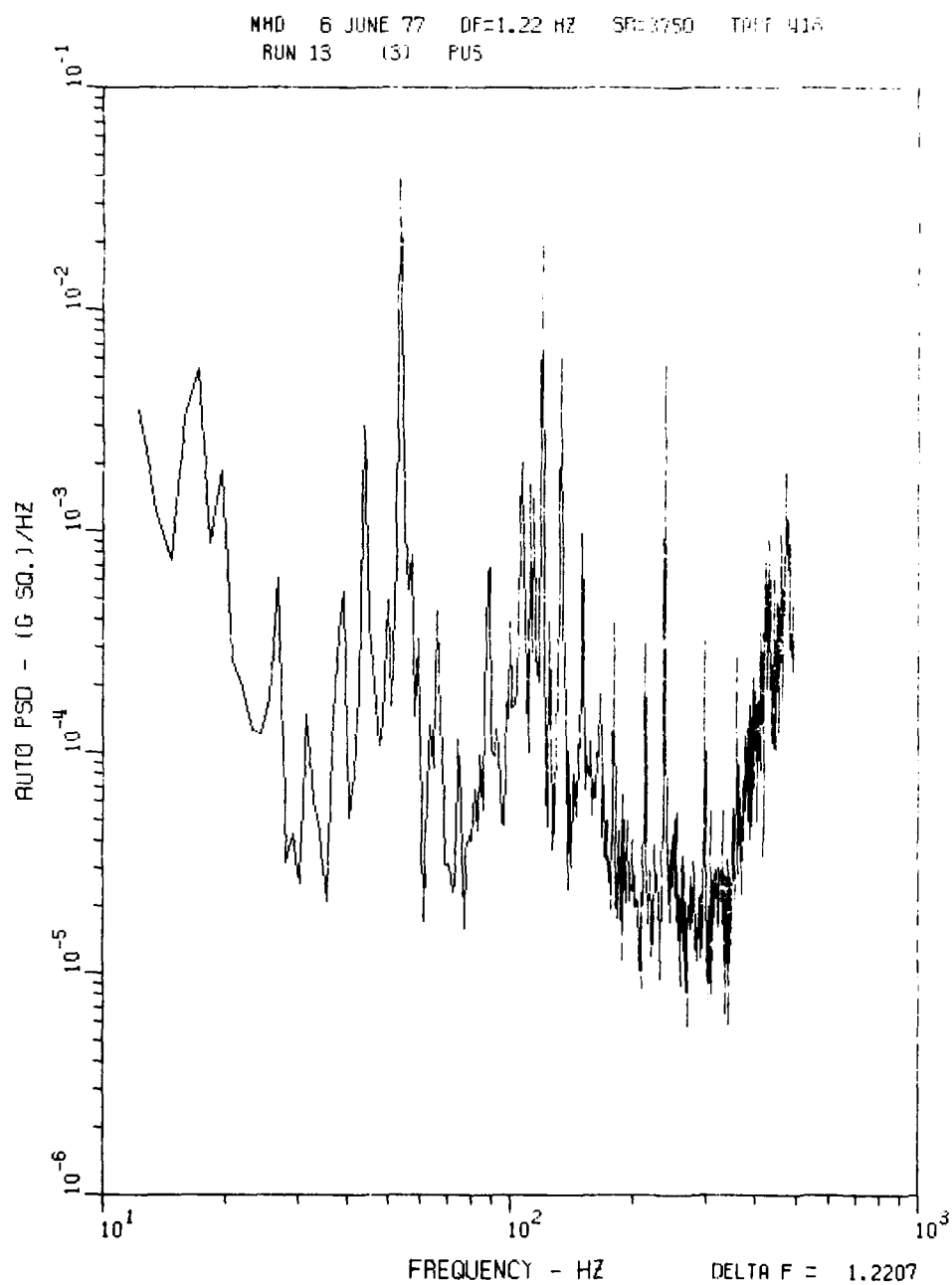


Figure 79. Channel Five PSD, 0-500 Hz, Run LWC 013

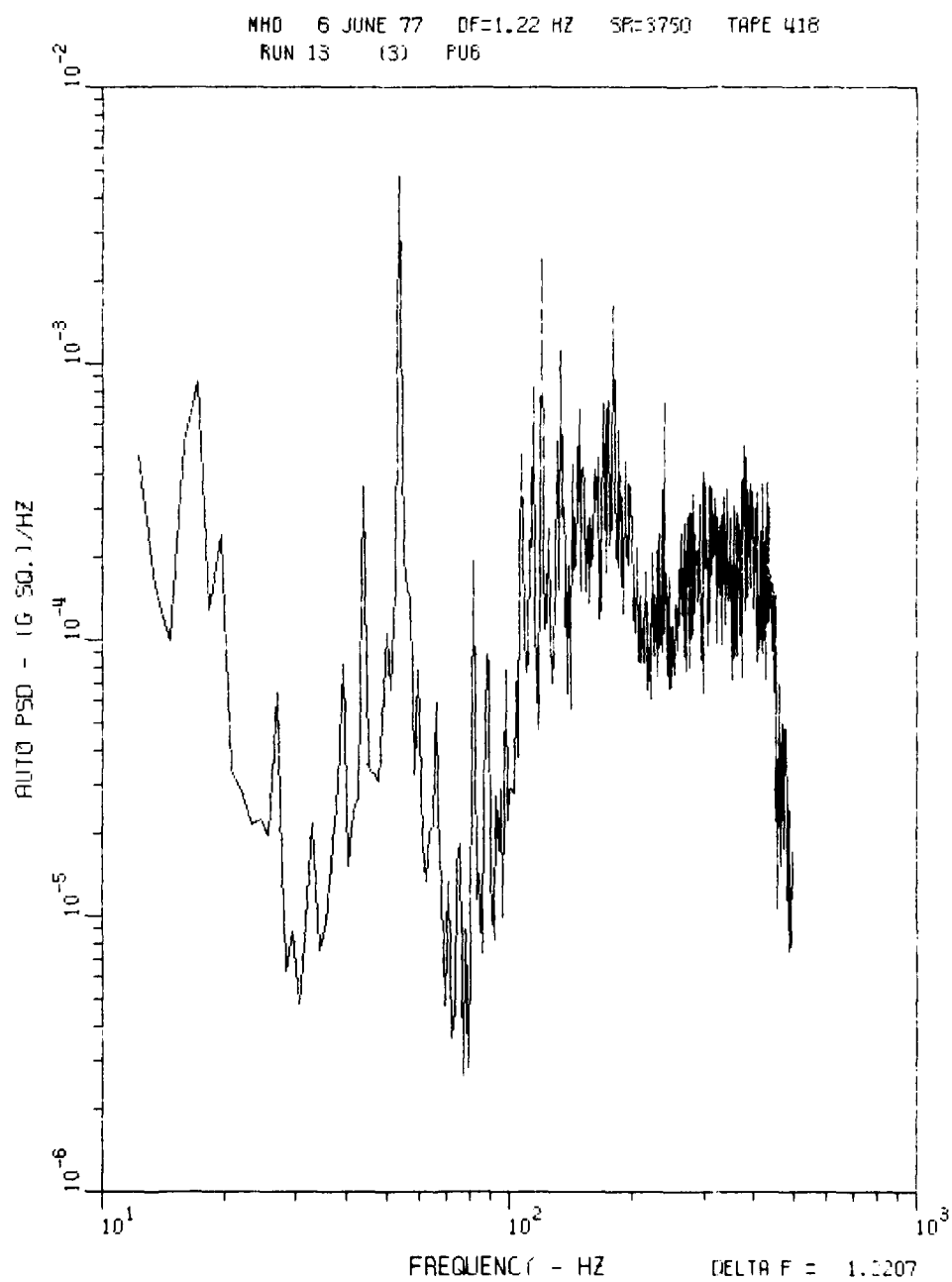


Figure 80. Channel Six PSD, 0-500 Hz, Run LWC 013

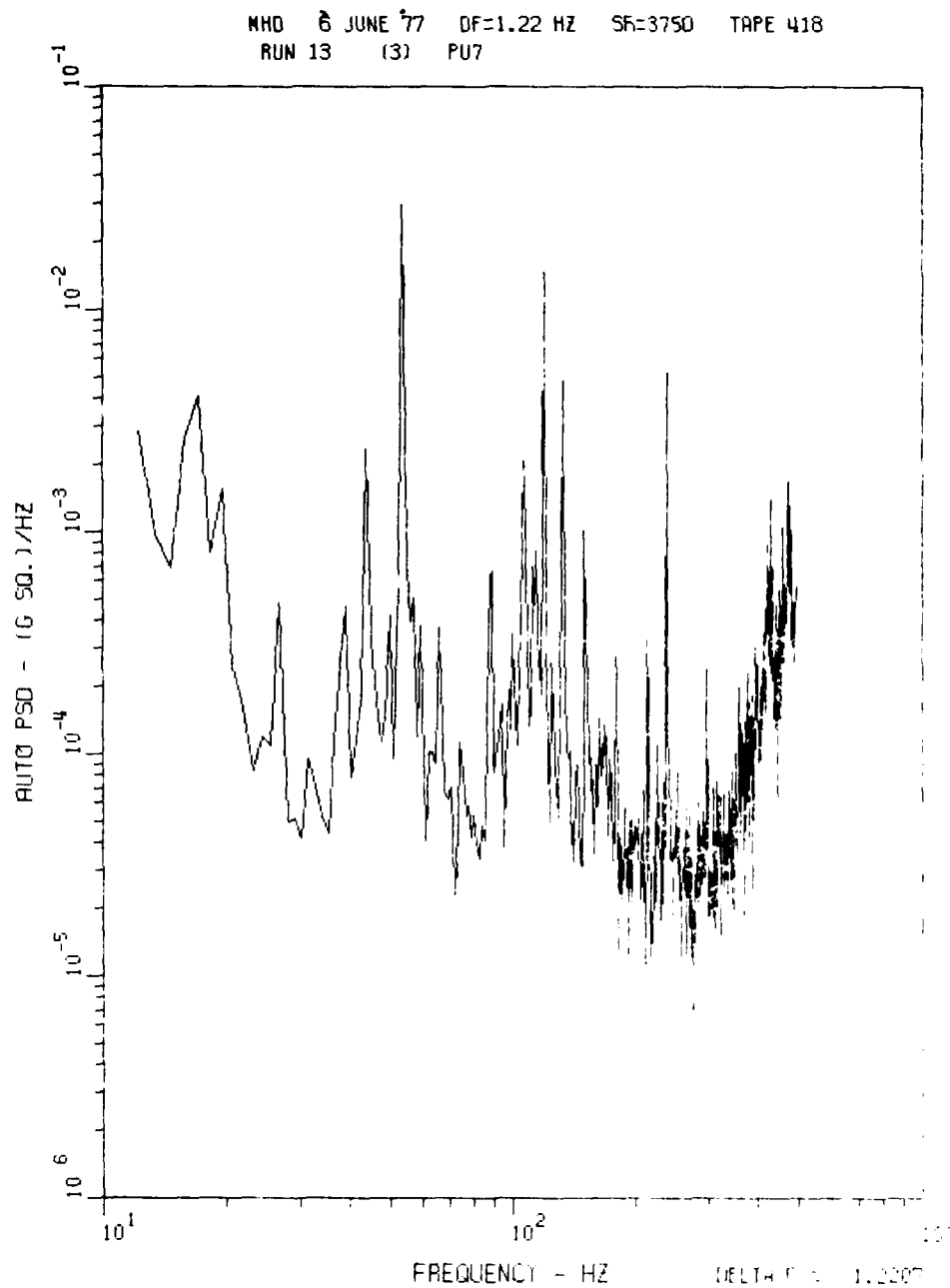


Figure 81. Channel Seven PSD, 0-500 Hz, Run LWC 013



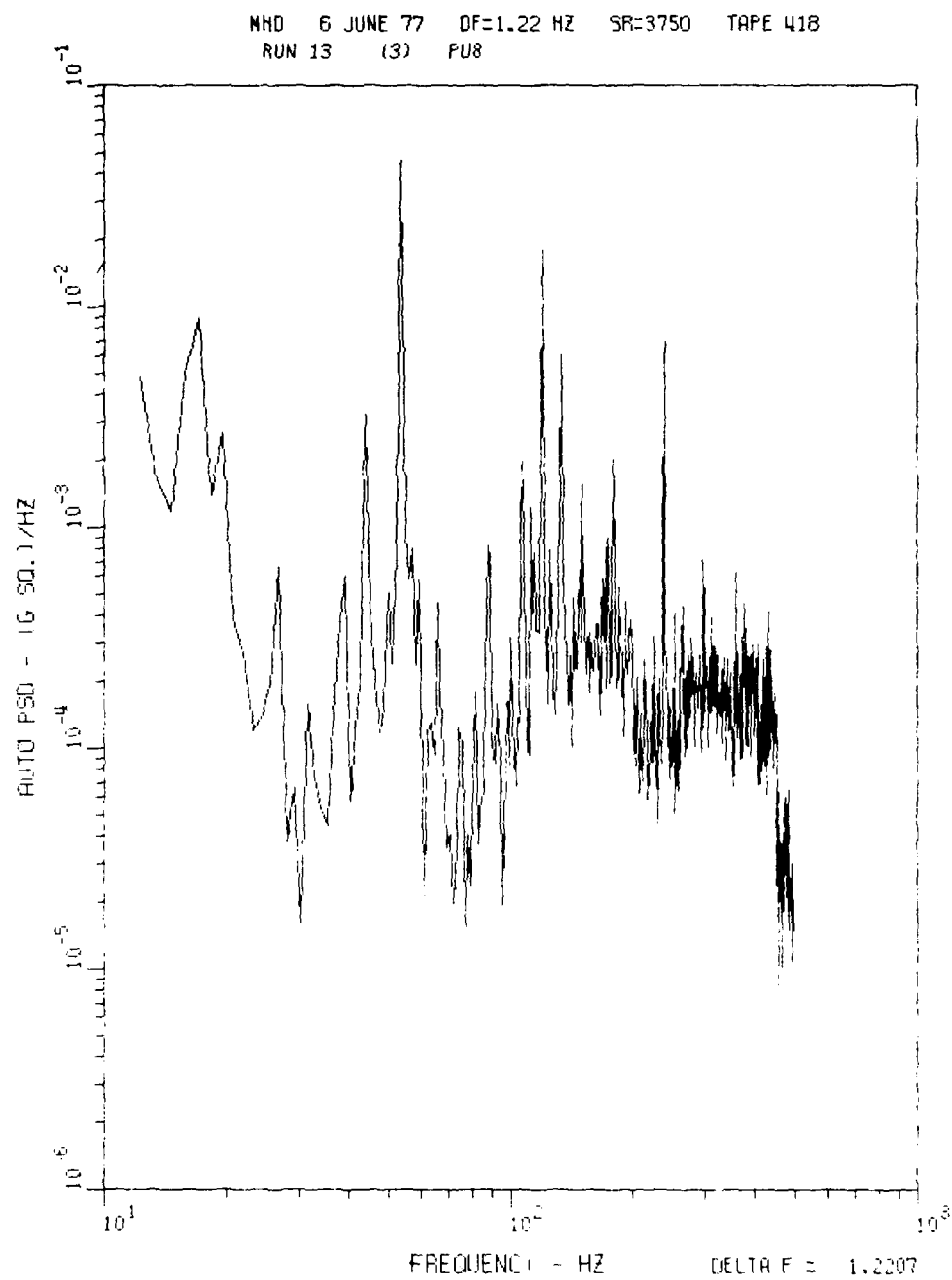


Figure 82. Channel Eight PSD, 0-500 Hz, Run LWC 013

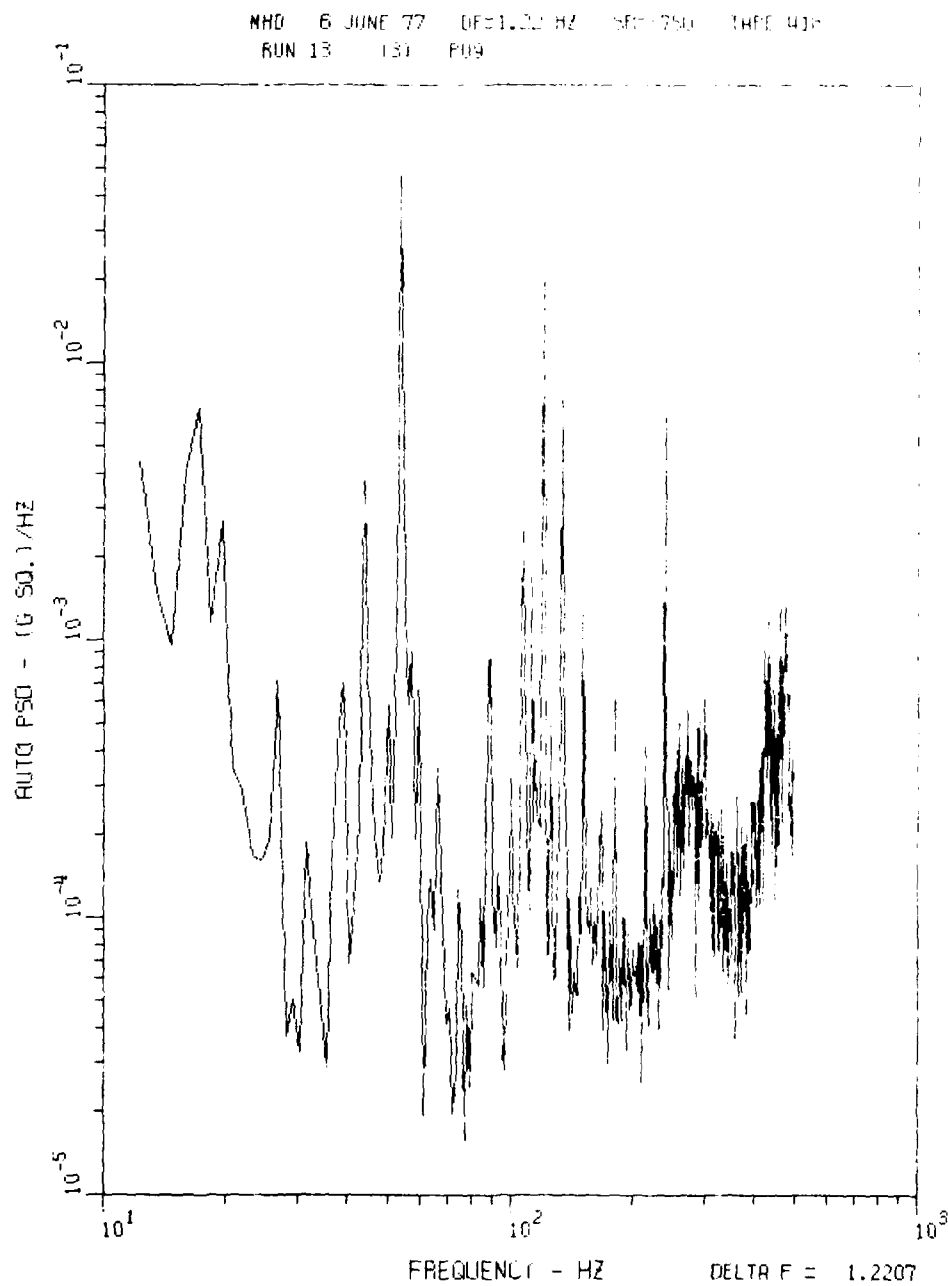


Figure 83. Channel Nine PSD, 0-500 Hz, Run LWC 013

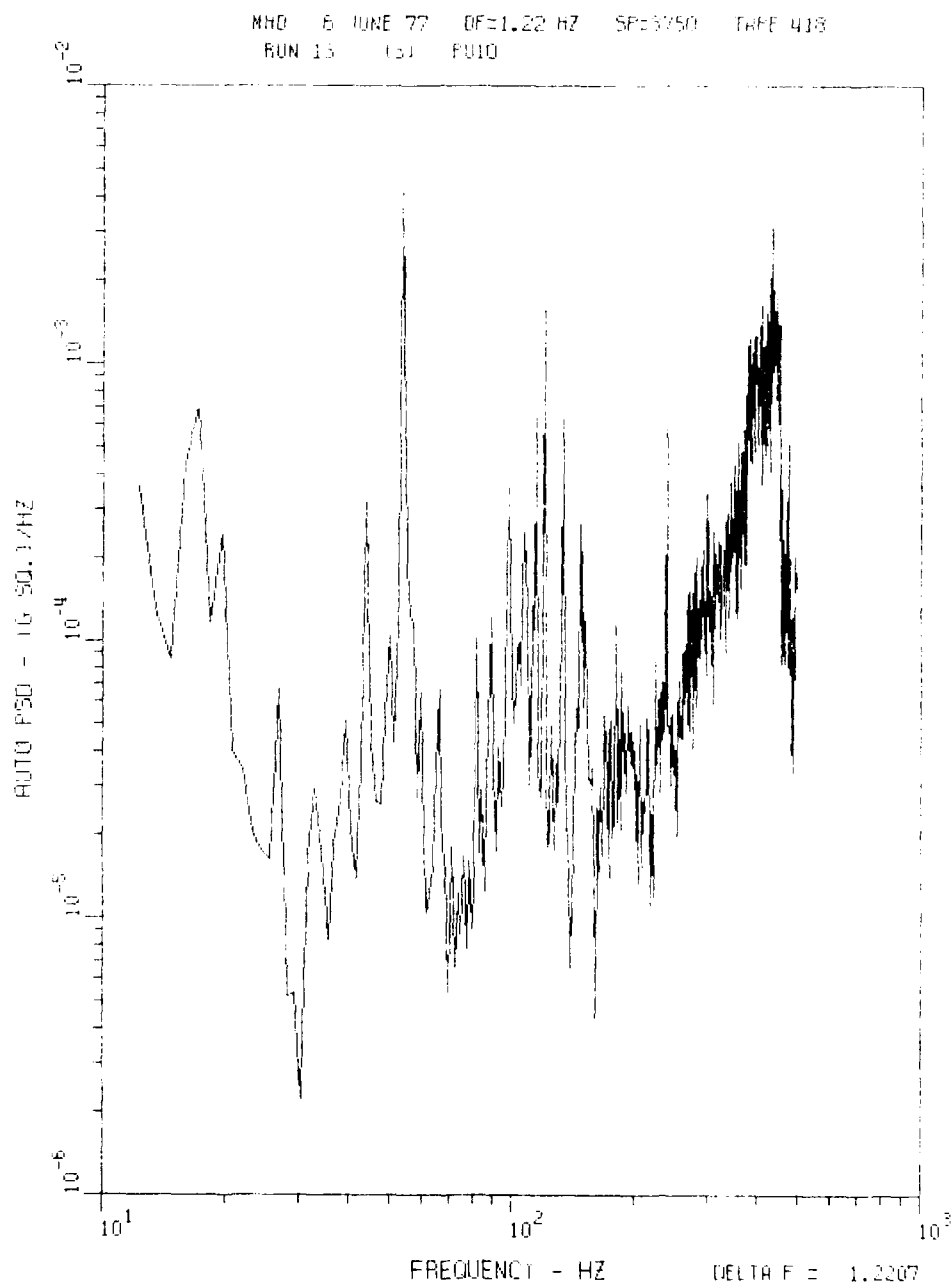


Figure 84. Channel Ten PSD, 0-500 Hz, Run LWC 013

NHD 6 JUNE 77 DF=1.22 HZ SR=3750 TAPE 418  
RUN 13 (3) PU11

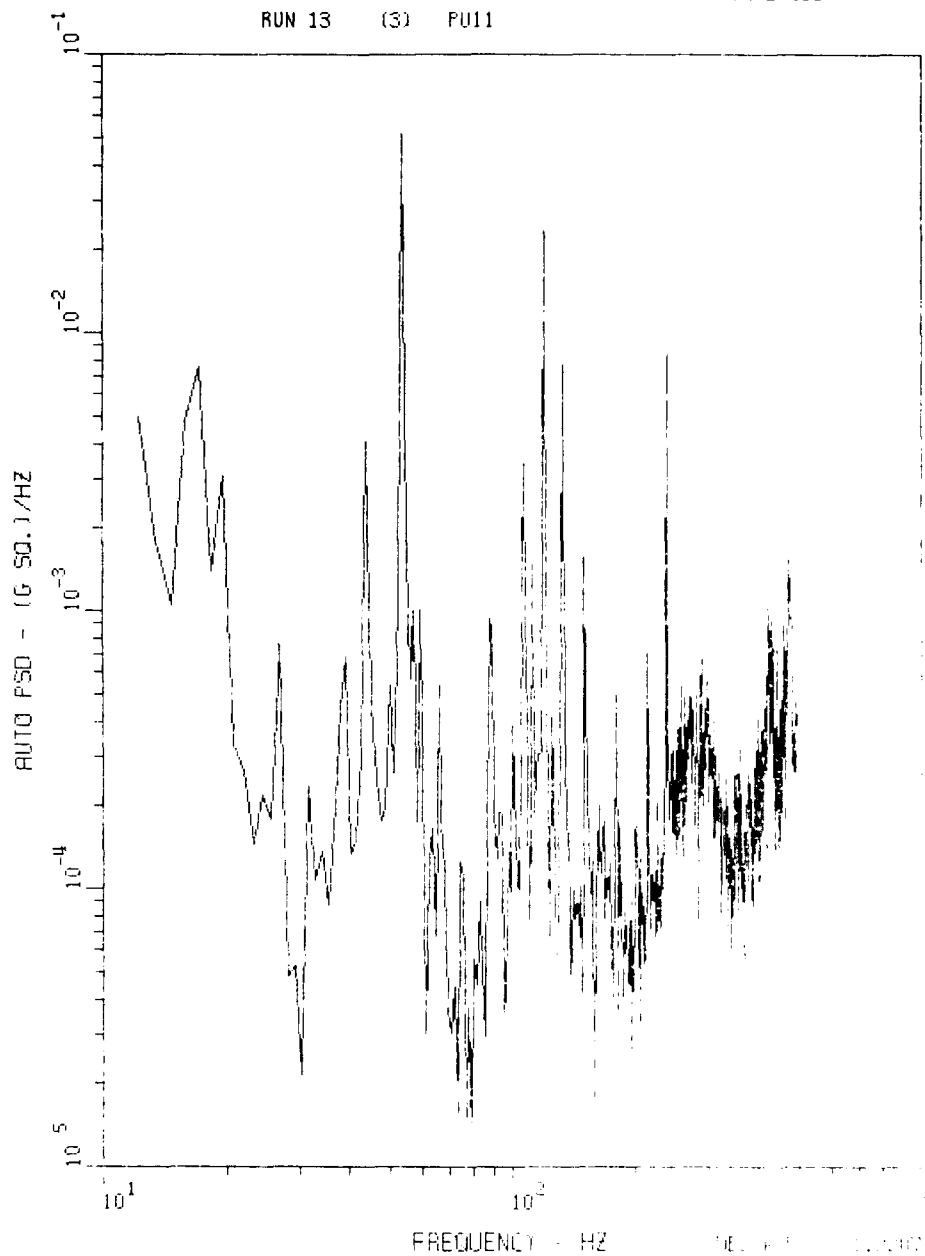


Figure 85. Channel Eleven PSD, 0-500 Hz, Run LWC 013

MHD 6 JUNE 77 DF=1.22 HZ SR=3750 TAPE 418  
 RUN 13 (3) PU12

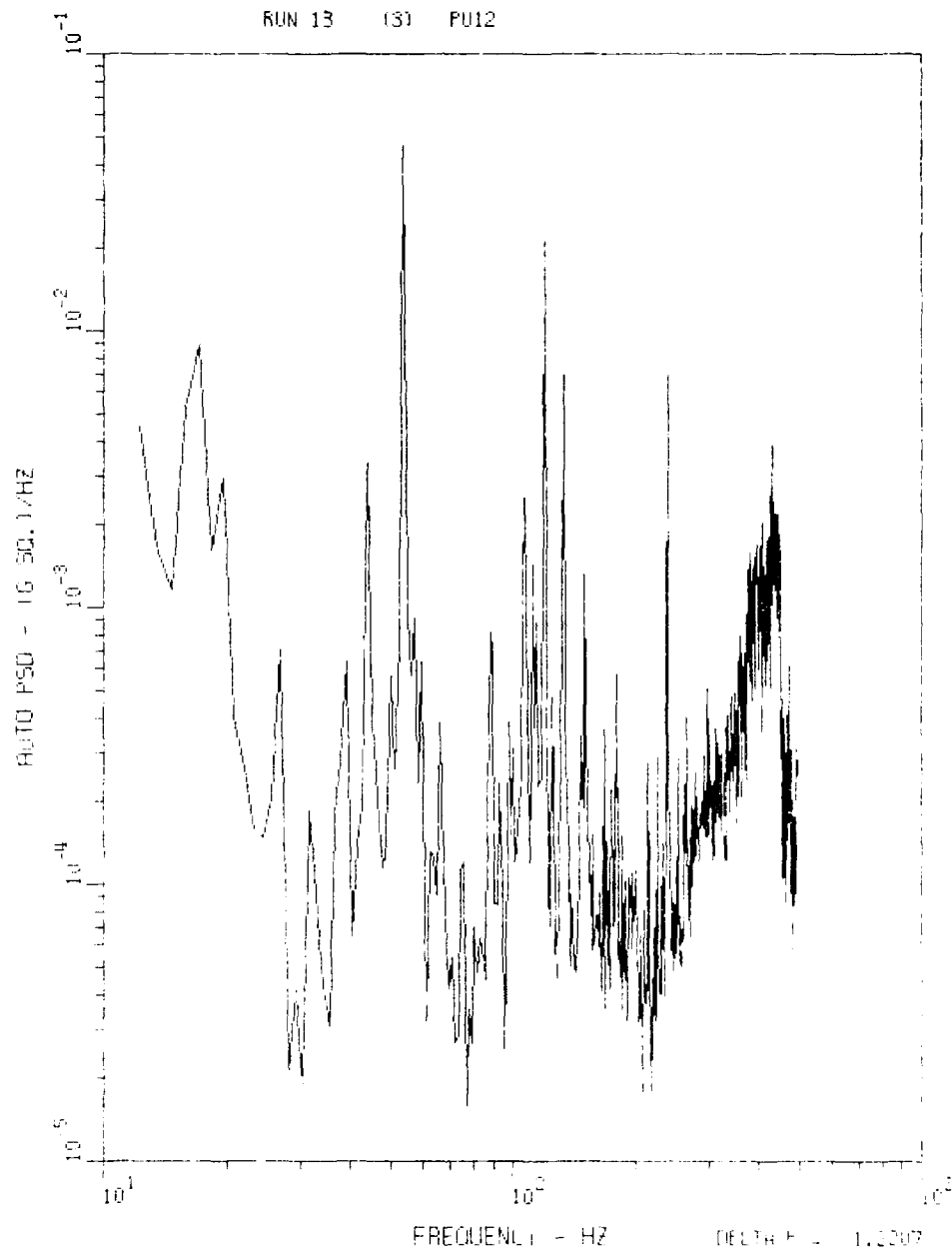


Figure 86. Channel Twelve PSD, 0-500 Hz, Run LWC 013

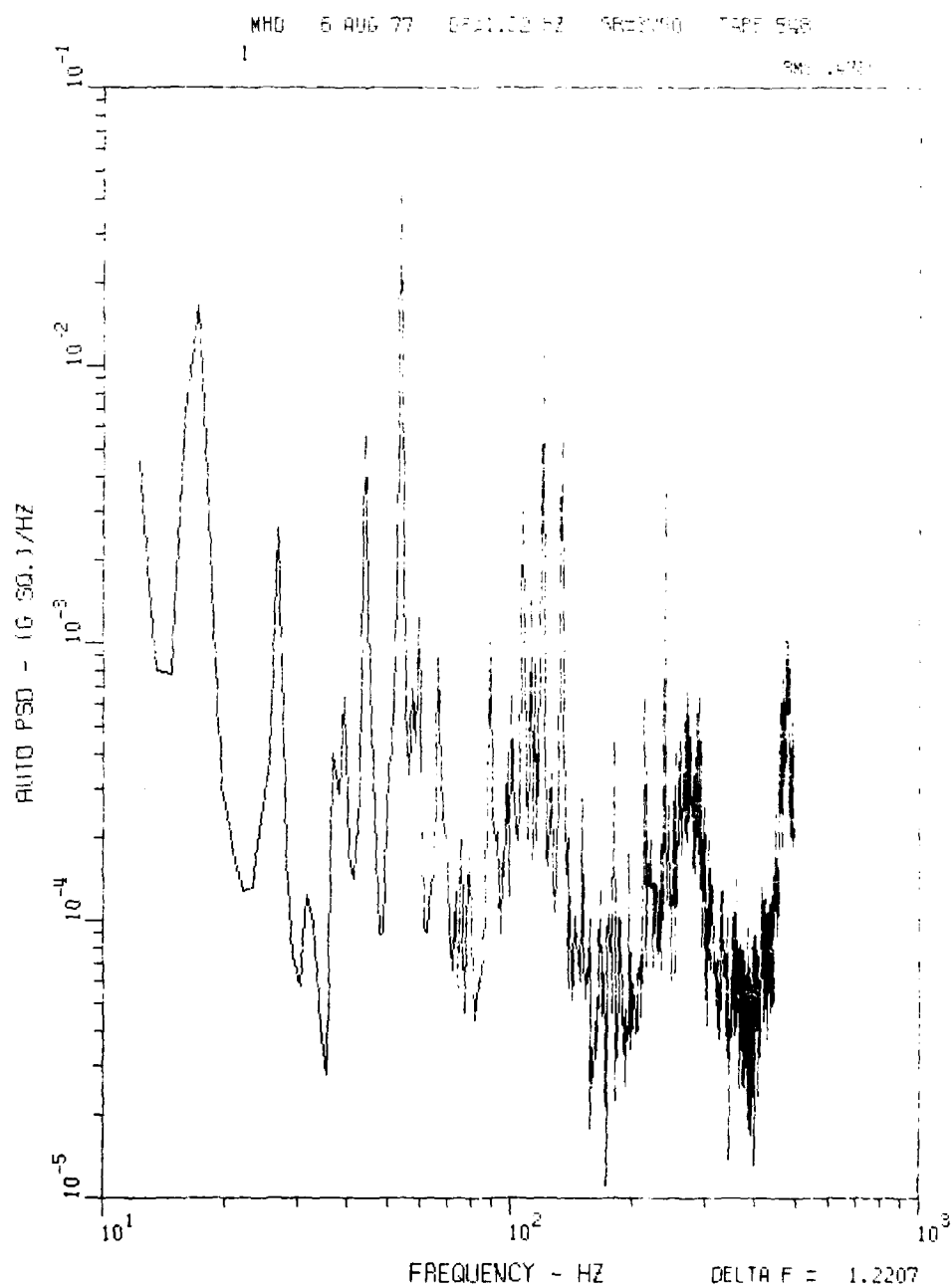


Figure 87. Channel One PSD, 0-500 Hz, Run LWC 023

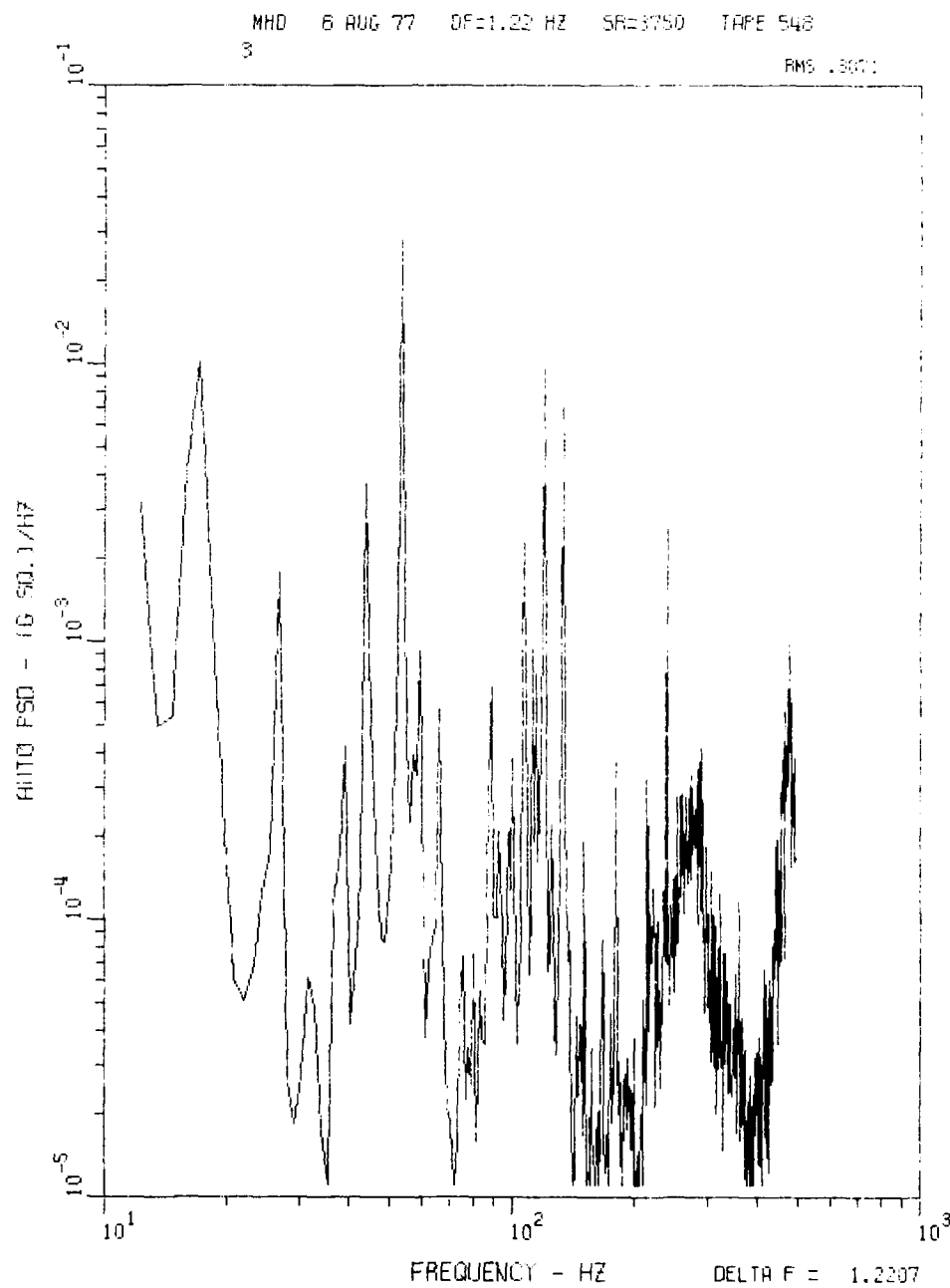


Figure 88. Channel Three PSD, 0-500 Hz, Run LWC 023

MHD 6 AUG 77 DF=1.22 HZ SR=3750 TAPE 548

4

RMS .5015

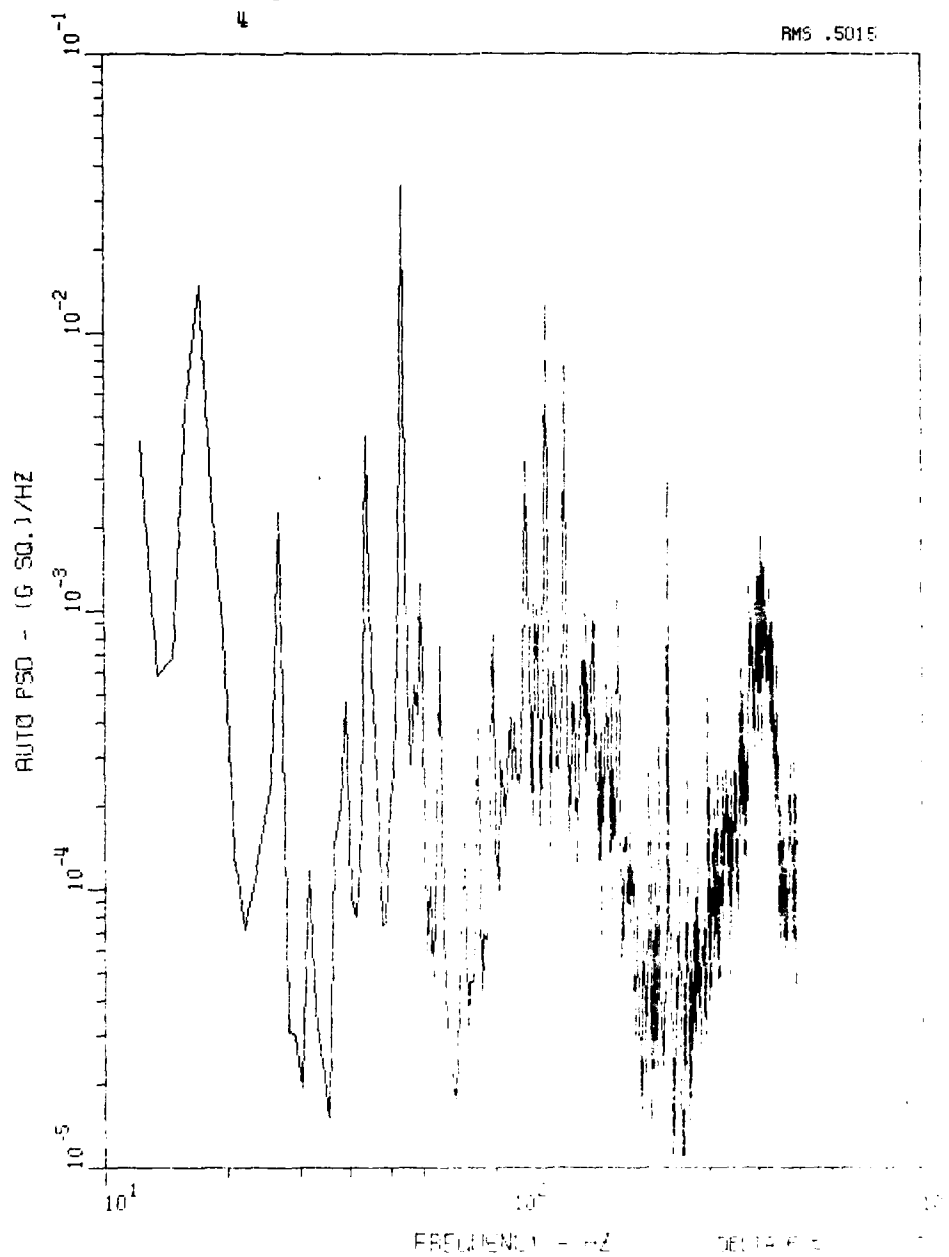


Figure 89. Channel Four PSD, 0-500 Hz, Run LWC 023



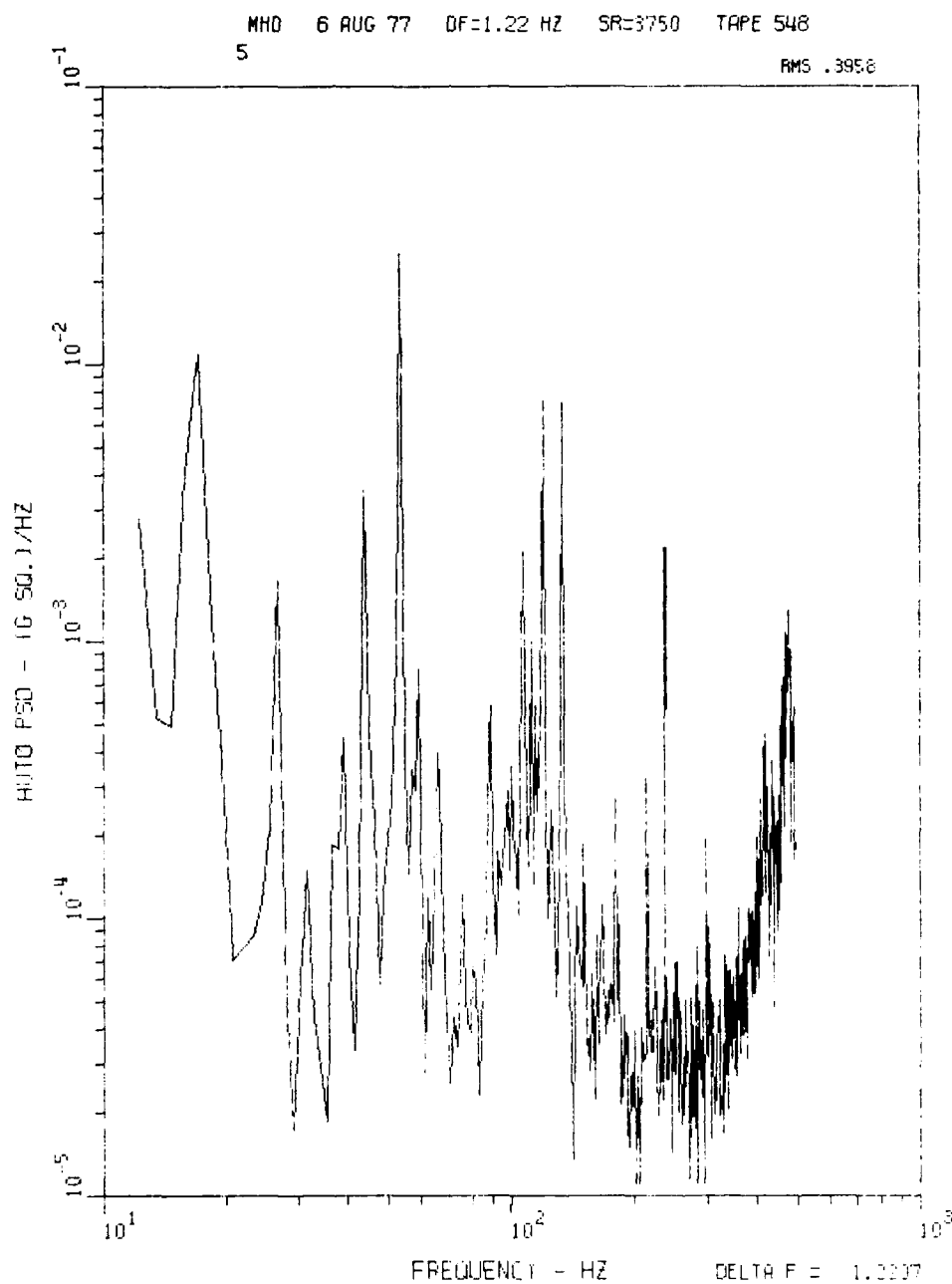


Figure 90. Channel Five PSD, 0-500 Hz, Run LWC 023

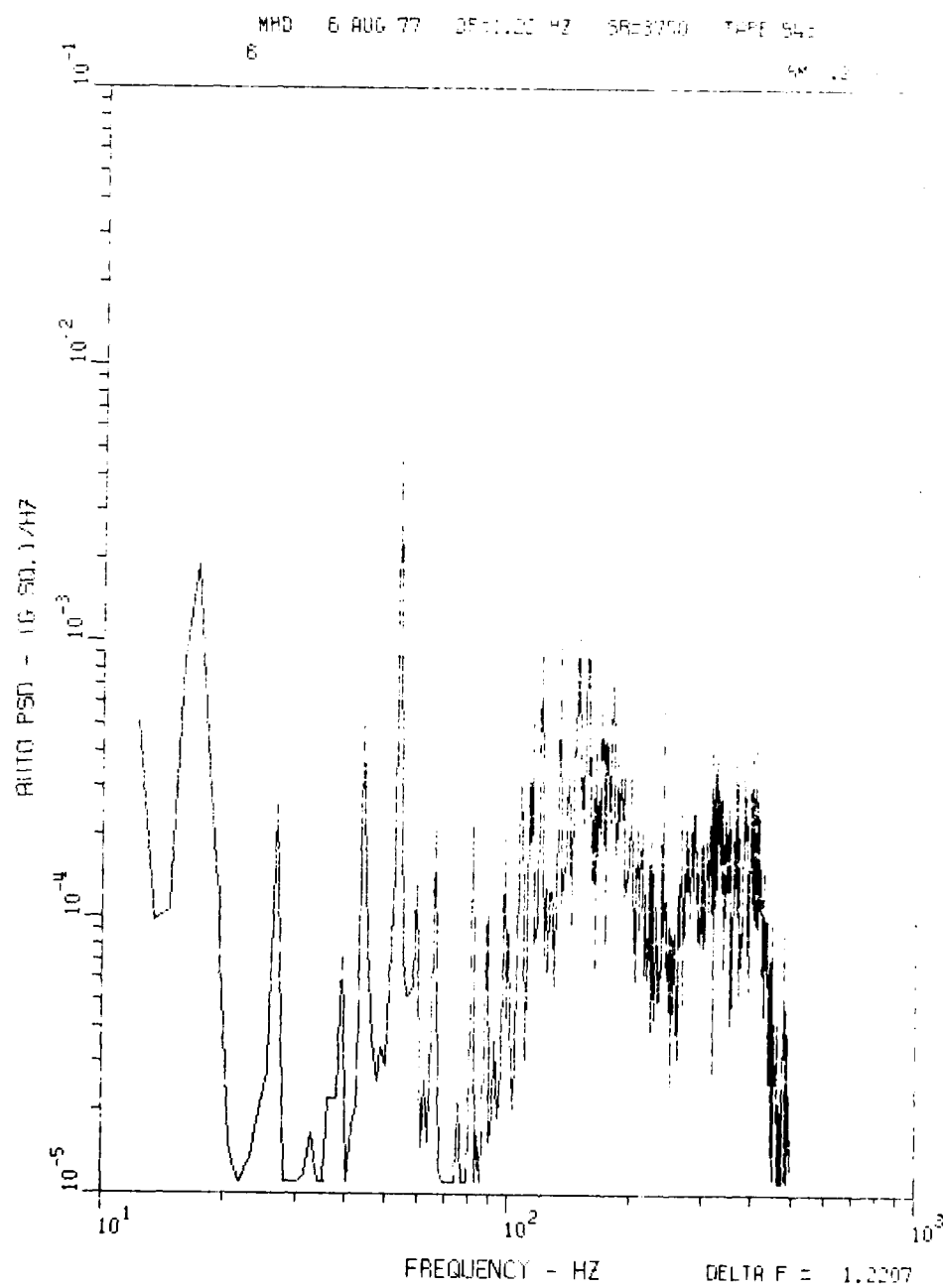


Figure 91. Channel Six PSD, 0-500 Hz, Run LWC 023

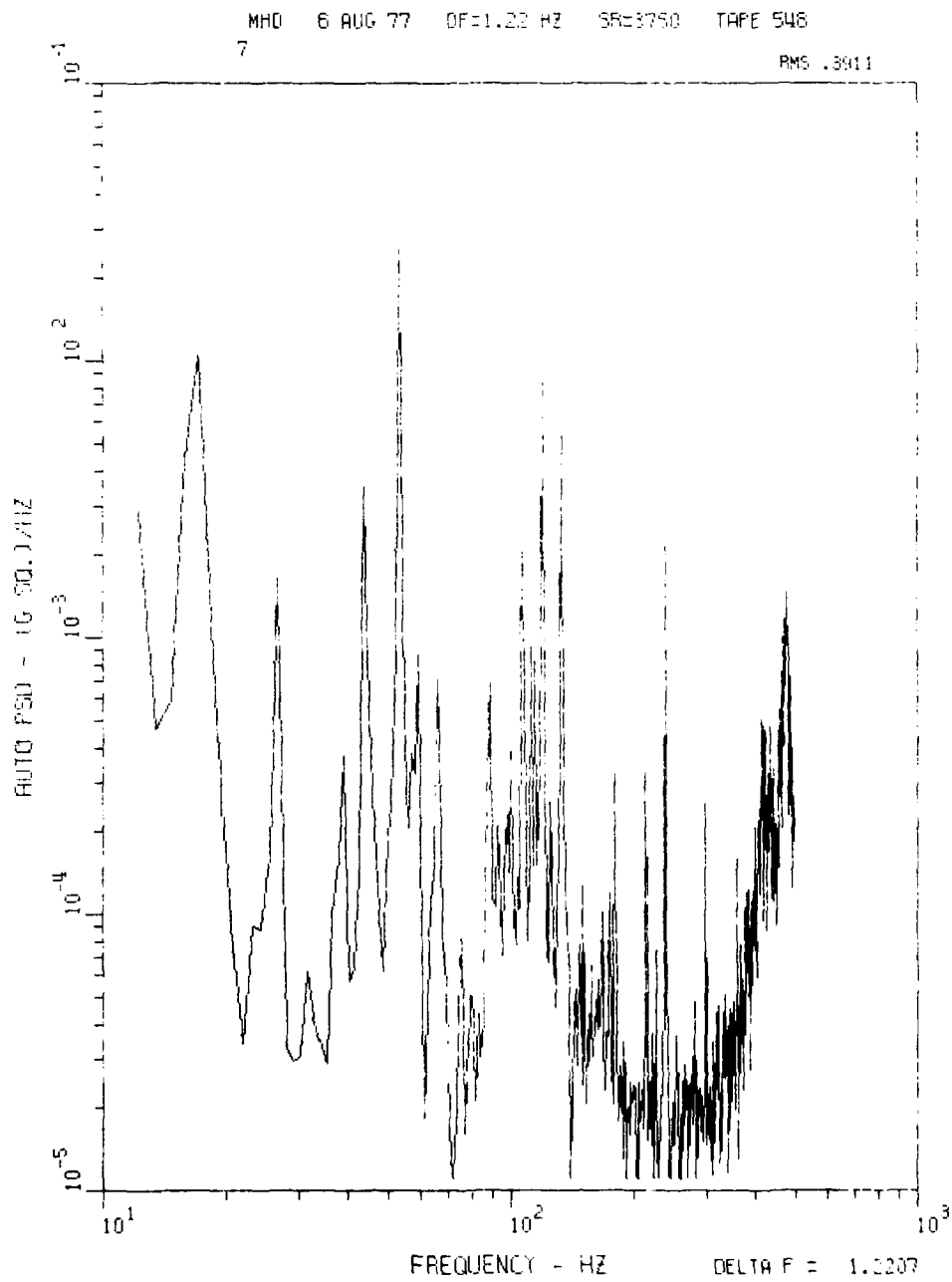


Figure 92. Channel Seven, PSD, 0-500 Hz, Run LWC 023

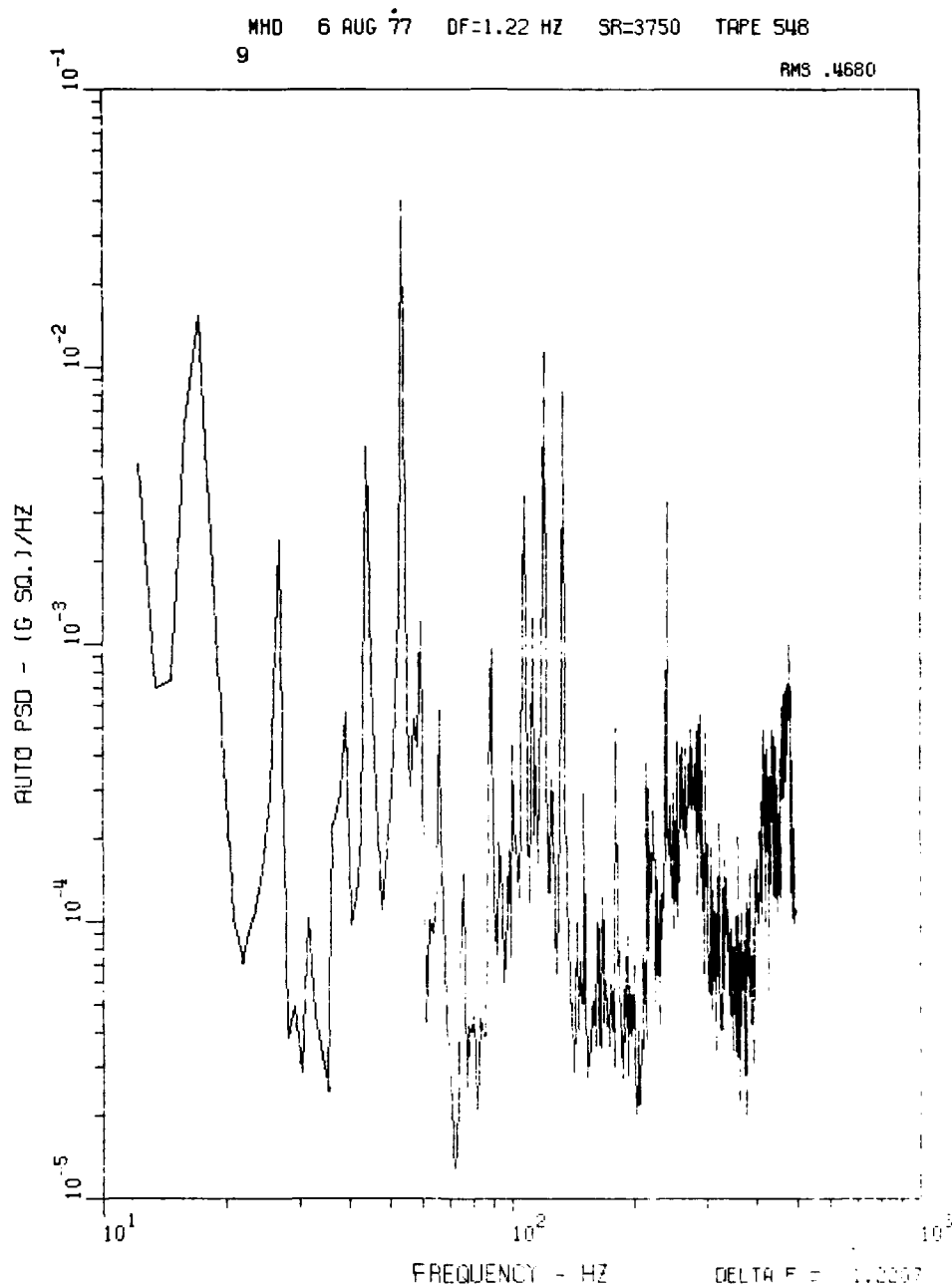


Figure 93. Channel Nine PSD, 0-500 Hz, Run LWC 023

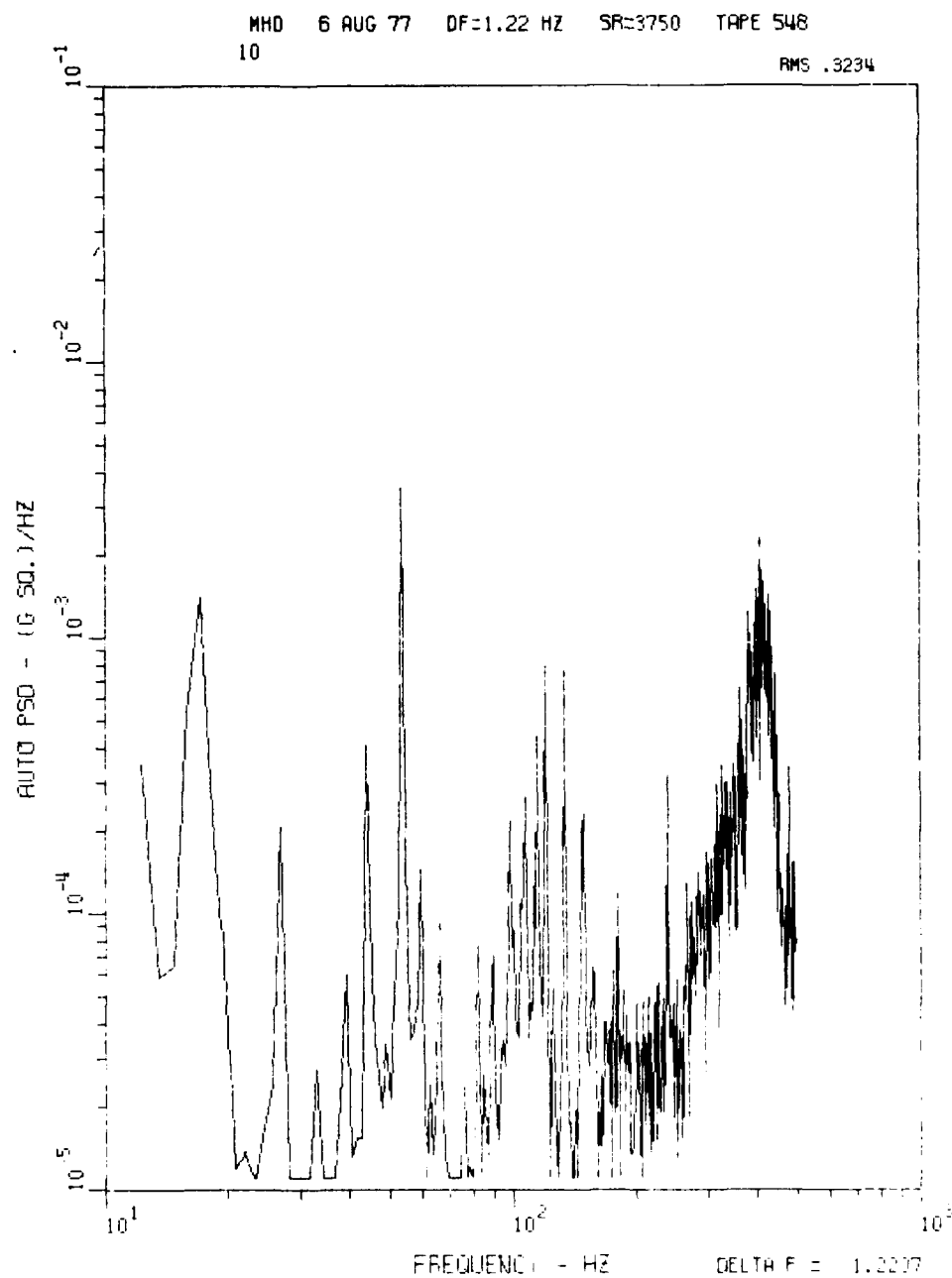


Figure 94. Channel Ten PSD, 0-500 Hz, Run LWC 023

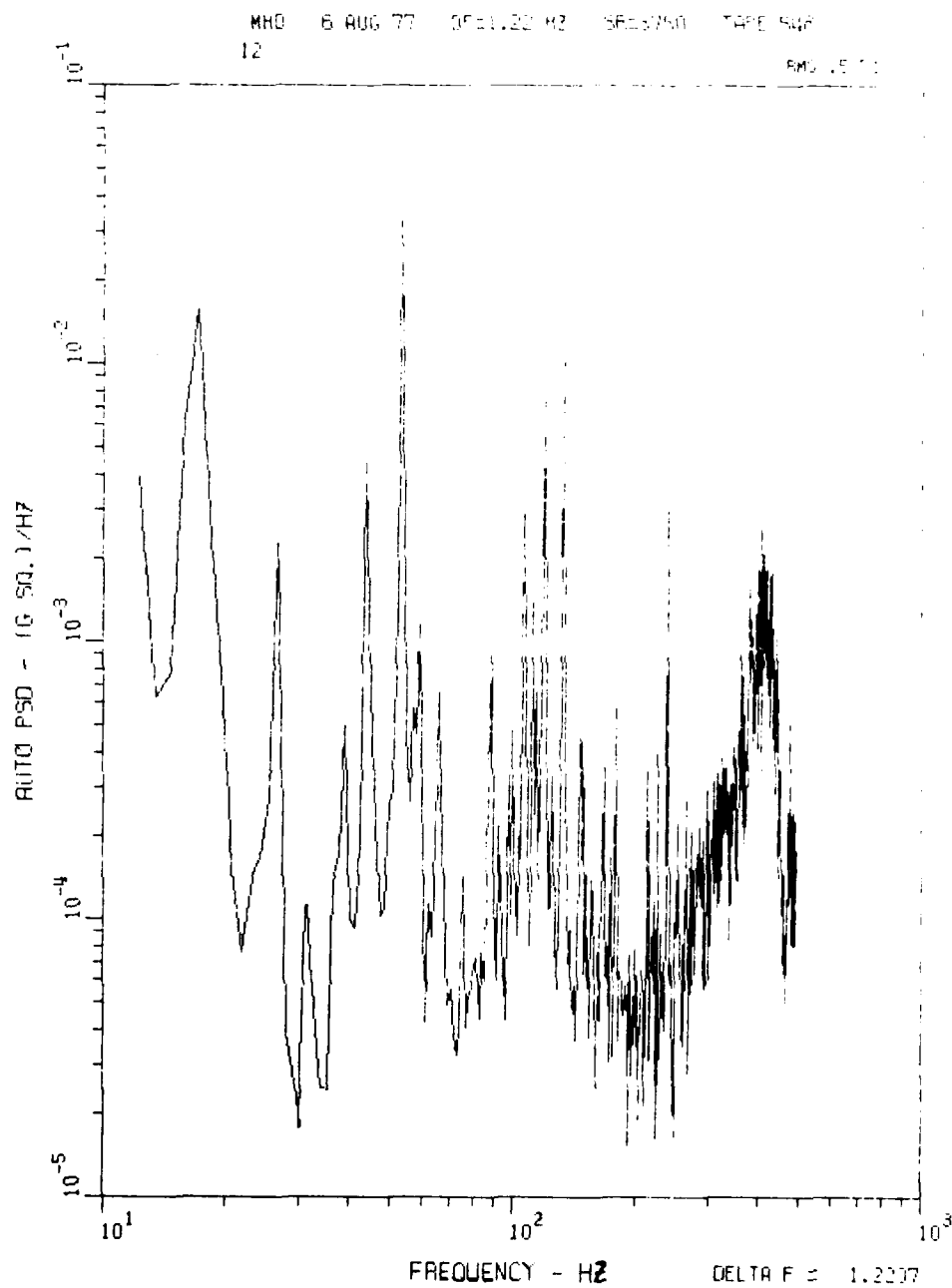


Figure 95. Channel Twelve PSD, 0-500 Hz, Run LWC 023

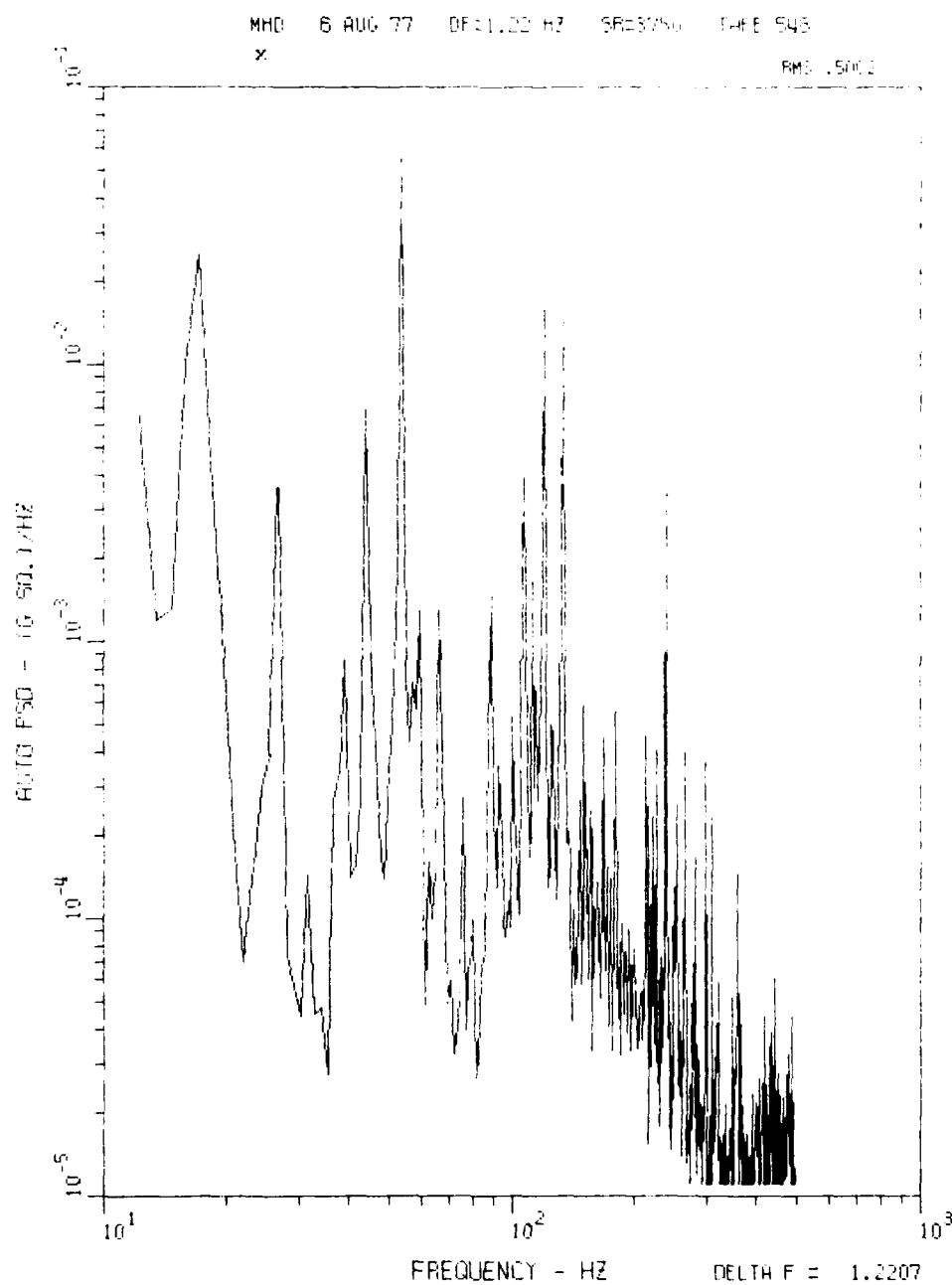


Figure 96. Channel x PSD, 0-500 Hz, Run LWC 023

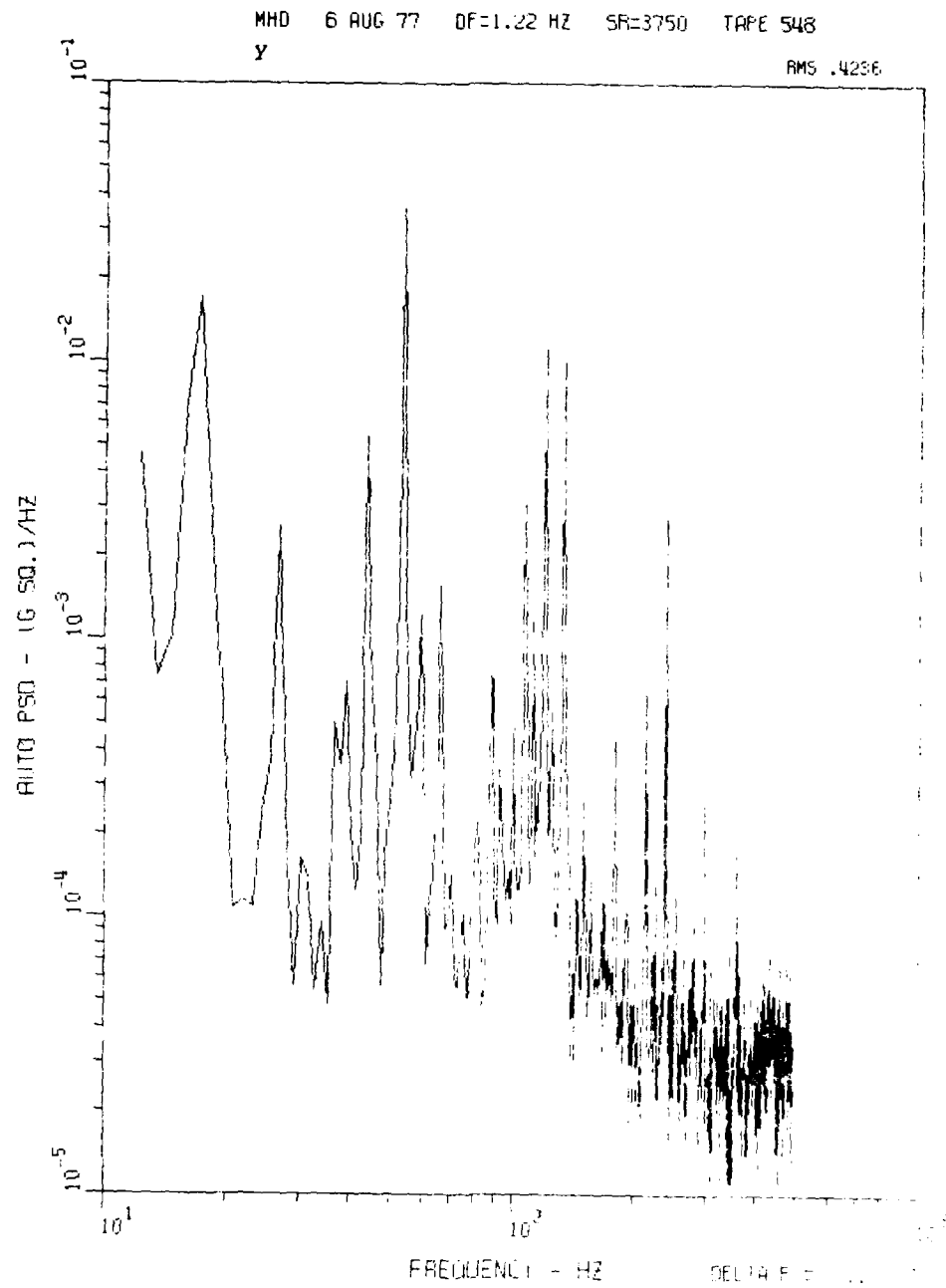


Figure 97. Channel y PSD, 0-500 Hz, Run LWC 023



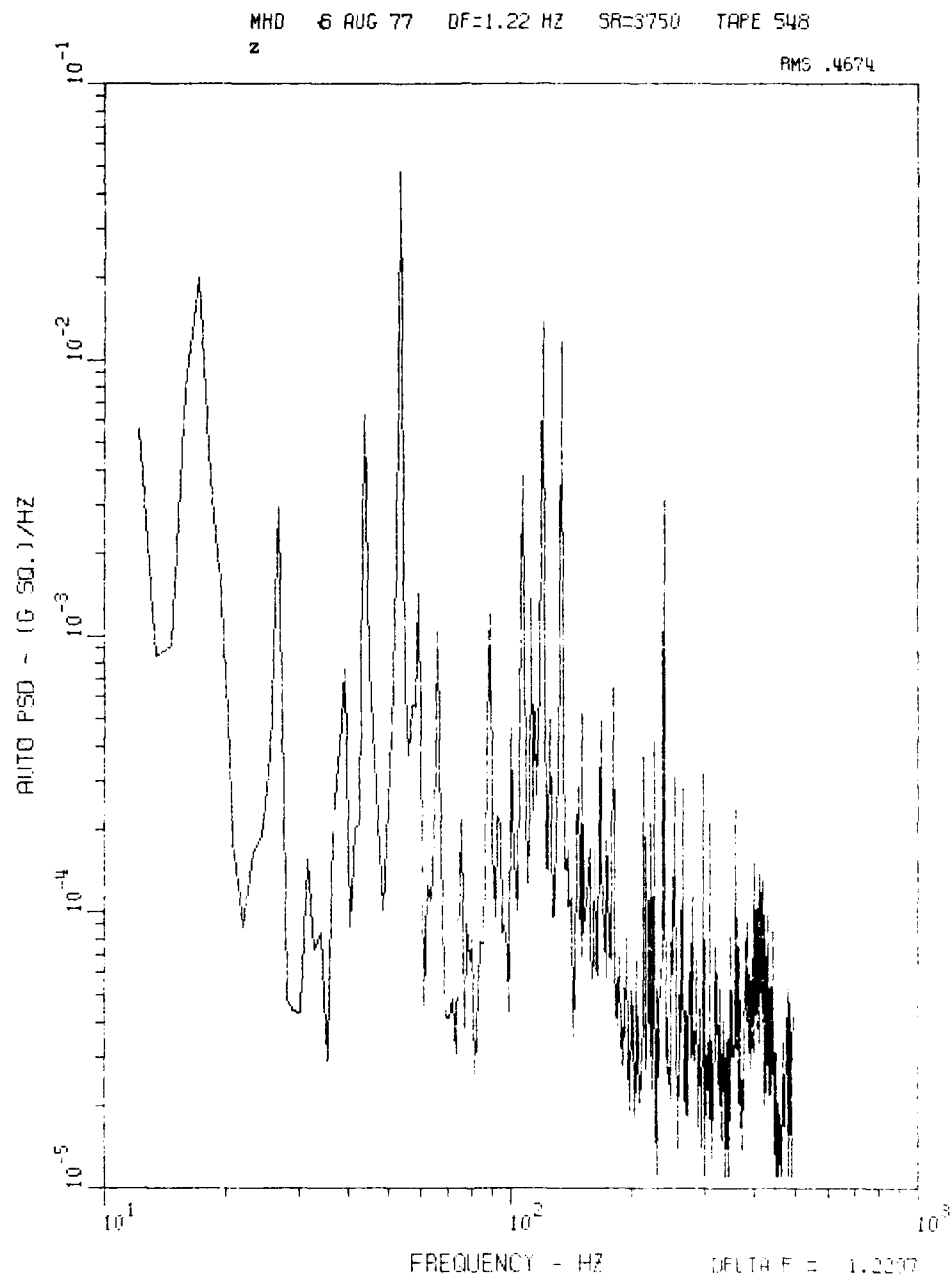


Figure 98. Channel z PSD, 0-500 Hz, Run LWC 023

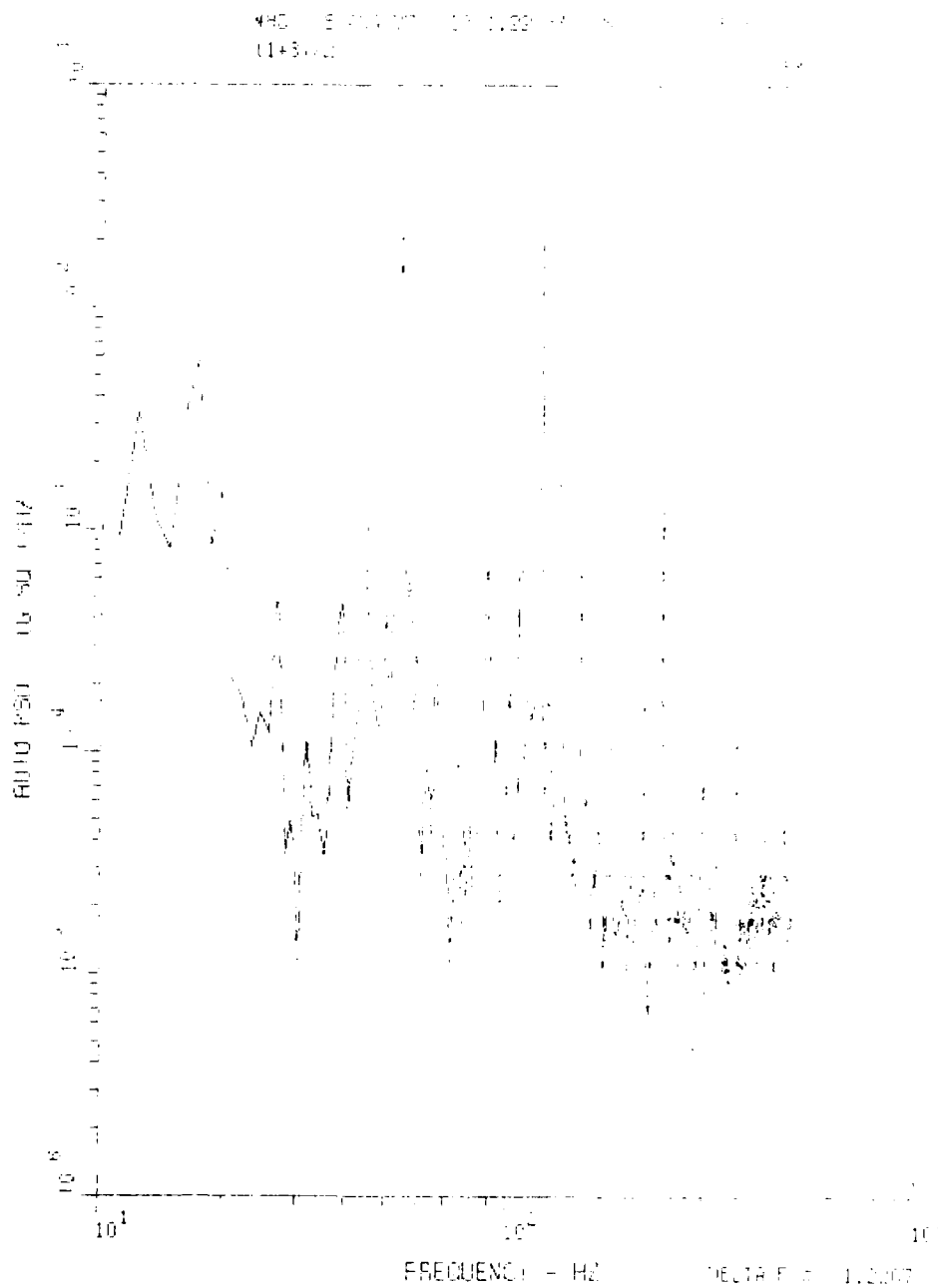


Figure 99. PSD for Channels (1+3)/2, 0-500 HZ, Run LWC 013

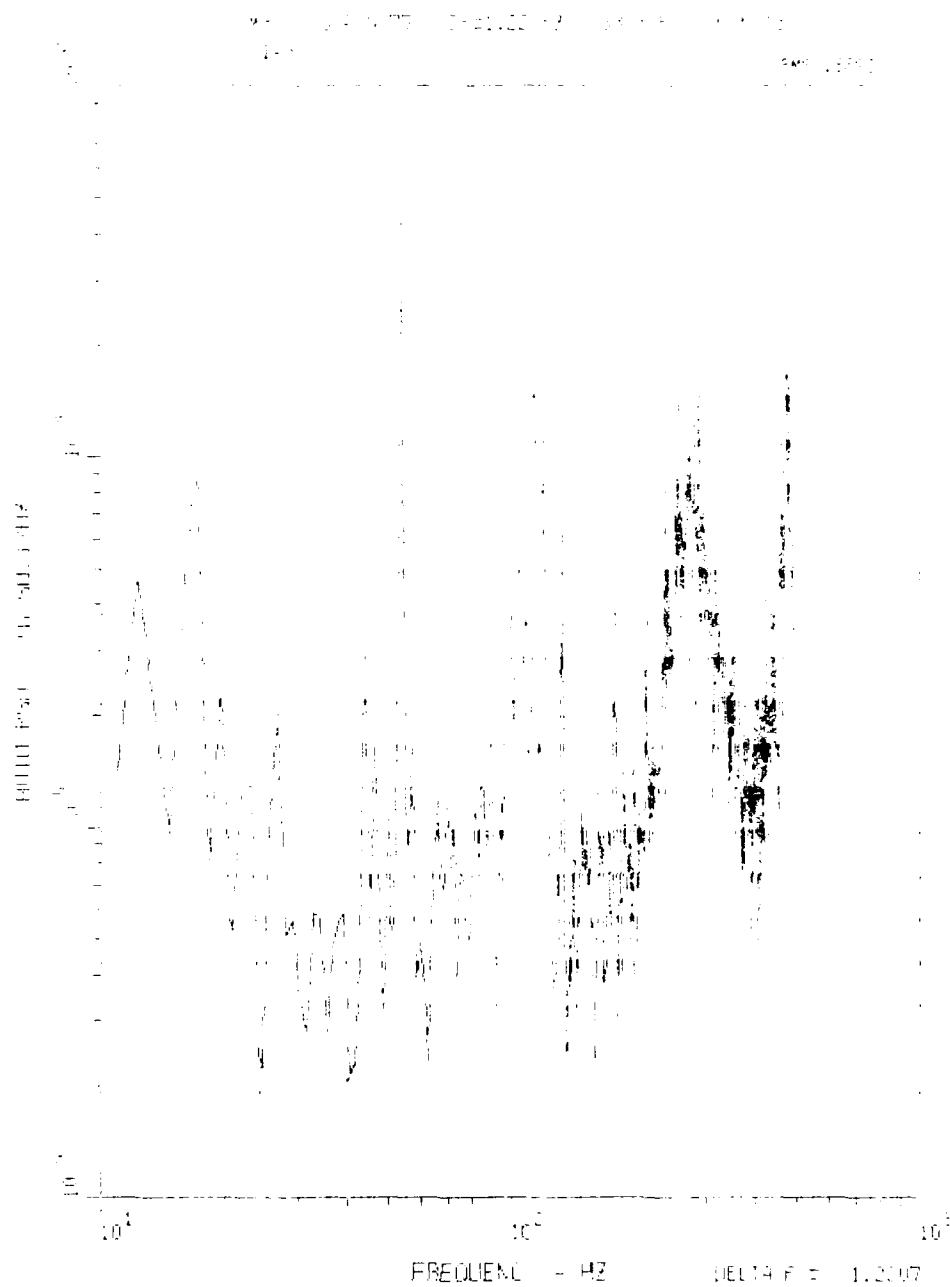


Figure 100. PSD for Channels 1-3, 0-500 Hz, Run LWC 013

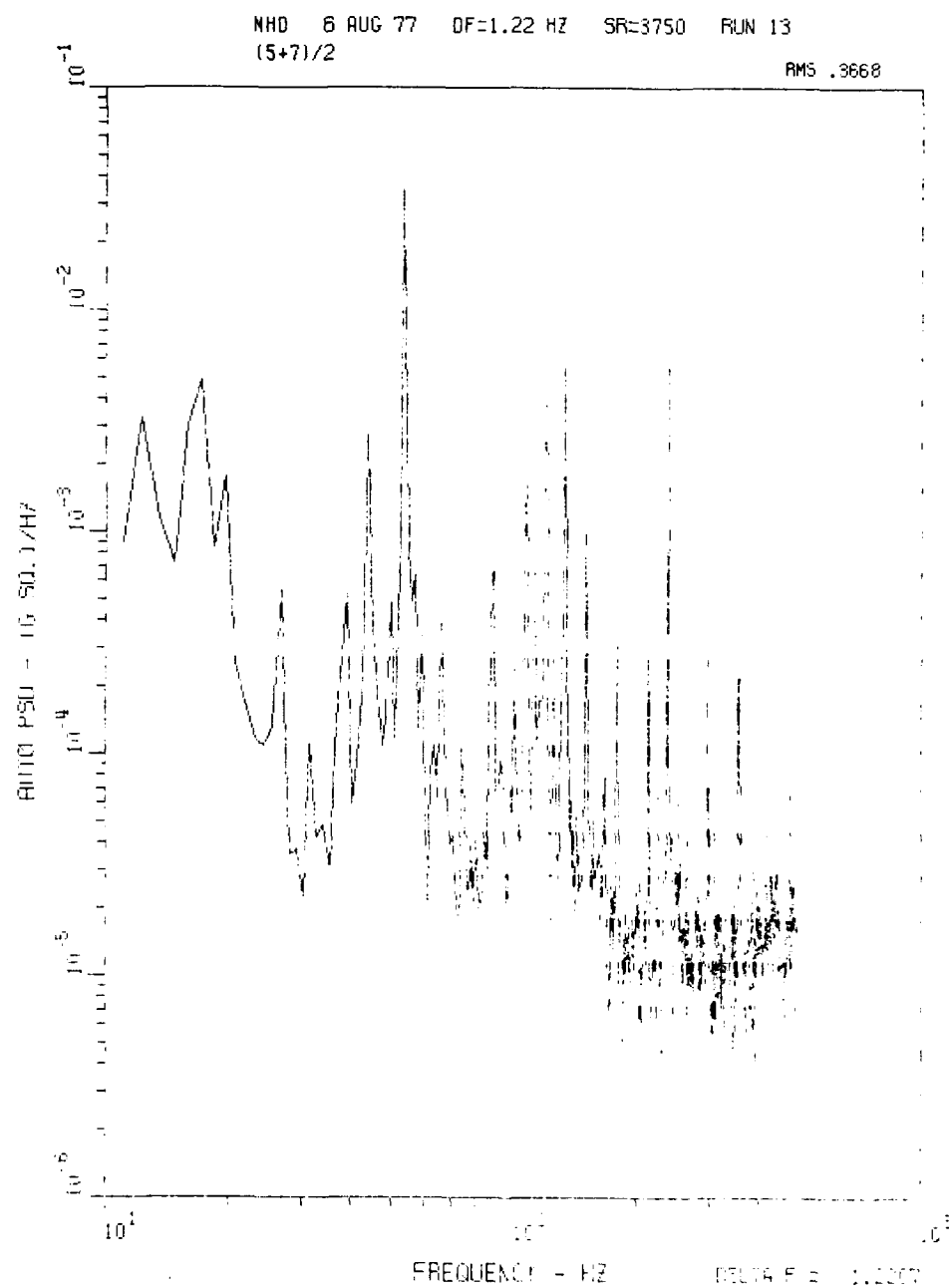


Figure 101. PSD for Channels (5+7)/2, 0-500 Hz, Run LWC 013

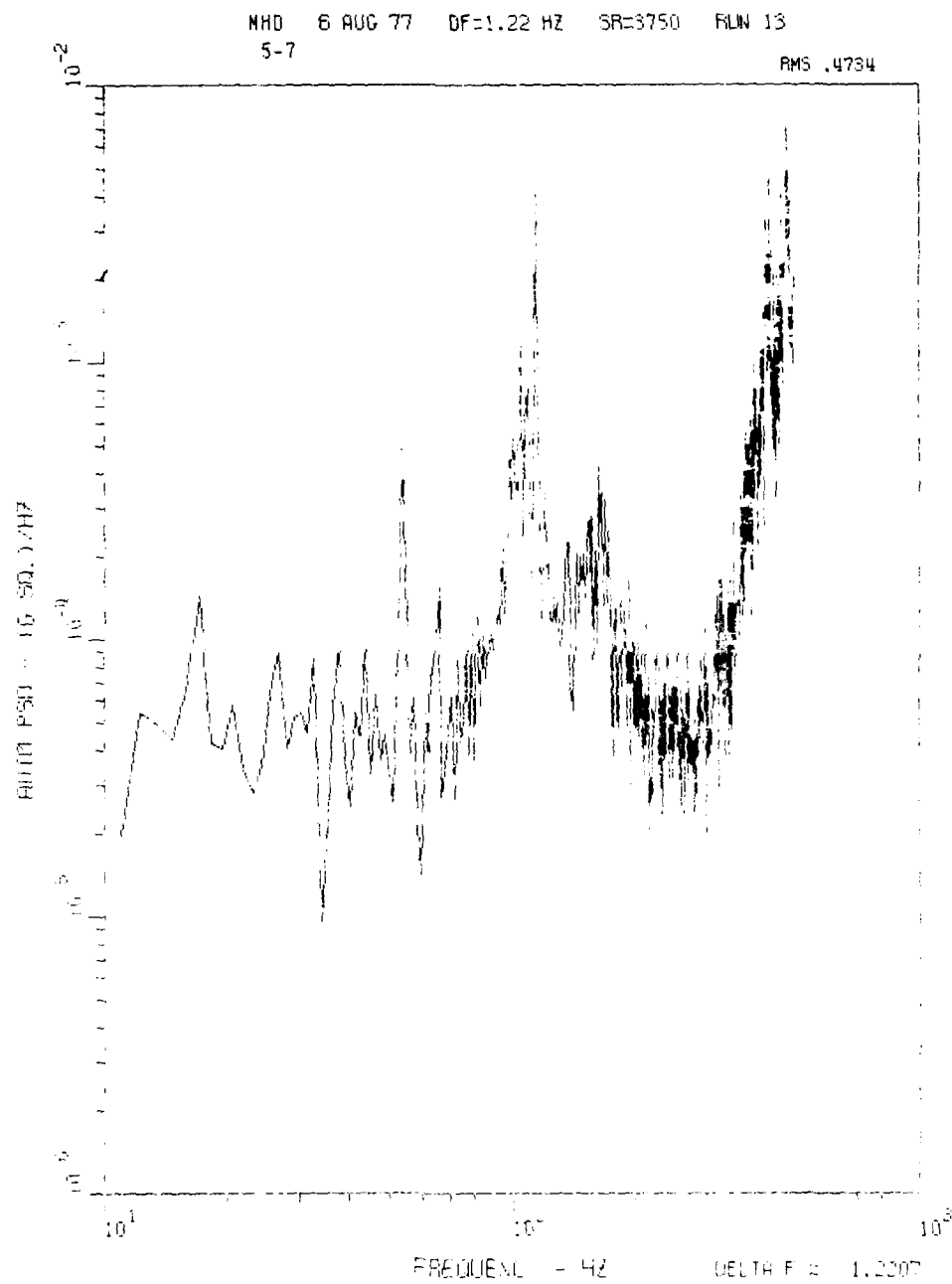


Figure 102. PSD for Channels 5-7, 0-500 Hz, Run LWC 013

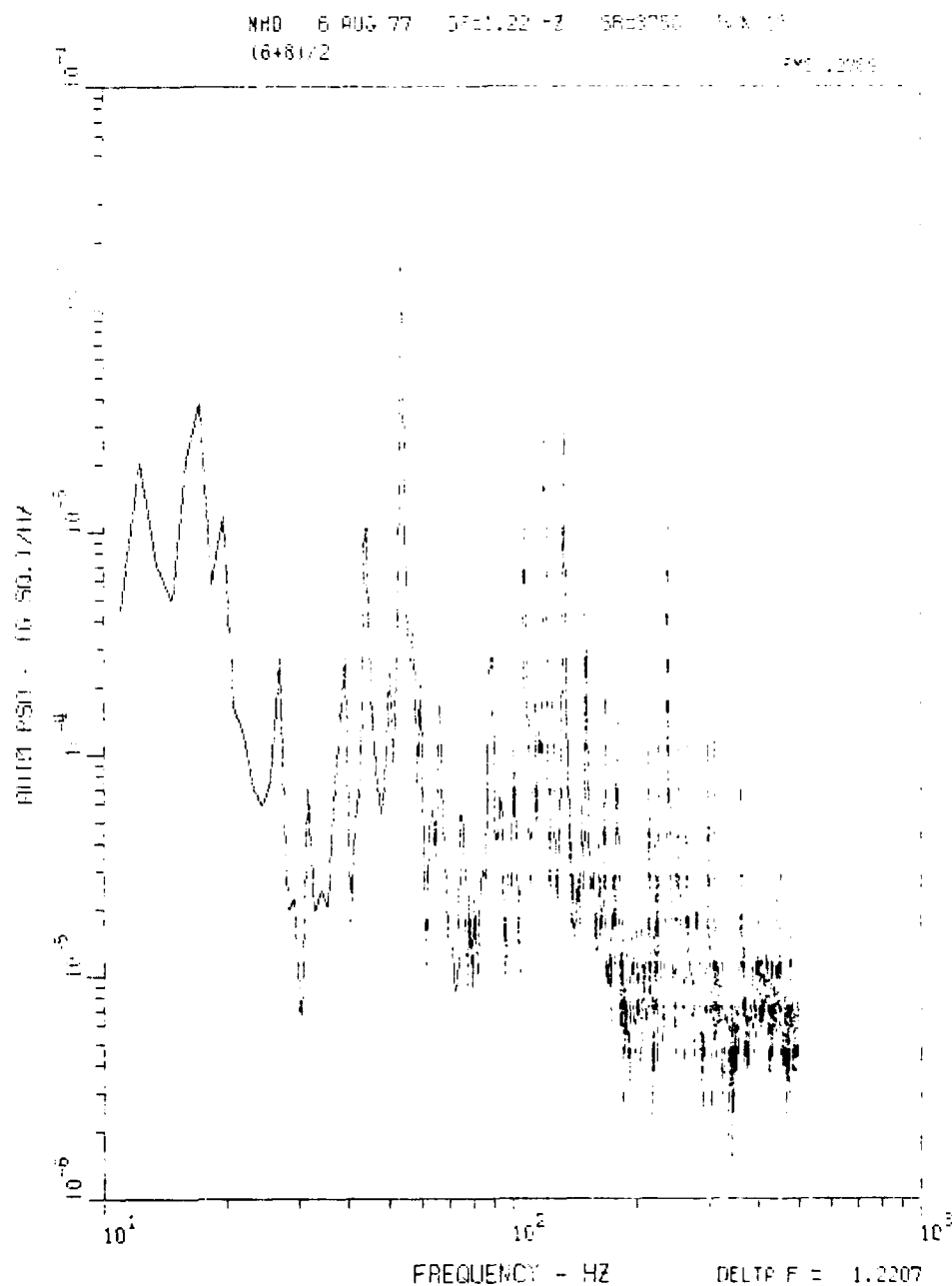


Figure 103. PSD for Channels (6+8)/2, 0-500 Hz, Run LNC 013

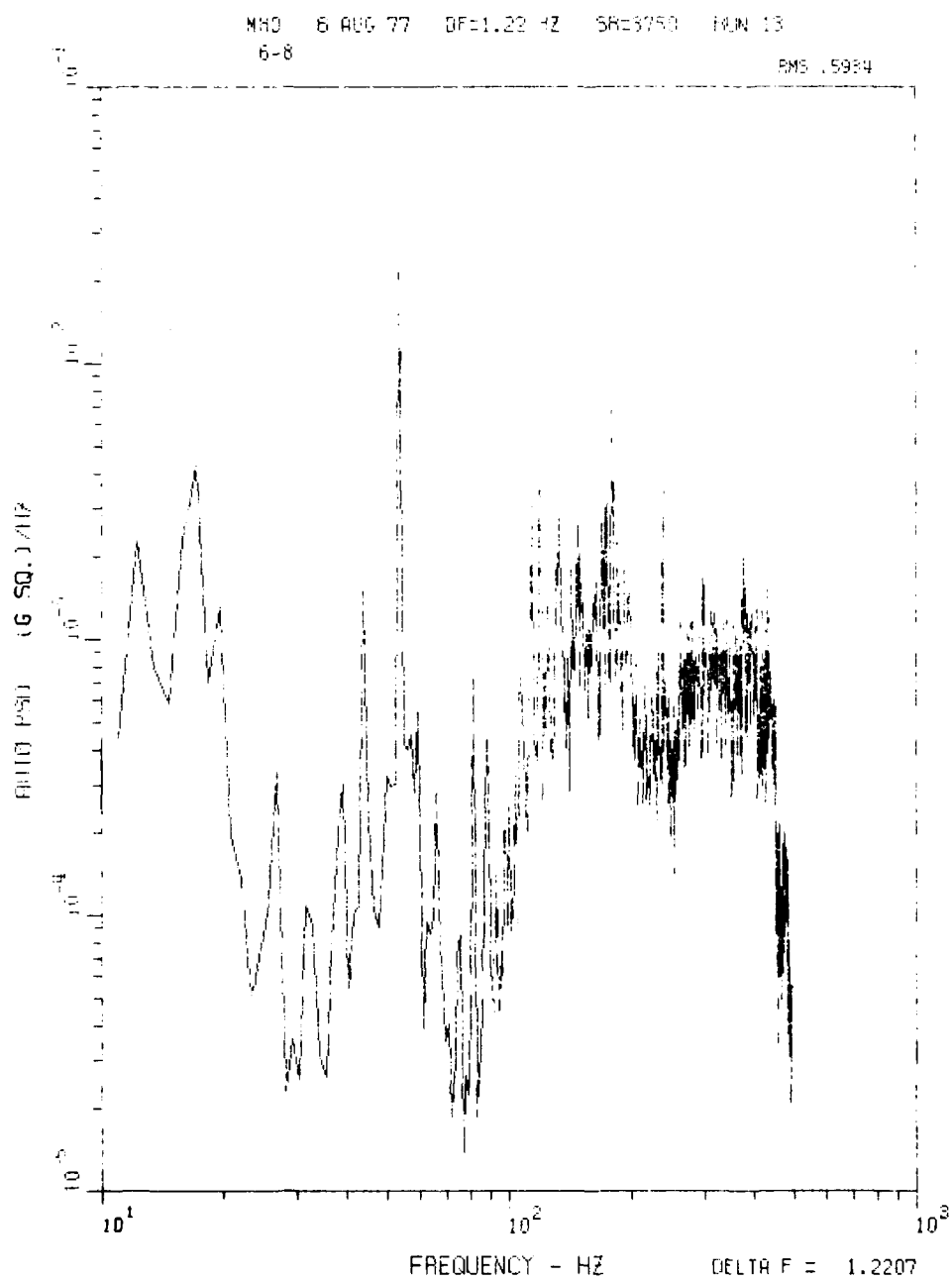


Figure 104. PSD for Channels 6-8, 0-500 Hz, Run LWC 013

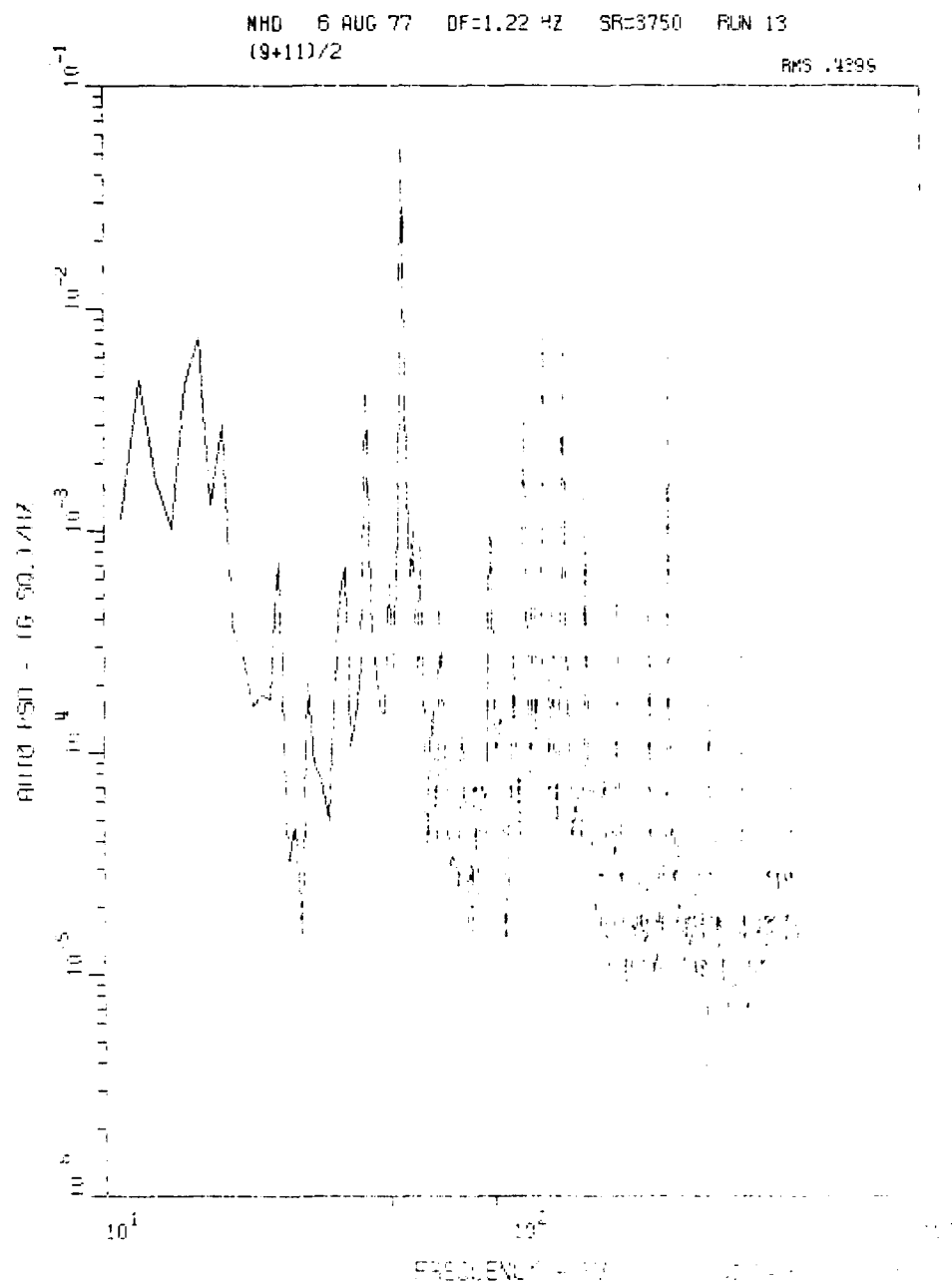


Figure 105. PSD for Channels (9+11)/2, 0-500 Hz, Run LWC 013



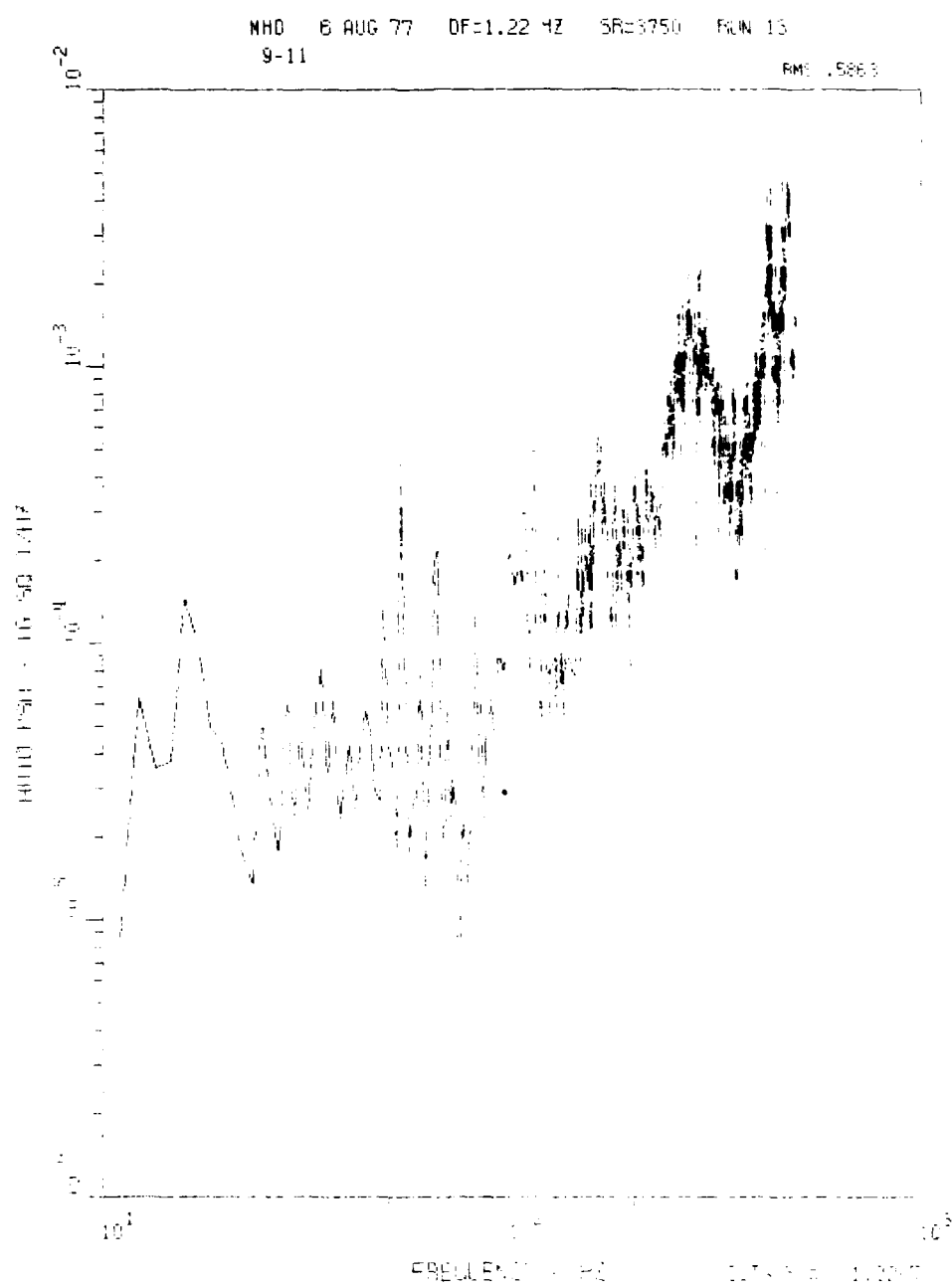


Figure 106. PSD for Channels 9-11, 0-500 Hz, Run LWC 013



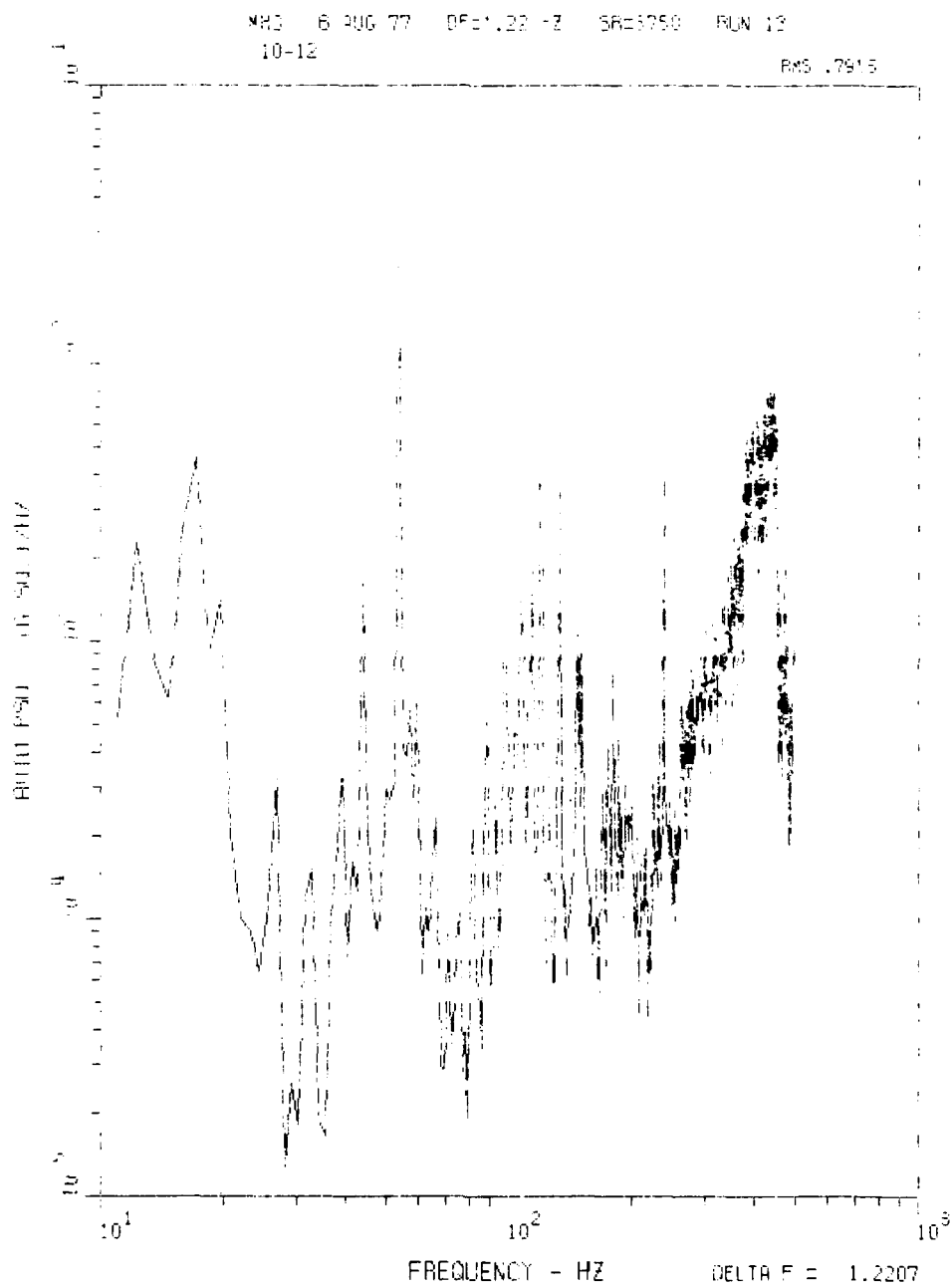
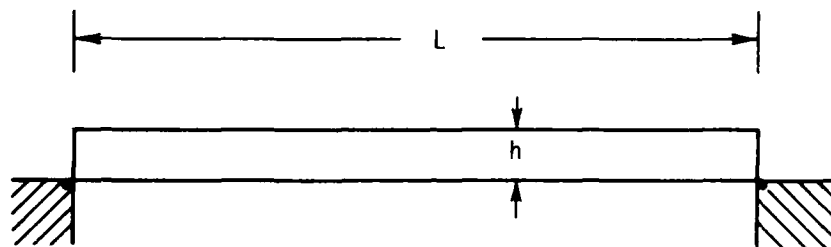


Figure 108. PSD for Channels 10-12, 0-500 Hz, Run LWC 013

a. Pinned-pinned beam



b. Modeshape for  $n^{\text{th}}$  mode

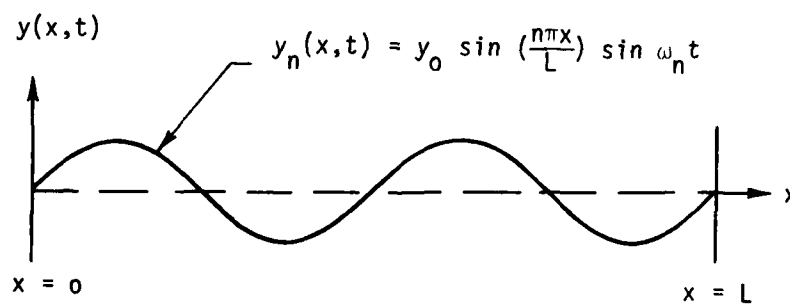


Figure 109. Beam Approximation to MHD Channel Modes

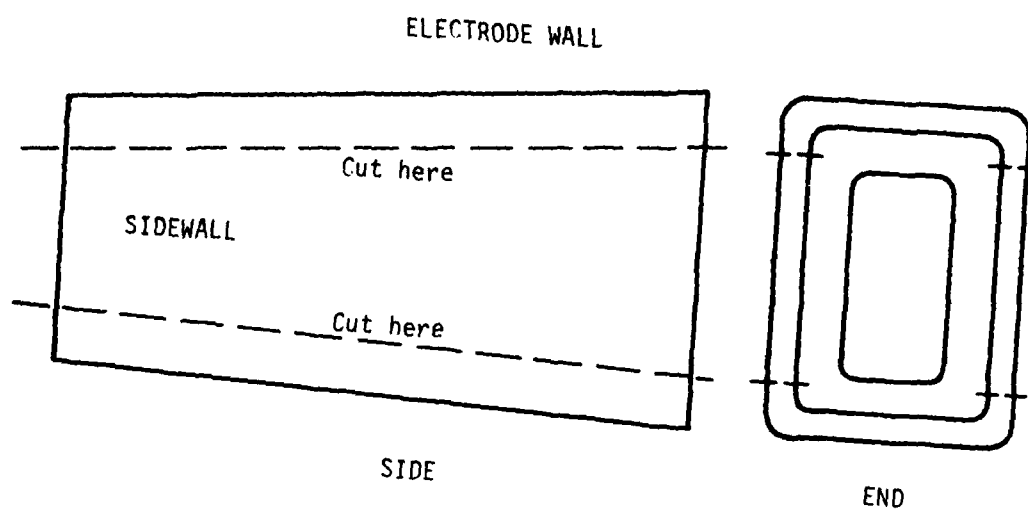


Figure 110. How the Lightweight Channel Was Cut Apart After Tests  
(Not to scale)

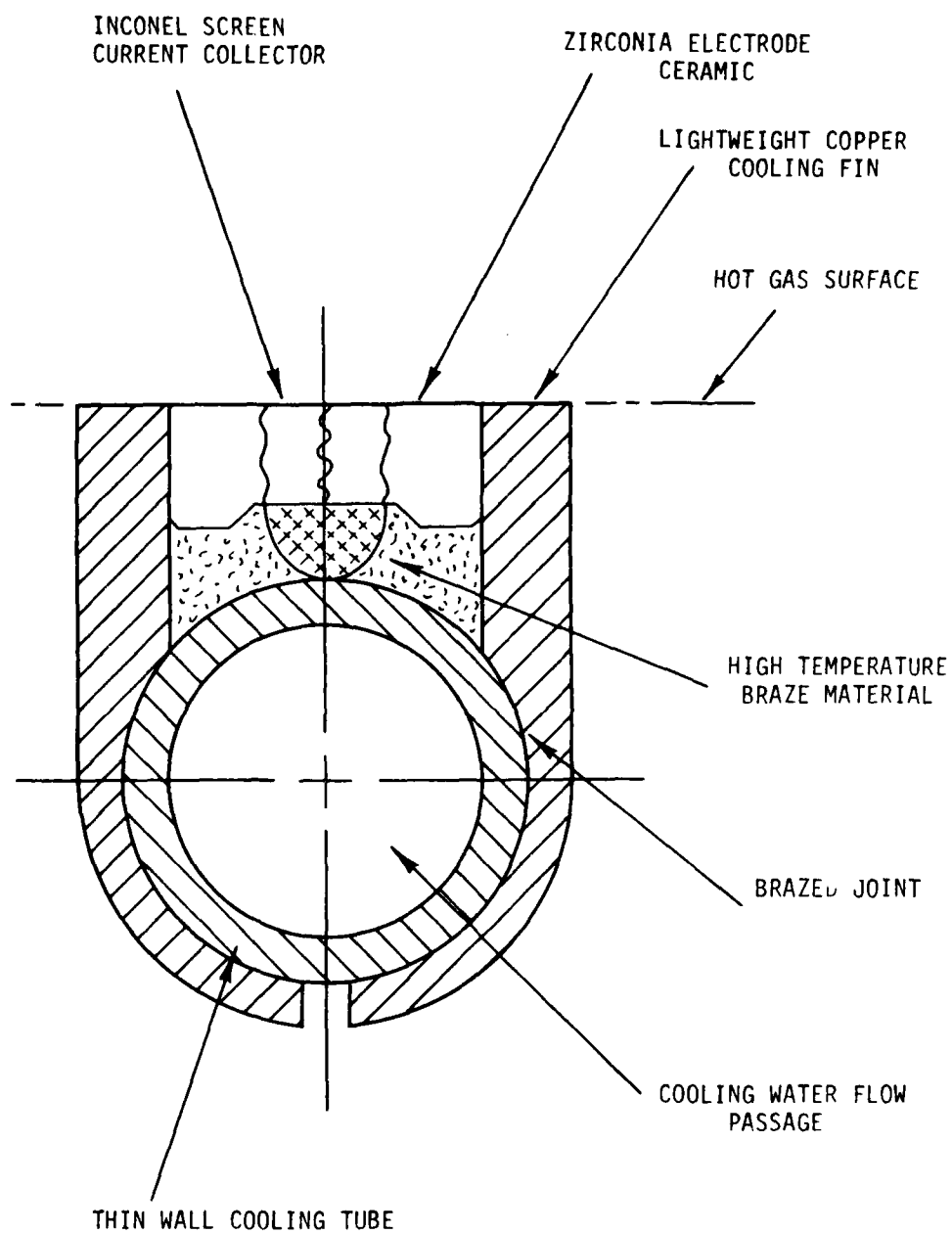


Figure 111. Typical Cross Section of Electrode Wall

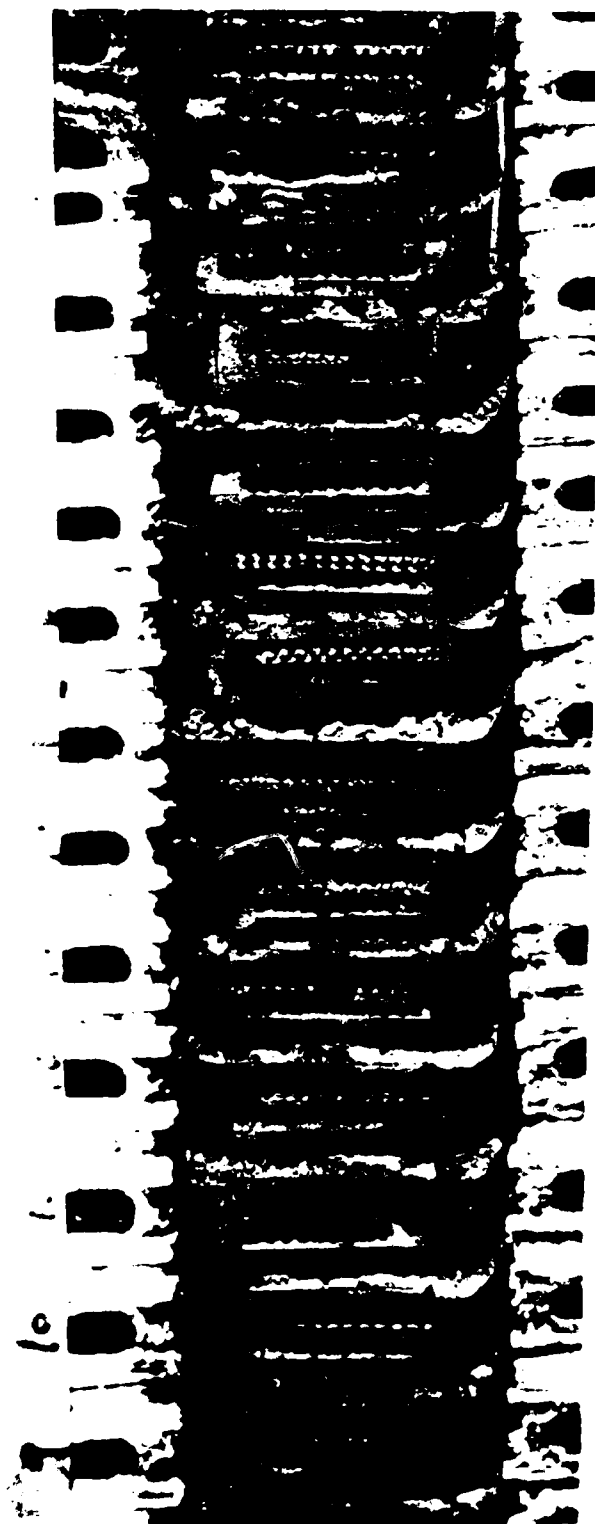


Figure 112. Some Anode Wall Electrodes Near the Upstream End of the Channel

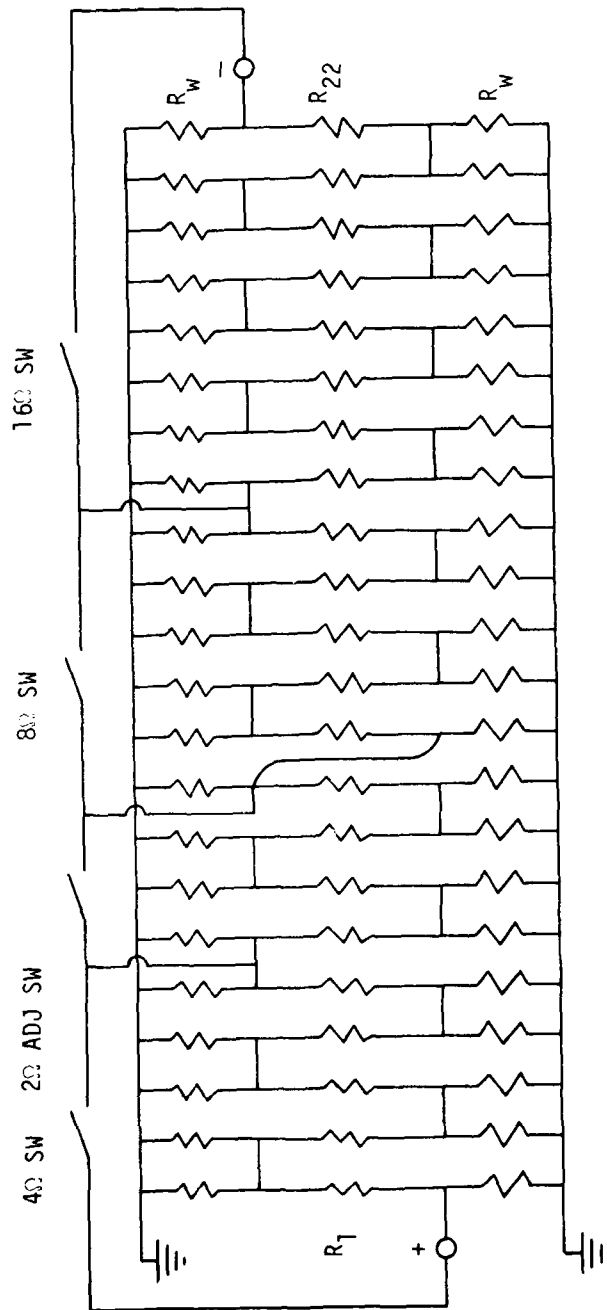


Figure 113. Cathode Wall Electrodes Near Middle of Channel



Figure 114. Channel Sidewall





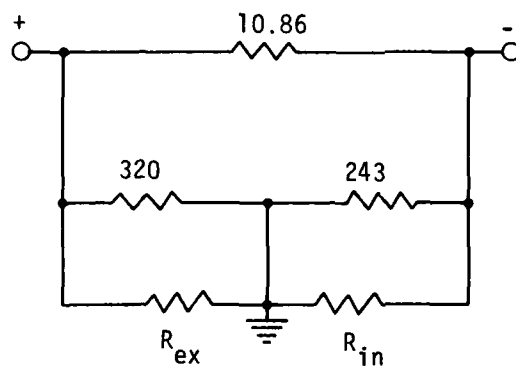
$R_0 \dots R_{22}$  = SS resistor tubes

$R_w$  = resistance of water paths of each water hose.

By changing switch combinations possible resistances between + and - terminals were:

4.19, 6.57, 8.46, 10.86, 12.63, 15.74 ohms.

Figure 115. Main Load Resistor Schematic



$R_{ex}$  = resistance between last MHD electrode and gnd.

$R_{in}$  = resistance between first MHD electrode and gnd.

$R_{ex} \gg R_{in}$

Figure 116. Main Load Resistor Circuit and Leakage Through Water Paths  
When Main Load = 10.86 Ohms; Equivalent Circuit

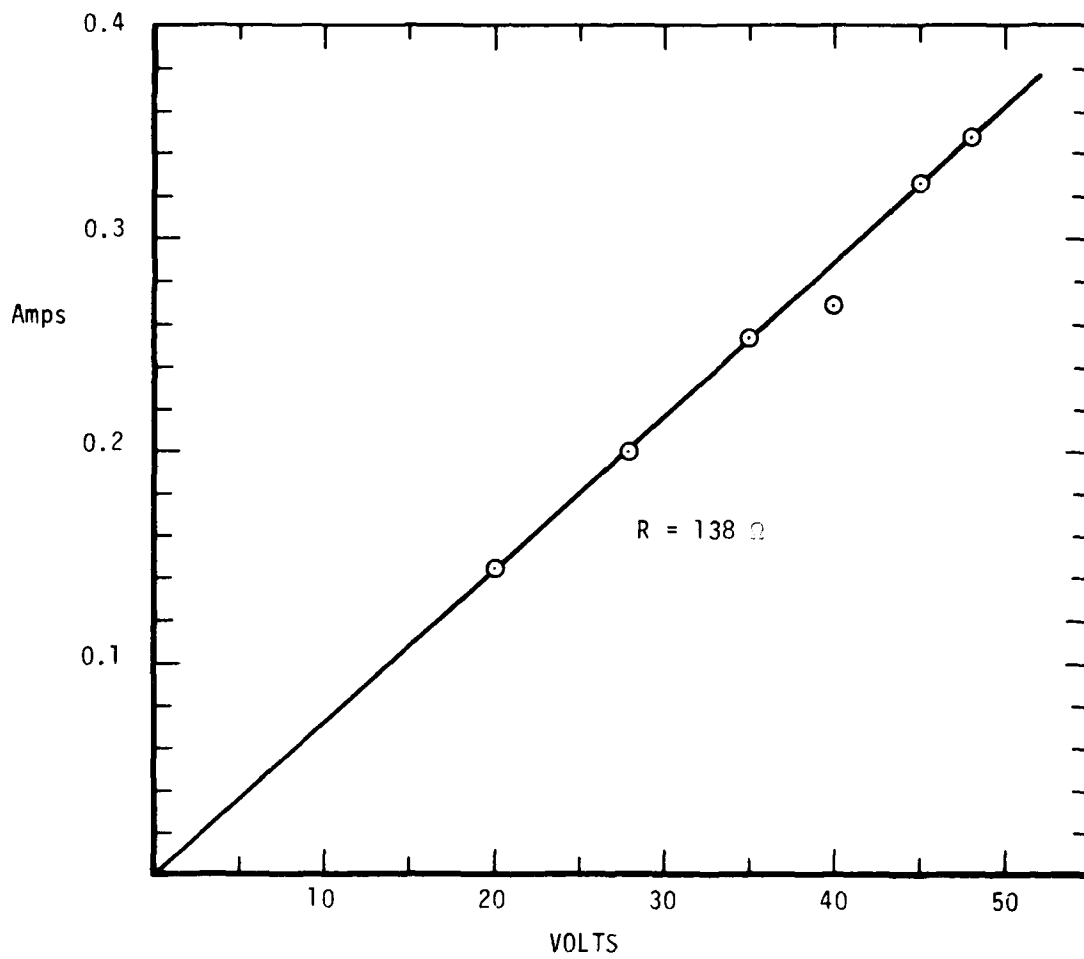


Figure 117.  $V/I$  for Current Leakage in Water Around Main Load Resistor to Ground

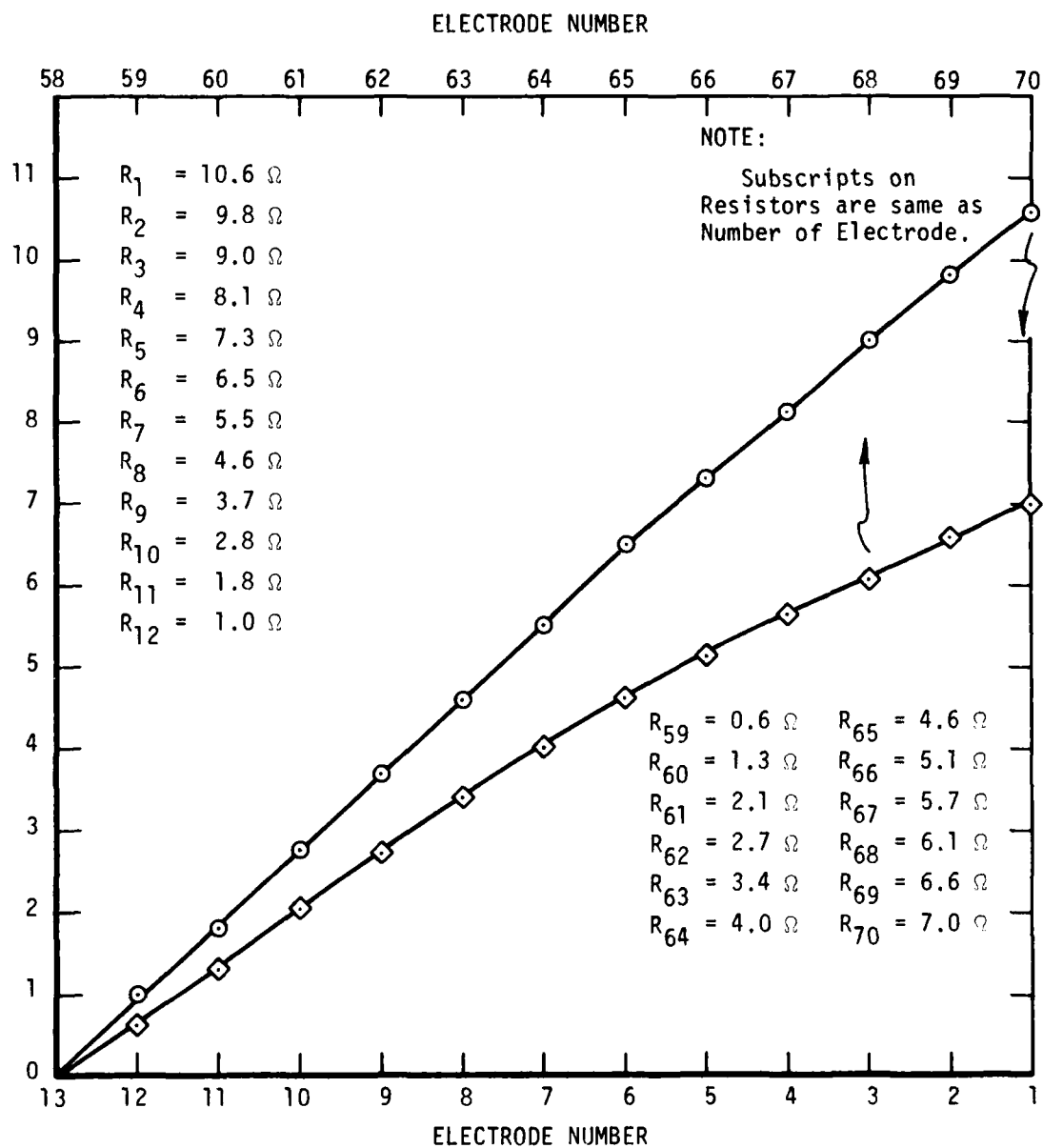


Figure 118. Ballast Resistors for LW MHD Channel

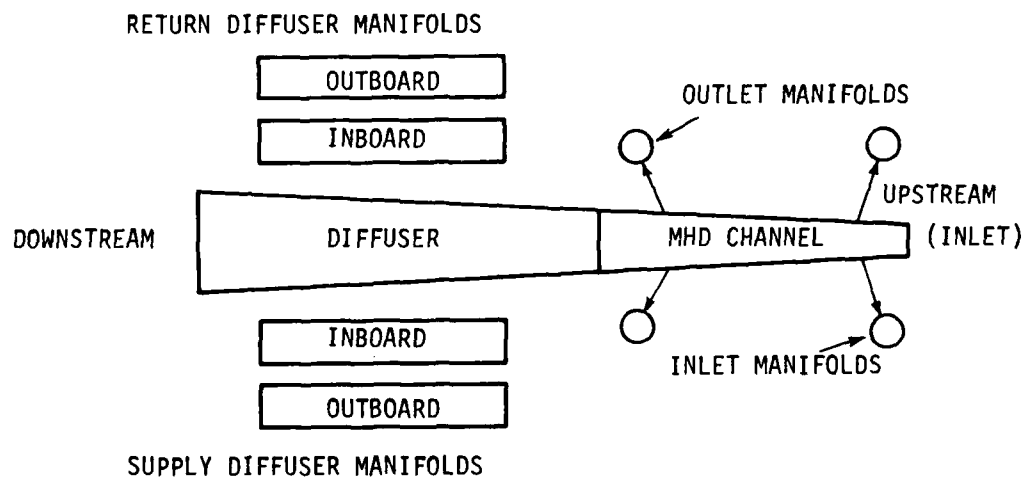


Figure 119. Top View, Schematic of MHD Channel and Diffuser Water Supply and Return

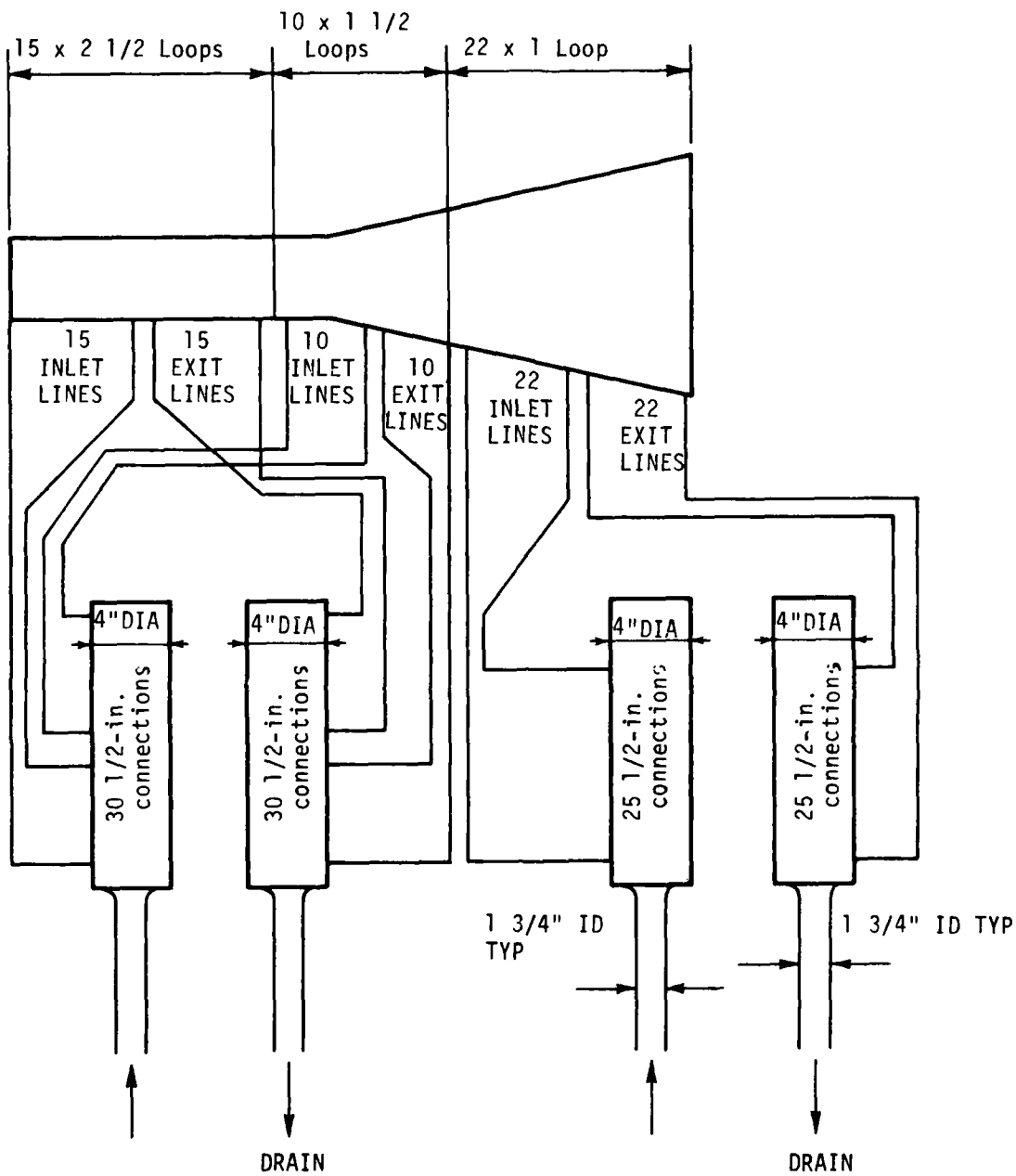


Figure 120. Cooling Water Connections for the Diffuser

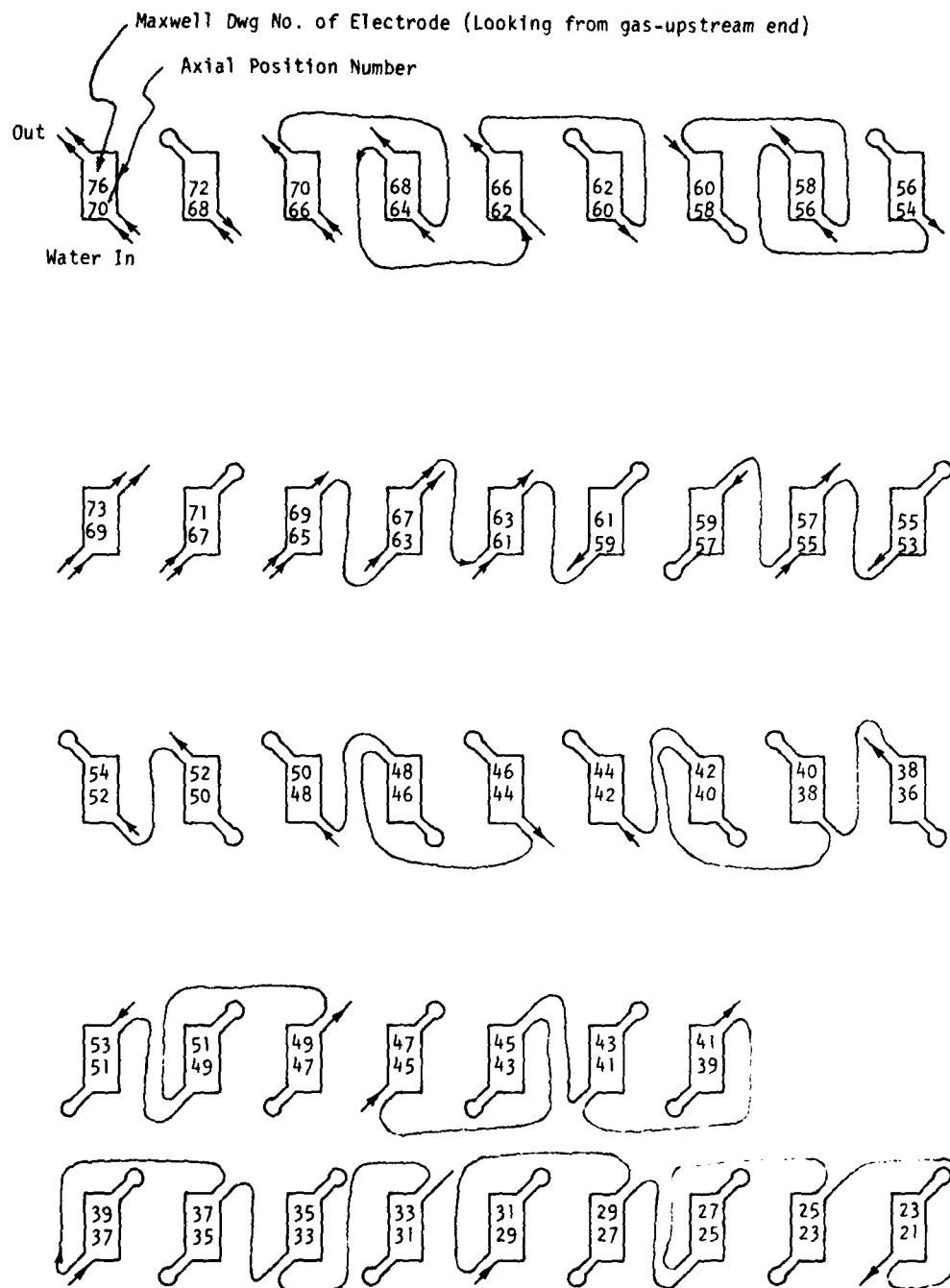


Figure 121. MHD Channel Electrode Water Circuit Schematic

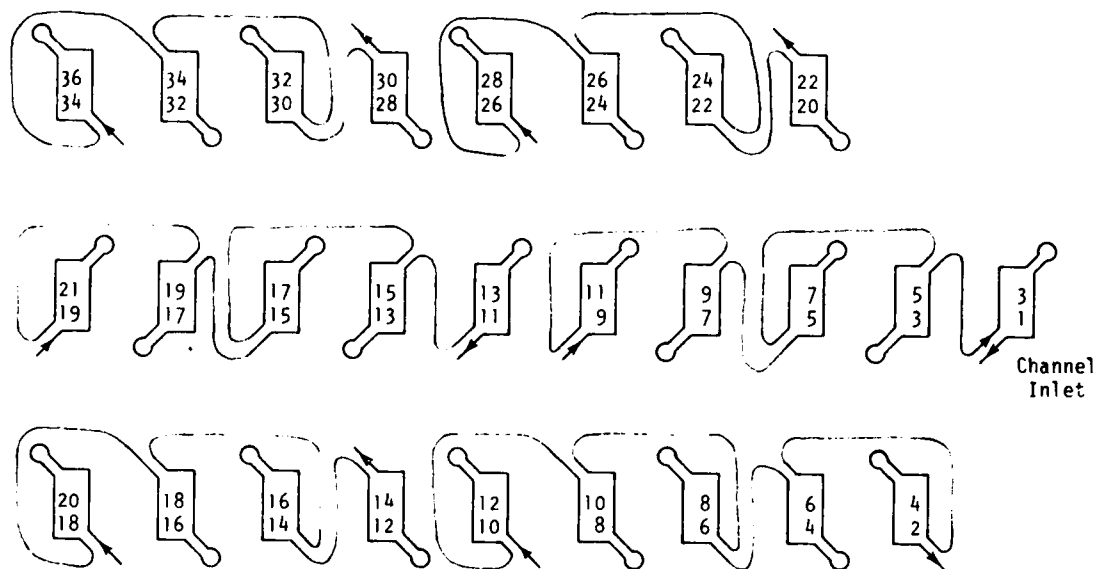


Figure 121. (Continued)

NOTE: There are 70 Electrodes. Electrode Dwg. Nos. 75, 74, 65, 64 are not present. 31 Inlets; 31 Outlets. The top number in each frame is Maxwell Dwg No.; Bottom Number is Channel Axial Position Sequence.



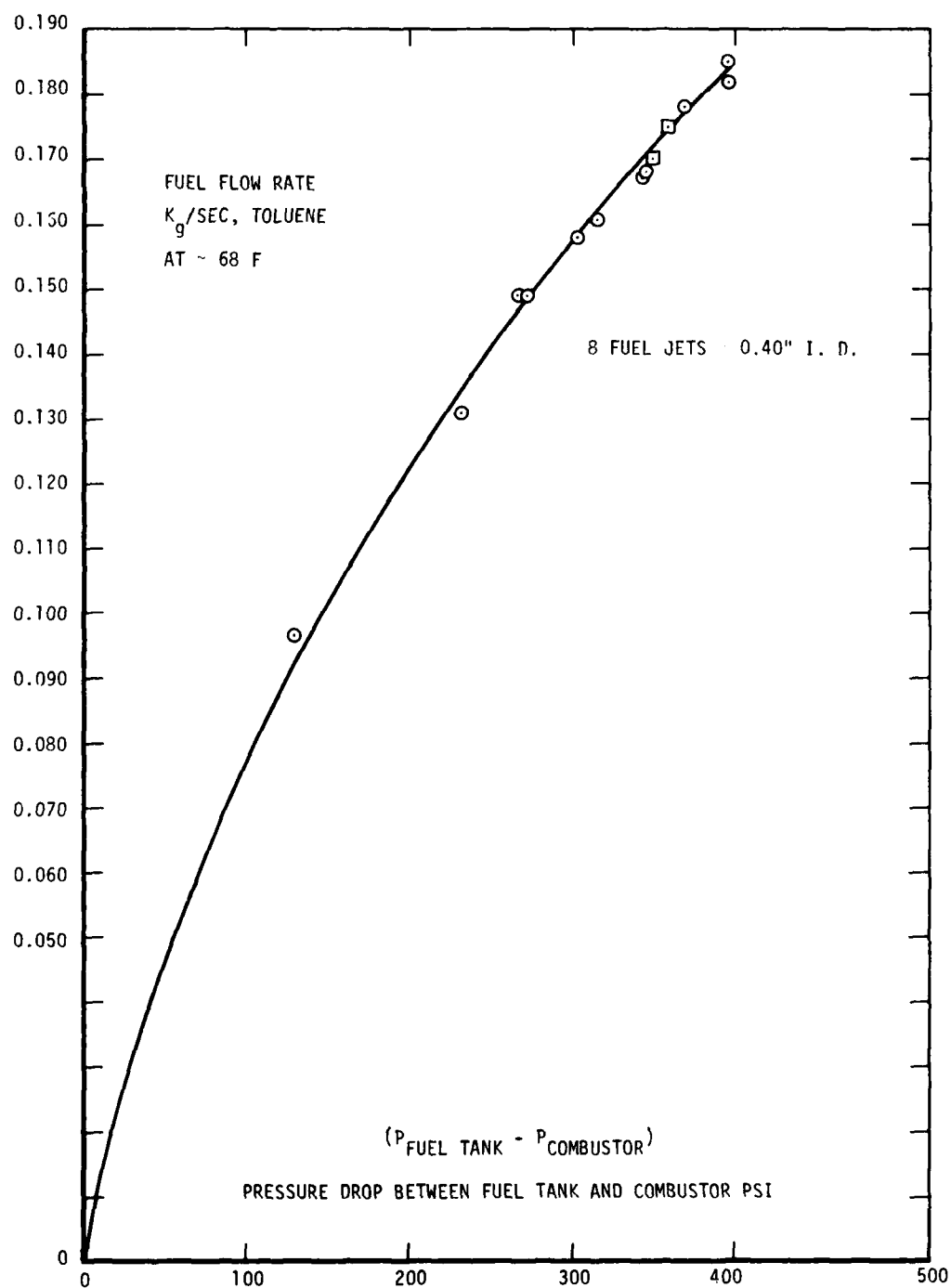


Figure 122. Fuel Flow Rate vs Fuel Line Pressure Drop

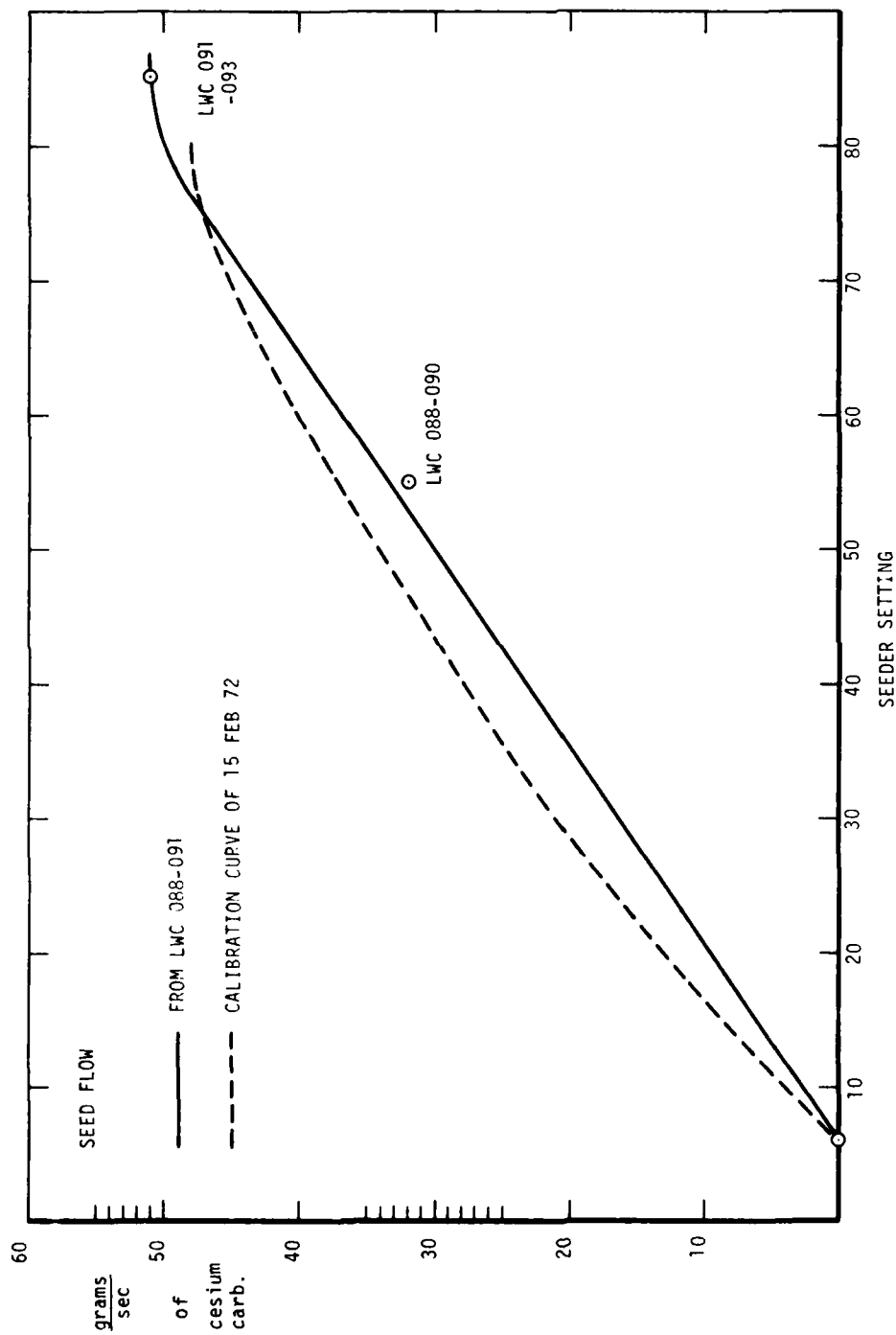


Figure 123. Seed Flow vs. Seeder Dial Setting

REFERENCES

1. D. W. Swallom, O. K. Sonju, D. E. Meader and G. T. Heskey, Magnetohydrodynamic Channel Development, AFAPL-TR-78-41, June 1978.
2. James F. Holt, Power Tests with the AFAPL KIVA-I MHD Generator, AFAPL-TR-74-99, May 1975.
3. James F. Holt and Daniel W. Swallom, Engineering Considerations for Combustion Driven Magnetohydrodynamic Generators, Tenth Intersociety Energy Conversion Engineering Conference, University of Delaware, Newark, Delaware, August, 1975, p. 524.
4. R. V. Shanklin III et al, KIVA-I Extended Duration MHD Generator Development, AFAPL-TR-75-27, June 1975.
5. W. Unkel and C. H. Kruger, Transient Response of MHD Generators, Symposium Engineering Aspects of Magnetohydrodynamics, Stanford University, Stanford, California, March 1973, p. II.9.1.
6. Richard E. Eckels, MHD High Energy Fuel Development Program, AFAPL-TR-78-10, March, 1978.
7. Fluid Meters, Sixth Edition, ASME, 1971.
8. D. W. Swallom, O. K. Sonju, D. E. Meader, and H. Becker, High Power Magnetohydrodynamic System, AFAPL-TR-78-51, Volume 1 (AD-A064796), July, 1978.

